UNIVERSITY OF MILAN

FACULTY OF MEDICINE

Doctoral School in Biotechnology applied to Medical Sciences

Title:
The IgLON family member Negr1 promotes neuronal arborization and migration via FGFR2.

Author:
Francesca Pischedda
Advisor:
Prof. Grazia Pietrini
Co-Advisor:
Dr. Giovanni Piccoli

INDEX

ABSTRACT

Negr1 is a member of IgLON adhesion protein family but its functions are largely unknown.

In our previous work ((Pischedda et al. 2014), APPENDIX I) we identified Negr1 as a developmentally regulated synaptic protein. Thus we examined the consequences of Negr1 acute down regulation. Strikingly, we found that Negr1 ablation impairs neuronal maturation in vitro.

In this project we demonstrated thanks to complementary biochemical and imaging approaches that Negr1 organizes trans-synaptic heterodimer and influences neurites outgrowth via MAPK signaling. In detail, we demonstrated that ectopic Negr1 is sufficient to improve neurite arborization and to rescue the morphological phenotype observed in Negr1 silenced cells.

This function is dependent on the activation of MAPK pathway through tyrosine kinase receptors. In fact, we found that Negr1 physically and functionally interacts with FGFR2, modulates FGFR2 response to FGF and consequently influences MAPK pathway.

FGFR2 pathway plays an important role during brain development. Not surprisingly, our investigation of the radial migration of newly generated cortical neurons revealed that Negr1-FGFR2 cross-talk controls cortical organization in vivo.

Noteworthy, mutations in NEGR1 and FGFR2 genes have been recently identified as ASD candidates.

Autism spectrum disorder (ASD) affects 0.9% of children and it is recognized as the most genetic of all developmental neuropsychiatric syndromes. Connectivity dysfunctions have been suggested as causative alterations in ASD.

Given the functional, physical and genetic correlation among Negr1 and FGFR2 and the impact of Negr1 on neuron morphology and migration, Negr1-FGFR2 molecular cross talk might arise as a key mechanism during CNS development.

1. INTRODUCTION

1.1 Neurite outhgrowth

Neurite outgrowth is a fundamental process that allows the establishment of a functional network in the developing brain.

During development of the nervous system, axons require a mechanism which guide them to their specific targets. This process is regulated by a large panel of guidance molecules.

Neurons need a permissive adhesive substratum to extend their axons. There are two major categories of adhesive cues: ECM (extracellular matrix) components, whose elements are localized in interstices or basement membrane, and CAMs (cell adhesion molecules) expressed both on neuronal and non-neuronal cells membrane. For example the ECM component laminin promotes the extension of those growth cones expressing the receptors for the integrin family (Bozyczko e Horwitz 1986; Jessell 1988; Letourneau 1978).

Neurons demonstrate selective affinity for different ECM molecules according to the particular panel of integrine receptors that they express (McKerracher, Chamoux, e Arregui 1996).

Neurons and glia express a wide variety of CAMs that allow the axons to interact with other cellular component or with themselves.

CAMs molecules are in fact the physical linkers between ECM and the intracellular cytoskeleton.

Furthermore, CAMs act also as receptor and activate intracellular cascade, such as the FAK-MAPK pathway (Fiol et al. 1994; Bechara et al. 2007; Maness e Schachner 2007) .

A wide variety of CAMs direct growing axons toward their targets via growth-promoting and inhibiting effects during development, and maintain the precise patterns of neuronal connectivity in the mature nervous system (Doherty, Fazeli, e Walsh 1995).

Thus guidance cues include a large variety of molecular signals, including electrical and chemical gradients and physical protein interaction tigthly regulated in a spatio-temporal manner(Raper e

Mason 2010).

Axons extending through the developing nervous system encounter many competing guidance signals arising from a variety of sources that need to be integrated into a single and reproducible command. For example axons simultaneously interact with ECM, glial cells and neuronal membrane, each one expressing multiple permissive, trophic and modulatory signals all at the same time (Fig. 1).

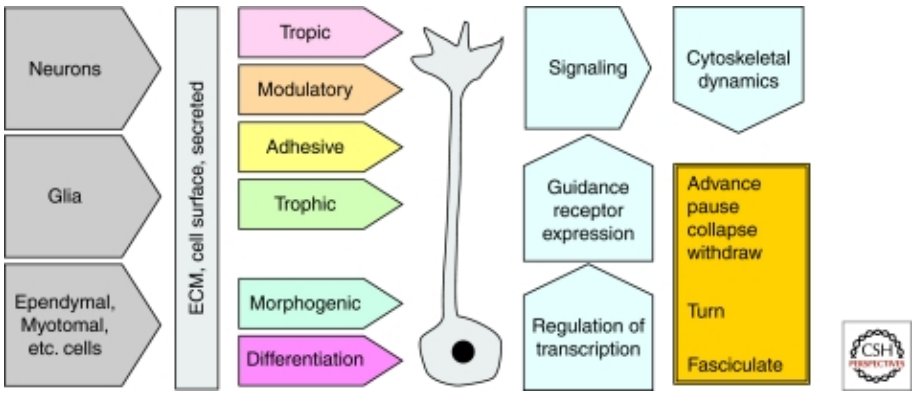

Fig. 1. Neurite outhgrowth modulatory signals.

Along their path, axons pass contact to both neuronal and non-neuronal cells. These cells expose on their surface or release into interstitial spaces and the ECM a multitude of signaling molecules, such as differentiation, modulation or tropic factors. As a result, a growth cone may advance, pause, collapse, withdraw, turn or fasciculate with other axons (adapted from (Raper e Mason 2010).

Given that many of the molecules and relative receptors involved in axonal growth and neuronal maturation have been identified, now the main goal is to understand how they cooperate to guide the establishment of a functional neuronal network.

1.2 IgLON CAMs family

The formation of the neuronal network requires the establishment of functional neuronal contacts, the synapse. One of the earliest and most critical steps in the formation of synaptic contact is the induction and adhesion of precisely opposed pre-synaptic and post-synaptic structures. Numerous neural recognition molecules involved in regulation of synaptic contact formation via homo/-hetero dimerization have been now identified.

Neurons exhibit at their cell surface different types of cell adhesion molecules (CAMs) and related signalling molecules. Many of CAMs belong to one of three most important families: the cadherin(Takeichi et al. 1988), integrin (Ruoslahti 1988), and immunoglobulin superfamily (Williams e Barclay 1988). Among them, major role is played by the molecules belonging to the immunoglobulin superfamily (IgSF): integrins, receptor tyrosine kinases (including ephrin receptors), neuroligins, neurexins, neuropilins and plexins. These molecules interact in a developmental and spatial specific manner thus allowing the establishment of the correct pattern of synaptic contact.

The IgSF proteins encompass one or more extracellular Ig-like domains and execute important functions in the establishment and remodeling of the CNS (Salzer e Colman 1989).

IgSF proteins such as neural cell adhesion molecule (NCAM), F3, TAG-1, L1, and NgCAM include also several fibronectin type-III-like repeats in addition to five or six immunoglobulin (Ig)-like domains, whereas Thy-1, myelin-associated glycoprotein, SC1 and telencephalin are composed by only Ig-like domain(s).

Many neural IgSF proteins do not include a transmembrane domain and are anchored to the plasma membrane via a glycosylphosphatidylinositol (GPI) bridge.

LAMP (Levitt 1984), OBCAM (Schofield et al. 1989), neurotrimin (Ntm) (Struyk et al. 1995) and Negr1 (Kilon) (Funatsu et al. 1999) are classified as a subgroup of IgSF named as IgLON. IgLONs

are expressed at higher levels in the cerebral cortex and limbic system (Levitt 1984; Struyk et al. 1995). Each IgLON member is highly glycosylated, binds the membrane by a GPI-anchor and includes three C2-type Ig-like domains (Fig. 2).

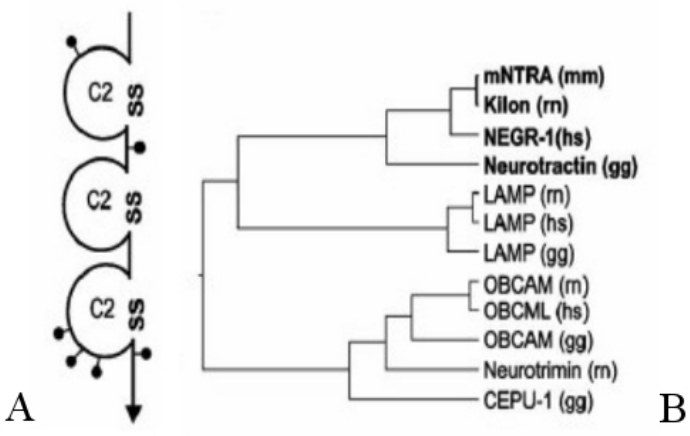

Fig. 2. Molecular structure and classification of IgLON family members.

(A) Structure of the three C2-type Ig-like domains in IgLON family members. **(B)** IgLON family members.

Experimental evidence suggested that IgLONs modulate synaptic functions, synaptic formation and plasticity (Hashimoto, Maekawa, e Miyata 2009). Furthermore, electron microscopic observations showed the synaptic localization of LAMP (Zacco et al. 1990), Negr1 and OBCAM (Miyata et al. 2003) in adult brains.

Recently, *in vitro* experiments performed in cultured hippocampal neurons have shown that Negr1 and OBCAM are directly implicated in synapse formation (Yamada et al. 2007; Hashimoto et al. 2008). IgLON members show heterophilic and homophilic binding within the plane of the plasma membrane and might function in molecular complexes.

It has been supposed that different homo/heterophilic dimers of IgLON members characterized by different affinities exist within the plasma membrane; *in vitro* evidences suggest that IgLON

homo/heterodimerization might have a dual impact on neurites extension (Schäfer et al. 2005; Orlando D Gil et al. 2002).

For example LAMP, which is an early marker of cortical and sub-cortical limbic regions, can act in two different ways. On one hand it facilitates the extension of neurites from thalamic neurons expressing LAMP and promotes the outgrowth of limbic axons. On the other hand, it inhibits branch formation and acts as repulsive signal during axonal guidance in neurons which do not express LAMP (Mann et al. 1998; Pimenta e Levitt 2004).

Neurotrimin (Ntm) is highly expressed in thalamus, subplate, lower cortical laminae of forebrain, hippocampus, olfactory bulb, dorsal root ganglia and spinal cord (Struyk et al. 1995).

Ntm binds neurons that express Ntm at high levels e.g., dorsal root ganglion (DRG) and hippocampal neurons. Interestingly, Ntm promotes neurite outgrowth of DRG neurons, but it inhibits the outgrowth of sympathetic neurons lacking Ntm expression (Orlando D Gil et al. 2002). Thus, both LAMP and Ntm promote *via* homophilic interactions neurite outgrowth, whereas the lack of homophilic partner or in presence of heterophilic interactions they have the opposite function (Orlando D Gil et al. 2002; Hashimoto et al. 2008). OBCAM expression was found in dendritic spines of neurons in cerebral cortex and hippocampus (Miyata et al. 2003) and regulates proliferation and cell size of cortical astrocytes (Sugimoto, Maekawa, e Miyata 2010).

OBCAM is able to bind homophylically and heterophilically with other members of IgLON family(Lodge et al. 2000). In conclusion, each IgLON is expressed on different neuronal surfaces and can form homo and hetero dimers with different functional consequences.

Thus, IgLON expression pattern may generate a complex molecular finger-print that can be instrumental for the establishment of proper neuronal connectivity.

1.3 Negr1 (Kilon)

Negr1 is a member of the IgLON family. Negr1 mRNA is transcribed from a large gene (> 800 kb) (NEGR1, 1p31.1) that includes 7 exons for a total of 5809 bp. More than 8000 SNPs have been identified in the gene region, 7 in the coding region. NEGR1 gene codes for a protein detected with an apparent MW of 50 kDa, but it shifts at 36 kDa after de-glycosylation.

This corresponds to the expected size deduced from the amino acid sequence (Schäfer et al. 2005).

Negr1 is highly expressed in the brain, but not in adult liver, spleen, kidney, or lung (figure 4A).

The expression gradually increased during postnatal brain development, reaching a steady-state level in adulthood (Schäfer et al. 2005). In the adult murine brain, it is expressed quite ubiquitously with higher levels in fore-brain regions (hippocampus, frontal cortex, amygdala) (figure 4B).

Western blotting analysis (figure 4C) and immuno-histochemistry approaches (figure 4D) confirmed that Negr1 is expressed by forebrain neurons with higher expression in hippocampus (both DG and CA1-3) and frontal cortex (all layers) (Schafer, M., unpublished data).

Furthermore, *in vitro* studies demonstrated high levels of Negr1 in axonal growth cones in early stages, whereas its localization is mostly confined in dendritic spines in late cultures (Hashimoto et al. 2008). *In vitro* studies suggested that Negr1 may act as a trans-neural growth promoting factor in regenerative axon sprouting (Schäfer et al. 2005). Moreover, Negr1 over-expression affects the number of synapses with different outcome depending on culture stages: at early stages Negr1 over-expression decreases the number of synapses, conversely in later stage it is positively associated with synapses number (Hashimoto, Maekawa, e Miyata 2009; Hashimoto et al. 2008).

Recently, we showed that Negr1 also controls dendritic arborization and spine density in cortical neurons *in vitro* and *in vivo* ((Pischedda et al. 2014) APPENDIX 1).

Thus, Negr1 appears to be an important cell adhesion molecule involved in the control of neurite outgrowth and synapses formation with putative critical function in the adult brain.

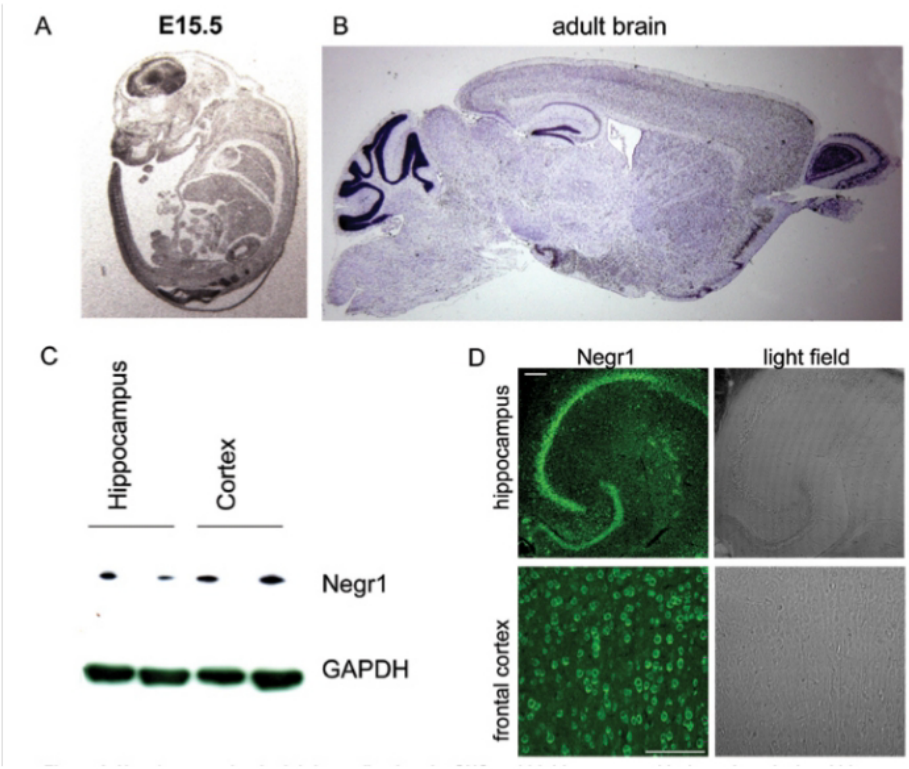

Fig. 3. Analysis of Negr1 Expression. (A) In situ hybridization with Negr1 specific probes in E 15.5 mouse embryos. Negr1 mRNA appears expressed in the brain, olfactory bulb and spinal cord. (B) Negr1 mRNA expression increases during post-natal development. High expression was found in hyppocampus and frontal cortex. (C) Western blotting analysis with Negr1 specific antibody (D) Immuno-fluorescence staining with Negr1 specific antibodies confirmed Negr1 protein expression in adult brain hippocampus and in frontal cortex. Scale bar=150 μm. (Schafer, M., unpublished data)

1.4 Ectodomain shedding and IgLON

It has been demonstrated that several membrane bound proteins involved in neuronal development are released from the membrane and exert their activity as soluble factors activating intracellular cascades (Alfandari et al. 2001; Black 2002).

The process at the bases of the release of the extracellular portion of proteins by proteolitical cleavage is called ectodomain shedding. This modification deeply influences protein function. (Black 2002).

ADAMs (for "a disintegrin and metalloprotease domain") are a family of transmembrane glycoprotein able to execute the ectodomain shedding on different molecules. These protein are important for fertilization, myogenesis and neurogenesis (Seals e Courtneidge 2003).

In humans, there are 19 genes coding for ADAM proteins. In total, considering also the other species, 34 ADAM gene have been described.

ADAMs are composed by several domains. Starting from the N-terminal: a prodomain, a metalloprotease domain, a disintegrine domain, a cysteine rich domain, a EGF-like domain, and a cytoplasmic tail (Seals e Courtneidge 2003)(Fig. 4).

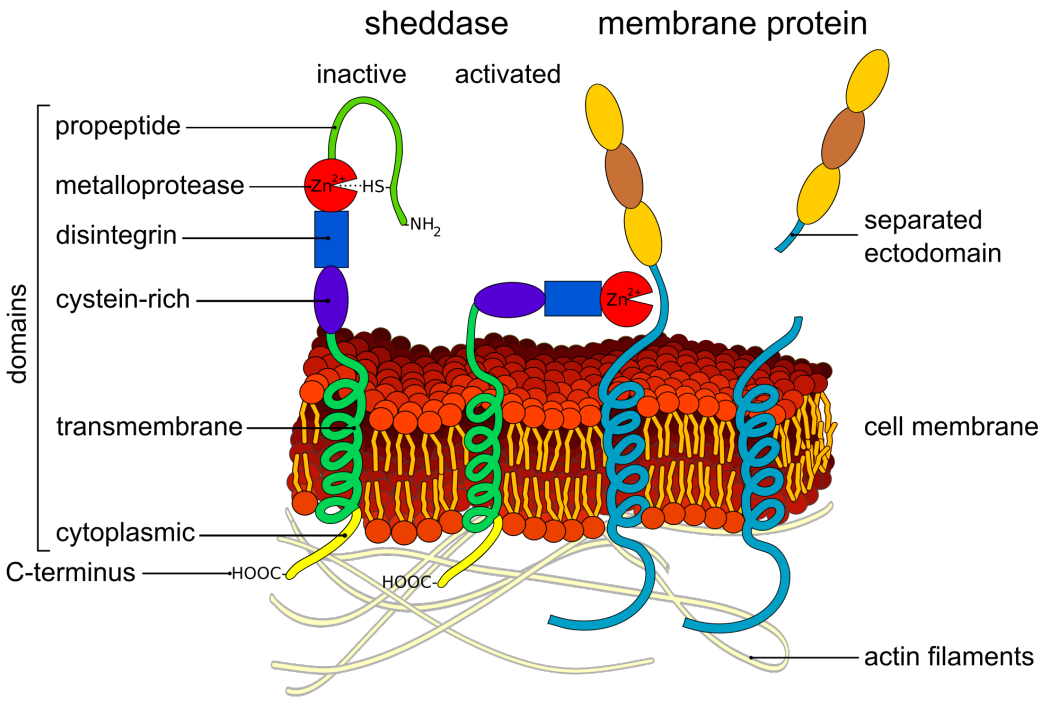

Fig. 4. ADAM domains and ectodomain shedding. (adapted from (Seals e Courtneidge 2003), review)

ADAMS proteins are involved in the cleavage of several proteins. For example MBP (Myelin Basic Protein) is processed exclusively by ADAM10, while TNF (Tumor Necrosis Factor) alpha is shed by ADAM 17/ TACE (Tumor Necrosis Factor-α-Converting Enzyme) (Chantry, Gregson, e Glynn 1989).

Furthermore, the proteolytic processing of APP (amyloid precursor protein) is an essential event in the ezyogenesis of Alzheimer's disease. Buxbaum, J. D., et al underlined in 1998 the role of ADAM 9, ADAM 10, and ADAM17 in the cleavage of APP, suggesting an essential role for these proteins in CNS (central nervous system) (Buxbaum et al. 1998). Fibronectin repeats (FN) of IgSF proteins could be proteolitically processed by ADAM protein family, leading to the release in the cellular media of extracellular portions of the protein. One of the first protein identified as a target for ectodomain shedding was L1 (Rathjen e Schachner 1984) which is processed by ADAM10 into 85 and 32 KDa active fragments (Mechtersheimer et al. 2001).

ADAMs may also play a pivotal role in the transfer of information from the cell to its environment

and vice-versa. Thus, is clear that ADAMs family members are positioned to play important roles in development, cell signaling, and disease pathologies.

In fact, ADAMs are involved in shedding of cytokines and cytokine receptors (Black 2002), growth factor (Izumi et al. 1998; Merlos-Suárez et al. 2001; Sunnarborg et al. 2002) and extracellular matrix components such as type IV collagen and fibronectin. It has been speculated that such activity may assist cellular migration (Alfandari et al. 2001).

Interestingly, recent *in vitro* data indicates that IgLONs, and Negr1 in particular, can be released *via* shedding into neuronal media and it regulates as soluble factor neurite outgrowth in mature cortical neurons (Sanz, Ferraro, e Fournier 2015).

Combining mass spectrometry, biochemistry and neuronal morphology analysis Sanz and colleagues found that the treatment of mature neurons with pan-metalloproteinase inhibitors correlates with a severe impairment in neurite outgrowth.

1.5 FGFRs role in neuronal morphology

Trophic molecules like neurothrophins and growth factor support growth cone motility (Connolly, Seeley, e Greene 1985; Reichardt 2006). In particular, the presence of trophic factor gradient guides axonal outgrowth *in vitro* (Gundersen e Barrett 1979; Letourneau 1978) acting as chemo-attractant for axons near-by when they become very close to their target (Patel et al. 2000; Genç et al. 2004).

The mammalian FGF (fibroblast growth factor) family comprises 18 molecules, which exert their actions through four highly conserved tyrosine kinase receptors (FGFR 1, FGFR2, FGFR3 and FGFR4) (Turner e Grose 2010).

FGFs are glycoproteins secreted and generally sequestered very fast by heparan sulphate proteoglycans (HPSGs) present in the extracellular matrix (ECM), as well as on the cell surface.

FGFs are released from the ECM by heparinases, proteases or specific FGF-binding proteins and subsequently bind first to cell surface HPSGs and then to FGFRs to trigger signalling cascades.(Ori et al. 2009).

Moreover, cell surface HPSGs are important to stabilize the FGF-FGFR interaction.

In conclusion FGF-FGFR and HPSG exists and executes cellular function as a ternary complex (Harmer et al. 2004; Mohammadi, Olsen, e Goetz 2005).

FGFRs control a multitude of cellular processes including cell growth, differentiation, migration and survival and have been related to a number of physiological and pathological processes.

The structure of FGFRs consists of three immunoglobulin (Ig) domains (Ig1–Ig3), a transmembrane helix and a cytoplasmic tyrosine kinase domain.

FGFR binding to FGF results in the dimerization of the receptor leading to auto-phosphorylation of the intracellular tyrosine kinase domains. This event triggers a complex intracellular pathway that involves AKT, Ras and PKC activation (Sternberg e Gullick 1990).

FGFRs play essential roles in almost every step during axonal elongation (Goetz e Mohammadi

2013) . Axonal path-finding in the visual system and in the peripheral nervous system rely on guidance mechanisms involving FGFRs (Haupt e Huber 2008). In particular, FGFR2 signalling regulates axon patterning modulating the expression of the repulsive guidance cue Sema3A during innervation (Kettunen et al. 2007).

The FGFR–ligand interaction occurs through the Ig2 and Ig3 modules, while the Ig1 module is thought to have mostly a regulatory function (Christensen et al. 2006).

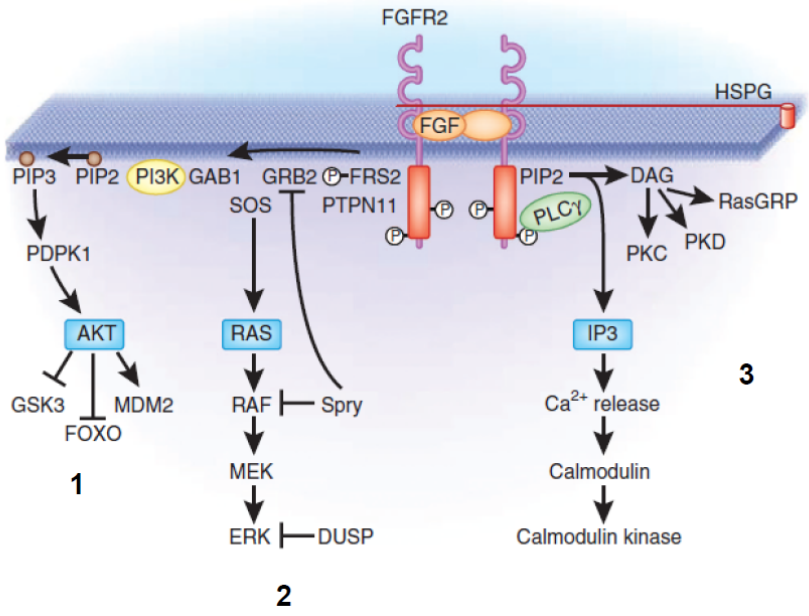

Fig. 5. FGFR2 signaling cascades. The main intracellular pathway triggered by FGFR2-FGFs interaction. FGFR2 transduces FGF signals to **1)** ERK, **2)** PI3K-Akt, **3)** Ca^{2+}, and diacylglycerol (DAG) signaling cascades. The FGF–ERK signaling cascade is mainly involved in cell proliferation. The FGF–PI3K signaling cascade is important for cell survival and polarity control. The regulator factor Sprouty inhibits the FGF–ERK signaling cascade acting on GRB2 and RAF, whereas DUSP (dual-specificity phosphatase) inhibits the FGF–ERK signaling cascade at ERK. The regulation of FGFR2 signaling passes by the balance of FGFs, heparan-sulfate proteoglycan (HSPG), FGFR2 isoforms, and endogenous inhibitors (adapted from (Katoh 2009)).

FGFs are not the only agonists able to activate FGFRs, for example FGFR1 signaling can also be triggered by cell adhesion molecules such as L1 or N-cadherin.

NCAM provides another example of cell adhesion molecule activating FGFRs through direct interaction (Kiselyov et al. 2005; Kochoyan et al. 2008). In 2003 Kielyov *et al*. for the first time reported that NCAM directly binds to FGFR1 and activates an intracellualr signalling that stimulates neurite outgrowth s (Kiselyov et al. 2005). Later Cavallaro's group reported that NCAM is a non-canonical ligand for FGFR1 and its binding to the receptor induces different cellular responses than the ones mediated by FGFs (Ditlevsen et al. 2008; Francavilla et al. 2009).

Whereas FGF induces degradation of the receptor, NCAM promotes its stabilization and recycling into the membrane, resulting in FGFR1 sustained activation. Moreover, in contrast to FGF, NCAM promotes cell migration inducing FGFR1 recycling and Src kinases activation (Francavilla et al. 2009). NCAM binding to FGFRs activates numerous signaling pathways including these requiring the activation of PKCβII (protein kinase CβII), PLCγ (phospholipase Cγ) and Src kinases, which ultimately lead to ERK kinases (extracellular signal-regulated kinases) phosphorylation (Fig. 6; (Cavallaro e Dejana 2011; Ditlevsen et al. 2008; Francavilla et al. 2009; Lin et al. 2009)).

NCAM binds and co-localize also with FGFR2 during early embryonal development.

However, the physiological role of this interaction on neuronal migration is still not resolved(Christensen et al. 2006; Vesterlund et al. 2011).

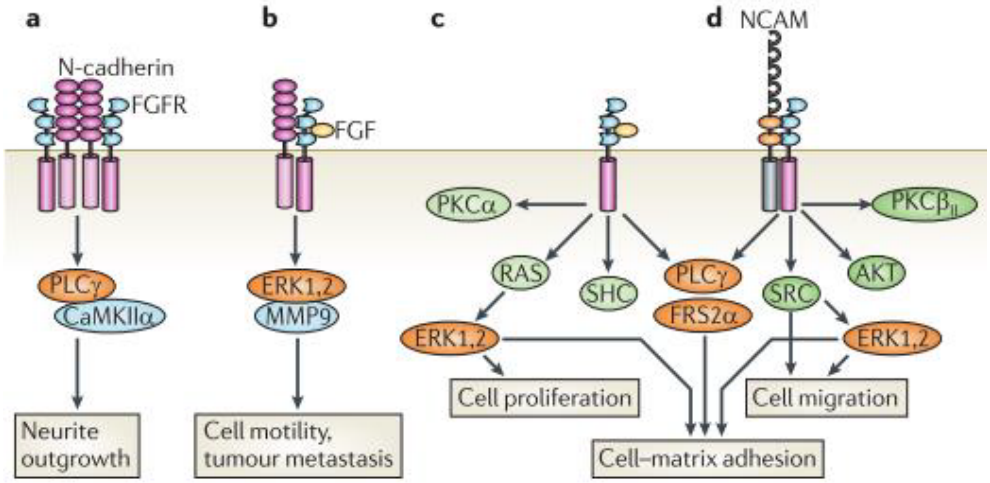

Fig. 6. FGFR signaling can be mediated by NCAM and N-cadherin. a) N-cadherin can bind to FGFR in ligand-independent manner and activate intracellular signaling pathway. N-cadherin-induced activation of PLCγ and calmodulin-dependent protein kinase IIα (CaMKIIα) stimulates neurite outgrowth. b) N-cadherin binding to FGFR causes a sustained activation of the receptor by FGF. This leads to the phosphorylation of ERK and matrix metalloprotease 9 (MMP9), which in turn promotes cell motility. c) and d) FGFR activation by FGF or NCAM triggers different signaling pathway . The interaction of FGFR with NCAM ultimately leads to cell migration *via* activation of proteins belonging to the Src family and subsequent phosphorylation of ERK kinases (adapted from (Cavallaro e Dejana 2011)).

1.6 Neuronal migration and CAMs

The correct positioning of newborn neurons in the cortex assures their proper identity and connectivity patterns (Evsyukova, Plestant, e Anton 2013). Pyramidal neurons and interneurons migrate remarkably long distances from their place of birth in telencephalon to their final position in the developing neocortex. There are two main types of migration in the cortex: pyramidal neurons radial migration and interneurons tangential migration. In 1972 Rakic revealed that pyramidal neurons align with the radial glial fibers during their migration (Rakic 1972).

This finding shed light on a possible role of radial glia in controlling the lamination of the cortex.

Newborn pyramidal neurons make their first step in radial migration by detaching from the neuroepithelium at the ventricular surface. Then, they move to the SVZ (Subventricular Zone) where they extend and retract their processes in all directions to adopt a multipolar morphology.

Then, they "wait" in the SVZ where they move tangentially in a random fashion for 24h. Subsequently, many critical signaling cues are activated and neurons acquire a polarized shape with a leading process (future dendrite) in the front of the cell and a trailing process (future axon) on the rear of the body. However, before acquiring a bipolar morphology many neurons will move retrogradly back to VZ (Ventricular Zone). Finally, when all neurons undergo multipolar-to-bipolar transition, they align with the radial glial fibers and begin their glial-driven locomotion through dense cellular environment toward the CP (Cortical Plate).

During this phase of migration, neurons repeat several important behaviors i) extension and retraction of the leading process; ii) formation of the membrane swellings in the leading process; iii) shift of centrosome into the swelling; iv) nucleokinesis – nucleus and soma movement to the front of the cell and v) trailing process retraction (Kriegstein e Noctor 2004; Nguyen e Hippenmeyer 2014) (Fig. 7).

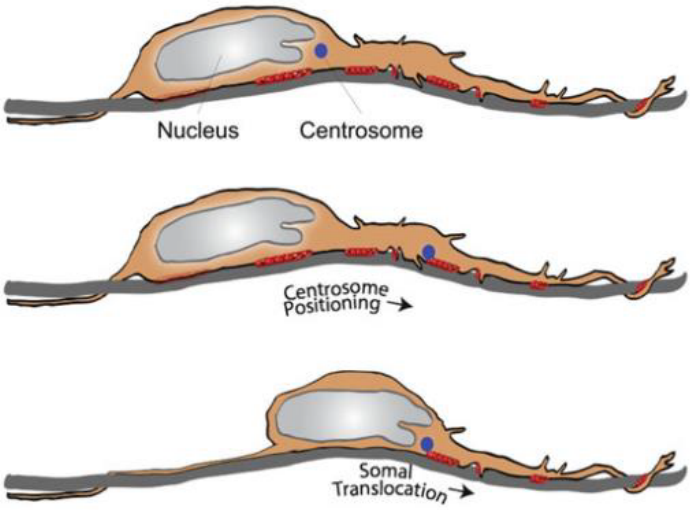

Fig. 7. Nucleokinesis of the migrating neuron. The centrosome is positioned into the neuronal leading process. Subsequently, the nucleus moves to the front of the cell (adapted from Cellular and Molecular Control of Neuronal Migration; Nguyen, Laurent, Hippenmeyer, Simon 2014).

When the neuron reaches the correct location within the cortex its leading process attaches to the MZ (Marginal Zone) and "pulls" up the soma and nucleus to the top of CP.

This process, called terminal somal translocation, helps the neuron to make final adjustments of its position within the specific layer where it will reach the complete maturation (Fig. 8; (Ayala, Shu, e Tsai 2007; Kriegstein e Noctor 2004; Nguyen e Hippenmeyer 2014)).

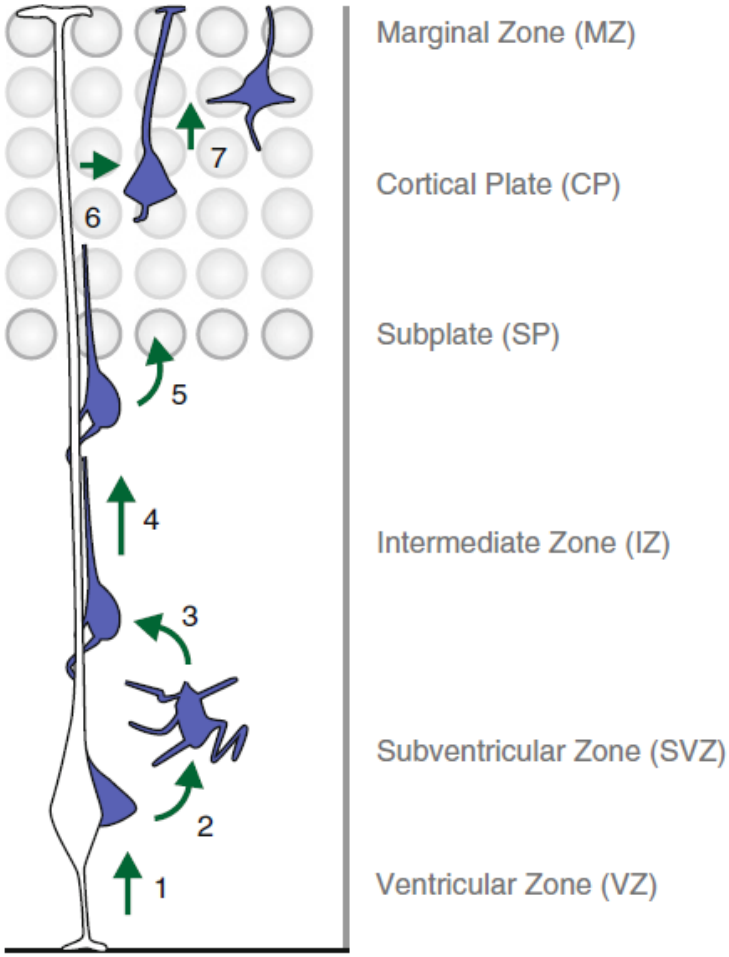

Fig. 8. Radial migration of pyramidal neurons. During the migration to their final position, neurons **1)** detach from neuroepithelium at the ventricular zone; 2) move to SVZ and acquire a multipolar morphology; **3)** undergo multipolar-to-bipolar morphology transition; acquire a polarized morphology with the leading process heading toward the pia surface and the trailing process heading toward VZ; **4)** continue its migration along radial glia fibers; **5)** reach the SP and enter the CP where **6)** detach from the radial glia and the leading process attaches to the MZ; **7)** undergo terminal somal translocation to reach its final position in the cortex (adapted from (Nguyen e Hippenmeyer 2014))

Cell adhesion molecules (CAMs) play a pivotal role in the contest of neuronal migration.

For example, NCAM has been described as a modulator of migration, axon growth, axon fasciculation and pathfinding (Bonfanti 2006). Accordingly, also FGFR signaling has a prominent role in the migration of a variety of cell types, including neurons (Hasegawa et al. 2004; Lin et al. 2009; Smith et al. 2006).

NCAM and FGFs are therefore involved in multiple feedback mechanisms through which neurons control the specification, migration, and differentiation of precursor cells in the cerebral cortex. Interestingly, recent data pointed out that FGFR2 may play a major role in this respect.

The selective deletion of FGFR2 in radial glial progenitor cells results in decreased cortical volume and decreased pyramidal cell number and density in the neocortex. Furthermore, the volume of subcortical white matter is dramatically reduced due to decreased number of axonal fibers in FGFR2 KO model (Vaccarino et al. 2009).

1.7 Cerebral Cortex Maldevelopment

Neuronal Migration Disorders (NMD) are caused by ectopic positioning and impaired differentiation of cortical grey matter (Copp e Harding 1999). NMD are a heterogeneous group of disorders with a range of clinical and pathological features. NMD are one of the most significant causes of neurological, developmental, intellectual disabilities and epileptic seizures (Copp e Harding 1999; Verrotti et al. 2010).

A wide range of diseases -including common disorders like schizophrenia, developmental epilepsy, autism spectrum disorder, bipolar disorder or mental retardation- are caused by mutations in specific genes involved in neuronal migration.

1.7.1 Autism Spectrum Disorders

Autism refers to an etiologically and clinically heterogeneous group of neurodevelopmental disorders which are replaced by one umbrella term "Autism Spectrum Disorder" (ASD).

The Diagnostic and Statistical Manual-Fourth Edition (DSM-IV), published by the American Psychiatric Association, includes under ASD: Autistic Disorder, Asperger's Disorder, and Pervasive Developmental Disorder Not Otherwise Specified (PDD-NOS) (Fig.9).

Fig. 9. ASD

Studies conducted in twins show that autism is a highly genetic disorder, with average concordance of 65% for identical twins and 9% for fraternal twins (Folstein e Rosen-Sheidley 2001; Miles 2011; Smalley, Asarnow, e Spence 1988).

Interestingly, there is almost 4:1 male to female gender ratio in ASD, with a prevalence of 0.6 (Banerjee, Riordan, e Bhat 2014; Veenstra-Vanderweele, Christian, e Cook 2004).

Patients with autism display three core symptoms: social behavior impairment, language impairment and repetitive and stereotyped behaviors. However, they may experience also comorbid symptoms like anxiety and depression, seizures, attention deficits, aggressive behavior, sleep disorders and sensory processing impairment (Spooren et al. 2012).

Interestingly, cell adhesion molecules (CAMs) have been largely implicated in ASD (Ye, Liu, e Wu

2010).

The best characterized synaptic CAM pathways implicated in ASDs are those involving neuroligins (NLGNs) and neurexins (Tabuchi et al. 2007; Glessner et al. 2009).

Recently, several independent genetic studies have strongly associated a poorly described adhesion molecule, Negr1, to ASD (Pinto et al. 2010; Pinto et al. 2010; Casey et al. 2012; Girirajan et al. 2012; Michaelson et al. 2012) (Table. 1).

Interestingly, alteration of Negr1 protein/gene expression has been described in other two neurological disorders characterized by marked connectivity dysfunctions, namely schizophrenia (Maccarrone et al. 2013) and dyslexia (Veerappa et al. 2013), suggesting that Negr1 plays pivotal role in functional CNS establishment.

Intriguingly, as demonstrated for Negr1, also FGFR2 has been recently associated to ASD (Hussman et al. 2011; Neale et al. 2012).

ASD candidates			
Gene symbol or Locus	**Cytoband**	**Type**	**Associated condition**
B3GALT6	1p36.33	gene	*de novo* deletion
CA6	1p36.2	gene	rare CNV
MTF1	1p34.3	gene	association
RIMS3	1p34.2	gene	*de novo* deletion
NEGR1	1p31.1	gene	translocation breakpoint
DPYD	1p21.3	gene	*de novo* deletion
GPR89A	1q21.1	gene	rare CNV
RFWD2	1q25.1-q25.2	gene	rare CNV
PAPPA2	1q25.2	gene	rare CNV
ASTN1	1q25.2	gene	paralogue of *ASTN2*
DISC1	1q42.1	gene	association
DPP10	2q14.1	gene	rare CNV, paralogue of *DPP6*
GALNT13	2q24.1	gene	rare CNV
SLC4A10	2q24.2	gene	*de novo* deletion
SCN7A	2q24.3	gene	rare CNV

Table. 1. ASD gene candidates. A translocation breakpoint has been found in NEGR1 gene in a family affected by ASD (adapted from (Pinto et al. 2010).

2. OBJECTIVE OF THE THESIS

In our previous work ((Pischedda et al. 2014); appendix I) by combining d LC-MS/MS, biochemistry and morphological analysis to study synaptic proteins, we discovered that Negr1 is highly enriched in synaptosomes and that its expression increases with neuronal maturation.

Next, we demonstrated that Negr1 silencing induced a significant decrease in the number and length of neuronal processes in mature neurons, thus causing a severe reduction of the overall complexity of neurite arborization *in vitro* and *in vivo*.

Strikingly, it has been recently demonstrated that IgLONs family members, including Negr1 can be shed from the surface of cortical neurons through a metalloproteases dependent proteolysis (Sanz et al., 2015).

We thus hypothised a triple effect for Negr1: I) the cis effect, in which the protein exerts its activity in the cell expressing the protein; II) the soluble effect, in i.e Negr1 acts as a released factor upon shedding; III) the trans effect, in which Negr1 exposed on neuronal membrane interacts with proteins present on the juxtaposed cells.

Since Negr1 is a synaptic protein involved in neuronal maturation the objective of this thesis was to investigate its role in the development of a mature and functional cortical network.

3. RESULTS

3.1 Negr1 in morphology

3.1.1 Negr1 modulates neuritic tree acting *in cis* and *in trans*

Recent evidence suggested that IgLONs members, including Negr1, are released into neuronal media via metalloproteinase and that metalloproteinase activity on IgLONs has an impact on neuronal maturation (Sanz, Ferraro, e Fournier 2015). We have previously showed that Negr1 influences neuritic tree development (Pischedda et al. 2014). At the light of all these findings, Negr1 may influence neuronal morphology acting *in cis* as membrane bound protein and/or *in trans* as a soluble protein. To investigate these two scenarios, we infected cortical neurons at DIV4 with viruses expressing GFP marker together with either Negr1 specific siRNA (siNegr1) or scramble control (siControl) following two experimental paradigms: 1) cultures infected with a high viral titer (MOI= 3); 2) cultures infected with a low viral titer (MOI=0.3). In both cases, cultures were processed for subsequent investigation at DIV18. Biochemical and imaging analysis showed that the titer of infection was directly correlated to the extent of Negr1 protein reduction and to infection efficiency (Fig. 10A-C). Next we studied the morphology of GFP positive neurons in the two different conditions. Interestingly we reported that cultures exposed to high viral titer show a more pronounced reduction in terms of neurite number and length than cultures exposed to low viral titer (Fig. 10D-E). Given that the two experimental settings were distinguished by the number of down regulated neurons in the culture rather than the efficiency of Negr1 silencing at the single cell level, such outcome may suggest that the overall amount of Negr1 (membrane bound and released) influences neuronal morphology.

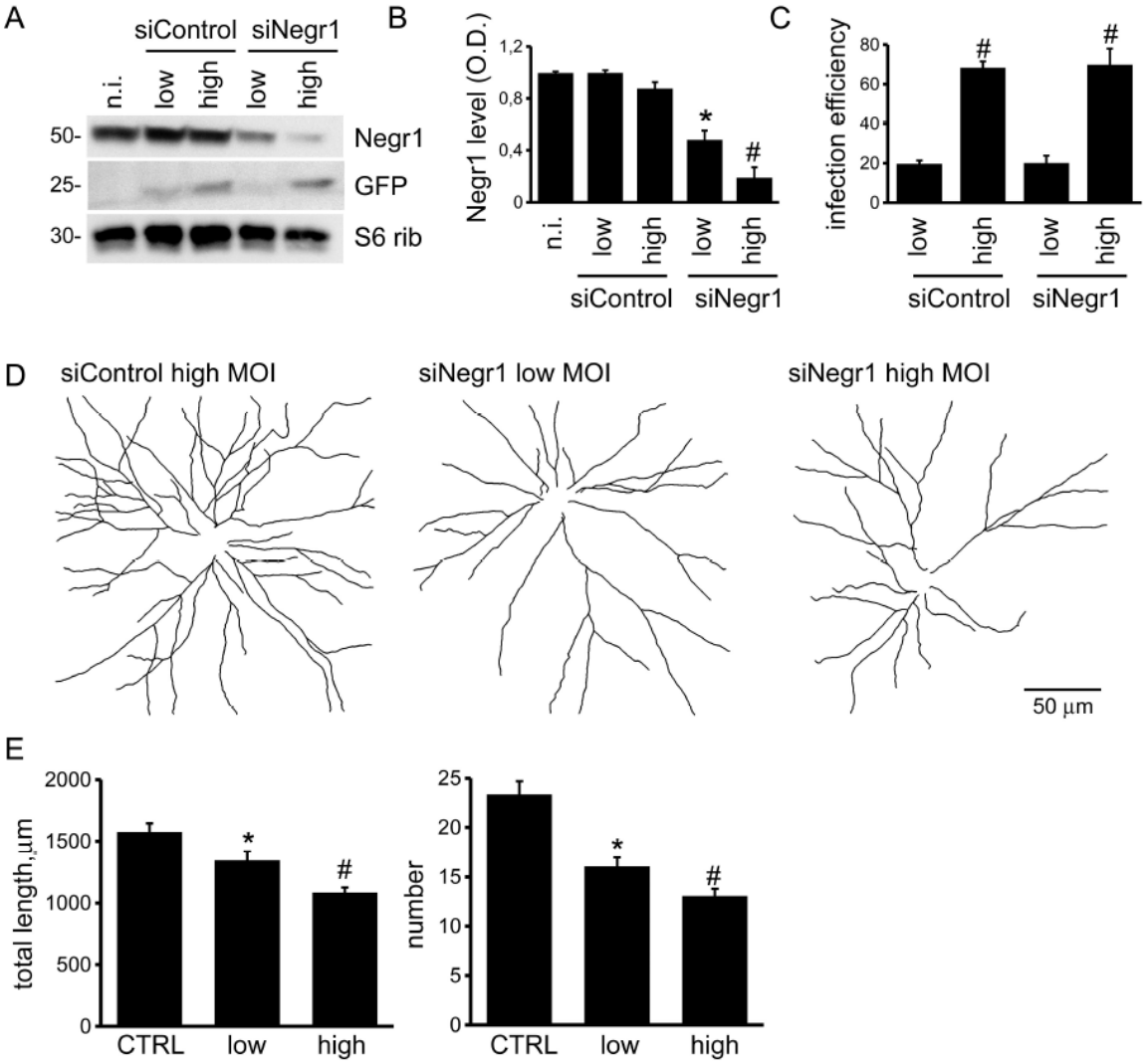

Fig 10. Negr1 influences neuritic tree. Cortical neurons were infected at DIV4 with low (MOI= 0.3) or high (MOI=3) titer of viruses expressing GFP and scramble siRNA (siControl) or siRNA against Negr1 (siNegr1). Cells were solubilized and then assayed for western-blotting at DIV18 (A). The graph reports the optical density of the band relative to Negr1 protein, normalized versus S6 ribosomial protein (S6 rib) value. Data are expressed as mean ± SEM, n=4. * $p<0.05$ vs not infected (n.i.), # $p<0.05$ vs low infection (B). Infection with low or high viral titer resulted in different infection efficiency, evaluated as fraction of GFP positive cells within the entire population, stained with DAPI. Data are expressed as mean ± SEM; * $p<0.05$ vs siControl (CTRL), # $p<0.05$ vs low infection. Scale bar= 50 um

3.1.2 Negr1 shedding by ADAM10 modulates neuritic tree

To confirm the biological relevance of Negr1 as soluble factor, we investigated in detail the presence of Negr1, NCAM and S6 ribosomial protein, a well established cytoplasmic marker, in samples prepared from neuronal culture at DIV18 or from the relative conditioned media.

As expected, we detected the three protein in the cellular lysate, but only Negr1 and NCAM in the media. It is well established that NCAM can be released in media by shedding via ADAM10 (Brennaman, Moss, e Maness 2014). Interestingly, when we treated neurons from DIV10 to DIV18 with the well established ADAM10 inhibitor, GI 254023X (20mM, every second day), we noticed a robust reduction of the fraction of NCAM and Negr1 protein released in the media (Fig. 11A-C).

These experiments suggest that Negr1 can be shed from neuronal membrane by ADAM10.

Sanz and colleagues showed that metalloproteinase inhibitors severely impaired proper neuronal morphological development in a IgLON dependent manner (Sanz, Ferraro, e Fournier 2015).

Consequently, we studied the morphological phenotype in cortical cultures treated with DMSO or with ADAM inhibitor GI 254023X (20mM, every second day) from DIV10 to 18.

Noteworthy, we noticed that ADAM chronic inhibition affected neuritic outgrowth (Fig. 11 D-E). ADAM10 shed several membrane proteins involved in neurite outgrowth, including NCAM, N-Cadherin and L1-NCAM (Brennaman, Moss, e Maness 2014; Jorissen et al. 2010; Mechtersheimer et al. 2001; Paudel et al. 2013). Thus we assessed the direct contribution of soluble Negr1 to the regulation of neuron morphology executed by ADAM10. To this aim we purified on streptavidin resin 2XStrep-FLAG Negr1 (rNegr1) from transfected HEK293 cell.

Protein purity was assessed by silver-staining (Fig. 11F). Negr1 is highly and specifically glycosylated in vivo (Miyata et al. 2003).

Upon western-blotting, we detected rNegr1 as a band with an apparent molecular weight (MW) of 50 KDa, corresponding to the glycosylated form of Negr1. Upon incubation with the N-linked

deglycosilase PNGase, we detected instead a band at apparent MW 38 KDa, corresponding to the predicted MW, as annotated in Expasy database (entry: Q80Z24) (Fig. 11G).

Thus, expression of rNegr1 resulted in a protein that resembled the feature of endogenous Negr1. Purified rNegr1 was administered to either DMSO or ADAM10 inhibitor treated cortical neuron at DIV10 at concentration of 40 ng/ml. Cells were fixed at DIV18 and processed for immunofluorescence. Interestingly, we observed that rNegr1 treatment was able to rescue the morphological phenotype due to ADAM10 inhibition. Furthermore rNegr1 treatment was associated to an increase of neurite number and length in DMSO treated neuron (Fig. 11D-E). All together these data suggest that soluble Negr1 released by ADAM10 positively modulates neuronal morphology.

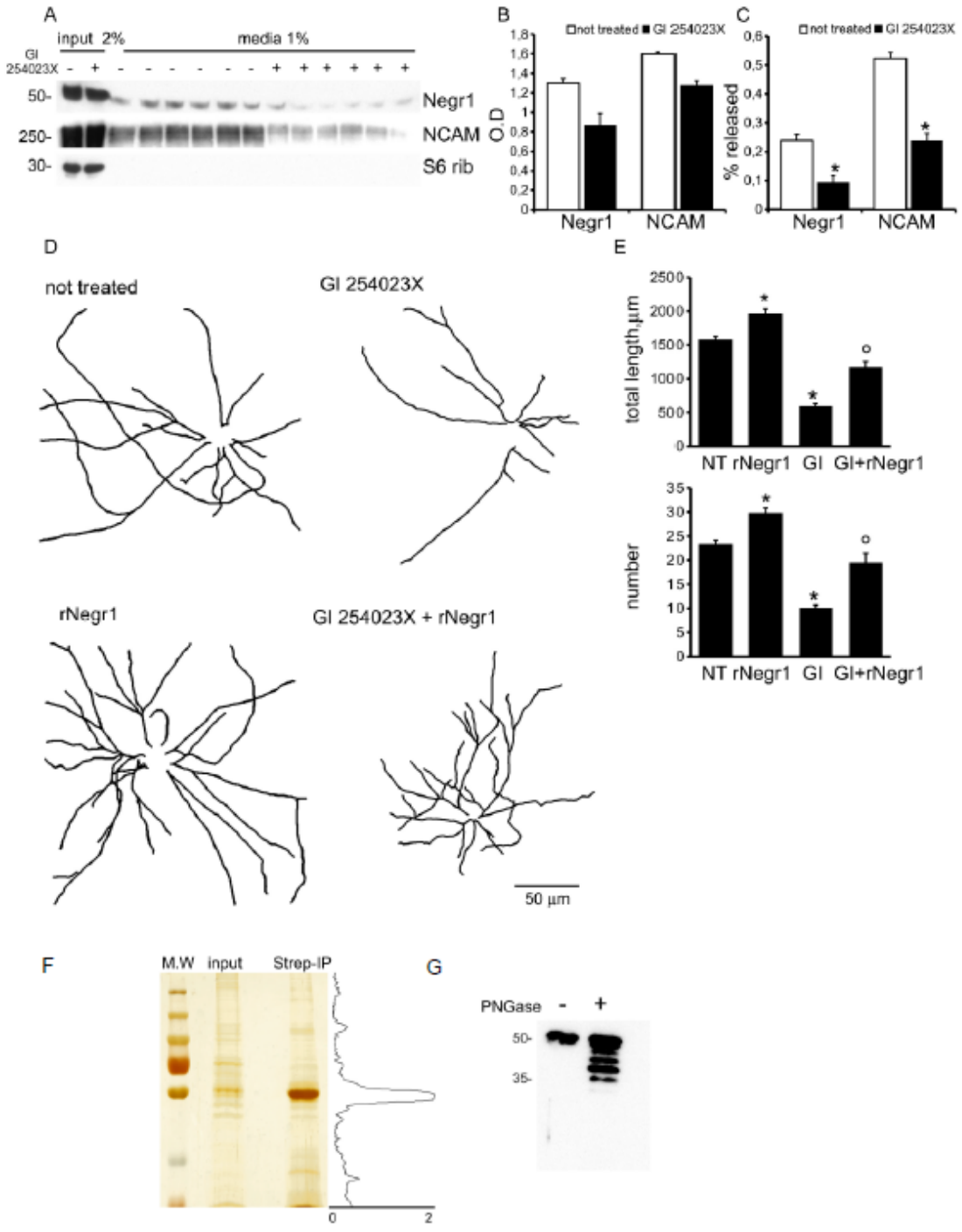

Fig. 11. ADAM10 activity modulates neuritic tree. Cortical neurons were infected at DIV4 with siControl and then treated every second day with DMSO (20 mM, not treated) or with ADAM10 inhibitor GI 254023X (20 mM) from DIV10 to DIV18. Cells and relative conditioned media were assayed for western-

blotting to measure NCAM, Negr1 and S6 ribosomial protein level (A). Graphs show NCAM, Negr1level in the cellular lysate expressed as optical density, normalized versus and S6 ribosomial protein (S6 rib) value (B) and the extent of Negr1 and NCAM release in media expressed as percentage of the relative amount measured in cellular lysate (C). Data are reported as mean ± SEM; n= 6, * $p<0.05$ vs not treated. Cortical neurons were infected with siControl virus at DIV4 and treated every second day from DIV10 to DIV18 with DMSO (not treated, NT) or with ADAM10 inhibitor GI 254023X (20 mM, GI) and/or recombinant Negr1 (40 ng/ml, single administration at DIV 10, rNegr1). Neurons were processed for immunofluorescence at DIV18 and GFP positive neurons imaged via confocal microscopy. Panels show camera lucida tracing (D). Graphs show neurite total length and number (E). Data are reported as mean ± SEM; * $p<0.001$ vs not treated (NT); ° p 0.001 vs GI 254023X (GI). Scale bar= 50 um . Protein purity and glicosylation assessed by silver-staining (F) and western blotting (G).

3.1.3 Negr1 impact on neuritic outgrowth requires ERK1/2 phosphorylation

ERK1/2 pathway had been recognized as a key player in neurite outgrowth (Maness e Schachner 2007). Thus we wondered if soluble Negr1 might influence neuronal morphology via ERK1/2 signalling. To this aim, we administered MEK inhibitor U0126 from DIV10 to DIV 18 (100 nM, daily) to rNegr1 or control treated neurons.

As expected, MEK inhibition significantly impaired neuron morphology. Noteworthy, Negr1 treatment was not able to rescue the morphological effect due to MEK inhibitors, neither in term of total process length or number (Fig. 12A-B). All together these data suggest that Negr1 influence neuritic tree outgrowth activating a pathway that requires proper ERK1/2 phosphorylation.

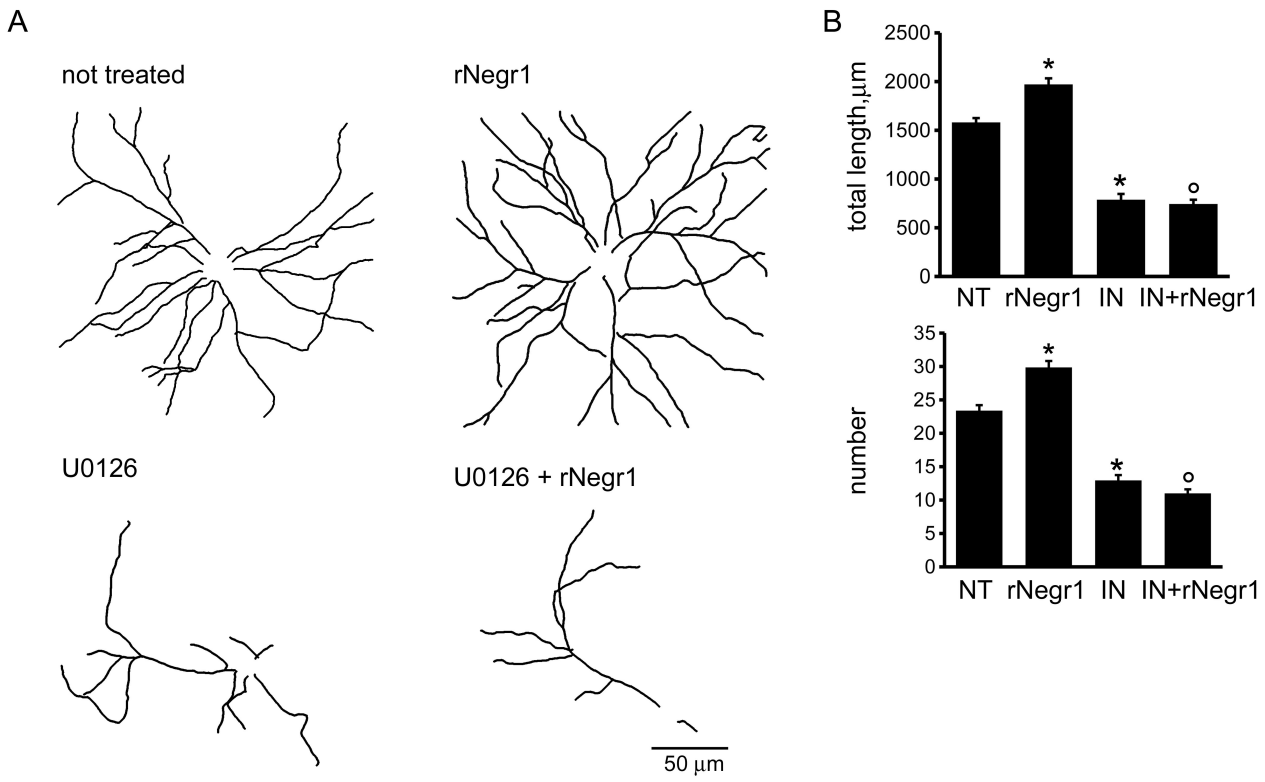

Fig. 12. MEK inhibition abolishes morphological effect of Negr1. Cortical neurons were infected with siControl virus at DIV4 and treated every second day from DIV10 to DIV18 with DMSO or with MEK

inhibitor U0126 (100 nM, IN) and/or recombinant Negr1 (40 ng/ml, single administration at DIV 10, rNegr1). Neurons were processed for immunofluorescence at DIV18 and infected GFP positive neurons imaged via confocal microscopy. Panels show camera lucida tracing (A). Graphs show neurite total length and number (B). Data are reported as mean ± SEM; * $p<0.001$ vs not treated (NT), ° $p<0.001$ vs rNegr1. Scale bar= 50 um

The role of Negr1 in neurite guidance has been already characterized (Schäfer et al. 2005).
Therefore, we investigated further the functional correlation among ERK1/2, Negr1 and neurite outgrowth. First we checked whether rNegr1 was correctly shuffled to the plasma membrane in a heterologous cellular system. Thus, we co-transfected HEK293 cells with strep-FLAG Negr1 and GFP, fixed and stained them with rat anti-FLAG antibody in non-permeabilizing condition followed by incubation with rabbit anti-FLAG in permeabilizing conditions. Laser microscopy demonstrated that rNegr1 is expressed at the extracellular membrane (Fig. 13).

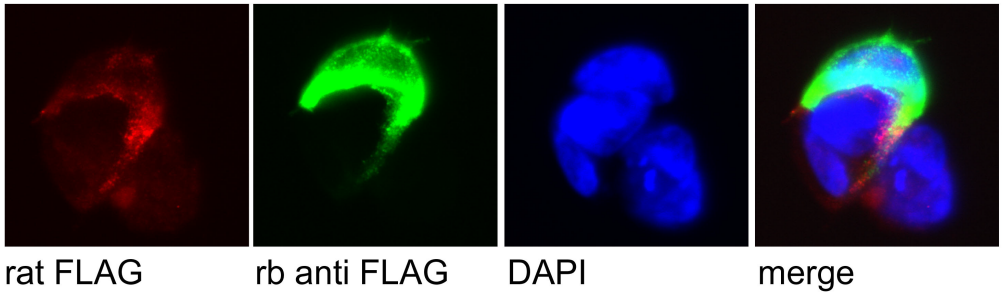

Fig. 13. rNegr1 localization. We tested rNegr1 expression combining both non-permeabilizing (rat anti-FLAG) and permibilizing (rabbit anti-FLAG) staining. Negr1 is expressed at the extracellular membrane.

Thus, we seeded on DIV1 cortical neurons HEK293 cells expressing GFP or an unrelated transmembrane protein fused to GFP, GFP-Rhodopsin, or rNegr1. Mixed cultures of neurons and HEK293T cells were fixed at DIV5 and processed for immunocitochemistry with an antibody specific for neuronal-process, β-tubulin-III (Fig. 14 A). In order to statistically estimate the effect of

rNegr1 heterologous expression, we quantify the number and the length of the β-tubulin-III processes those approached and passes above transfected HEK293 cells in the different experimental conditions. We found that β-tubulin-III positive neurites stopped upon contact with rNegr1-expressing HEK293T cells, whereas they were able to pass above control cells, despite an overall similar length (Fig. 14B-C).

To demonstrate the functional correlation between rNegr1 expression on HEK293 cells and neurites phenotype, we treated living mixed culture with rat anti-FLAG antibody (AB) during the co-culturing period. The idea behind this strategy is that once bound to the FLAG epitope fused to Negr1, anti-FLAG antibody may mask rNegr1 protein via steric hindrance.

Interestingly, in presence of the anti-FLAG antibody, we experienced that neurites recover the capability to pass above rNegr1 expressing HEK293 cells. No effect was observed upon incubation with rat IgG (data not shown). Eventually, we treated neuron-HEK293 co-cultures with MEK inhibitor UO126 (100 nM) from DIV1 to DIV4. In presence of MEK inhibitor, we noticed a partial rescue of the number of processes able to cross Negr1 expressing cells. All together these data suggest that Negr1 influence neuritic tree outgrowth activating upon the physical interaction of two juxtaposed membrane a pathway that requires proper ERK1/2 phosphorylation.

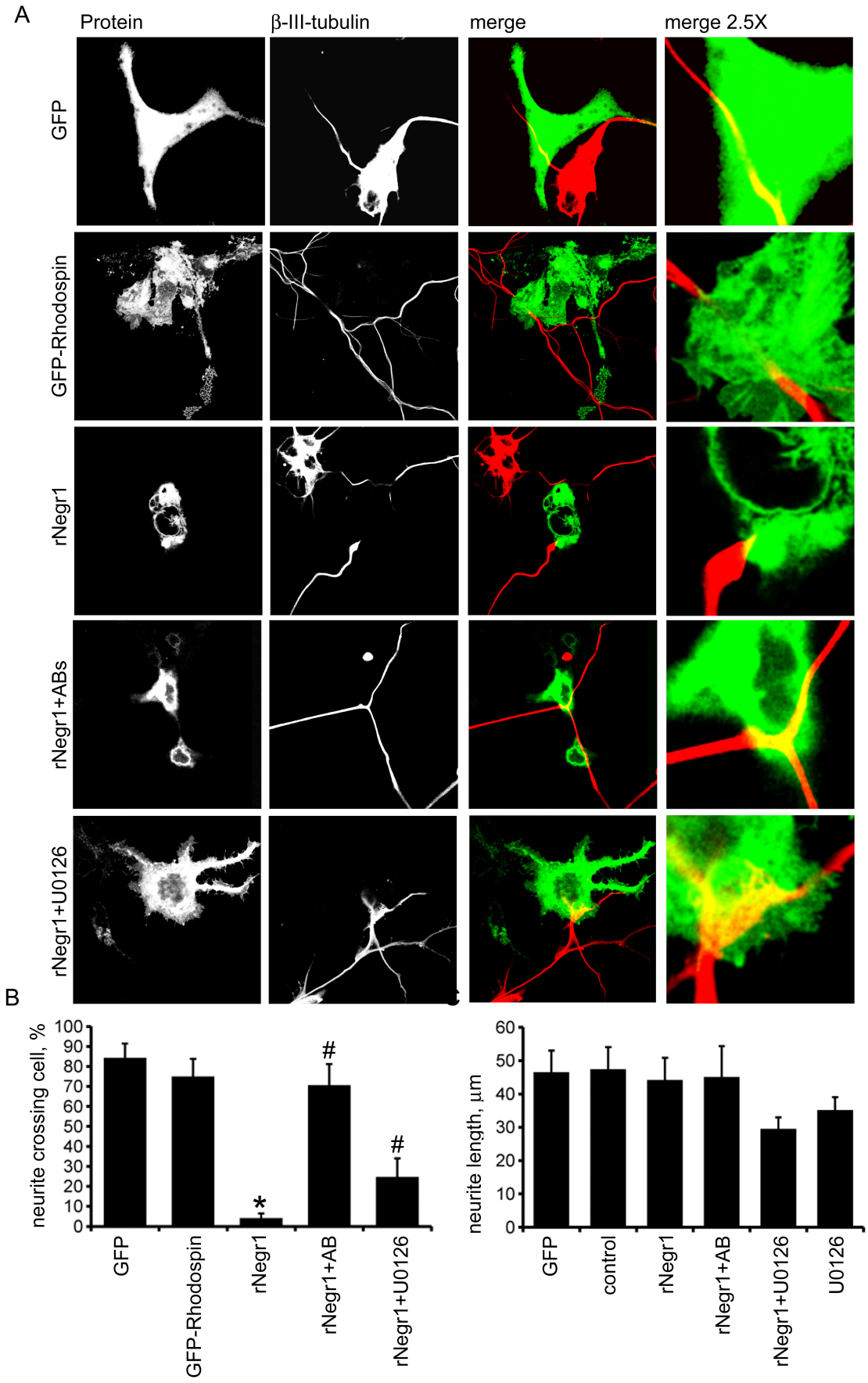
A
Protein
β-III-tubulin
merge
merge 2.5X
GFP
GFP-Rhodospin
rNegr1
rNegr1+ABs
rNegr1+U0126
B
neurite crossing cell, %
100
90
80
70
60
50
40
30
20
10
0
*
#
#
GFP
GFP-Rhodospin
rNegr1
rNegr1+AB
rNegr1+U0126
neurite length, µm
60
50
40
30
20
10
0
GFP
control
rNegr1
rNegr1+AB
rNegr1+U0126
U0126

Fig 14. Negr1 controls neurite guidance *via* MAPK. Cortical neurons were co-cultured at DIV1 with HEK293 cells transfected with GFP, GFP-Rhodopsin or rNegr1. The cultures were fixed at DIV4 and stained with antibodies against FLAG (green) and β-III-tubulin (red). Merge and higher magnification (merge 2.5X) are shown. Scale bar= 25 mm (A). Where indicated, co-cultures were treated with anti-FLAG antibodies (ABs; 10mg/ml) or MEK inhibitor U0126 (100 nM) for 48 hours before fixation. The graphs report the number of β-III-tubulin positive processes able to pass above HEK293 cells transfected as indicated (B) and the average length of neurites (C). Data are reported as mean ± S.E; n= 24, * $p<0.05$ vs control, # $p<0.05$ vs rNegr1.

3.1.4 Negr1 induces the formation of gap-junction.

It is now clear that neuron communicate also through the formation of inter-cellular channels (Cheung, Chever, e Rouach 2014). Inter-cellular connections such as connexin-43 gap junctions allow direct electrical and metabolic communication between two adjacent cells; they are therefore vital to many physiological processes. Besides connexins, other gap junction forming proteins have been recently characterized, the pannexin proteins (Penuela et al. 2014). Although still debated, it has been shown that pannexin 1 and 3 can form functional large pore gap junctions (Sahu, Sukumaran, e Bera 2014). Studies examining the distribution and functional role of connexins and pannexins indicate that they may allow cell-to-cell coupling among neurons, astrocytes and microglia. The process instructing the formation of inter-cellular channels is far from understood. Strickingly we discovered that Negr1 is sufficient to instruct the formation of gap-junction between neuronal and not neuronal cells. Our experimental strategy implied the co-culture among primary neurons and not neuronal HEK293 cells expressing td-Tomato and Negr1 or only td-Tomato.

Co-cultures were left running for two days, then fixed and analysed by confocal-microscopy. Interestingly, we found that neurons in contact with HEK293 over-expressing td-Tomato and Negr1 became td-Tomato positive. Instead in the co-culture including neurons and HEK293 expressing just the fluorescent reporter, td-Tomato remained confined only in HEK293 cells (Fig. 15).

Furthermore, when we treated cortical cultures with conditioned media obtained from td-Tomato and Negr1 expressing HEK293 cells, we did not observe td-Tomato positive neurons. Thus we may exclude the involvement of vesicle-driven DNA/protein transfer. Instead we deem that this phenomenon, known as dye coupling, may reflect the formation of physical junction between two adjacent cells.

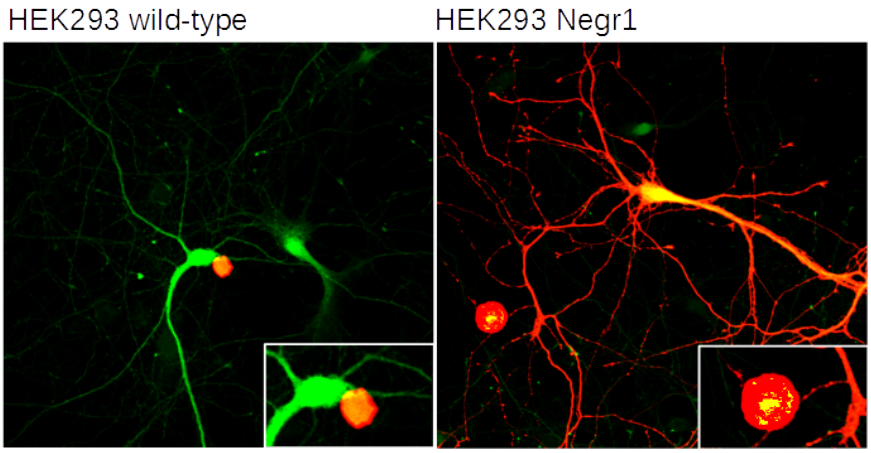

Fig. 15. Negr1 is sufficient to instruct the formation of intercellular channels. Cortical neurons were infected with GFP (green) expressing viruses at DIV4 and then co-coltured from DIV10 to DIV12 in presence of HEK cells expressing Td-Tomato (red) and either empty vector (left) or Negr1 construct (right). Inserts show HEK-neuron contact point at higher magnification. We observed a transfer of Td-Tomato from Negr1 expressing HEK cells to neurons.

3.1.5 Soluble Negr1 influences neuron morphology acting via FGFR2

Biochemical studies showed that IgLON protein can form stable homodimers (Miyata et al. 2003). Thus we wondered whether soluble rNegr1 may execute its function via binding with endogenous Negr1 expressed on neuronal membrane. To this aim we investigated the impact of soluble rNegr1 on cortical culture down-regulated for endogenous Negr1 expression.

Cortical neurons were infected at DIV4 with viruses expressing GFP together with Negr1 specific siRNA (siNegr1) or scramble siRNA (siControl) and treated at DIV10 with soluble rNegr1. As already observed, the abolishment of endogenous Negr1 expression correlated with a reduction of neuritic tree complexity (Pischedda et al. 2014). Interestingly, rNegr1 treatment was able to fully

rescue the morphological phenotype due to Negr1 silencing (Fig. 16). This evidence suggests that the formation of Negr1 homodimer is not instrumental for the morphological effect associated to the treatment with soluble Negr1.

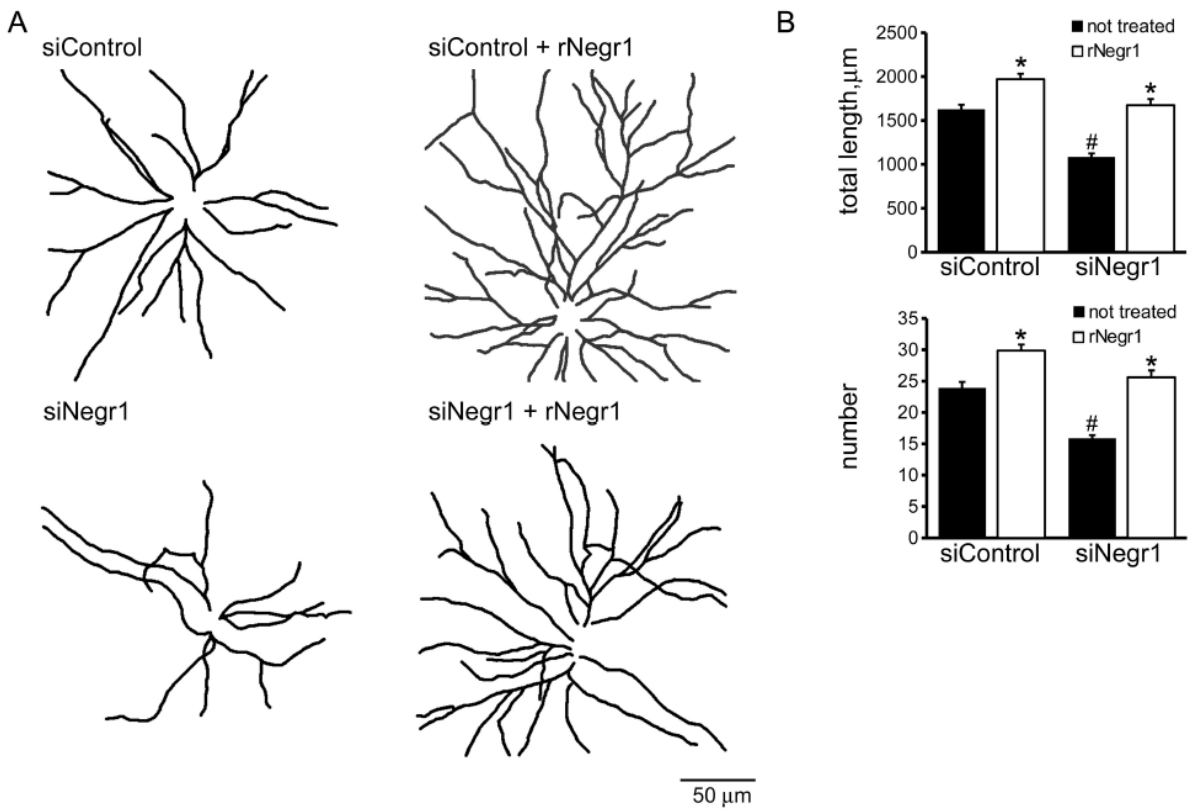

Fig. 16. Homodimerization is not essential to execute rNegr1 morphological effect. Cortical neurons were infected with siControl or siNegr1 virus at DIV4 and treated with recombinant Negr1 (40 ng/ml, single administration at DIV 10, rNegr1). Neurons were processed for immunofluorescence at DIV18 and infected GFP positive neurons imaged via confocal microscopy. Panels show camera lucida tracing (A). Graphs show neurite total length and number (B). Data are reported as mean ± SEM; * $p<0.001$ vs not treated, same infection, # $p<0.001$ vs siControl, same treatment. Scale bar= 50 um

Soluble Negr1 may associate with other protein to influence neurite outgrowth. It has been demonstrated that IgLON members are able to influence tyrosine kinase associate receptor (RTK) (McKie et al. 2012). Furthermore, it is well established that RTK can influence via ERK1/2 pathway neuronal morphology (Hausott et al. 2009). Consequently, we screened a battery of RTK agonists for their ability to rescue the phenotype associated to Negr1 silencing.

Cortical neurons were treated from DIV10 to 18 with IGF (5 ng/ml), FGFb (20 ng/ml) and FGF7

(20 ng/ml). Interestingly, we noticed a complete rescue of the morphological phenotype due to Negr1 silencing only upon chronic treatment with FGF7, a specific FGFR2 agonist.

Similarly, when we administered RTK agonist to control infected cells, only FGF7 treatment was associated to a significant increase in neuritic tree complexity (Fig. 17).

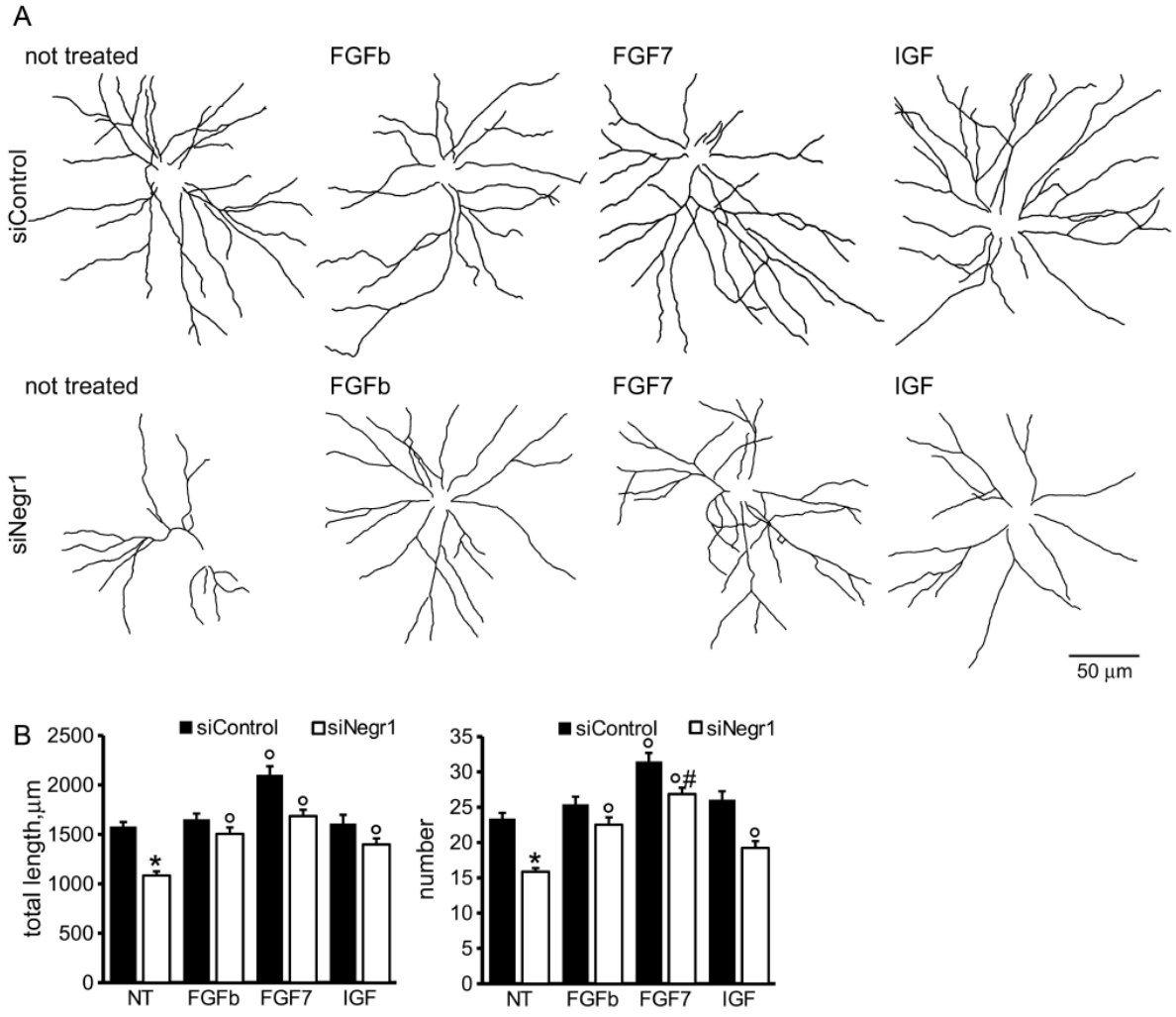

Fig. 17. FGFR2 activation ameliorates morphological effect due to Negr1 down-regulation.

Cortical neurons were infected with siControl or siNegr1 virus at DIV4 and treated daily from DIV10 to DIV18 with IGF (5 ng/ml), FGFb (20 ng/ml) and FGF7 (20 ng/ml). Neurons were processed for immunofluorescence at DIV18 and infected GFP positive neurons imaged via confocal microscopy. Panels show camera lucida tracing (A). Graphs show neurite total length and number (B). Data are reported as mean ± SEM; * $p<0.001$ vs siControl, same treatment, ° $p<0.001$ vs not treated, same infection (NT), # $p<0.01$ vs FGFb, same infection. Scale bar= 50 um

To further appreciate the functional correlation among Negr1, FGFR2 and neurite outgrowth, we studied neuron morphology upon acute FGFR2 silencing. To this aim, we took advantage of a selective silencing construct targeting FGFR2 mRNA sequence (Zhou et al. 2006).

Cortical neurons were infected at DIV4 with siFGFR2 or control virus, treated or not with soluble rNegr1 at DIV10 and imaged at DIV18. We noticed that FGFR2 silencing was associated to a robust reduction of neuritic tree complexity. Furthermore we did not observe any increase in neurite number or total length upon rNegr1 treatment in siFGFRF2 neurons (Fig. 18 A-B). Dendritic spines constitute the main postsynaptic elements of excitatory synapses (Tada e Sheng 2006). Previous reports, including our own, indicated that Negr1 modulated dendritic spine number (Hashimoto, Maekawa, e Miyata 2009; Pischedda et al. 2014). Thus we imaged dendritic protrusions treated or not with soluble rNegr1. The quantification of spine number and morphology indicated that rNegr1 treatment correlates with an increase in total spine number.

To investigate the potential involvement of FGFR2 on this effect, we treated or not with rNegr1 neuronal cultures down-regulated for FGFR2 expression. Interestingly we noticed that FGFR2 silencing did not have an impact on spine number in control treated cultures but abolished the positive effect reported upon Negr1 treatment (Fig. 18 C-D). Eventually, we investigated whether Negr1 may activate FGFR2 dependent intracellular pathway.

To this aim, wild-type and siFGFR2 infected neurons were treated with rNegr1 (40 ng/ml, 10 minutes) and processed for western blotting to assess the activation of ERK1/2 pathway. Interestingly, we noticed that acute Negr1 treatment induced ERK1/2 phosphorylation in wild-type neurons but not in siFGFR2 cells (Fig. 18 E-F).

All together these findings suggest that soluble Negr1 influences neuron morphology in a FGFR2 dependent manner.

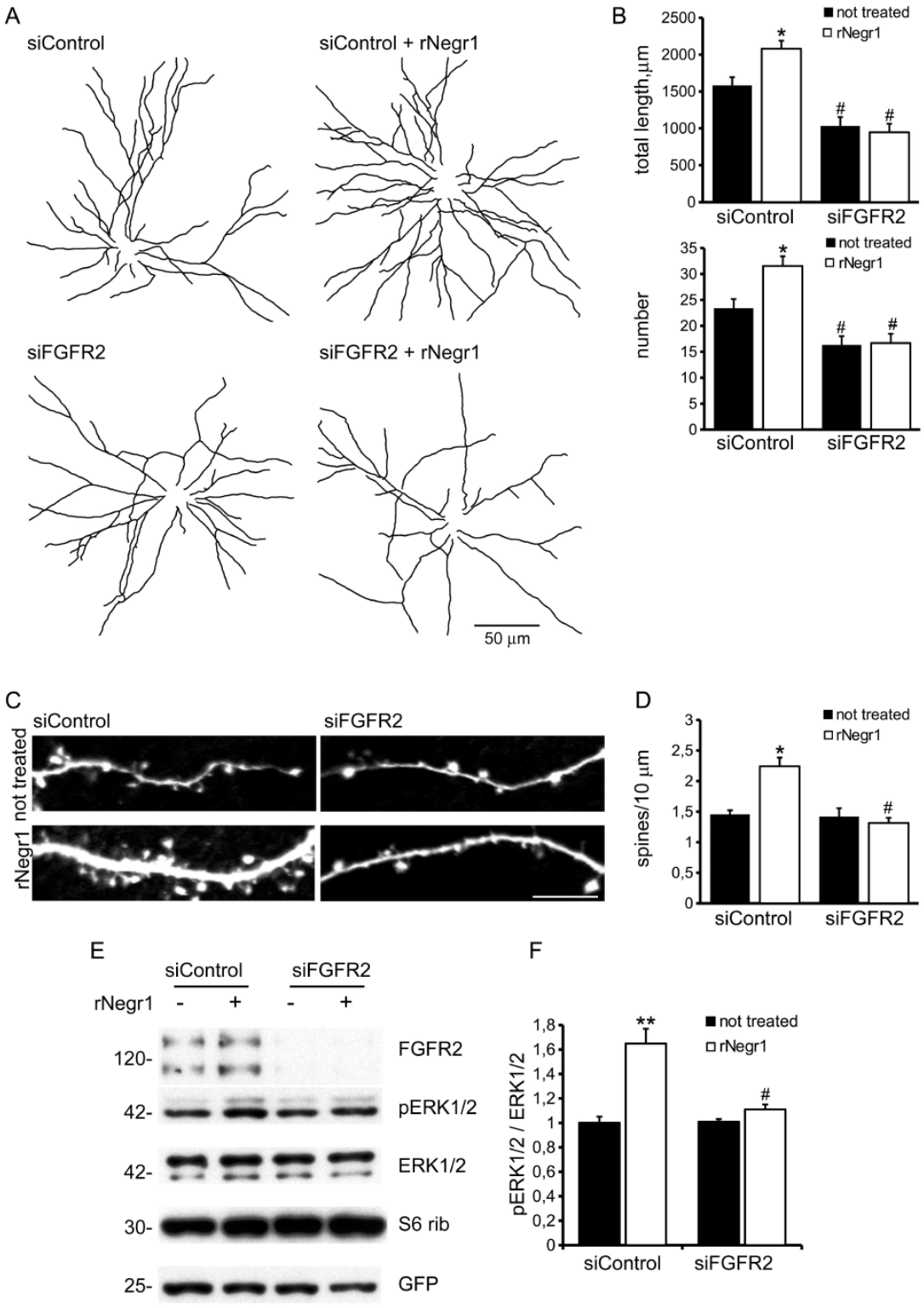

Fig. 18. Negr1 modulates neuron morphology via FGFR2. Cortical neurons were infected at DIV4

with virus expressing siControl or siRNA against FGFR2 (siFGR2) and treated at DIV10 with recombinant Negr1 (40 ng/ml, rNegr1). Neurons were processed for immunofluorescence at DIV18 and infected GFP positive neurons imaged via confocal microscopy. Panels show camera lucida tracing (A). Graphs show neurite total length and number (B). Data are reported as mean ± SEM; * $p<0.001$ vs not treated, same infection, # $p<0.01$ vs siControl, same treatment. Scale bar= 50 um. Dendritic spines were recognized as mushroom like protrusions decorating the neurites (C). Spine density was calculated as protrusion number along 10 mm of neuritic length. Data are reported as mean ± SEM; * $p<0.001$ vs not treated, same infection, # $p<0.01$ vs siControl, same treatment. Scale bar= 10 (D). Cortical neurons were infected with virus expressing siControl or siRNA against FGFR2 (siFGR2) and treated with recombinant Negr1 (40 ng/ml, rNegr1 30 minutes). Neurons were processed for western-blotting to investigate ERK1/2 phosphorylation (E). The graph reports p-ERK1/2 level normalized versus total ERK1/2 amount (F). Data are expressed as mean ± SEM n=5. ** $p<0.01$ vs not treated, same infection; # $p<0.05$ vs siControl, same treatment.

3.2.2 Negr1 forms hetero complex with FGFR2

The functional interaction between soluble Negr1 and FGFR2 suggested the existence of Negr1-FGFR2 heterocomplex.

Since that is known from literature that IgLON family protein are able to form homo-hetero complex (O D Gil et al. 1998; Orlando D Gil et al. 2002; Schäfer et al. 2005) first we assessed the capability of Negr1 to form homo-dimers. Thus we assayed wild-type and FLAG-Negr1 stable cells N2A for their propensity to aggregate *in vitro*, being cellular cluster formation a read-out of protein interaction. Cells were dissociated and collected in a buffer not permissive for cell-to-cell aggregation and then incubated in adhesion permissive condition.

We noticed that Negr1 expressing cells formed multi-cellular aggregates when compared with wild-type counterpart (Fig 19A), suggesting that Negr1 forms homo-dimer *in trans*.

Negr1 belongs to the group of cell adhesion molecules, which are localized to the membrane raft via glycosylphosphatidylinositol (GPI) anchor and lack transmembrane and intracellular domains.

Thus, Negr1 possibly requires interactions with other receptors to exert its biological functions. Other IgLON family members interact physically and functionally with receptors associated to tyrosine kinase activity (McKie et al. 2012).

Thus, we screened Negr1 and control cell via FLAG immuno-precipitation upon chemical cross-linking by western-blotting. We found that Negr1 binds FGFR2, but not with FGFR1 (Fig. 19B). These results were supported by immunoprecipitation of endogenous Negr1 protein carried on adult brain lysate (Fig. 19C). To further verify Negr1 and FGFR2 interaction we took advantage of the overlay assay, that investigates the interaction of protein left in native condition.

Thus we incubated living wild-type and FGFR2 over-expressing cells with purified recombinant FLAG-Negr1 protein. After incubation, we processed the cells for imaging purposes with anti-FLAG antibody. We detected FLAG signal only in FGFR2-overexpressing culture (Fig. 19D, panels I-III vs panels IV-VI).

FGFb induces FGFRs internalization (Francavilla et al. 2009).

Interestingly, upon FGFb treatment, we identified FLAG-positive aggregates in the perinuclear region (Fig. 19D, panels VII-IX). This evidence indicates that Negr1 internalizes together with FGFR2. All together these data suggest that Negr1 interacts with FGFR2 (Fig. 19).

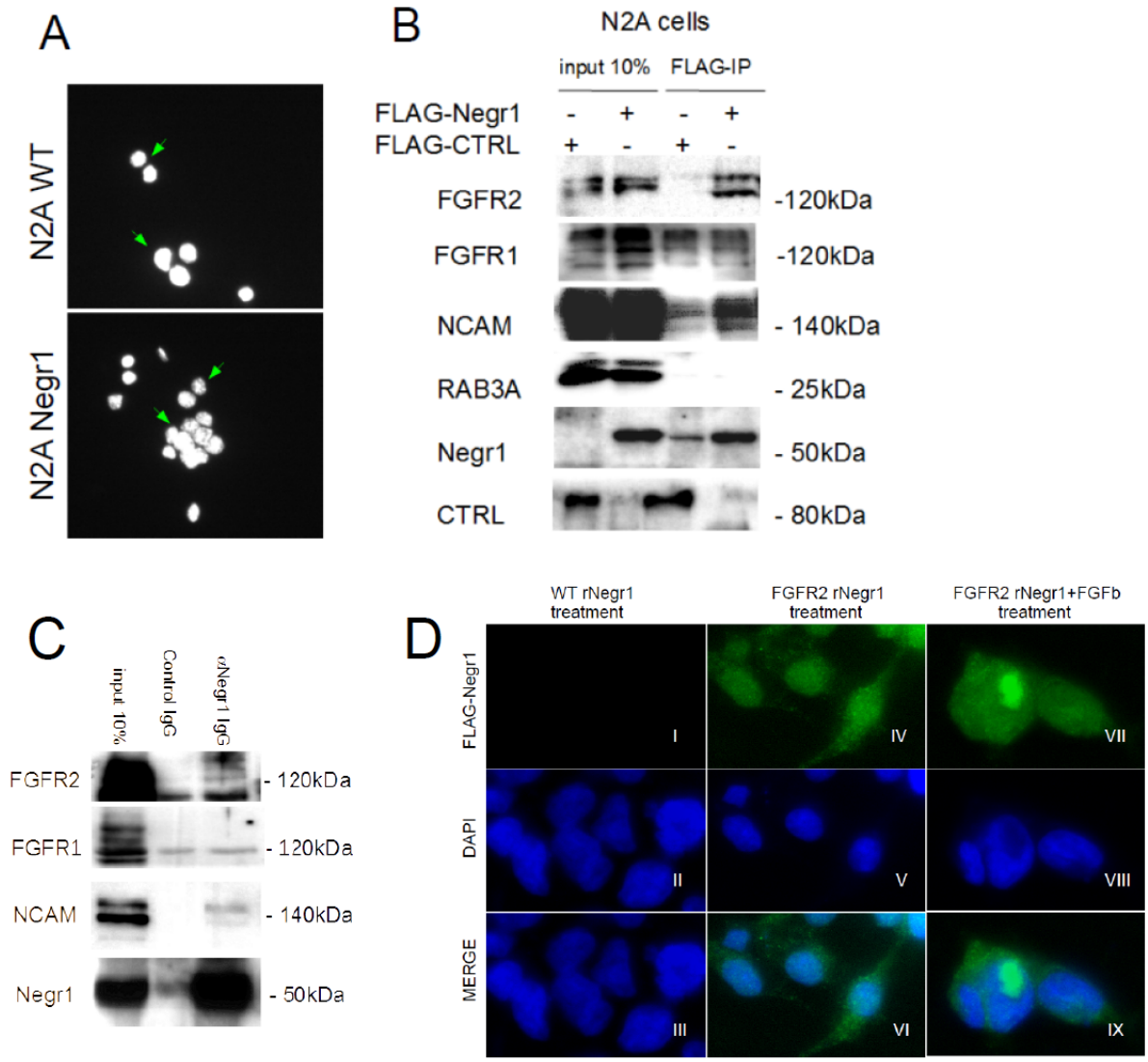

Fig 19. Negr1 interacts with FGFR2. (A) Negr1 expression induces the formation of multi-cellular aggregates. Wild-type or Negr expressing N2A were assayed for cluster formation. (B) Negr1 interacts with FGFR2. N2A wild-type or expressing FLAG-Negr1 were chemically cross-linked, solubilized and then processed for FLAG-immunoprecipitation. Upon western-blotting, samples were decorated with indicated antibodies. (C) Purified FLAG-Negr1 interacts with FGFR2. Wild-type or myc-FGFR2 expressing cells were exposed to purified soluble FLAG-Negr1 (40 ng/ml, 1h 4°C). Cell were fixed either directly after the incubation with Negr1 or upon FGFb stimulation (20 ng/ml, 1h, 37°C).

3.2.3 Negr1 modulates FGFR2 signalling acting both *in cis* and *in trans*

Next, we investigated whether physical interaction of Negr1 with FGFR2 receptor may modulate FGFR2 signalling. Since FGFR2 stimulation activates different pathways that all impinge on ERK1/2 phosphorylation (Maness e Schachner 2007), we investigated the impact of Negr1 on FGFR2 induced ERK1/2 phosphorylation. To this aim, we investigated by biochemistry neuronal culture infected at DIV4 with viruses expressing scramble siRNA (siCTRL), Negr1 siRNA (siNEGR1) or FGFR2 siRNA (siFGFR2). Cultures were treated or not with FGFb (pan FGFR agonist) 20 ng/ml, FGF7 (specific for FGFR2) 20 ng/ml and EGF 10 ng/ml (EGFR agonist) for 10 minutes at 37°C.

By judging P-ERK fold over basal condition, we noticed that Negr1 silencing impaired culture answer to FGF7, while FGFb and EGF stimulation resulted not affected. Similarly, FGFR2 silencing reduced cellular response to FGF7 only (Fig. 20 A-B).

Interestingly, upon Negr1 silencing we observed a robust and significant reduction also in FGFR2 expression. This suggest that Negr1 could be important also for FGFR2 stabilization in the membrane. To understand more in detail the mechanism underlying FGFR2 down regulation we analyzed FGFR2 sub-cellular localization. To this aim, we processed by membrane fractionation assays silenced and control neurons treated or not with FGFb. We observed a significant FGFR2 downregulation in total lisate obtained from silenced neurons in comparison with controls. Furthermore, FGFb was able to induce FGFR2 downregulation in control neurons but did not affect receptor levels in silenced neurons. Interestingly, we noticed that the amount of FGFR2 protein present in the membrane fraction remain unaffected upon FGF stimulation or Negr1 silencing (Fig. 21 A-B). These results suggest that Negr1 may be implicated in the regulation of FGFR2 trafficking.

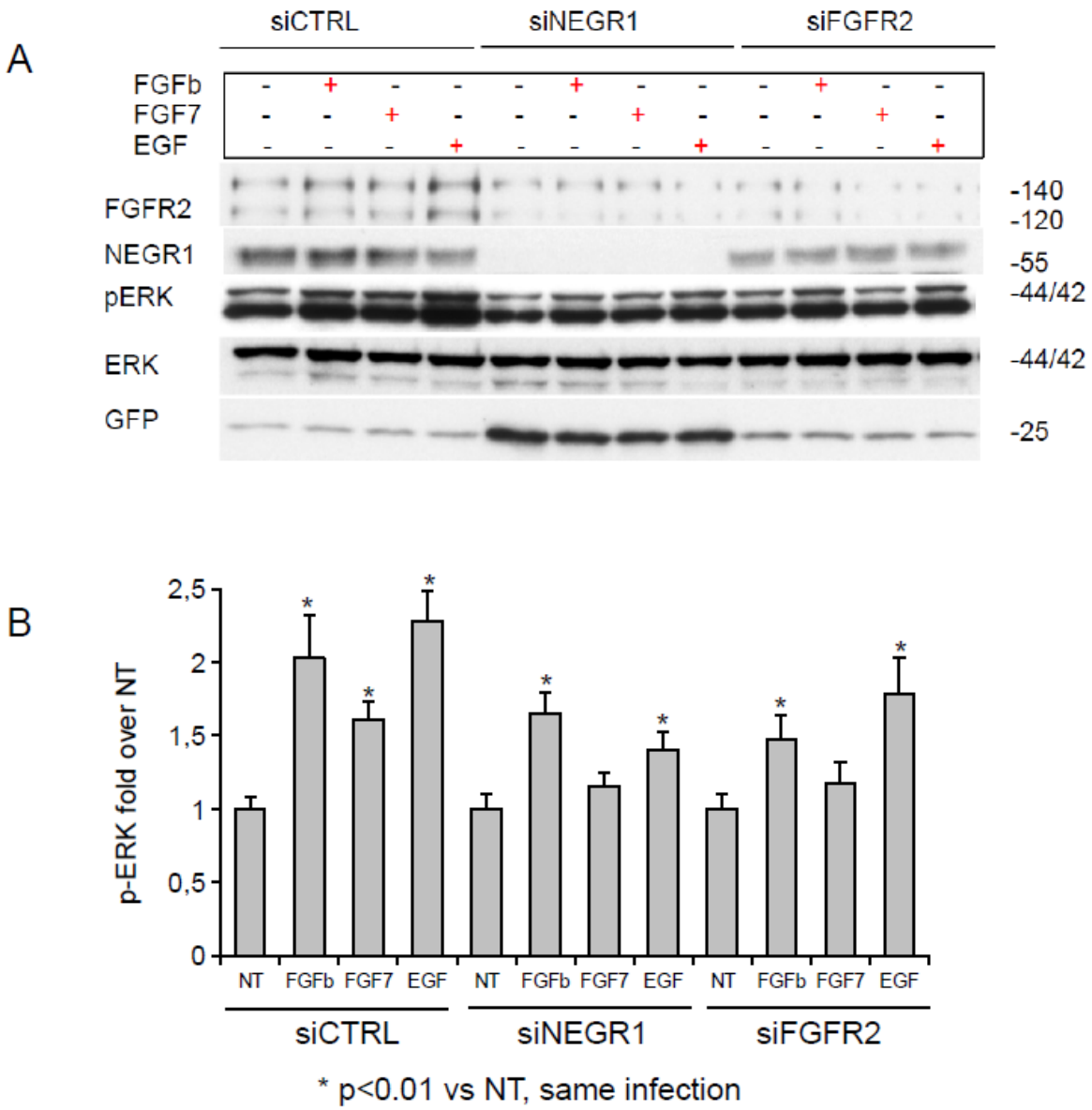

Fig 20. Negr1 influences FGFR2 signalling *in cis*. (A) Cortical neurons were infected at DIV4 with control siRNA (siCTRL) , Negr2 siRNA (siNEGR1) or FGFR2 siRNA (siFGFR2) and treated at DIV16 with FGFb (20 ng/ml), FGF7 (20 ng/ml) or EGF (5 ng/ml) for 1h at 37°C then processed for western-blotting . (B) The graph reports pERK1/2/total ERK1/2 fold over untreated condition. Data are expressed as mean ±S.E; n=6, ** p<0.01 ANOVA.

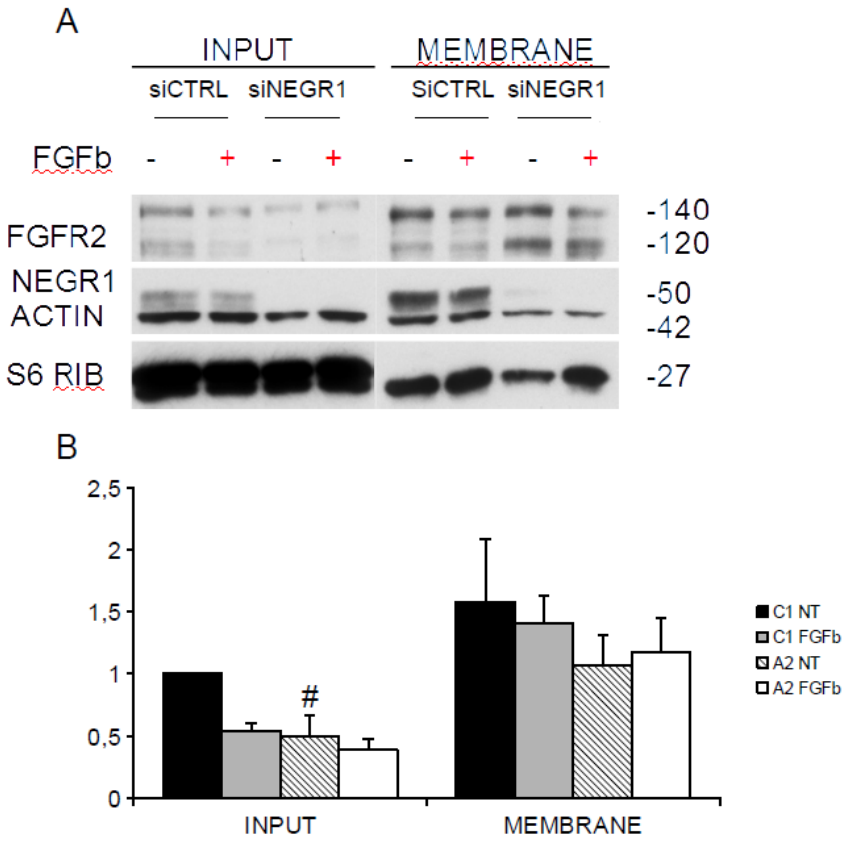

Fig. 21. Negr1 silencing modulates FGFR2 expression. Membrane fractionation of siCTRL and siNEGR1 infected neurons (A). We observed a robust and significant reduction of FGFR2 level in silenced culture in comparison with control neurons. Otherwise, FGFR2 levels in membrane remained similar (B). Data are expressed as mean ±S.E; n=3, # $p<0.01$ ANOVA.

Our data suggest that Negr1 modulates FGFR2 activity; however, given that Negr1 is expressed as membrane bound protein, two scenarios are possible: Negr1 binds FGFR2 expressed on the same cell as membrane bound protein (*in cis*); Negr1 binds FGFR2 expressed on juxtaposed cell (*in trans*). Thus, we decided to dissect the potential effect on ERK phosphorylation due to *in trans* Negr1-FGFR2 interaction. To this aim, we seeded at DIV16 wild-type or FLAG-Negr1 expressing HEK293 cells on cortical neuronal cultures. Cultures were processed for western-blotting at DIV18. We found a robust increase in pERK1/2 level when neurons where co-cultured with FLAG-Negr1 cells. Strikingly, increase in ERK phosphorylation was lost once we seeded FLAG-Negr1 cells on neurons infected at DIV4 with siNEGR1 or siFGFR2, i.e. lacking Negr1 or FGFR2 expression (Fig. 22A-B). Altogether, these data suggest that Negr1 positively triggers ERK pathway acting *in trans* on Negr1-FGFRF2 heterodimer.

Furthermore, IgLON molecules have been recently shown to increase FGFR2 stability (McKie et al. 2012). Interestingly, when Negr1-HEK293 cells are co-cultured together with primary cortical neurons we observed not only an increase in pERK levels but also a robust upregulation of FGFR2 in neurons in comparison with neurons cultured alone (Fig 23). This suggest that Negr1 is important to control FGFR2 signaling and trafficking also *in trans*.

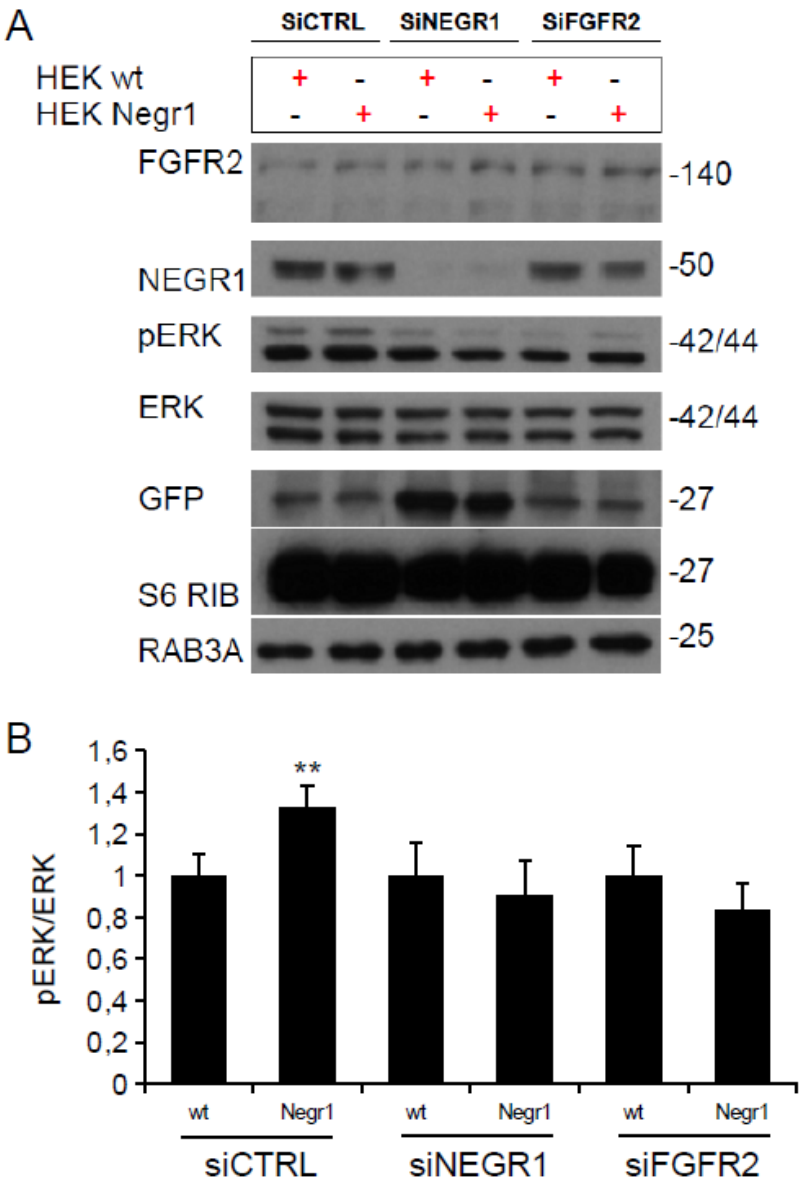

Fig 22. Negr1 influences FGFR2 signalling *in trans*. (A) DIV4 cortical cultures were infected with control siRNA (siCTRL) , Negr2 siRNA (siNEGR1) or FGFR2 siRNA (siFGFR2), co-cultured at DIV16 with wild-type or FLAG-Negr1 expressing cells and processed at DIV18 for western blotting. (B) The graph reports pERK1/2 to total ERK1/2 ratio. Data are expressed as mean ± S.E; n=6, ** $p<0.01$ ANOVA.

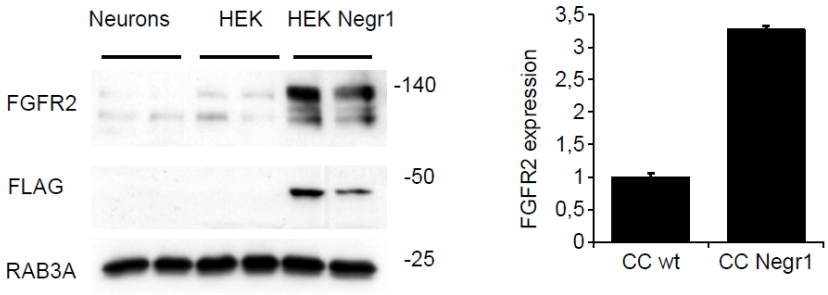

Fig 23. Negr1 stabilizes FGFR2 *in trans*. Western blot analysis of FGFR2 levels in co-culture assay. FGFR2 expression increases co-cultivating neurons with HEK-Negr1 in comparision with HEK wt. Data are expressed as mean ± S.E; n=3, ** $p<0.01$ ANOVA.

3.2 Negr1 in migration

3.2.1 Negr1 expression is temporally and spatially regulated *in vivo*

To start the investigation on the role of Negr1 in *in vivo* development, we first performed *in situ* hybridization in the mouse brain with specific probes for Negr1 mRNA expression (Fig. 24).

In the embryonic brain (E18), we found that Negr1 mRNA expression was high in the ventricular zone (SVZ), and at the border between the intermediate zone (IZ) and cortical plate (E18; Fig. 24). At later stages, P7, adult), Negr1 mRNA expression appeared progressively more confined to layer IV. Interestingly, Negr1 expression was also spatially regulated as its mRNA was detectable at higher levels in some brain areas (e.g., somatosensory and visual cortices, hippocampus), than in others (e.g., motor and prefrontal cortices, Fig. 24).

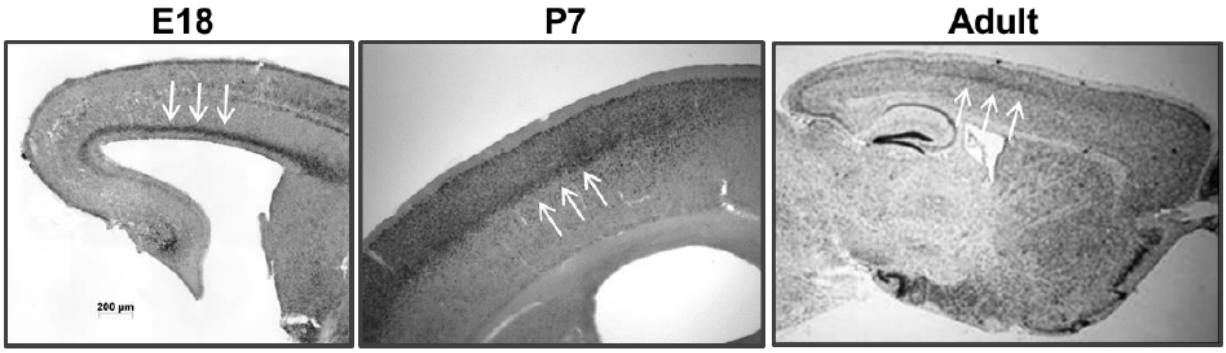

Fig. 24. Negr1 expression is temporally and spatially regulated *in vivo.* *In situ* hybridization showing expression of Negr1 at the indicated ages. White arrows point to strong expression of Negr1 in VZ (E18) and in layer IV (P7, adult).

3.2.4 Manipulation of Negr1 expression affects late-born neuron migration *in vivo.*

Given the expression of Negr1 mRNA in the somatosensory cortex in new-born neurons committed to layer II/III, we wondered whether Negr1 may have a role in the development of these neurons. To this aim, we used RNA interference against Negr1 (Negr1 siRNA) and cDNA encoding for WT Negr1 (Negr1 cDNA;(Pischedda et al. 2014); APPENDIX I) to manipulate the expression levels of Negr1 in the developing somatosensory cortex, where its expression is the strongest.

We took advantage of standard *in utero* electroporation and we introduced scrambled siRNA (control), Negr1 siRNA or Negr1 cDNA into the lateral ventricle of E15.5 mice *in utero,* and transfected these constructs into a subpopulation of neural precursors and their progeny of newborn neurons committed to migrate to the layer II/III of the somatosensory cortex (Fig.25A; (Saito e Nakatsuji 2001)).

All constructs were co-electroporated with EGFP for visualization of transfected cells (Bony et al. 2013; Cancedda et al. 2007). After allowing for *in vivo* development, we analyzed the migration in coronal brain slices obtained from mouse embryos at pups at P7 (Fig 25) and adult mice at P35 (Fig. 26). By P7, control and cDNA-transfected cells reached cortical layer II/III, whereas a large number of Negr1 siRNA-expressing cells were arrested in layer V and appeared not able to cross the border between layer IV and layer V (Figure 25B). We defined these cells as "ectopic" neurons, as they stopped in an ectopic layer. We quantified the number of these ectopic neurons at P7, and normalized them to the total number of transfected cells (Figure 25C).

We found that in animals transfected with Negr1 siRNA 16.49 ± 1.96 % of migrating cells were arrested in layer V, with an ~30 folds increase compared to controls (Fig. 25C, Control 0.51 ± 0.17 %, Negr1 cDNA 1.27 ± 0.31 %; one way ANOVA Dunn's *post-hoc*: ***$p < 0.001$).

The effect of Negr1 downregulation on ectopic cells arrested in layer V persisted also at P35, indicating a long-lasting effect (Fig. 26; Control 0.20 ± 0.20 %; Negr1 siRNA 5.63 ± 0.62 %; Student's *t*-test: *** $p < 0.001$).

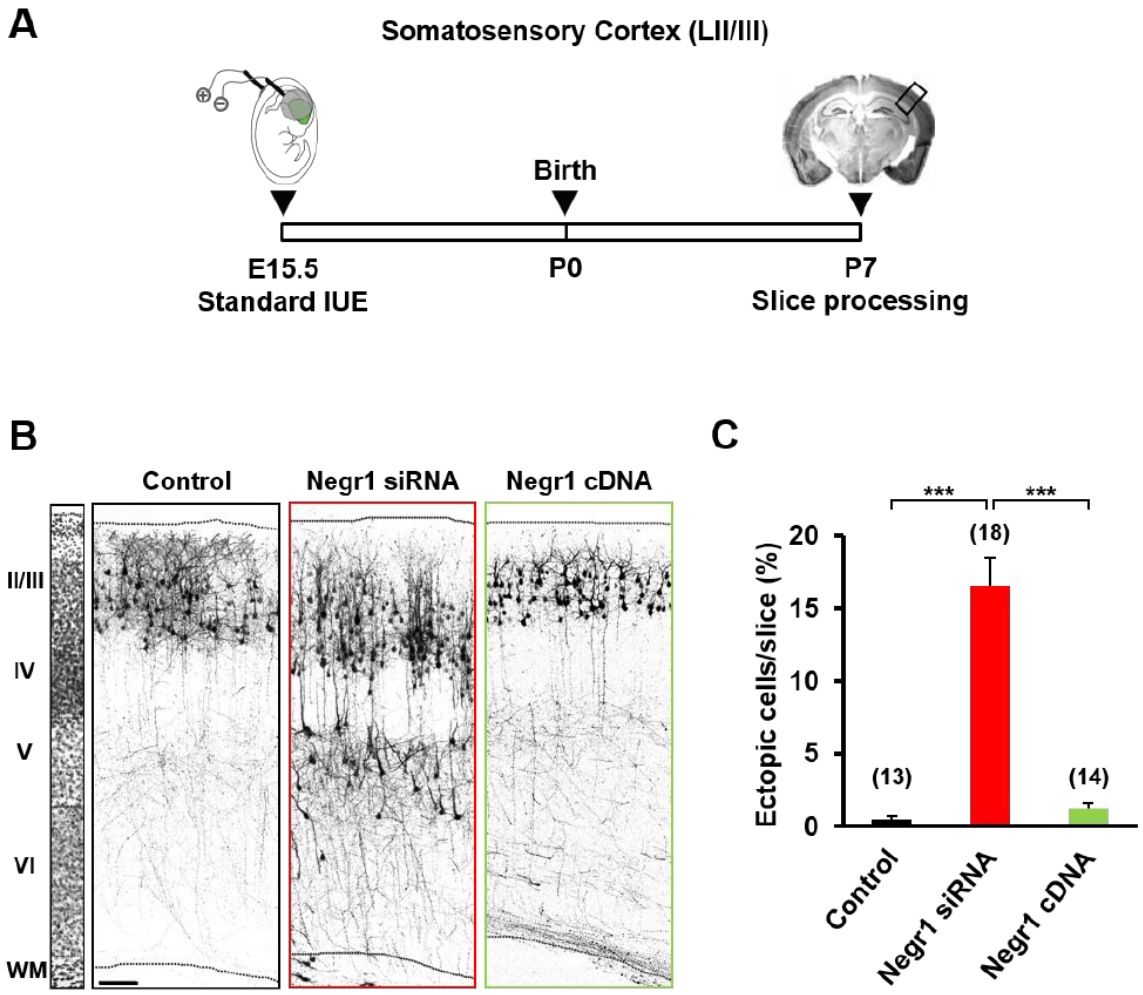

Fig. 25. Negr1 downregulation, but not overexpression, causes accumulation of ectopic cells in layer V at P7 *in vivo.* (A) Schematic cartoon of the experimental protocol with processing at P7. (B) Confocal images of GFP fluorescence in coronal sections of somatosensory cortices at P7 after *in utero* transfection (at E15.5) with control siRNA (black), functional Negr1 siRNA (red) or Negr1 cDNA (green). Slices were counterstained with DAPI (left). Scale bar, 100µm. WM = white matter. (C) Quantification of the number of control, Negr1 siRNA- and Negr1 cDNA-expressing neurons that did not complete their migration. Data are expressed as average percentage (± SEM) of the total number of fluorescent cells in the section. Asterisks: statistically significant difference (One-way ANOVA; Dunn's *post-hoc*: ***$p < 0.001$). Numbers in parenthesis: total number of animal processed (1 slice/animal).

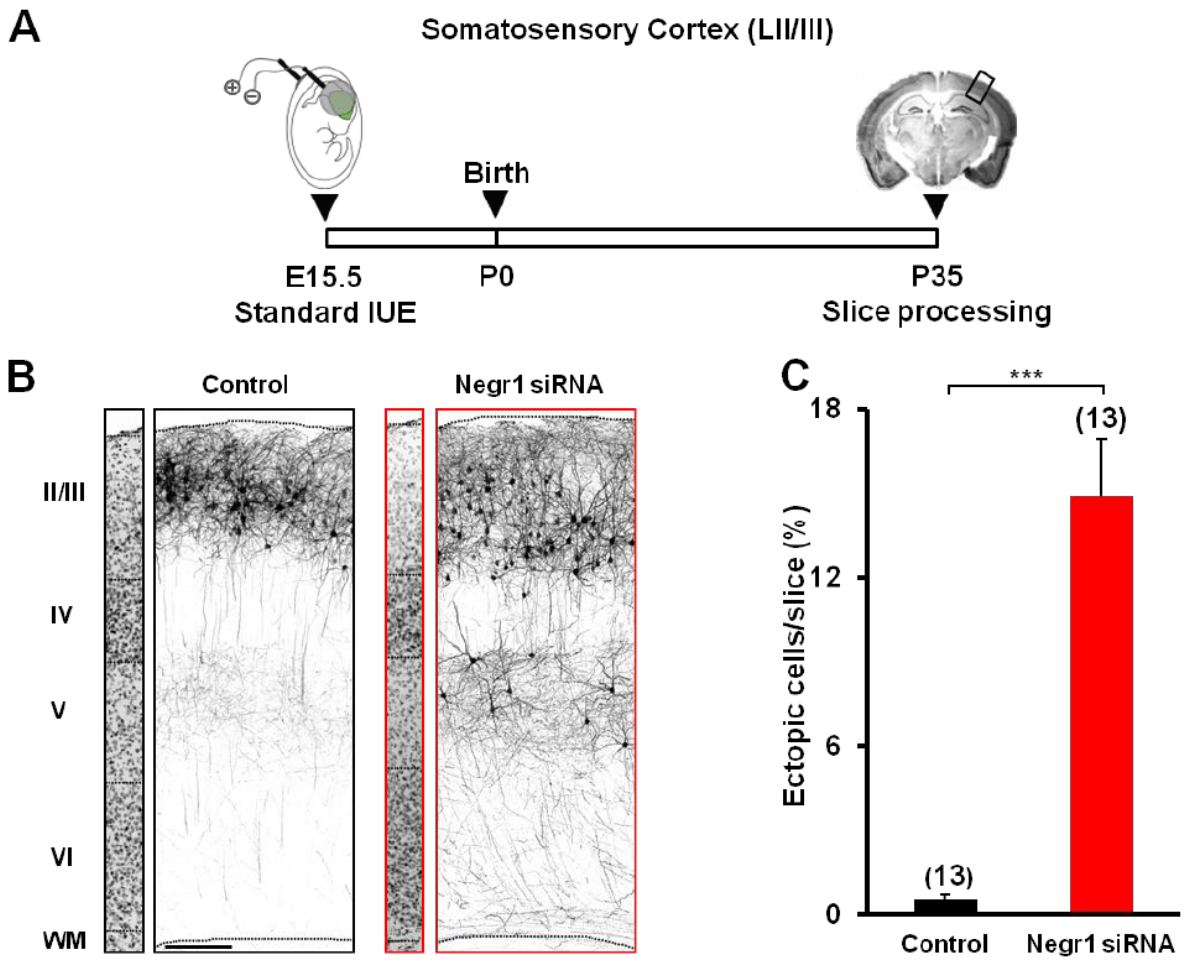

Fig 26. The effect of Negr1 downregulation on neuronal migration is long-lasting. (A) Schematic cartoon of the experimental protocol with processing in adulthood. (B) Confocal images of GFP fluorescence in coronal sections of somatosensory cortices at P35 after *in utero* transfection (at E15.5) with scrambled siRNA (Control, black) or Negr1 siRNA (red). Slices were counterstained with DAPI (left). Scale bar, 100µm. (C) Quantification of the number of control or Negr1 siRNA-expressing neurons that did not complete their migration. Data are expressed as average percentage (± SEM) of the total number of fluorescent cells in the section. Asterisks: statistically significant difference (Student's *t*-test: *** $p < 0.001$). Numbers in parenthesis: total number of animal processed (1 slice/animal).

5.DISCUSSION

In this study we have shown that Negr1 plays a key role in controlling neurite outgrowth and neuronal migration. Our main hypothesis is that Negr1 contributes to the proper formation and stabilization of neuronal network. Furthermore, we brought evidences that Negr1 regulates neuronal morphology and migration during development of the central nervous system.

Interestingly, Sanz et al demonstrated recently that IgLON family protein are actively released in neuronal media and their shedding is important for a proper neuronal maturation (Sanz, Ferraro, e Fournier 2015).

Our data suggest that Negr1 acts as a soluble factor, binds FGFR2 expressed in membrane and triggers MAPK signaling pathway. Several experimental findings connect ADAM10 mediated shedding and FGFR2 to the regulation of neuronal functional and morphological maturation.

ADAM10 modulates axonal growth via the cleavage of different membrane proteins including L1-NCAM, N-cadherin and NCAM (Hinkle et al. 2006; Mechtersheimer et al. 2001; Paudel et al. 2013). NCAM ectodomain in particular can stimulate neurite outgrowth triggering ERK1/2 signalling via binding with B1 integrin (Diestel et al. 2005). Finally, it has been demonstrated that NCAM binds and activates FGFR1 and 2 (Francavilla et al. 2009; Francavilla et al. 2007; Kiselyov et al. 2005).

Our data suggest that ADAM10 shedding releases Negr1 in the extracellular media.

In their work, Sanz and colleagues did not notice any difference in term of Negr1 release upon ADAM10 acute silencing (Sanz, Ferraro, e Fournier 2015). Instead in our study we abolished ADAM10 activity via ADAM10 specific inhibitor. In fact, upon chronic treatment we observed a robust reduction in Negr1 release. Our different experimental approach may account for the opposite outcome we reported here.

Thus our data suggest a mechanism implying that soluble Negr1 influences positively neuron

maturation stimulating via FGFR2 ERK1/2 intracellular signalling cascade, i.e acting *in trans*. Nevertheless, a role for Negr1 *in cis* has to be taken in account. In our previous publication (Pischedda et al. 2014), we showed that acute Negr1 down-regulation impairs severely neurite outgrowth. In this study, we analyzed more in detail the impact of acute negr1 down-regulation.

In particular, we noticed a clear morphological defect also upon infection with low titer of Negr1 siRNA viruses. In such condition, scarce and isolated Negr1 silenced neurons were surrounded by cells expressing and therefore releasing Negr1. Interestingly, also in this experimental setting we observed a clear impairment of neuritic tree complexity upon Negr1 silencing.

However the magnitude of the effect was lower than the one reported upon high viral titer infection, i.e upon massive and general down regulation of Negr1 protein level in the culture.

These results may suggest that Negr1 influences neuronal development acting both *in cis* and *in trans* and that the two mechanisms contribute to determine neurite outgrowth.

It has been demonstrated that IgLON proteins are able not only to bind RTKs but and also to modulate their activity (McKie et al. 2012).

Here, taking advantage of immunoprecipitation and in cell overlay assay we found that Negr1 binds FGFR2. While our data suggest that Negr1 acts *in trans* via FGFR2, we cannot exclude the existence of Negr1 and FGFR2 complex *in cis*. In fact, we can speculate that membrane bound Negr1 may form a heterocomplex with FGFR2. As reported for NCAM, Negr1 *in cis* interaction can influence FGFR2s downstream signalling upon agonist binding (including potentially soluble Negr1 itself as well as FGFs) (Francavilla et al. 2007; Francavilla et al. 2009).

In the attempt to analyze the cis effect of Negr1-FGFR2 co-expression, we treated neurons with different growth factor such as EGF, FGFb and FGF7.

The biochemical analysis of pERK levels showed that Negr1 silencing impaired cellular answer to FGF7 (a specific agonist of FGFR2), while FGFb and EGF stimulation resulted not affected. Similarly, FGFR2 silencing reduced cellular response to FGF7 only.

This suggest that the potential heterocomplex formed by Negr1 and FGFR2 expressed on the same cell does not induce ERK1/2 phosphorylation by itself, but it is instead important for FGFR2 response to its specific agonist.

Thus we conclude that Negr1 has a regulatory role for FGFR2 *in cis.*

Finally, given that Negr1 is expressed as membrane bound protein, two scenarios are possible: Negr1 binds FGFR2 expressed on the same cell as membrane bound protein (*in cis*); Negr1 binds FGFR2 expressed on juxtaposed cell (*in trans)*.

Thus, we decided to dissect the potential effect on ERK phosphorylation due to *in trans* Negr1-FGFR2 interaction taking advantage of the co-culture assay. We found a robust increase in pERK1/2 level when neurons where co-cultured with Negr1 positive cells. Strikingly, increase in ERK phosphorylation was lost once we seeded Negr1 cells on neurons lacking Negr1 or FGFR2 expression. Altogether, these data suggest that Negr1 positively triggers ERK pathway acting *in trans* on Negr1-FGFRF2 heterodimer present on the justaxposed neuronal membrane.

In conclusion, our data show that Negr1 activates *in trans* and as soluble factor FGFR2 while it modulates FGFR2 *in cis.*

Furthermore, we demonstrated that Negr1 might influence FGFR2 protein level.

In particular, we deem that Negr1 may influence the amount of FGFR2 within the recycling pool and/or discriminate between recyling and lysosomial degradation. Our working hypothesis is that Negr1 co-expression may be important to support ERK activation regulating both FGFR2 signaling and trafficking inside the cell.

Given the pivotal role played by FGFR2 during CNS development, it is tempting to speculate that Negr1 might be involved in the formation of neuronal network.

Neuron migration requires several mechanisms, such as the recognition of the proper path and the ability to move long distances. Many external factors might negatively influences a proper neural migration and result in a misplacement of cells.

Examples of such external influences are alcohol, cocaine or radiation, which may lead to numerous mental disorders. Furthermore, mutations in genes that regulate this migration have recently been shown to cause some rare genetic forms of mental retardation, schizophrenia and epilepsy.

FGFRs have been largely studied as key regulators of neuronal migration via ERK1/2 kinases (Cavallaro e Dejana 2011; Francavilla et al. 2009). Importantly, conditional knock out of ERK1/2 leads to perturbation in cortical lamination with decreased number of pyramidal neurons in layer II/III and increased number of neurons in layer V (Pucilowska et al. 2012).

ERK pathway and NCAM activation of FGFR1 have been extensively linked to the modulation of neuronal proliferation and migration during embryonic brain development (Francavilla et al. 2007).

Fibroblast growth factors play multiple roles in the central nervous system (CNS) and control the size of the cerebral cortex (Shin et al. 2004; Vaccarino et al. 2009) as well as its patterning (Fukuchi-Shimogori e Grove 2001; O'Leary e Nakagawa 2002; Garel, Huffman, e Rubenstein 2003; Hébert e Fishell 2008).

Several FGF ligands, including FGF2, 3, 7, 8, 10, 15, 17, and 18, are expressed in the rostral telencephalic midline and early cortical primordium (Fukuchi-Shimogori e Grove 2001; Garel, Huffman, e Rubenstein 2003; Cholfin e Rubenstein 2007), and have been demonstrated to regulate neurogenesis (Raballo et al. 2000; Borello et al. 2008). Amongst the four FGFR, only FGFR1-3 are expressed in the developing CNS (Ford-Perriss, Abud, e Murphy 2001).

Recent studies have demonstrated that FGFRs regulate CNS growth, including the hippocampus (Ohkubo et al. 2004) and the cerebral cortex (Kang et al. 2009). Once neural progenitors have been generated in the developing brain and spinal cord, FGFs play important roles in their survival and expansion (Vaccarino et al. 2009; Diez del Corral et al. 2003; Inglis-Broadgate et al. 2005).

Furthermore FGF signalling has a prominent role in the migration of neurons.

FGFs secreted by neurons of the cerebral cortex signal back to cortical progenitors, as shown by the FGF18-dependent expression of the Ets transcription factors Pea3, Erm, and Er81 by VZ cells

(Hasegawa et al. 2004).

Blocking FGF signalling leads to neuronal migration defects, suggesting that FGF mediates a feedback loop through which neurons that have reached their final position control the migratory behaviour and laminar position of the next wave of neurons (Hasegawa et al. 2004).

Migration of young post-mitotic neurons from the ventricular zone to the cortical plate where they differentiate is a key event in cortical development. Neuronal migration disorders lead neurons to move and differentiate in an abnormal position (Rakic 1988). Ectopic positioning and impaired differentiation of cortical grey matter cause pathologies called Neuronal Migration Disorders (NMD) (Copp e Harding 1999).

In fact, periventricular and subcortical neuronal displacement have been described in the brain of patients suffering from epilepsy (Barkovich e Kjos 1992; Flint e Kriegstein 1997).

Moreover, discrete intracortical disorganization also have been described in the brains of patients affected by dyslexia schizophrenia and autism (Jones 1995).

Autism refers to an etiologically and clinically heterogeneous group of neurodevelopmental disorders and is included in Neuronal Migration Disorders.

Both Negr1 and FGFR2 are implicated in Autism Spectrum Disorders (ASD) (Kaminsky et al. 2011; Marshall et al. 2008; Michaelson et al. 2012; Pinto et al. 2010; Wentz et al. 2014).

However, ASD is a highly heterogeneous disorder with thousands of genes and molecular mechanisms involved in its etiology. For this reason a very large effort has been recently put on research focusing on finding convergent pathways affected by ASD genes during human development (Li e Reiser 2011; Parikshak et al. 2013; Pinto et al. 2014). In this context is very interesting that many of ASD genes are enriched in cortical pyramidal neurons of superficial layers (Parikshak et al. 2013) and patches of abnormal laminar cytoarchitecture have been found in patients suffering from ASD (Stoner et al. 2014).

Taking advantage of standard *in utero* electroporation Laura Cancedda's group in Genova silenced

Negr1 into a subpopulation of neural precursors and their progeny of newborn neurons committed to migrate to the layer II/III of the somatosensory cortex. By P7, large number of Negr1 silenced cells were arrested in layer V and appeared not able to cross the border between layer IV and layer V. We defined these cells as "ectopic" neurons, as they stopped in an ectopic layer and this effect is long lasting until P35.

Furthermore, we found that acute down regulation of FGFR2 results in strikingly similar migration defect with neurons arrested in layer V, as seen upon Negr1 knockdown.

Finally, clear signaling cross talk between Negr1 and FGFR2 is strengthen by the fact that Negr1 downregulation and FGFR2 overexpression in the same cell can completely rescue the migration defect, proving for the first time an *in vivo* involvement of both molecules in the same signaling pathway (Laura Cancedda, IIT Genova. Data not shown).

Because we found that: Negr1 miRNA is present in high levels in layer IV of the somatosensory cortex, is able to modulate FGFR2 signaling both *in cis* and *in trans* and furthermore MAPK are fundamental for neuronal migration, we hypothesized that Negr1 expressed by layer IV neurons could interact *in trans* with FGFR2-Negr1 complex located on neurons committed to layer II/III and it could regulate their migration to the superficial layers of the cortex *via* pERK modulation.

ASD is characterized by complex behavioral defects, including emotional and motivation impairments. USVs are socially-relevant communication sounds emitted by pups as a result of separation from the mother and are widely used as an easy method to measure social and communications behaviors in various models of neurodevelopmental disorders (Fischer e Hammerschmidt 2011; Ju et al. 2014; Lai et al. 2014; Scattoni, Ricceri, e Crawley 2011).

In particular, USVs provide sensitive insight into the early emotional development of the pup (Gulia et al. 2014; Wöhr e Schwarting 2008) and, reduced number of USV calls with unusual patterns have been reported in several mice models of ASD (Fujita et al. 2008; Scattoni, Ricceri, e Crawley 2011).

Thus, we investigated ultrasonic vocalizations (USV) in mice soon after birth to test possible defects in communication skills. We found that pups after Negr1 or FGFR2 downregulation in the somatosensory cortex, a region believed to be analogous to the language area in the human cortex (Sia, Clem, e Huganir 2013), display reduction in the number of ultrasonic vocalization calls with lower probability of emitting complex calls. Interestingly, ERK kinases activation restored this aberrant behavior (Laura Cancedda, IIT Genova. Data not shown).

These data suggest that Negr1 is important not only for neuronal maturation, but also for neuronal migration during the formation of cortical layers.

But how Negr1 could regulate *via* FGFR2 cortical cyto-architecture and neuronal maturation during development? We propose four models to explain the complex interconnession between Negr1-FGFR2 and MAPK signaling.

We can distinguish two main mechanisms underlying Negr1 effect on FGFR2 activity: *in cis* and *in trans*. In control neurons, which express both Negr1 and FGFR2 *in cis*, Negr1 binds and stabilizes FGFR2 on the membrane, thus allowing agonist binding and subsequent activation of ERK1/2 signaling. Upon agonist binding, Negr1- FGFR2 heterocomplex is internalized and recycles on the membrane, ready for a new cycle of activation (Fig. 27).

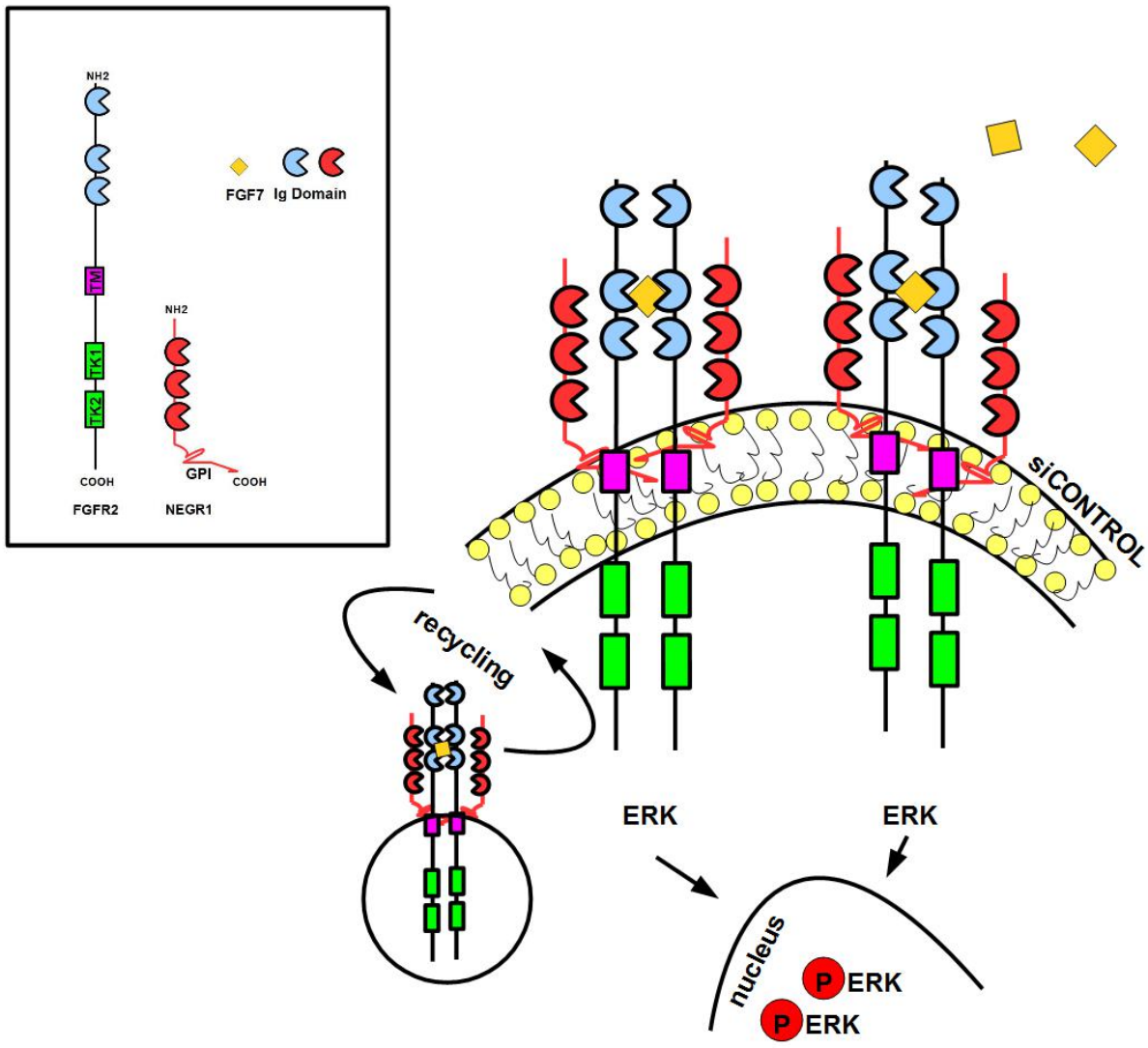

Fig 27. Negr1 action *in cis.* Negr1 binds FGFR2 regulating its response to FGF7.

When Negr1 is missing, FGFR2 is still exposed in membrane but answers less to FGF7 stimulation. Furthermore, our biochemical evidence suggests that Negr1 could impact on FGFR2 recycling.

It is known from the literature that growth factor receptors, more in the specific RTKs, activates alternative pathways upon internalization (Sorkin e von Zastrow 2009). Furthermore, recycling is a

fundamental process that disassembles FGF7-FGFR2 complex and allows the translocation of receptors' subunit back to the membrane. Given such crucial role of the recycling, any alteration of proper receptor trafficking may alter receptor activity. Finally, Negr1 may discriminate beetween the two fates that intra-cellular pool of FGFR2 might encounter: recycling or lysosomial degradation. In presence of Negr1, FGFR2 pool might be driven towards recycling, while in absence it is degraded.

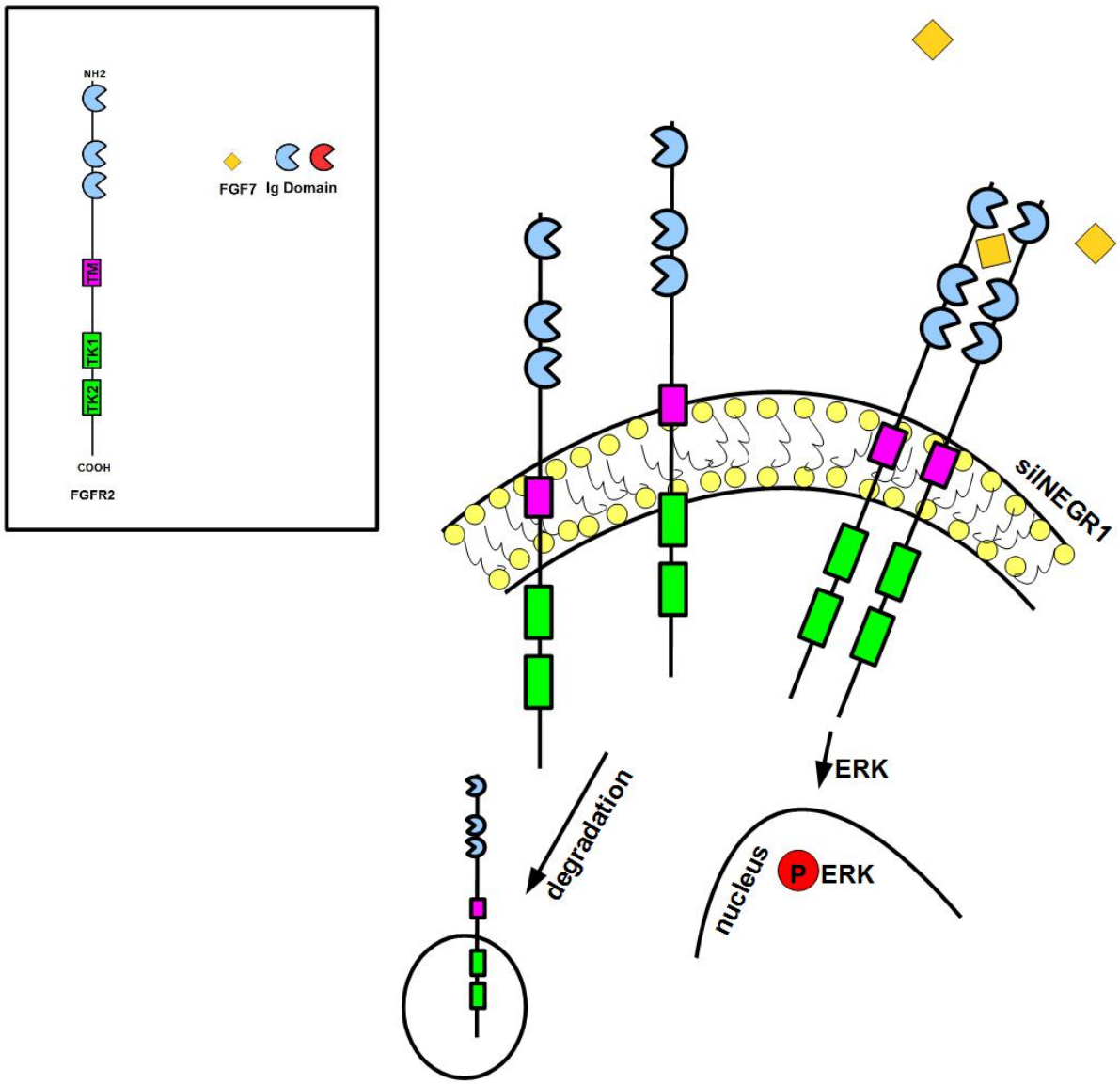

Fig. 28. Negr1 action *in cis.* If Negr1 is missing FGFR2 is still exposed in membrane but answers less to FGF7 stimulation.

Furthermore, we know from our biochemical data that Negr1 is important also *in trans*.

In fact, our coculture assay suggest that Negr1-HEK overexpressing cells are able to trigger MAPK signalling cascade in neurons. Interestingly we observed that at the same time Negr1 induces the stabilization of FGFR2 in neuronal cultures after 3 days *in vitro*.

All together these data suggest that Negr1 *in trans* activates ERK pathway maybe recruiting Negr1-FGFR2 heterodimer on the justaxposed membrane (Fig. 29).

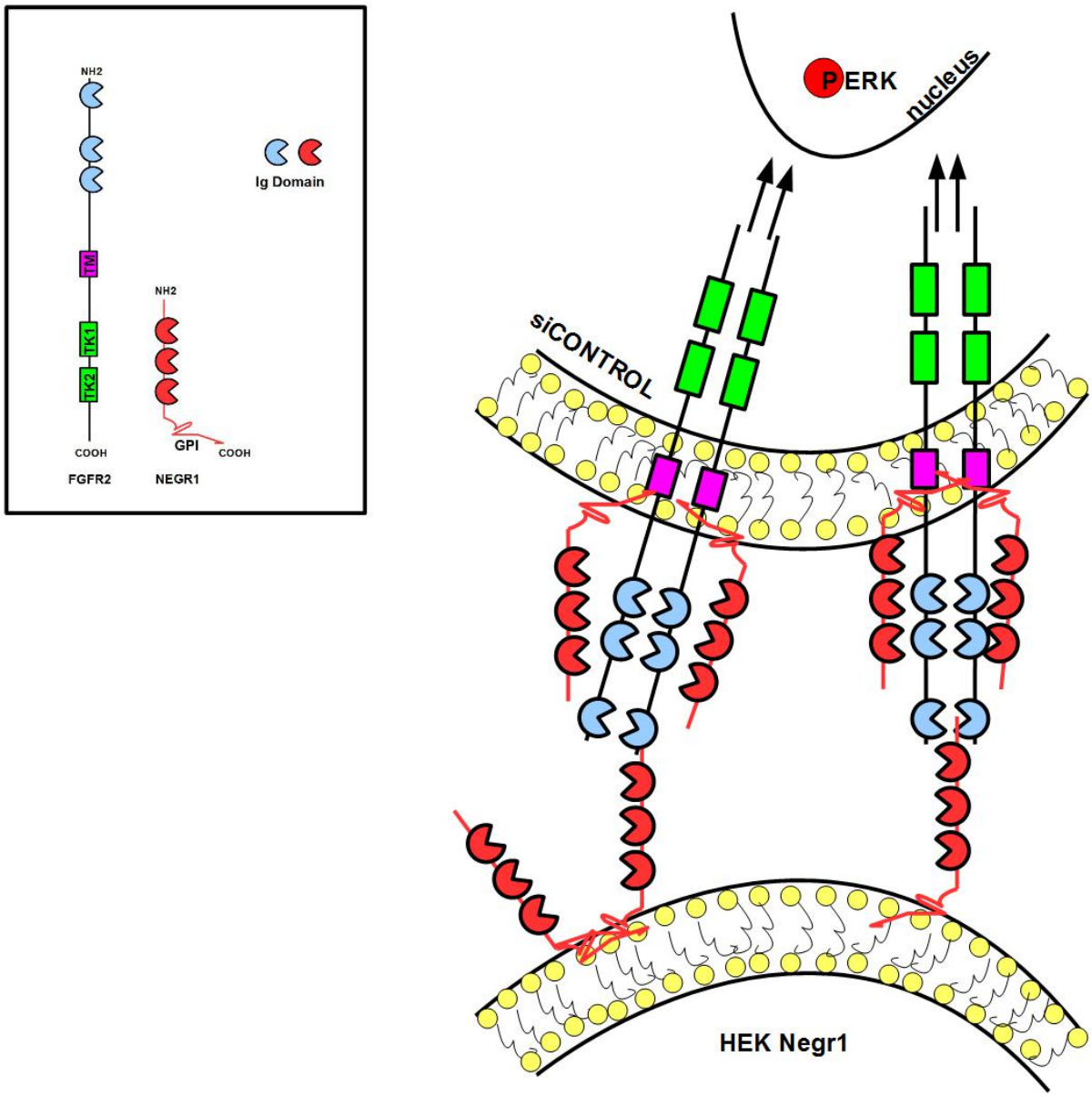

Fig. 29. Negr1 action *in trans.* Negr1 trans activates MAPK signaling in neurons.

In absence of Negr1, we did not observe an increase of ERK1/2 phosphorylation in silenced neurons co-cultivated together with Negr1-HEK cells. This outcome might arise from the absence of proper Negr1-FGFR2 heterocomplex on neuronal membrane: in such condition, Negr1 exposed from HEK cells cannot trigger any signalling pathways.

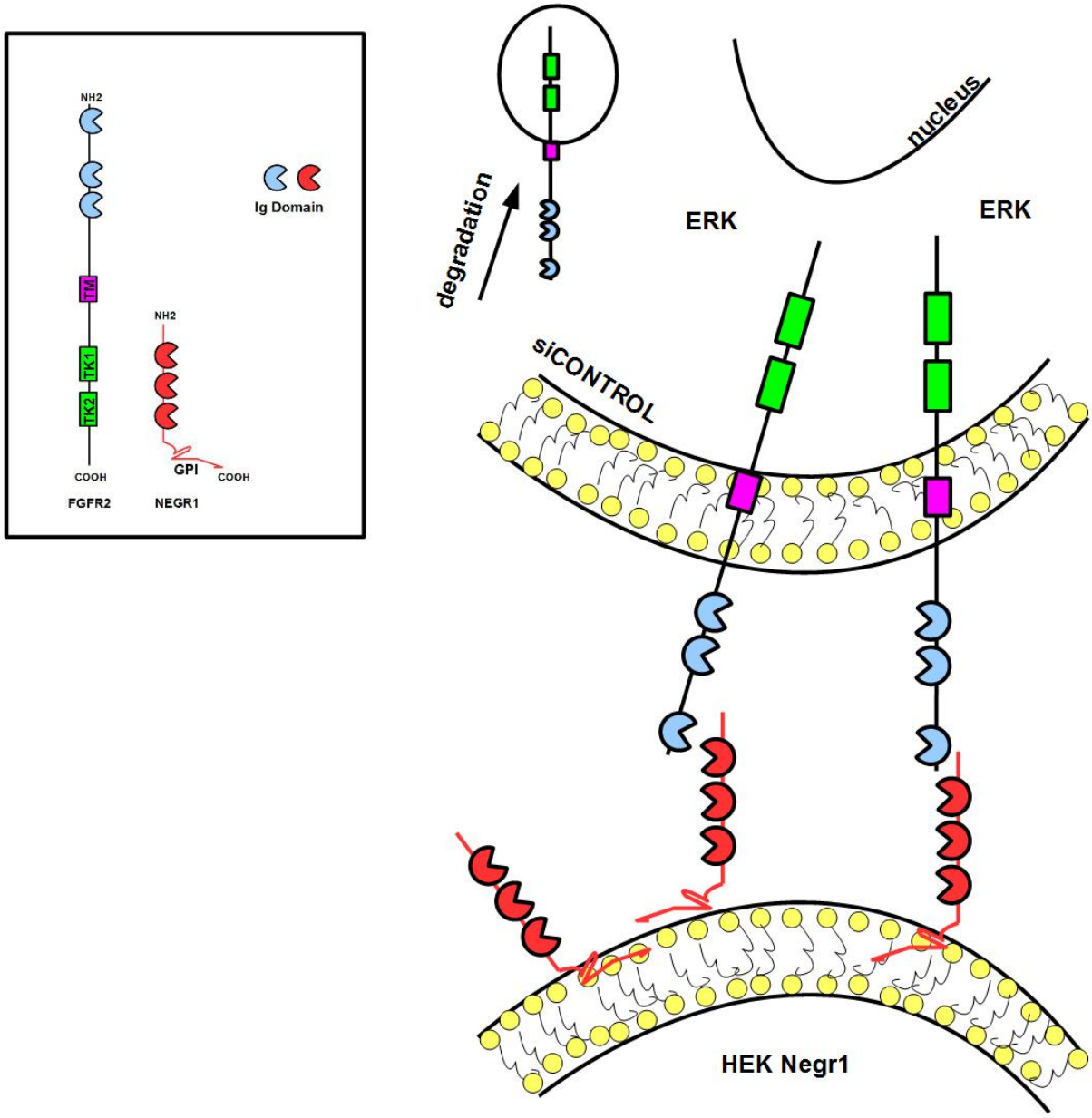

Fig 30. Negr1 action *in trans*. In absence of proper Negr1-FGFR2 heterocomplex on neuronal membrane Negr1 exposed on HEK cells is unable to trigger ERK1/2 signaling.

To support our hypotesis, in a recent paper (Song et al. 2015) Song and colleagues discovered a role for Slitrk -a transmembrane protein- in regulating TrkB-BDNF trafficking and signaling.

Slitrk isotypes are highly expressed in the CNS, where they mediate neurite outgrowth, synaptogenesis, and neuronal survival exactly like IgLON family proteins.

They report that Slitrk5 through direct interaction with TrkB receptors is able to modulate brain-derived neurotrophic factor (BDNF)-dependent biological responses.

Under basal conditions, Slitrk5 interacts primarily with a trans-synaptic binding partner; however, upon BDNF stimulation, Slitrk5 shifts to *cis*-interactions with TrkB. In the absence of Slitrk5, TrkB has a reduced rate of ligand-dependent recycling and altered responsiveness to BDNF treatment. Furthermore, they discovered that Slitrk5 mediates optimal targeting of TrkB receptors to Rab11-positive recycling endosomes through recruitment of a Rab11 effector protein, Rab11-FIP3 (Fig 31).

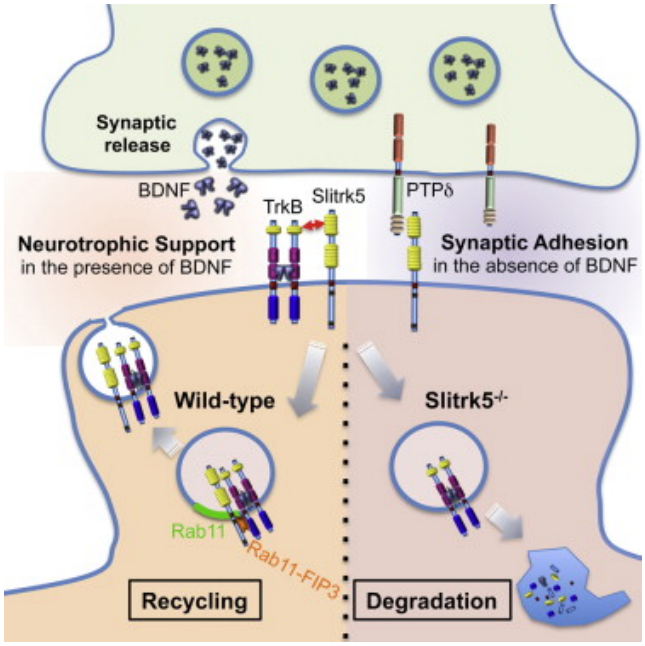

Fig 31. Slitrk5 regulates TrkB-BDNF trafficking and signaling *via* supporting RAB11 recycling at early endosomes (adapted from (Song et al. 2015)).

Negr1 may execute its function following a mechanism similar to the one proposed for Slitrk5.

In fact, we hypothesize a double action for Negr1: *in cis*, it interacts directly with the receptor, mediates its biological response to agonist and influences receptor trafficking. *In trans* it interacts with Negr1-FGFR2 heterocomplex formed on the justaxposed membrane triggering FGFR2 signaling and supporting synaptic stabilization.

All these mechanisms may be called in action during neuronal migration.

Our main hypothesis is that neurons migrating from the ventricular zone (VZ) reach layer IV where Negr1 is highly expressed. If the migrating neurons express both Negr1-FGFR2, the heterocomplex is assembled and the receptor is functionally exposed in membrane and triggers ERK intracellular cascade. The recycling is functional so the signalling is long-lasting and the neuron can go further reaching layer II-III of the cortex. If migrating neuron lacks Negr1 or FGFR2 expression it is blocked to layer IV - we called these neurons "ectopic neurons"- causing maldevelopment of the cortex (Fig. 32)

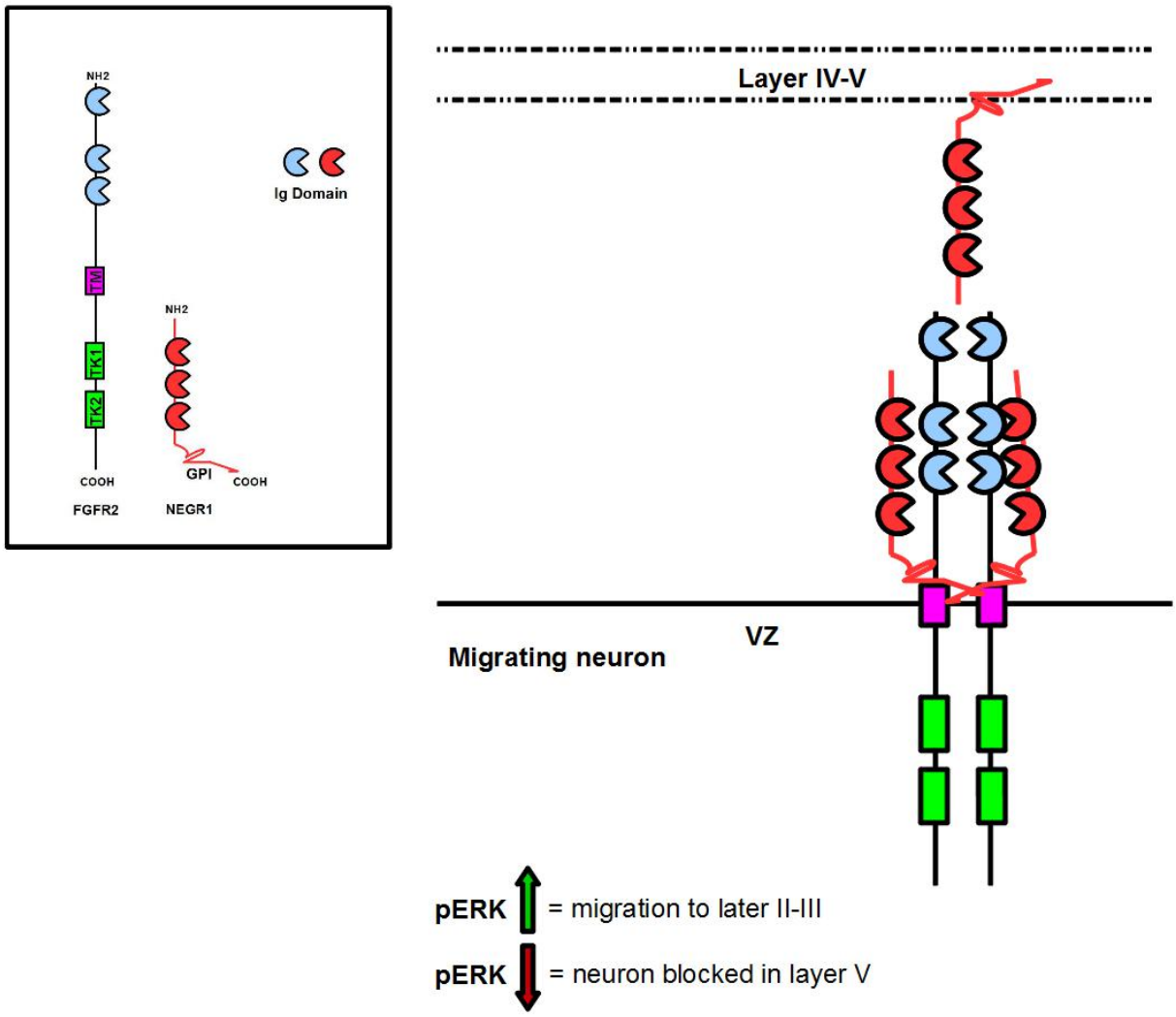

Fig. 32. Model for migration. Negr1-FGFR2 is important for the proper migration of neurons from ventricular zone to cortical layer II-III.

6.CONCLUSION

ASD affects 0.9% of children, and it is recognized as the most genetic of all developmental neuropsychiatric syndromes (82-92% accordance in monozygotic twins, 90% familiar component). Interestingly, many genes associated with ASD are fundamental in establishing neuronal networks, and connectivity dysfunctions are causative alterations in ASD.

Cell adhesion molecules (CAM) and FGFR members drive neuronal wiring during development and thus not surprisingly mutations in CAM and FGFR proteins have been widely identified as ASD risk factors. In detail, mutations in NEGR1 and FGFR2 genes have been recently indicated as relevant ASD candidates. Therefore, given the functional, physical and genetic correlation among Negr1 and FGFR2, the study of Negr1 may disclose a pathway where different risk factors for autism converge and therefore result in a powerful tool to disclose the pathogenesis of ASD.

Early educational intervention is the cornerstone for ASD management, indicating an early temporal window during development for successful therapy. On the other hand, huge effort has been spent to delineate a pharmacological treatment for ASD.

Yet, only antipsychotics Risperidone and Aripiprazole are currently accepted as treatments. Moreover, these drugs only address comorbid clinical symptoms, rather than the underlying ASD pathology. Large evidence points to defects in the development of neuronal networks as underlying causes of ASD. Thus, understanding the molecular mechanisms underlying Negr1 signaling in physiological and pathological brain will possibly pave the way to clarifying the developmental aspect at the basis of ASD. Finally, our study will directly tackle whether somatosensory deficits contribute to social impairment in ASD, addressing a big issue in the field. Our project will open new fields of research for the design of alternative pharmacological treatments.

7. EXPERIMENTAL PROCEDURES

Constructs generation for Lentivirus production and *in utero* electroporation. Negr1 and FGFR2 target sequences were identified, synthesized and cloned into GFP-expressing pLVTH, as previously described (Bauer et al., 2009; Pischedda et al., 2013; Zhou et al., 2006). All recombinant lentiviruses were produced by transient transfection of HEK293T cells according to standard protocols (Wiznerowicz and Trono, 2003). Primary neuronal cultures were transduced with viruses at multiplicity of infection (MOI) 3 if not otherwise specified. mNegr1 cDNA (Addgene clone C3342IRCKp5014P057-rzpdm13-21) was cloned into strep-FLAG pcDNA3.1 vector (Gloeckner et al., 2009). FGFR2 cDNA has been purchased from GeneCopoeia [ORF expression clone for FGFR2 (NM_010207.2)].

Negr1 purification and deglycosylation. For protein purification, HEK293 cells transfected with strep-FLAG Negr1 were lysed in RIPA buffer (150mM NaCl, 50mM HEPES, 0,5% NP40, 1% Sodium-deoxycholate) for one hour at 4°C and then processed for streptavidin immunoprecipitation. Protein were eluted from STREP resin in elution buffer (2.5 mM Desthiobiotin, 100 mM Tris-HCL, 150mM NaCl, 1mM EDTA) in mild agitation for one hour at 4°C. The protein concentration was measured via standard Bradford assay (Bio-Rad) and protein purity was assessed by SDS-PAGE followed by silver staining. Where indictaed, after purification strep-FLAG Negr1 was treated with PNGase F (5 units, 20 minutes, 37°C) (Sigma-Aldrich, Germany) and then analyzed by western blotting.

Neuronal cultures and drugs. The cortical neuron cultures were prepared from embryonic day 16 (E16) wild type CD1 mouse cortex (Harlan, Udine, Italy). E0 was considered the day at which the copulation plug was observed in the mother. One day before the dissection day (D-day), the

coverslips were placed in 24-well plates (First multiwell plate, Euroclone), coated and incubated for no more than 16 hours with 250 µl/coverslip of poly-L-lysine (Sigma Aldrich) 50µg/ml in PBS buffer pH 7.4. On D-day the polylysine solution was removed and the coverlips were rinsed three times with sterile water, 10 minutes for each wash. After the last wash, the water was removed. The pregnant dam was killed using approved methods of euthanasia and the fetuses were removed from the uterus. The dissected brains were placed in a sterile 50 ml falcon containing ice cold HBSS 1X (HBSS 10X (Invitrogen) + HEPES 10mM pH 7.3 + 1%Pen/Strep) and kept in ice.

Using a dissecting microscope, the two hemispheres were separated, meninges and striatum removed, and the cortex dissected out. The cortexes were placed in a 15-ml conical centrifuge tube containing ice cold HBSS 1X. Working under a laminar flow hood, the cortexes were rinsed with 5 ml 37°C sterile HBSS 1X medium for three times. After the last wash, the medium was removed and the dissociating solution was added (9 ml 37°C HBSS 1X + 1 ml trypsin 10X).

After 15 minutes of incubation in a water bath at 37$_{o}$C the trypsine solution was gently removed leaving the cortexes at the bottom of the tube. The cortexes dissociation was made in 5 ml final volume of HBSS 1X by repeatedly pipetting them up and down in a Pasteur pipette.

Once the cortical neurons were separated, the cell density was calculated. An appropriate neuron complete medium (Neurobasal (Invitrogen) + 1% L-Glutamine + 1% Pen/Strep + B27 50X (Invitrogen)) volume containing 100.000 cells was added to each well containing the treated coverslip. The neurons in 24-well plates were used for IHC. For the biochemistry experiments, 300.000 cells were added in 1ml of medium and plated in 12-well plates (Euroclone). The neurons were maintained at 37°C and 5% CO_2 and the medium was changed once, three days after the dissection. In these cultures glial growth is reduced to less than 0.5% of the nearly pure neuronal population (Brewer et al., 1993). Neurons were treated daily with FGFb 20 ng/ml, FGF7/KGF 20 ng/ml, IGF 5 ng/ml (all from Peprotech, NJ USA) or every second day with GI 254023X 20mM (TOCRIS Bioscience, UK) or MEK inhibitor U0126 100nM (Sigma-Aldrich, Germany). Strep-

FLAG-Negr1 treatment, 40ng/ml, was performed at DIV10. All procedures involving animals complied with ARRIVE guidelines and were performed according to the National and Istitutional Animal regulation (IACUC 625).

HEK cells and cortical neurons co-culture. At DIV14 on cortical neurons culture HEK293T cells were seeded in ratio 300.000 neurons/100.000 HEK293 cells (3:1). For ERK kinases phosphorylation experiments cells were transfected with control vector or with Negr1 cDNA. Mixed cultures were cultured until DIV16 and then lysed and processed for western-blotting.

Membrane fractionation. Primary neuronal cultures were plated in 12 well plates (Euroclone) at the density of 600.000 cells *per* well and then transduced with siCTRL and siNEGR1 viruses at MOI 3 on DIV 1. Neurons on DIV 16 were then resuspended in 600 ul of isosmotic buffer (4mM HEPES, 32mM SUCROSE in PBS 1X) and spottered 10 times with glass potter. Then lysate was centrifuged for 10 minutes at 600g to separate nuclei (pellet). The supernatant was then centrifuged at 100.000g for 1 hour to separate citosol (supernatant) from membrane (pellet). The pellet was then lysed in RIPA buffer (150mM NaCl, 50mM HEPES, 0,5% NP40, 1% Sodium-deoxycholate) and processed for biochemical analysis.

Biochemistry and antibody. Neurons were washed in PBS and lysed in RIPA buffer (150mM NaCl, 50mM HEPES, 0,5% NP40, 1% Sodium-deoxycholate). After 1 h under mild agitation, lysate was clarified by centrifugation for 20 min at 16,000g. All procedures were performed at 4 °C. Protein sample were measured via standard Bradford assay (Bio-Rad. USA). For protein identification and relative quantification via Western blotting, a proper volume of sample containing an equal amount of proteins was diluted with 0.25% 5X Laemmli buffer and loaded onto 10% SDS-PAGE gels; the proteins were transferred onto nitrocellulose membrane (Sigma-Aldrich)

at 80 V for 120 min at 4 °C. The primary antibodies were applied overnight in a blocking buffer (20 mM Tris, pH 7.4, 150 mM NaCl, 0.1% Tween 20, and 5% nonfat dry milk); primary antibodies (source in parentheses) included rabbit anti- FGFR2 1:200 (Santa Cruz Biotechnology, USA), goat anti-Negr1 1:1000 (R&D, USA), mouse anti-NCAM 1:1000 (BD Biosciences, USA), rabbit anti-GFP 1:5000 (Life Technology, USA), mouse anti-Actin 1:2000 (Sigma-Aldrich), rabbit anti RpS6 1:2000, rabbit antip42/44(pERK) and rabbit anti-42/44 (ERK) (Cell Signaling, USA).

The secondary antibodies (HRP-conjugated anti-mouse, anti-rabbit, or anti-rat) (Jackson ImmunoResearch, UK) were used in a ratio of 1:8000. The signal was detected using an ECL detection system (GE Healthcare). Films were acquired on a GS-800 densitometer (BioRad) calibrated following the manufacturers' instructions, and protein abundance was estimated as a function of the optical density of a specific band quantified by ImageJ software (NIH). Unless otherwise stated, all the other chemicals were purchased from Applichem, Germany.

Cross-link assay. The N2A cells were cultured in monolayer in IWAKI plates (10 cm diameter) in 10 ml of culture medium DMEM (Dulbecco's Minimum Essential Medium) containing glutamine (2 mM), antibiotic (1% Penicillin/Streptomycin), and enriched with decomplemented fetal bovine serum (FBS) at 10%. Formaldehyde to a final concentration of 0.8% was added directly in the culture medium and the 10 ml dishes were put under mild agitation for 10 minutes at room temperature. Then glycine was added to a final concentration of 125 mM to neutralize the effect of formaldehyde. The plates were again put under mild agitation at room temperature for 10 minutes. Finally the cells were lysed in a lysis buffer containing 150 mM NaCl, 50 mM Hepes and 0.2% Triton X-100 and placed in agitation for 1 hour at 4°C. Finally the lysate was spin at 16.000g 10 minutes at 4°C.

Strep-IP. Streptactin Superflow beads (IBA) (50% in ethanol) were diluted 1:1 with wash buffer

containing NaCl 150 mM and Hepes 50 mM and centrifuged for 2 minutes at 2000g to purify the resine from ethanol. For a 10 ml dish we used 40 µl of purified beads. The lysate was added to the beads and put under mild agitation for 1 hour at 4°C . After the incubation the resine was washed twice with a wash buffer containing NaCl 150 mM, Hepes 50 mM, 0,1% Triton X-100. A brief centrifugation at 2000g followed each wash. Finally the resine was resuspended in 60 µl of SB2X.

Overlay assay. Living wild-type and FGFR2 over-expressing HEK cells were incubated with 1ug/ml of purified recombinant FLAG-Negr1 protein at 4°C for 1hour to increase the binding and at the same time reduce FGFR2 internalization. After 4°C incubation, cells were then treated with 20 ng/ml FGFb (peprotec) and put at 37°C for two hours to stimulate receptor internalization. Then cells were fixed in 4% paraformaldehyde-sucrose in PBS1X and incubated with anti-FLAG antibody. The fluorescence images were acquired using a LSM Zeiss 510 confocal microscope with Zeiss 20X objective (Karl Zeiss, Jena, Germany).

Co-clustering assay. Strep-FLAG-Negr1 and wt cells were dissociated in a solution not permissive for cell-to-cell aggregation (2 mM EDTA in PBS) and collected in eppendorf tubes. Then cells were counted and re-suspended in cell to cell adhesion permissive medium (HBSS 1X, MgCl 2 mM, CaCl 2 mM) at a concentration of 4 $x10_6$ cells/ml. Then 50.000 cells were seeded and incubated for 30 minutes at 37°C in a 24-well plate with coverslips. After the incubation, cells were fixed with a solution of paraformaldehyde (4%), sucrose (4%) and phosphate buffer (240 mM) for 10 minutes at room temperature.

Immunofluorescence and quantification. Neuronal cultures were infected with viruses at days in vitro (DIV) 1-2 or transfected at DIV4 with Lipofectamine 2000 following manifacture's protocol (Life Technology). For the immunostaining experiments, neurons were fixed at DIV 18 in 4% paraformaldehyde and 4% sucrose at room temperature. GFP positive neurons were randomly

chosen for quantification. The fluorescence images were acquired using a LSM Zeiss 510 confocal microscope with Zeiss 63X objective (Karl Zeiss, Jena, Germany) at a resolution of 2,048x2,048pixels, pixel size=0.098 mm. All the measurements were performed using NeuronStudio (available at http://research.mssm.edu/cnic/tools.html). Neurites were automatically traced and quantified by the software in terms of length, number and morphology (Rodriguez et al., 2008; Wearne et al., 2005). Data were then logged and analysed in Microsoft Excel.

***In Utero* Electroporation.** All experimental procedures and animal care were conducted in accordance with the IIT licensing and the Italian Ministry of Health. *In utero* electroporation was performed accordingly to our recent protocol (Szczurkowska et al., under revision in Nature Protocols, APPENDIX 6). Briefly, E13.5 and E15.5 timed-pregnant CD1 mice (Charles River SRL, Italy) were anesthetized with isoflurane (induction, 4.0%; surgery, 2.5%), and the uterine horns were exposed by laparotomy. The DNA (1.0 μg/μl in water) together with the dye Fast Green (0.3 mg/ml; Sigma, St. Louis, MO) was injected (3-4 μl) into right lateral ventricle of each embryos by glass micropipette at E13.5 (World Precision Instruments, USA) or a 30G needle at E15.5 (Pic indolor, Grandate, Italy). The embryo's head was carefully held between tweezer-type circular electrodes (3 mm diameter; Nepa Gene, Chiba, Japan) and 6 electric pulses were delivered with square-wave electroporation generator (CUY21EDIT; Nepa Gene) accordingly to electroporation protocol (amplitude, 25 and 30 V for E13.5 and E15.5, respectively; duration, 50 ms; intervals, 1s) After electroporation, embryos were handed back into the dam's abdominal cavity which allowed their further development.

Slice Histology and Immunostaining. E18 brains were dissected and fixed at least 24 hrs in 4 % PFA in PBS. P7 brains were fixed by transcardial perfusion of 4% PFA in PBS and cryopreserved in 30 % sucrose. Coronal sections 80 μm thick were obtained with a microtome-refrigerator

(Microm HM 450 Sliding Microtome equipped with Freezing Unit Microm KS34, Thermo Scientific). Free-floating sections first underwent antigen retrival in 10mM citric acid (pH6) for 10min at 95°C. Subsequently slices were permeabilized and blocked with PBS containing 0.3% Triton X-100 and 10% NGS. Primary antibodies were incubated in PBS containing 0.3% Triton X-100 and 5% NGS [rat anti-CTIP2, 1:100 (Abcam), rabbit anti-Cux1, 1:100 (Santa Cruz), rabbit anti-cFos, 1:1000 (Abcam)]. Immunostaining was detected using Alexa 543 or Alexa 647 fluorescent secondary antibody (Invitrogen), 1:600, incubated in PBS containing 0.3% Triton X-100 and 5 % NGS. Subsequently, cell-permeant nuclear counterstain was performed with Hoechst (2,5 μg/μL; Sigma). Finally, samples were mounted in Vectashield Mounting Medium (Vector Laboratories, Burlingame, CA) and acquired with confocal microscopy.

Statistical analysis

All data are expressed as mean ± SEM. Data were analyzed with an unpaired Student's t test (two classes) or ANOVA followed by Tuckey's post hoc test (more than two classes). The indication of the level of significance (p) are indicated throughout the text. For the analysis of neurons morphology in the different experimental condition we considered at least 12 cells randomly chosen in at least 4 experiments.

8.BIBLIOGRAPHY

Alfandari, D., H. Cousin, A. Gaultier, K. Smith, J. M. White, T. Darribère, e D. W. DeSimone. 2001. «Xenopus ADAM 13 Is a Metalloprotease Required for Cranial Neural Crest-Cell Migration». *Current Biology: CB* 11 (12): 918–30.

Ayala, Ramsés, Tianzhi Shu, e Li-Huei Tsai. 2007. «Trekking across the Brain: The Journey of Neuronal Migration». *Cell* 128 (1): 29–43. doi:10.1016/j.cell.2006.12.021.

Banerjee, Swati, Maeveen Riordan, e Manzoor A. Bhat. 2014. «Genetic Aspects of Autism Spectrum Disorders: Insights from Animal Models». *Frontiers in Cellular Neuroscience* 8: 58. doi:10.3389/fncel.2014.00058.

Barkovich, A. J., e B. O. Kjos. 1992. «Gray Matter Heterotopias: MR Characteristics and Correlation with Developmental and Neurologic Manifestations». *Radiology* 182 (2): 493–99. doi:10.1148/radiology.182.2.1732969.

Bechara, Ahmad, Julien Falk, Frédéric Moret, e Valérie Castellani. 2007. «Modulation of Semaphorin Signaling by Ig Superfamily Cell Adhesion Molecules». *Advances in Experimental Medicine and Biology* 600: 61–72. doi:10.1007/978-0-387-70956-7_6.

Black, Roy A. 2002. «Tumor Necrosis Factor-Alpha Converting Enzyme». *The International Journal of Biochemistry & Cell Biology* 34 (1): 1–5.

Bonfanti, Luca. 2006. «PSA-NCAM in Mammalian Structural Plasticity and Neurogenesis». *Progress in Neurobiology* 80 (3): 129–64. doi:10.1016/j.pneurobio.2006.08.003.

Bony, Guillaume, Joanna Szczurkowska, Ilaria Tamagno, Maya Shelly, Andrea Contestabile, e Laura Cancedda. 2013. «Non-Hyperpolarizing GABAB Receptor Activation Regulates Neuronal Migration and Neurite Growth and Specification by cAMP/LKB1». *Nature Communications* 4: 1800. doi:10.1038/ncomms2820.

Borello, Ugo, Inma Cobos, Jason E. Long, John R. McWhirter, Cornelis Murre, e John L. R. Rubenstein. 2008. «FGF15 Promotes Neurogenesis and Opposes FGF8 Function during Neocortical Development». *Neural Development* 3: 17. doi:10.1186/1749-8104-3-17.

Bozyczko, D., e A. F. Horwitz. 1986. «The Participation of a Putative Cell Surface Receptor for Laminin and Fibronectin in Peripheral Neurite Extension». *The Journal of Neuroscience: The Official Journal of the Society for Neuroscience* 6 (5): 1241–51.

Brennaman, Leann H., Marcia L. Moss, e Patricia F. Maness. 2014. «EphrinA/EphA-Induced Ectodomain Shedding of Neural Cell Adhesion Molecule Regulates Growth Cone Repulsion through ADAM10 Metalloprotease». *Journal of Neurochemistry* 128 (2): 267–79. doi:10.1111/jnc.12468.

Buxbaum, J. D., K. N. Liu, Y. Luo, J. L. Slack, K. L. Stocking, J. J. Peschon, R. S. Johnson, B. J. Castner, D. P. Cerretti, e R. A. Black. 1998. «Evidence That Tumor Necrosis Factor Alpha Converting Enzyme Is Involved in Regulated Alpha-Secretase Cleavage of the Alzheimer Amyloid Protein Precursor». *The Journal of Biological Chemistry* 273 (43): 27765–67.

Cancedda, Laura, Hubert Fiumelli, Karen Chen, e Mu-ming Poo. 2007. «Excitatory GABA Action Is Essential for Morphological Maturation of Cortical Neurons in Vivo». *The Journal of Neuroscience: The Official Journal of the Society for Neuroscience* 27 (19): 5224–35. doi:10.1523/JNEUROSCI.5169-06.2007.

Casey, Jillian P., Tiago Magalhaes, Judith M. Conroy, Regina Regan, Naisha Shah, Richard Anney, Denis C. Shields, et al. 2012. «A Novel Approach of Homozygous Haplotype Sharing Identifies Candidate Genes in Autism Spectrum Disorder». *Human Genetics* 131 (4): 565–79. doi:10.1007/s00439-011-1094-6.

Cavallaro, Ugo, e Elisabetta Dejana. 2011. «Adhesion Molecule Signalling: Not Always a Sticky Business». *Nature Reviews. Molecular Cell Biology* 12 (3): 189–97. doi:10.1038/nrm3068.

Chantry, A., N. A. Gregson, e P. Glynn. 1989. «A Novel Metalloproteinase Associated with Brain Myelin Membranes. Isolation and Characterization». *The Journal of Biological Chemistry*

264 (36): 21603–7.
Cheung, Giselle, Oana Chever, e Nathalie Rouach. 2014. «Connexons and Pannexons: Newcomers in Neurophysiology». *Frontiers in Cellular Neuroscience* 8: 348. doi:10.3389/fncel.2014.00348.
Cholfin, Jeremy A., e John L. R. Rubenstein. 2007. «Genetic Regulation of Prefrontal Cortex Development and Function». *Novartis Foundation Symposium* 288: 165–73; discussion 173–77, 276–81.
Christensen, Claus, Jes B. Lauridsen, Vladimir Berezin, Elisabeth Bock, e Vladislav V. Kiselyov. 2006. «The Neural Cell Adhesion Molecule Binds to Fibroblast Growth Factor Receptor 2». *FEBS Letters* 580 (14): 3386–90. doi:10.1016/j.febslet.2006.05.008.
Connolly, J. L., P. J. Seeley, e L. A. Greene. 1985. «Regulation of Growth Cone Morphology by Nerve Growth Factor: A Comparative Study by Scanning Electron Microscopy». *Journal of Neuroscience Research* 13 (1-2): 183–98. doi:10.1002/jnr.490130113.
Copp, A. J., e B. N. Harding. 1999. «Neuronal Migration Disorders in Humans and in Mouse Models--an Overview». *Epilepsy Research* 36 (2-3): 133–41.
Diestel, Simone, C. Leann Hinkle, Brigitte Schmitz, e Patricia F. Maness. 2005. «NCAM140 Stimulates Integrin-Dependent Cell Migration by Ectodomain Shedding». *Journal of Neurochemistry* 95 (6): 1777–84. doi:10.1111/j.1471-4159.2005.03475.x.
Diez del Corral, Ruth, Isabel Olivera-Martinez, Anne Goriely, Emily Gale, Malcolm Maden, e Kate Storey. 2003. «Opposing FGF and Retinoid Pathways Control Ventral Neural Pattern, Neuronal Differentiation, and Segmentation during Body Axis Extension». *Neuron* 40 (1): 65–79.
Ditlevsen, Dorte Kornerup, Sylwia Owczarek, Vladimir Berezin, e Elisabeth Bock. 2008. «Relative Role of Upstream Regulators of Akt, ERK and CREB in NCAM- and FGF2-Mediated Signalling». *Neurochemistry International* 53 (5): 137–47. doi:10.1016/j.neuint.2008.06.011.
Doherty, P, M S Fazeli, e F S Walsh. 1995. «The neural cell adhesion molecule and synaptic plasticity». *Journal of neurobiology* 26 (3): 437–46. doi:10.1002/neu.480260315.
Evsyukova, Irina, Charlotte Plestant, e E. S. Anton. 2013. «Integrative Mechanisms of Oriented Neuronal Migration in the Developing Brain». *Annual Review of Cell and Developmental Biology* 29: 299–353. doi:10.1146/annurev-cellbio-101512-122400.
Fiol, C. J., J. S. Williams, C. H. Chou, Q. M. Wang, P. J. Roach, e O. M. Andrisani. 1994. «A Secondary Phosphorylation of CREB341 at Ser129 Is Required for the cAMP-Mediated Control of Gene Expression. A Role for Glycogen Synthase Kinase-3 in the Control of Gene Expression». *The Journal of Biological Chemistry* 269 (51): 32187–93.
Fischer, J., e K. Hammerschmidt. 2011. «Ultrasonic Vocalizations in Mouse Models for Speech and Socio-Cognitive Disorders: Insights into the Evolution of Vocal Communication». *Genes, Brain, and Behavior* 10 (1): 17–27. doi:10.1111/j.1601-183X.2010.00610.x.
Flint, A. C., e A. R. Kriegstein. 1997. «Mechanisms Underlying Neuronal Migration Disorders and Epilepsy». *Current Opinion in Neurology* 10 (2): 92–97.
Folstein, S. E., e B. Rosen-Sheidley. 2001. «Genetics of Autism: Complex Aetiology for a Heterogeneous Disorder». *Nature Reviews. Genetics* 2 (12): 943–55. doi:10.1038/35103559.
Ford-Perriss, M, H Abud, e M Murphy. 2001. «Fibroblast growth factors in the developing central nervous system». *Clinical and experimental pharmacology & physiology* 28 (7): 493–503.
Francavilla, Chiara, Paola Cattaneo, Vladimir Berezin, Elisabeth Bock, Diletta Ami, Ario de Marco, Gerhard Christofori, e Ugo Cavallaro. 2009. «The Binding of NCAM to FGFR1 Induces a Specific Cellular Response Mediated by Receptor Trafficking». *The Journal of Cell Biology* 187 (7): 1101–16. doi:10.1083/jcb.200903030.
Francavilla, Chiara, Sébastien Loeffler, Daniele Piccini, Angelika Kren, Gerhard Christofori, e Ugo Cavallaro. 2007. «Neural Cell Adhesion Molecule Regulates the Cellular Response to

Fibroblast Growth Factor». *Journal of Cell Science* 120 (Pt 24): 4388–94. doi:10.1242/jcs.010744.
Fujita, Eriko, Yuko Tanabe, Akira Shiota, Masatsugu Ueda, Kiyotaka Suwa, Mariko Y. Momoi, e Takashi Momoi. 2008. «Ultrasonic Vocalization Impairment of Foxp2 (R552H) Knockin Mice Related to Speech-Language Disorder and Abnormality of Purkinje Cells». *Proceedings of the National Academy of Sciences of the United States of America* 105 (8): 3117–22. doi:10.1073/pnas.0712298105.
Fukuchi-Shimogori, T., e E. A. Grove. 2001. «Neocortex Patterning by the Secreted Signaling Molecule FGF8». *Science (New York, N.Y.)* 294 (5544): 1071–74. doi:10.1126/science.1064252.
Funatsu, N, S Miyata, H Kumanogoh, M Shigeta, K Hamada, Y Endo, Y Sokawa, e S Maekawa. 1999. «Characterization of a novel rat brain glycosylphosphatidylinositol-anchored protein (Kilon), a member of the IgLON cell adhesion molecule family». *The Journal of biological chemistry* 274 (12): 8224–30.
Garel, Sonia, Kelly J. Huffman, e John L. R. Rubenstein. 2003. «Molecular Regionalization of the Neocortex Is Disrupted in Fgf8 Hypomorphic Mutants». *Development (Cambridge, England)* 130 (9): 1903–14.
Genç, Bariş, P. Hande Ozdinler, April E. Mendoza, e Reha S. Erzurumlu. 2004. «A Chemoattractant Role for NT-3 in Proprioceptive Axon Guidance». *PLoS Biology* 2 (12): e403. doi:10.1371/journal.pbio.0020403.
Gil, O D, G Zanazzi, A F Struyk, e J L Salzer. 1998. «Neurotrimin mediates bifunctional effects on neurite outgrowth via homophilic and heterophilic interactions». *The Journal of neuroscience: the official journal of the Society for Neuroscience* 18 (22): 9312–25.
Gil, Orlando D, Li Zhang, Suzanne Chen, Y Q Ren, Aurea Pimenta, George Zanazzi, Dean Hillman, Pat Levitt, e James L Salzer. 2002. «Complementary expression and heterophilic interactions between IgLON family members neurotrimin and LAMP». *Journal of neurobiology* 51 (3): 190–204. doi:10.1002/neu.10050.
Girirajan, Santhosh, Jill A. Rosenfeld, Bradley P. Coe, Sumit Parikh, Neil Friedman, Amy Goldstein, Robyn A. Filipink, et al. 2012. «Phenotypic Heterogeneity of Genomic Disorders and Rare Copy-Number Variants». *The New England Journal of Medicine* 367 (14): 1321–31. doi:10.1056/NEJMoa1200395.
Glessner, Joseph T., Kai Wang, Guiqing Cai, Olena Korvatska, Cecilia E. Kim, Shawn Wood, Haitao Zhang, et al. 2009. «Autism Genome-Wide Copy Number Variation Reveals Ubiquitin and Neuronal Genes». *Nature* 459 (7246): 569–73. doi:10.1038/nature07953.
Goetz, Regina, e Moosa Mohammadi. 2013. «Exploring Mechanisms of FGF Signalling through the Lens of Structural Biology». *Nature Reviews. Molecular Cell Biology* 14 (3): 166–80. doi:10.1038/nrm3528.
Gulia, Kamalesh K., Niraj Patel, Arathi Radhakrishnan, e Velayudhan Mohan Kumar. 2014. «Reduction in Ultrasonic Vocalizations in Pups Born to Rapid Eye Movement Sleep Restricted Mothers in Rat Model». *PloS One* 9 (1): e84948. doi:10.1371/journal.pone.0084948.
Gundersen, R. W., e J. N. Barrett. 1979. «Neuronal Chemotaxis: Chick Dorsal-Root Axons Turn toward High Concentrations of Nerve Growth Factor». *Science (New York, N.Y.)* 206 (4422): 1079–80.
Harmer, Nicholas J., Leopold L. Ilag, Barbara Mulloy, Luca Pellegrini, Carol V. Robinson, e Tom L. Blundell. 2004. «Towards a Resolution of the Stoichiometry of the Fibroblast Growth Factor (FGF)-FGF Receptor-Heparin Complex». *Journal of Molecular Biology* 339 (4): 821–34. doi:10.1016/j.jmb.2004.04.031.
Hasegawa, Hiroshi, Shizuko Ashigaki, Masako Takamatsu, Rika Suzuki-Migishima, Norihiko Ohbayashi, Nobuyuki Itoh, Shinji Takada, e Yasuto Tanabe. 2004. «Laminar Patterning in

the Developing Neocortex by Temporally Coordinated Fibroblast Growth Factor Signaling». *The Journal of Neuroscience: The Official Journal of the Society for Neuroscience* 24 (40): 8711–19. doi:10.1523/JNEUROSCI.3070-04.2004.

Hashimoto, Takashi, Shohei Maekawa, e Seiji Miyata. 2009. «IgLON cell adhesion molecules regulate synaptogenesis in hippocampal neurons». *Cell Biochemistry and Function* 27 (7): 496–98. doi:10.1002/cbf.1600.

Hashimoto, Takashi, Mayumi Yamada, Shohei Maekawa, Toshihiro Nakashima, e Seiji Miyata. 2008. «IgLON cell adhesion molecule Kilon is a crucial modulator for synapse number in hippocampal neurons». *Brain Research* 1224 (agosto): 1–11. doi:10.1016/j.brainres.2008.05.069.

Haupt, Corinna, e Andrea B. Huber. 2008. «How Axons See Their Way--Axonal Guidance in the Visual System». *Frontiers in Bioscience: A Journal and Virtual Library* 13: 3136–49.

Hausott, Barbara, Isil Kurnaz, Srecko Gajovic, e Lars Klimaschewski. 2009. «Signaling by Neuronal Tyrosine Kinase Receptors: Relevance for Development and Regeneration». *Anatomical Record (Hoboken, N.J.: 2007)* 292 (12): 1976–85. doi:10.1002/ar.20964.

Hébert, Jean M., e Gord Fishell. 2008. «The Genetics of Early Telencephalon Patterning: Some Assembly Required». *Nature Reviews. Neuroscience* 9 (9): 678–85. doi:10.1038/nrn2463.

Hinkle, C. Leann, Simone Diestel, Jeffrey Lieberman, e Patricia F. Maness. 2006. «Metalloprotease-Induced Ectodomain Shedding of Neural Cell Adhesion Molecule (NCAM)». *Journal of Neurobiology* 66 (12): 1378–95. doi:10.1002/neu.20257.

Hussman, John P., Ren-Hua Chung, Anthony J. Griswold, James M. Jaworski, Daria Salyakina, Deqiong Ma, Ioanna Konidari, et al. 2011. «A Noise-Reduction GWAS Analysis Implicates Altered Regulation of Neurite Outgrowth and Guidance in Autism». *Molecular Autism* 2 (1): 1. doi:10.1186/2040-2392-2-1.

Inglis-Broadgate, Suzanne L., Rachel E. Thomson, Francesca Pellicano, Michael A. Tartaglia, Charlie C. Pontikis, Jonathan D. Cooper, e Tomoko Iwata. 2005. «FGFR3 Regulates Brain Size by Controlling Progenitor Cell Proliferation and Apoptosis during Embryonic Development». *Developmental Biology* 279 (1): 73–85. doi:10.1016/j.ydbio.2004.11.035.

Izumi, Y., M. Hirata, H. Hasuwa, R. Iwamoto, T. Umata, K. Miyado, Y. Tamai, et al. 1998. «A Metalloprotease-Disintegrin, MDC9/meltrin-gamma/ADAM9 and PKCdelta Are Involved in TPA-Induced Ectodomain Shedding of Membrane-Anchored Heparin-Binding EGF-like Growth Factor». *The EMBO Journal* 17 (24): 7260–72. doi:10.1093/emboj/17.24.7260.

Jessell, T. M. 1988. «Adhesion Molecules and the Hierarchy of Neural Development». *Neuron* 1 (1): 3–13.

Jones, Edward G. 1995. *Development of the Cerebral Cortex*.

Jorissen, Ellen, Johannes Prox, Christian Bernreuther, Silvio Weber, Ralf Schwanbeck, Lutgarde Serneels, An Snellinx, et al. 2010. «The Disintegrin/metalloproteinase ADAM10 Is Essential for the Establishment of the Brain Cortex». *The Journal of Neuroscience: The Official Journal of the Society for Neuroscience* 30 (14): 4833–44. doi:10.1523/JNEUROSCI.5221-09.2010.

Ju, Anes, Kurt Hammerschmidt, Martesa Tantra, Dilja Krueger, Nils Brose, e Hannelore Ehrenreich. 2014. «Juvenile Manifestation of Ultrasound Communication Deficits in the Neuroligin-4 Null Mutant Mouse Model of Autism». *Behavioural Brain Research* 270 (agosto): 159–64. doi:10.1016/j.bbr.2014.05.019.

Kaminsky, Erin B., Vineith Kaul, Justin Paschall, Deanna M. Church, Brian Bunke, Dawn Kunig, Daniel Moreno-De-Luca, et al. 2011. «An Evidence-Based Approach to Establish the Functional and Clinical Significance of Copy Number Variants in Intellectual and Developmental Disabilities». *Genetics in Medicine: Official Journal of the American College of Medical Genetics* 13 (9): 777–84. doi:10.1097/GIM.0b013e31822c79f9.

Kang, Wenfei, Li Chin Wong, Song-Hai Shi, e Jean M Hébert. 2009. «The transition from radial

glial to intermediate progenitor cell is inhibited by FGF signaling during corticogenesis». *The Journal of neuroscience: the official journal of the Society for Neuroscience* 29 (46): 14571–80. doi:10.1523/JNEUROSCI.3844-09.2009.

Katoh, Masaru. 2009. «FGFR2 Abnormalities Underlie a Spectrum of Bone, Skin, and Cancer Pathologies». *The Journal of Investigative Dermatology* 129 (8): 1861–67. doi:10.1038/jid.2009.97.

Kettunen, Päivi, Bradley Spencer-Dene, Tomasz Furmanek, Inger Hals Kvinnsland, Clive Dickson, Irma Thesleff, e Keijo Luukko. 2007. «Fgfr2b Mediated Epithelial-Mesenchymal Interactions Coordinate Tooth Morphogenesis and Dental Trigeminal Axon Patterning». *Mechanisms of Development* 124 (11-12): 868–83. doi:10.1016/j.mod.2007.09.003.

Kiselyov, Vladislav V., Vladislav Soroka, Vladimir Berezin, e Elisabeth Bock. 2005. «Structural Biology of NCAM Homophilic Binding and Activation of FGFR». *Journal of Neurochemistry* 94 (5): 1169–79. doi:10.1111/j.1471-4159.2005.03284.x.

Kochoyan, Artur, Flemming M. Poulsen, Vladimir Berezin, Elisabeth Bock, e Vladislav V. Kiselyov. 2008. «Study of the Interaction of the Ig2 Module of the Fibroblast Growth Factor Receptor, FGFR Ig2, with the Fibroblast Growth Factor 1, FGF1, by Means of NMR Spectroscopy». *FEBS Letters* 582 (23-24): 3374–78. doi:10.1016/j.febslet.2008.08.033.

Kriegstein, Arnold R., e Stephen C. Noctor. 2004. «Patterns of Neuronal Migration in the Embryonic Cortex». *Trends in Neurosciences* 27 (7): 392–99. doi:10.1016/j.tins.2004.05.001.

Lai, Jonathan K. Y., Monica Sobala-Drozdowski, Linghong Zhou, Laurie C. Doering, Paul A. Faure, e Jane A. Foster. 2014. «Temporal and Spectral Differences in the Ultrasonic Vocalizations of Fragile X Knock out Mice during Postnatal Development». *Behavioural Brain Research* 259 (febbraio): 119–30. doi:10.1016/j.bbr.2013.10.049.

Letourneau, P. C. 1978. «Chemotactic Response of Nerve Fiber Elongation to Nerve Growth Factor». *Developmental Biology* 66 (1): 183–96.

Levitt, P. 1984. «A monoclonal antibody to limbic system neurons». *Science (New York, N.Y.)* 223 (4633): 299–301.

Lin, Yongshun, Lijie Chen, Chunhong Lin, Yongde Luo, Robert Y. L. Tsai, e Fen Wang. 2009. «Neuron-Derived FGF9 Is Essential for Scaffold Formation of Bergmann Radial Fibers and Migration of Granule Neurons in the Cerebellum». *Developmental Biology* 329 (1): 44–54. doi:10.1016/j.ydbio.2009.02.011.

Li, Rongyu, e Georg Reiser. 2011. «Phosphorylation of Ser45 and Ser59 of αB-Crystallin and p38/extracellular Regulated Kinase Activity Determine αB-Crystallin-Mediated Protection of Rat Brain Astrocytes from C2-Ceramide- and Staurosporine-Induced Cell Death». *Journal of Neurochemistry* 118 (3): 354–64. doi:10.1111/j.1471-4159.2011.07317.x.

Lodge, A. P., M. R. Howard, C. J. McNamee, e D. J. Moss. 2000. «Co-Localisation, Heterophilic Interactions and Regulated Expression of IgLON Family Proteins in the Chick Nervous System». *Brain Research. Molecular Brain Research* 82 (1-2): 84–94.

Maccarrone, Giuseppina, Claudia Ditzen, Alexander Yassouridis, Christiane Rewerts, Manfred Uhr, Mathias Uhlen, Florian Holsboer, e Christoph W. Turck. 2013. «Psychiatric Patient Stratification Using Biosignatures Based on Cerebrospinal Fluid Protein Expression Clusters». *Journal of Psychiatric Research* 47 (11): 1572–80. doi:10.1016/j.jpsychires.2013.07.021.

Maness, Patricia F., e Melitta Schachner. 2007. «Neural Recognition Molecules of the Immunoglobulin Superfamily: Signaling Transducers of Axon Guidance and Neuronal Migration». *Nature Neuroscience* 10 (1): 19–26. doi:10.1038/nn1827.

Mann, F., V. Zhukareva, A. Pimenta, P. Levitt, e J. Bolz. 1998. «Membrane-Associated Molecules Guide Limbic and Nonlimbic Thalamocortical Projections». *The Journal of Neuroscience: The Official Journal of the Society for Neuroscience* 18 (22): 9409–19.

Marshall, Christian R., Abdul Noor, John B. Vincent, Anath C. Lionel, Lars Feuk, Jennifer Skaug, Mary Shago, et al. 2008. «Structural Variation of Chromosomes in Autism Spectrum Disorder». *American Journal of Human Genetics* 82 (2): 477–88. doi:10.1016/j.ajhg.2007.12.009.

McKerracher, L., M. Chamoux, e C. O. Arregui. 1996. «Role of Laminin and Integrin Interactions in Growth Cone Guidance». *Molecular Neurobiology* 12 (2): 95–116. doi:10.1007/BF02740648.

McKie, Arthur B., Sebastian Vaughan, Elisa Zanini, Imoh S. Okon, Louay Louis, Camila de Sousa, Mark I. Greene, et al. 2012. «The OPCML Tumor Suppressor Functions as a Cell Surface Repressor-Adaptor, Negatively Regulating Receptor Tyrosine Kinases in Epithelial Ovarian Cancer». *Cancer Discovery* 2 (2): 156–71. doi:10.1158/2159-8290.CD-11-0256.

Mechtersheimer, S., P. Gutwein, N. Agmon-Levin, A. Stoeck, M. Oleszewski, S. Riedle, R. Postina, et al. 2001. «Ectodomain Shedding of L1 Adhesion Molecule Promotes Cell Migration by Autocrine Binding to Integrins». *The Journal of Cell Biology* 155 (4): 661–73. doi:10.1083/jcb.200101099.

Merlos-Suárez, A., S. Ruiz-Paz, J. Baselga, e J. Arribas. 2001. «Metalloprotease-Dependent Protransforming Growth Factor-Alpha Ectodomain Shedding in the Absence of Tumor Necrosis Factor-Alpha-Converting Enzyme». *The Journal of Biological Chemistry* 276 (51): 48510–17. doi:10.1074/jbc.M103488200.

Michaelson, Jacob J., Yujian Shi, Madhusudan Gujral, Hancheng Zheng, Dheeraj Malhotra, Xin Jin, Minghan Jian, et al. 2012. «Whole-Genome Sequencing in Autism Identifies Hot Spots for de Novo Germline Mutation». *Cell* 151 (7): 1431–42. doi:10.1016/j.cell.2012.11.019.

Miles, Judith H. 2011. «Autism Spectrum Disorders--a Genetics Review». *Genetics in Medicine: Official Journal of the American College of Medical Genetics* 13 (4): 278–94. doi:10.1097/GIM.0b013e3181ff67ba.

Miyata, S, N Matsumoto, K Taguchi, A Akagi, T Iino, N Funatsu, e S Maekawa. 2003. «Biochemical and ultrastructural analyses of IgLON cell adhesion molecules, Kilon and OBCAM in the rat brain». *Neuroscience* 117 (3): 645–58.

Mohammadi, Moosa, Shaun K. Olsen, e Regina Goetz. 2005. «A Protein Canyon in the FGF-FGF Receptor Dimer Selects from an à La Carte Menu of Heparan Sulfate Motifs». *Current Opinion in Structural Biology* 15 (5): 506–16. doi:10.1016/j.sbi.2005.09.002.

Neale, Benjamin M., Yan Kou, Li Liu, Avi Ma'ayan, Kaitlin E. Samocha, Aniko Sabo, Chiao-Feng Lin, et al. 2012. «Patterns and Rates of Exonic de Novo Mutations in Autism Spectrum Disorders». *Nature* 485 (7397): 242–45. doi:10.1038/nature11011.

Nguyen, Laurent, e Simon Hippenmeyer. 2014. *Cellular and Molecular Control of Neuronal Migration*.

Ohkubo, Yasushi, Ayumi O. Uchida, Dana Shin, Juha Partanen, e Flora M. Vaccarino. 2004. «Fibroblast Growth Factor Receptor 1 Is Required for the Proliferation of Hippocampal Progenitor Cells and for Hippocampal Growth in Mouse». *The Journal of Neuroscience: The Official Journal of the Society for Neuroscience* 24 (27): 6057–69. doi:10.1523/JNEUROSCI.1140-04.2004.

O'Leary, Dennis D. M., e Yasushi Nakagawa. 2002. «Patterning Centers, Regulatory Genes and Extrinsic Mechanisms Controlling Arealization of the Neocortex». *Current Opinion in Neurobiology* 12 (1): 14–25.

Ori, Alessandro, Paul Free, José Courty, Mark C. Wilkinson, e David G. Fernig. 2009. «Identification of Heparin-Binding Sites in Proteins by Selective Labeling». *Molecular & Cellular Proteomics: MCP* 8 (10): 2256–65. doi:10.1074/mcp.M900031-MCP200.

Parikshak, Neelroop N., Rui Luo, Alice Zhang, Hyejung Won, Jennifer K. Lowe, Vijayendran Chandran, Steve Horvath, e Daniel H. Geschwind. 2013. «Integrative Functional Genomic Analyses Implicate Specific Molecular Pathways and Circuits in Autism». *Cell* 155 (5):

1008–21. doi:10.1016/j.cell.2013.10.031.
Patel, T. D., A. Jackman, F. L. Rice, J. Kucera, e W. D. Snider. 2000. «Development of Sensory Neurons in the Absence of NGF/TrkA Signaling in Vivo». *Neuron* 25 (2): 345–57.
Paudel, Sharada, Yeoun-Hee Kim, Man-Il Huh, Song-Ja Kim, Yongmin Chang, Young Jeung Park, Kyoo Won Lee, e Jae-Chang Jung. 2013. «ADAM10 Mediates N-Cadherin Ectodomain Shedding during Retinal Ganglion Cell Differentiation in Primary Cultured Retinal Cells from the Developing Chick Retina». *Journal of Cellular Biochemistry* 114 (4): 942–54. doi:10.1002/jcb.24435.
Penuela, Silvia, Luke Harland, Jamie Simek, e Dale W. Laird. 2014. «Pannexin Channels and Their Links to Human Disease». *The Biochemical Journal* 461 (3): 371–81. doi:10.1042/BJ20140447.
Pimenta, Aurea F., e Pat Levitt. 2004. «Characterization of the Genomic Structure of the Mouse Limbic System-Associated Membrane Protein (Lsamp) Gene». *Genomics* 83 (5): 790–801. doi:10.1016/j.ygeno.2003.11.013.
Pinto, Dalila, Elsa Delaby, Daniele Merico, Mafalda Barbosa, Alison Merikangas, Lambertus Klei, Bhooma Thiruvahindrapuram, et al. 2014. «Convergence of Genes and Cellular Pathways Dysregulated in Autism Spectrum Disorders». *American Journal of Human Genetics* 94 (5): 677–94. doi:10.1016/j.ajhg.2014.03.018.
Pinto, Dalila, Alistair T Pagnamenta, Lambertus Klei, Richard Anney, Daniele Merico, Regina Regan, Judith Conroy, et al. 2010. «Functional impact of global rare copy number variation in autism spectrum disorders». *Nature* 466 (7304): 368–72. doi:10.1038/nature09146.
Pischedda, Francesca, Joanna Szczurkowska, Maria Daniela Cirnaru, Florian Giesert, Elena Vezzoli, Marius Ueffing, Carlo Sala, et al. 2014. «A Cell Surface Biotinylation Assay to Reveal Membrane-Associated Neuronal Cues: Negr1 Regulates Dendritic Arborization». *Molecular & Cellular Proteomics: MCP* 13 (3): 733–48. doi:10.1074/mcp.M113.031716.
Pucilowska, Joanna, Pavel A. Puzerey, J. Colleen Karlo, Roberto F. Galán, e Gary E. Landreth. 2012. «Disrupted ERK Signaling during Cortical Development Leads to Abnormal Progenitor Proliferation, Neuronal and Network Excitability and Behavior, Modeling Human Neuro-Cardio-Facial-Cutaneous and Related Syndromes». *The Journal of Neuroscience: The Official Journal of the Society for Neuroscience* 32 (25): 8663–77. doi:10.1523/JNEUROSCI.1107-12.2012.
Raballo, R., J. Rhee, R. Lyn-Cook, J. F. Leckman, M. L. Schwartz, e F. M. Vaccarino. 2000. «Basic Fibroblast Growth Factor (Fgf2) Is Necessary for Cell Proliferation and Neurogenesis in the Developing Cerebral Cortex». *The Journal of Neuroscience: The Official Journal of the Society for Neuroscience* 20 (13): 5012–23.
Rakic, P. 1972. «Extrinsic Cytological Determinants of Basket and Stellate Cell Dendritic Pattern in the Cerebellar Molecular Layer». *The Journal of Comparative Neurology* 146 (3): 335–54. doi:10.1002/cne.901460304.
Rakic, P. 1988. «Defects of neuronal migration and the pathogenesis of cortical malformations». *Progress in brain research* 73: 15–37.
Raper, Jonathan, e Carol Mason. 2010. «Cellular Strategies of Axonal Pathfinding». *Cold Spring Harbor Perspectives in Biology* 2 (9): a001933. doi:10.1101/cshperspect.a001933.
Rathjen, F. G., e M. Schachner. 1984. «Immunocytological and Biochemical Characterization of a New Neuronal Cell Surface Component (L1 Antigen) Which Is Involved in Cell Adhesion». *The EMBO Journal* 3 (1): 1–10.
Reichardt, Louis F. 2006. «Neurotrophin-Regulated Signalling Pathways». *Philosophical Transactions of the Royal Society of London. Series B, Biological Sciences* 361 (1473): 1545–64. doi:10.1098/rstb.2006.1894.
Ruoslahti, E. 1988. «Fibronectin and its receptors». *Annual review of biochemistry* 57: 375–413. doi:10.1146/annurev.bi.57.070188.002111.

Sahu, Giriraj, Sunitha Sukumaran, e Amal Kanti Bera. 2014. «Pannexins Form Gap Junctions with Electrophysiological and Pharmacological Properties Distinct from Connexins». *Scientific Reports* 4: 4955. doi:10.1038/srep04955.

Saito, T., e N. Nakatsuji. 2001. «Efficient Gene Transfer into the Embryonic Mouse Brain Using in Vivo Electroporation». *Developmental Biology* 240 (1): 237–46. doi:10.1006/dbio.2001.0439.

Salzer, J L, e D R Colman. 1989. «Mechanisms of cell adhesion in the nervous system: role of the immunoglobulin gene superfamily». *Developmental neuroscience* 11 (6): 377–90.

Sanz, Ricardo, Gino B. Ferraro, e Alyson E. Fournier. 2015. «IgLON Cell Adhesion Molecules Are Shed from the Cell Surface of Cortical Neurons to Promote Neuronal Growth». *The Journal of Biological Chemistry* 290 (7): 4330–42. doi:10.1074/jbc.M114.628438.

Scattoni, M. L., L. Ricceri, e J. N. Crawley. 2011. «Unusual Repertoire of Vocalizations in Adult BTBR T+tf/J Mice during Three Types of Social Encounters». *Genes, Brain, and Behavior* 10 (1): 44–56. doi:10.1111/j.1601-183X.2010.00623.x.

Schäfer, Michael, Anja U. Bräuer, Nicolai E. Savaskan, Fritz G. Rathjen, e Thomas Brümmendorf. 2005. «Neurotractin/kilon Promotes Neurite Outgrowth and Is Expressed on Reactive Astrocytes after Entorhinal Cortex Lesion». *Molecular and Cellular Neurosciences* 29 (4): 580–90. doi:10.1016/j.mcn.2005.04.010.

Schofield, P R, K C McFarland, J S Hayflick, J N Wilcox, T M Cho, S Roy, N M Lee, H H Loh, e P H Seeburg. 1989. «Molecular characterization of a new immunoglobulin superfamily protein with potential roles in opioid binding and cell contact». *The EMBO journal* 8 (2): 489–95.

Seals, Darren F., e Sara A. Courtneidge. 2003. «The ADAMs Family of Metalloproteases: Multidomain Proteins with Multiple Functions». *Genes & Development* 17 (1): 7–30. doi:10.1101/gad.1039703.

Shin, Dana M., Sailaja Korada, Rossana Raballo, Cooduvalli S. Shashikant, Antonio Simeone, Jane R. Taylor, e Flora Vaccarino. 2004. «Loss of Glutamatergic Pyramidal Neurons in Frontal and Temporal Cortex Resulting from Attenuation of FGFR1 Signaling Is Associated with Spontaneous Hyperactivity in Mice». *The Journal of Neuroscience: The Official Journal of the Society for Neuroscience* 24 (9): 2247–58. doi:10.1523/JNEUROSCI.5285-03.2004.

Sia, G. M., R. L. Clem, e R. L. Huganir. 2013. «The Human Language-Associated Gene SRPX2 Regulates Synapse Formation and Vocalization in Mice». *Science (New York, N.Y.)* 342 (6161): 987–91. doi:10.1126/science.1245079.

Smalley, S. L., R. F. Asarnow, e M. A. Spence. 1988. «Autism and Genetics. A Decade of Research». *Archives of General Psychiatry* 45 (10): 953–61.

Smith, Karen Müller, Yasushi Ohkubo, Maria Elisabetta Maragnoli, Mladen-Roko Rasin, Michael L. Schwartz, Nenad Sestan, e Flora M. Vaccarino. 2006. «Midline Radial Glia Translocation and Corpus Callosum Formation Require FGF Signaling». *Nature Neuroscience* 9 (6): 787–97. doi:10.1038/nn1705.

Song, Minseok, Joanna Giza, Catia C. Proenca, Deqiang Jing, Mark Elliott, Iva Dincheva, Sergey V. Shmelkov, et al. 2015. «Slitrk5 Mediates BDNF-Dependent TrkB Receptor Trafficking and Signaling». *Developmental Cell* 33 (6): 690–702. doi:10.1016/j.devcel.2015.04.009.

Sorkin, Alexander, e Mark von Zastrow. 2009. «Endocytosis and Signalling: Intertwining Molecular Networks». *Nature Reviews. Molecular Cell Biology* 10 (9): 609–22. doi:10.1038/nrm2748.

Spooren, Will, Lothar Lindemann, Anirvan Ghosh, e Luca Santarelli. 2012. «Synapse Dysfunction in Autism: A Molecular Medicine Approach to Drug Discovery in Neurodevelopmental Disorders». *Trends in Pharmacological Sciences* 33 (12): 669–84. doi:10.1016/j.tips.2012.09.004.

Sternberg, M. J., e W. J. Gullick. 1990. «A Sequence Motif in the Transmembrane Region of

Growth Factor Receptors with Tyrosine Kinase Activity Mediates Dimerization». *Protein Engineering* 3 (4): 245–48.
Stoner, Rich, Maggie L. Chow, Maureen P. Boyle, Susan M. Sunkin, Peter R. Mouton, Subhojit Roy, Anthony Wynshaw-Boris, Sophia A. Colamarino, Ed S. Lein, e Eric Courchesne. 2014. «Patches of Disorganization in the Neocortex of Children with Autism». *The New England Journal of Medicine* 370 (13): 1209–19. doi:10.1056/NEJMoa1307491.
Struyk, A F, P D Canoll, M J Wolfgang, C L Rosen, P D'Eustachio, e J L Salzer. 1995. «Cloning of neurotrimin defines a new subfamily of differentially expressed neural cell adhesion molecules». *The Journal of neuroscience: the official journal of the Society for Neuroscience* 15 (3 Pt 2): 2141–56.
Sugimoto, Chiaki, Shohei Maekawa, e Seiji Miyata. 2010. «OBCAM, an Immunoglobulin Superfamily Cell Adhesion Molecule, Regulates Morphology and Proliferation of Cerebral Astrocytes». *Journal of Neurochemistry* 112 (3): 818–28. doi:10.1111/j.1471-4159.2009.06513.x.
Sunnarborg, Susan Wohler, C. Leann Hinkle, Mary Stevenson, William E. Russell, Christina S. Raska, Jacques J. Peschon, Beverly J. Castner, et al. 2002. «Tumor Necrosis Factor-Alpha Converting Enzyme (TACE) Regulates Epidermal Growth Factor Receptor Ligand Availability». *The Journal of Biological Chemistry* 277 (15): 12838–45. doi:10.1074/jbc.M112050200.
Tabuchi, Katsuhiko, Jacqueline Blundell, Mark R Etherton, Robert E Hammer, Xinran Liu, Craig M Powell, e Thomas C Südhof. 2007. «A neuroligin-3 mutation implicated in autism increases inhibitory synaptic transmission in mice». *Science (New York, N.Y.)* 318 (5847): 71–76. doi:10.1126/science.1146221.
Tada, Tomoko, e Morgan Sheng. 2006. «Molecular Mechanisms of Dendritic Spine Morphogenesis». *Current Opinion in Neurobiology* 16 (1): 95–101. doi:10.1016/j.conb.2005.12.001.
Takeichi, M., K. Hatta, A. Nose, e A. Nagafuchi. 1988. «Identification of a Gene Family of Cadherin Cell Adhesion Molecules». *Cell Differentiation and Development: The Official Journal of the International Society of Developmental Biologists* 25 Suppl (novembre): 91–94.
Turner, Nicholas, e Richard Grose. 2010. «Fibroblast Growth Factor Signalling: From Development to Cancer». *Nature Reviews. Cancer* 10 (2): 116–29. doi:10.1038/nrc2780.
Vaccarino, Flora M., Elena L. Grigorenko, Karen Müller Smith, e Hanna E. Stevens. 2009. «Regulation of Cerebral Cortical Size and Neuron Number by Fibroblast Growth Factors: Implications for Autism». *Journal of Autism and Developmental Disorders* 39 (3): 511–20. doi:10.1007/s10803-008-0653-8.
Veenstra-Vanderweele, Jeremy, Susan L Christian, e Edwin H Cook Jr. 2004. «Autism as a paradigmatic complex genetic disorder». *Annual Review of Genomics and Human Genetics* 5: 379–405. doi:10.1146/annurev.genom.5.061903.180050.
Veerappa, Avinash M., Marita Saldanha, Prakash Padakannaya, e Nallur B. Ramachandra. 2013. «Family-Based Genome-Wide Copy Number Scan Identifies Five New Genes of Dyslexia Involved in Dendritic Spinal Plasticity». *Journal of Human Genetics* 58 (8): 539–47. doi:10.1038/jhg.2013.47.
Verrotti, Alberto, Alberto Spalice, Fabiana Ursitti, Laura Papetti, Rosanna Mariani, Antonella Castronovo, Mario Mastrangelo, e Paola Iannetti. 2010. «New Trends in Neuronal Migration Disorders». *European Journal of Paediatric Neurology: EJPN: Official Journal of the European Paediatric Neurology Society* 14 (1): 1–12. doi:10.1016/j.ejpn.2009.01.005.
Vesterlund, Liselotte, Virpi Töhönen, Outi Hovatta, e Juha Kere. 2011. «Co-Localization of Neural Cell Adhesion Molecule and Fibroblast Growth Factor Receptor 2 in Early Embryo Development». *The International Journal of Developmental Biology* 55 (3): 313–19.

doi:10.1387/ijdb.103240lv.
Wentz, Elisabet, Mihailo Vujic, Ewa-Lotta Kärrstedt, Anna Erlandsson, e Christopher Gillberg. 2014. «A Case Report of Two Male Siblings with Autism and Duplication of Xq13-q21, a Region Including Three Genes Predisposing for Autism». *European Child & Adolescent Psychiatry* 23 (5): 329–36. doi:10.1007/s00787-013-0455-1.
Williams, A F, e A N Barclay. 1988. «The immunoglobulin superfamily--domains for cell surface recognition». *Annual review of immunology* 6: 381–405. doi:10.1146/annurev.iy.06.040188.002121.
Wöhr, Markus, e Rainer K. W. Schwarting. 2008. «Maternal Care, Isolation-Induced Infant Ultrasonic Calling, and Their Relations to Adult Anxiety-Related Behavior in the Rat». *Behavioral Neuroscience* 122 (2): 310–30. doi:10.1037/0735-7044.122.2.310.
Yamada, Mayumi, Takashi Hashimoto, Noriko Hayashi, Maiko Higuchi, Akira Murakami, Toshihiro Nakashima, Shohei Maekawa, e Seiji Miyata. 2007. «Synaptic adhesion molecule OBCAM; synaptogenesis and dynamic internalization». *Brain research* 1165 (agosto): 5–14. doi:10.1016/j.brainres.2007.04.062.
Ye, Haihong, Jianghong Liu, e Jane Y Wu. 2010. «Cell adhesion molecules and their involvement in autism spectrum disorder». *Neuro-Signals* 18 (2): 62–71. doi:10.1159/000322543.
Zacco, A, V Cooper, P D Chantler, S Fisher-Hyland, H L Horton, e P Levitt. 1990. «Isolation, biochemical characterization and ultrastructural analysis of the limbic system-associated membrane protein (LAMP), a protein expressed by neurons comprising functional neural circuits». *The Journal of neuroscience: the official journal of the Society for Neuroscience* 10 (1): 73–90.
Zhou, Yong-Xing, Nicole C. Flint, Joshua C. Murtie, Tuan Q. Le, e Regina C. Armstrong. 2006. «Retroviral Lineage Analysis of Fibroblast Growth Factor Receptor Signaling in FGF2 Inhibition of Oligodendrocyte Progenitor Differentiation». *Glia* 54 (6): 578–90. doi:10.1002/glia.20410.

9.FIGURE INDEX

10.ABBREVIATION INDEX

ADAM- disintegrin and metalloprotease domain

APP - Amyloid Precursor Protein

ASD - Autism Spectrum Disorders

CAM - Cell Adhesion Molecule

CaMKIIα - Calmodulin-Dependent Protein Kinase IIα

cAMP - Cyclic AMP

CDK5 - Cyclin-Dependent Kinase 5

cDNA – Complementary DNA

CNV - Copy Number Variation

CP - Cortical Plate

DISC1 - Disrupted in Schizophrenia 1

DNA –Deoxyribonucleic Acid

DRG- Dorsal Root Ganglion

DSM-IV - Diagnostic and Statistical Manual-Fourth Edition

E18 – Embryonic Day 18

ECM - Extracellular Matrix

EGF - Epidermal Growth Factor

EGFP – Enhanced Green Fluorescent Protein

ERK - Extracellular Regulated Kinases

FAK - Focal Adhesion Kinase

FGFb – basic Fibroblast Growth Factor

FGF7- Fibroblast Growth Factor 7

FGFR – Fibroblast Growth Factor Receptor

FNIII - Fibronectin-type III

GABA - γ-aminobutyric Acid

GFP- Green Fluorescent Protein

GM - Gray Matter

GPI - Glycophosphatidyl Inositol Anchor

GWAS - Genome-Wide Association Studies

HPSGs - Heparan Sulphate Proteoglycans

IgCAM - Immunoglobulin-like Cell Adhesion Molecule

IgSF - Immunoglobulin Superfamily

IUE – *In Utero* Electroporation

IZ – Intermediate Zone

Kilon - Kindred of IgLON

KO – Knock Out

LAMP - Limbic Dystem-Associated Membrane Protein

MAPK - mitogen-activated protein kinase

MBP - Myelin Basic Protein

MMP9 - Matrix Metalloprotease 9

mRNA – Messenger RNA

MZ - Marginal Zone

NCAM - Neuronal Cell Adhesion Molecule

NE - Neuroepithelial Cell

Negr1- Neuronal Growth Regulator 1 Protein

Nlgn – Neuroligin

NMD - Neuronal Migration Disorders

Nrxn – Neurexin

Ntm – Neurotrimin

OBCAM – Opioid Binding Cell Adhesion Molecule

P7 – Postnatal Day 7

PDD-NOS - Pervasive Developmental Disorder Not Otherwise Specified

PKCβII - protein kinase CβII

PLCγ - Phospholipase Cγ

PSA - Polysialic Acid

RGC - Radial Glial Cell

RNA – Ribonucleic Acid

rNegr1 – recombinant Negr1

RTK - Receptors Associated to Tyrosine Kinase

Sema3A - Semaphorin 3A

siRNA – Small Interfering RNA

SNV - Single Nucleotide Variation

SP – Subplate

SVZ - Subventricular Zone

TACE - Tumor Necrosis Factor-α-Converting Enzyme

TNF - Tumor Necrosis Factor

TUBA1A - Alpha 1 Tubulin

USV - ultrasonic vocalization

VZ - Ventricular Zone

WM - White Matter

WT – Wild Type

11.APPENDIX I

A Cell Surface Biotinylation Assay to Reveal Membrane-associated Neuronal Cues: Negr1 Regulates Dendritic Arborization*[S]

Francesca Pischedda‡, Joanna Szczurkowska§, Maria Daniela Cirnaru‡, Florian Giesert¶, Elena Vezzoli‖, Marius Ueffing‡‡, Carlo Sala‡, Maura Francolini‖, Stefanie M. Hauck‡‡, Laura Cancedda§, and Giovanni Piccoli‡§§**

A complex and still not comprehensively resolved panel of transmembrane proteins regulates the outgrowth and the subsequent morphological and functional development of neuronal processes. In order to gain a more detailed description of these events at the molecular level, we have developed a cell surface biotinylation assay to isolate, detect, and quantify neuronal membrane proteins. When we applied our assay to investigate neuron maturation *in vitro*, we identified 439 differentially expressed proteins, including 20 members of the immunoglobulin superfamily. Among these candidates, we focused on Negr1, a poorly described cell adhesion molecule. We demonstrated that Negr1 controls the development of neurite arborization *in vitro* and *in vivo*. Given the tight correlation existing among synaptic cell adhesion molecules, neuron maturation, and a number of neurological disorders, our assay results are a useful tool that can be used to support the understanding of the molecular bases of physiological and pathological brain function. ***Molecular & Cellular Proteomics 13: 10.1074/mcp.M113.031716, 733–748, 2014.***

Genetic analysis indicates that 20% to 30% of the total open reading frame encodes for integral membrane proteins (1). Although less abundant than cytosolic proteins, membrane-passing proteins contribute to the regulation of all major cell processes and signaling pathways. In particular, membrane proteins play an important role in the establishment of functional neuronal circuitries during development. This process initially entails the growth, guidance, and stabilization of neuronal processes (axons and dendrites) in a timely, ordered manner involving cell surface molecules that sense the extracellular surroundings and activate signaling cascades (2).

Then, specialized cell-to-cell connections, the synapses, are formed. These connections allow information to flow from one neuron to another and relay the precise juxtaposition and interactions between the pre- and postsynaptic membrane proteins to support their final functional establishment. Several families of synaptic transmembrane or membrane proteins, such as semaphorin, neuroligin, neurexin, and the immunoglobulin superfamily (IgSF),[1] are implicated in neurite formation and synapse establishment (3). However, the picture of membrane proteins expressed in neurons is still far from being completely resolved, and it is expected that many other key molecules are awaiting identification (4). Thus, uncovering the nature of the dynamic multiprotein complexes expressed at the plasma membrane will possibly strongly support the understanding of the mechanism controlling structural and functional neuron development. Here, we describe a biochemical approach to isolate and quantify proteins exposed at the extracellular side of the plasma membrane. Our assay utilized affinity purification on streptavidin resin of biotinylated membrane proteins extracted from a crude synaptosomal preparation. We combined this cell surface biotinylation assay with MS/MS analysis and label-free quantification to investigate protein patterns characterizing immature and mature neuronal cultures. Our analysis identified a panel of 439 differentially expressed proteins, including 109 membrane proteins. In particular, we found that the expression profile of 20 cell adhesion molecules belonging to the IgSF was tightly correlated to neuronal maturation. Among our hits, we focused on Negr1, and we demonstrated that it

From the ‡Institute of Neuroscience CNR, 20129 Milano, Italy; §Istituto Italiano di Tecnologia, 16163 Genova, Italy; ¶Institute of Developmental Genetics, Helmholtz Zentrum München (GmbH), German Research Center for Environmental Health, 85764 Neuherberg, Germany; ‖Department of Medical Biotechnology and Translational Medicine, Università degli Studi di Milano, 20129 Milano, Italy; **Institute for Ophthalmic Research, Eberhard Karls University Tübingen, 72076 Tübingen, Germany; ‡‡Research Unit Protein Science, Helmholtz Zentrum München (GmbH), German Research Center for Environmental Health, 85764 Neuherberg, Germany

Received June 26, 2013, and in revised form, November 22, 2013.
Published, MCP Papers in Press, December 31, 2013, DOI 10.1074/mcp.M113.031716

Author contributions: L.C. and G.P. designed the research; L.C., S.H., and G.P. wrote the manuscript; F.P., J.S., M.D.C., M.F., E.V., S.H., and F.G. performed experiments; M.U., C.S., and S.H. provided data analysis expertise.

[1] The abbreviations used are: IgSF, immunoglobulin superfamily; DIV, days *in vitro*; CAM, cell adhesion molecule; SV, synaptic vesicle; P2, crude synaptosomal pellet; S2, cytosomal supernatant; GO, gene ontology.

plays a key role in regulating neuronal morphological development *in vitro* and *in vivo*.

EXPERIMENTAL PROCEDURES

Lentiviral Vector Constructs, Virus Production, and Plasmids—Negr1 target sequences were identified using Ambion Web-based oligo-search software, and four silencing sequences for Negr1 (A2, 5′-CACCCTTTGATGCTCCATCTT-3′; B1, 5′-AAGATGGAGCATCAAAGGGTG-3′; D4, 5′-AATGTTGATGTAACAGATG-3′; C8, 5′-CTGGAGGCTGTAGTCTCTT-3′) were selected, synthesized, and cloned into GFP-expressing pLVTH, as previously described (5). In brief, oligonucleotides coding for a 5′-pseudoBglII site, a sense-oligonucleotide-loop-antisense-oligonucleotide transcription termination site, and a 3′pseudo-XbaI restriction site were purchased from Metabion, Martinsried, Germany. Sense and antisense oligos were annealed and subsequently phosphorylated. The fragments were cloned 3′ to the H1 promoter of pBC KS+(ClaI)-H1, resulting in pBC KS+(ClaI)-sh. The H1sh cassettes were isolated with ClaI, blunted, and cloned into the blunted ClaI/BamH1 site of pLV transfer vector. pLV is a modified plasmid transfer vector derived from original pLVTH (6) in which the BamH1-tetO-H1-ClaI fragment has been excised. All recombinant lentiviruses were produced by means of transient transfection of HEK293T cells according to standard protocols (6). Primary neuronal cultures were transduced with viruses at multiplicity of infection 1. mNegr1 cDNA (Addgene clone C3342IRCKp5014P057-rzpdm13–21) was cloned into strep-FLAG pcDNA3.1 vector. For rescue experiments, we introduce into mNegr1 cDNA via site-directed mutagenesis two silent mutations in the region targeted by miRNA A2 using the following primer: 5′-GCCGTGGACAACATGCTCGTCAGGAAAGGTGACACAGCG-3′.

Neuronal Cultures—Cortical neuron cultures were prepared from mouse embryos (E17.5–18.5; strain C57BL/*6*). High-density (750 to 1000 cells/mm^2) and medium-density (150 to 200 cells/mm^2) neuronal cultures were plated and grown on six-well plastic tissue culture plates (Iwaki, Bibby Sterilin, Staffordshire, UK) or on 12-mm-diameter coverslips put into 24-well plastic tissue culture plates as previously described (Iwaki, Bibby Sterilin, Staffordshire, UK) (7). In these cultures glial growth is reduced to less than 0.5% of the nearly pure neuronal population (8). Neuronal cultures were infected with viruses at days *in vitro* (DIV) 1 to 2 or transfected at DIV4 with Lipofectamine 2000 following the manufacturer's protocol (Lifetech, Carlsbad, CA).

Cell Surface Biotinylation Assay and Western Blotting—Neurons were incubated at DIV6 or DIV16 with 0.5 mg/ml nonpermeable biotin (NHS-biotin, Sigma-Aldrich) in PBS for 30 min under gentle agitation. After incubation, cells were washed with 100 mM glycine in PBS three times and PBS once, with each washing lasting 10 min.

Subsequently, subcellular fractions were produced as previously described (9). Briefly, high-density cultures were collected in HEPES-buffered sucrose (0.32 M sucrose, 4 mM HEPES pH 7.4) and spun at 600*g* for 5 min to pellet the nuclear fraction. The resulting supernatant was centrifuged at 10,000*g* for 15 min to obtain a cytosolic supernatant (S2) and a crude synaptosomal pellet (P2). The P2 fraction was solubilized in a dedicated lysis buffer (150 mM NaCl, 1% Nonidet P-40, 0.4% n-dodecyl-β-D-maltoside, 0.1% SDS, and 50 mM HEPES, pH 7.4) for 1 h. The lysates from P2 and S2 were spun for 20 min at 16,000*g*, and the supernatant was added to streptavidin-agarose beads and put under mild agitation for 1 h. After the incubation, the resin was washed twice with a wash buffer containing 150 mM NaCl, 50 mM Hepes, 0.1% Triton X-100. A brief centrifugation at 2000*g* followed each wash. Proteins were eluted in 60 μl of 2X Laemmli buffer. To assay protein expression *in vivo*, C57BL/*6* mice were sacrificed when indicated. Cortexes were isolated and homogenized manually in lysis buffer. After 1 h under mild agitation, lysate was clarified by centrifugation for 20 min at 16,000*g*. All procedures described here were performed at 4 °C. The protein concentration in each sample was measured via standard Bradford assay (Bio-Rad). For protein identification and relative quantification via Western blotting, a proper volume of sample containing an equal amount of proteins was diluted with 0.25% 5X Laemmli buffer and loaded onto 4–12% NuPAGE gels (Invitrogen); the proteins were transferred onto nitrocellulose membrane (Sigma-Aldrich) at 80 V for 120 min at 4 °C. The primary antibodies were applied overnight in a blocking buffer (20 mM Tris, pH 7.4, 150 mM NaCl, 0.1% Tween 20, and 5% nonfat dry milk); primary antibodies (source in parentheses) included rabbit anti-NR2A 1:1000, goat anti-Negr1 1:1000 (R&D, Minneapolis, MN), rabbit anti-HSP90 1:1000, rabbit anti-NSF 1:1000, rabbit anti RpS6 1:2000 (Cell Signaling, Danvers, MA), mouse anti-NCAM 1:1000 (BD Biosciences), mouse anti-PSD-95 1:5000 (NeuroMab, Davis, CA), mouse anti-MAP2 1:1000, mouse anti-SNAP-25 1:1000, mouse anti-Synaptophysin 1:1000, mouse anti-syntaxin 1A 1:1000, mouse anti-actin 1:1000, mouse anti-α-tubulin 1:1000 (Sigma-Aldrich), and mouse anti-Na/K ATPase α 1:2000 (10) (a generous gift from Grazia Pietrini, University of Milano). The secondary antibodies (HRP-conjugated anti-mouse, anti-rabbit, or anti-rat) (Jackson ImmunoResearch, Suffolk, UK) were used in a ratio of 1:8000. The signal was detected using an ECL detection system (GE Healthcare). Films were acquired on a GS-800 densitometer (BioRad) calibrated following the manufacturers' instructions, and protein abundance was estimated as a function of the optical density of a specific band quantified by ImageJ software (NIH). Unless otherwise stated, all the other chemicals were purchased from Applichem, GmBH, Darmstadt, Germany.

Electron Microscopy—Specimens from neurons at different DIV were prepared for electron microscopy as previously described (11). Briefly, neuronal cultures were fixed in cacodylate buffered with 3% glutaraldehyde for 12 h and subsequently Epon-embedded. Ultrathin sections were cut, mounted on copper grids, contrasted with uranyl acetate and lead citrate, and observed with an electron microscope (Zeiss EM10 at 60 kV). Electron microscopy images were processed on ImageJ (NIH), and single vesicles and synaptic structures were annotated manually. Throughout the text, *n* refers to the number of neurons measured. For transmission electron microscopy analysis of the P2 fraction, samples were fixed with 2% glutaraldehyde in cacodylate buffer (Na-cacodylate 0.1 M, pH 7.4) and processed for transmission electron microscopy. Briefly, after fixation the samples were post-fixed with osmium tetroxide (2% OsO_4 in 0.1 M cacodylate buffer), rinsed, stained with 1% uranyl acetate in water for 45 min, dehydrated, and embedded in epoxy resin (Epon 812, Electron Microscopy Science, Hatfield, PA). The resin was then baked for 48 h at 60 °C. Thin sections (70 nm) were obtained with an ultramicrotome (Reichert Ultracut E, Leica Microsystems, Heerbrugg, Switzerland). Samples were observed with a Philips CM10 transmission electron microscope at 80 kv, and images were acquired using a Morada Olympus digital camera.

Immunofluorescence and Quantification—For the immunostaining experiments, neurons were fixed in 4% paraformaldehyde and 4% sucrose at room temperature or 100% methanol at −20 °C. Primary and secondary antibodies were applied in GDB buffer (30 mM phosphate buffer, pH 7.4, containing 0.2% gelatin, 0.5% Triton X-100, and 0.8 M NaCl) for two hours at room temperature or overnight at 4 °C. Primary antibodies included goat anti-OPCML 1:500, goat anti-NEGR1 1:500 (R&D), mouse anti-LSAMP 1:1000 (DSHB, Iowa City, Iowa), mouse anti-PSD-95 1:500 (NeuroMab), Alexa phalloidin-546 1:2000 (Invitrogen), rabbit anti-MAP2 1:400 (Millipore, Billerica, MA), and mouse anti-Na/K ATPase α 1:100. GFP-positive neurons were randomly chosen for quantification in at least four independent experiments for each condition. The fluorescence images were acquired using an LSM Zeiss 510 confocal microscope with a Zeiss 63× objective (Karl Zeiss, Jena, Germany) at a resolution of 2048 × 2048

pixels, with a pixel size of 0.098 μm. All the measurements were performed using NeuronStudio. Neurites and dendritic spines were automatically traced and quantified by the software in terms of length, number, and morphology (12, 13). Data were then logged and analyzed in Microsoft Excel.

Exo-endocytotic Assay—The endocytosis assay to monitor synaptic vesicle (SV) recycling was performed as previously described with minor modifications (14, 15). Briefly, rabbit polyclonal antibodies directed against the intravesicular domain of synaptotagmin1 (Synaptic Systems, Goettingen, Germany) were diluted in Tyrode solution (124 mM NaCl, 5 mM KCl, 5 mM $CaCl_2$, 1 mM $MgCl_2$, 30 mM glucose, 25 mM HEPES, pH 7.4) and applied for 5 min at room temperature. After fixation and permeabilization, a synaptophysin counterstain (mouse anti-synaptophysin 1:400, Sigma-Aldrich) was performed to visualize the totality of synaptic vesicles. Images were acquired by means of confocal microscopy, processed, and quantitatively analyzed with ImageJ software, as previously described (16).

Mass Spectrometry—Protein samples derived from cellular fractions before Strep pull-down were processed via filter-aided sample preparation as described elsewhere (17). Samples generated via Strep pull-downs were directly digested on bead after reduction and alkylation and repetitive washes with 6 M urea followed by one wash in 5 M NaCl. The peptides generated by tryptic digests were acidified and then subjected to LC-MS/MS as described elsewhere (18). Briefly, LC-MS/MS analysis was performed on an Ultimate3000 nano-HPLC system (Dionex, Sunnyvale, CA) coupled to an LTQ OrbitrapXL mass spectrometer (Thermo Fisher Scientific) by a nanospray ion source. Tryptic peptides were automatically injected and loaded at a flow rate of 30 μl/min in 95% buffer C (0.5% trifluoroacetic acid in HPLC-grade water) and 5% buffer B (98% acetonitrile and 0.1% formic acid in HPLC-grade water) onto a nano trap column (100 μm inner diameter × 2 cm, packed with Acclaim PepMap100 C18, 5 μm, 100 Å; Dionex). After 5 min, peptides were eluted and separated on the analytical column (75 μm inner diameter × 15 cm, Acclaim PepMap100 C18, 3 μm, 100 Å; Dionex) by a linear gradient from 5% to 40% of buffer B in buffer A (2% acetonitrile and 0.1% formic acid in HPLC-grade water) at a flow rate of 300 nl/min over 120 min. Remaining peptides were eluted by a short gradient from 40% to 100% buffer B in 5 min. The eluted peptides were analyzed by the LTQ OrbitrapXL mass spectrometer. From the high-resolution mass spectrometry prescan with a mass range of 300–1500, the 10 most intense peptide ions were selected for fragment analysis in the linear ion trap, if they exceeded an intensity of at least 200 counts, and if they were at least doubly charged. The normalized collision energy for collision-induced dissociation was set to a value of 35, and the resulting fragments were detected with normal resolution in the linear ion trap. The lock mass option was activated, and the background signal with a mass of 445.12002 was used as the lock mass (19). Every ion selected for fragmentation was excluded for 30 s by means of dynamic exclusion. The acquired spectra were processed and analyzed using Mascot Daemon (V2.4.1) with the following settings: cystein carbamidomethylation as a fixed modification; methionine oxidation and asparagine/glutamine deamidation as variable modifications; and one missed cleavage allowed. Mass tolerances for parent and fragment peptides were set at 10 ppm and 0.6 Da, respectively. The database used was the Ensembl Mouse database (version GRCm38; 51,372 sequences, 23,210,570 residues) For the qualitative analysis, Mascot result files were analyzed by Scaffold software (V4.0.7, Proteome Software Inc., Portland, OR) to validate MS/MS-based peptide and protein identifications. Peptide identifications were accepted if they could be established at greater than 95% probability as specified by the Peptide Prophet algorithm (20). Protein identifications were accepted if they could be established at greater than 99% probability and contained at least two identified unique peptides. Protein probabilities were assigned by the Protein Prophet algorithm (21). Protein and peptide false discovery rates were fixed at 1% and 0.1%, respectively. Proteins that contained similar peptides and could not be differentiated based on MS/MS analysis alone were grouped to satisfy the principles of parsimony. All identified proteins with their respective numbers of uniquely identified peptides are listed in supplemental Table S1. All identified peptides are listed in supplemental Table S2.

For relative quantification based on peptide intensities, three independent biological replicates for each experimental condition were analyzed. The raw files were directly imported into Progenesis Software (version 4.0, Nonlinear Dynamics, Newcastle upon Tyne, UK) and processed as described elsewhere (18). Briefly, profile data of the MS scans and MS/MS spectra were transformed into peak lists with Progenesis LC-MS using a proprietary algorithm and then stored in peak lists comprising *m/z* and abundance values. One sample was set as a reference, and the retention times of the other sample within were aligned (three to five manual landmarks, followed by automatic alignment) to create maximal overlay of the two-dimensional feature maps. Features with only one charge or more than seven charges were masked at this point and excluded from further analysis. Samples were then allocated to experimental groups (DIV6 and DIV16, respectively). For quantification, all unique peptides (with Mascot percolator score ≥ 13) of an identified protein were included and the cumulative abundance for that protein was calculated by summing the abundances of all peptides allocated to the respective protein normalized *versus* the total peptide abundance. No minimal thresholds were set for the method of peak picking or selection of data to use for quantification. Based on the cumulative intensities, a ratio between DIV16 and DIV6 was calculated for each protein and evaluated statistically via *t* test. All identified proteins with their respective cumulated peptide intensities from each sample are listed in supplemental Table S3. Peptide quantification is reported in supplemental Table S4.

In Utero Electroporation—*In utero* electroporation was performed with the standard configuration, as described elsewhere (22). In brief, the day of mating (limited to 4 h in the morning) was defined as embryonic day zero (E0), and the day of birth was defined as postnatal day zero (P0). E15.5 timed-pregnant CD1 mice (Harlan Italy SrL, Correzzana, Italy) were anesthetized with isoflurane (induction, 4%; surgery, 2.5%), and the uterine horns were exposed by laparotomy. The DNA (1 to 2 μg/μl in water) together with Fast Green dye (0.3 mg/ml; Sigma, St. Louis, MO) was injected (5 to 6 μl) through the uterine wall into one of the lateral ventricles of each embryo by a 30-gauge needle (Pic indolor, Grandate, Italy). After the uterine horn had been soaked with a PBS solution, the embryo's head was carefully held between tweezer-type circular electrodes (3-mm diameter, Nepa Gene, Chiba, Japan). For the electroporation, six electrical pulses (amplitude, 30 V; duration, 50 ms; intervals, 1 s) were delivered with a square-wave electroporation generator (CUY21EDIT, Nepa Gene, Ichikawa-City, Chiba, Japan; ECM 830, BTX, Harvard Apparatus, Holliston, MA). After electroporation, the uterine horns were returned into the abdominal cavity and embryos were allowed to continue their normal development.

Real-time Reverse-transcription PCR—Quantitative real-time RT-PCR was performed as previously described (23). In short, RNA extracted by the RNeasy Mini Kit (Qiagen, Hilden, Germany) was reverse transcribed using SuperScript®-VILO (Invitrogen, #11904–018). For quantification of *Negr1* and *Ncam1* transcripts, real-time PCR was performed using the ABI PRISM 7900 Sequence Detection System (Applied Biosystems, Carlsbad, CA) and TaqMan® reaction mixes for murine *Negr1* (Mm01317328_m1, Applied Biosystems), *Ncam1* (Mm01149710_m1, Applied Biosystems), and *Actb* (actin, beta) (NM_007393.1, Applied Biosystems). All samples were measured in

triplicate. The relative expression of endogenous *Negr1* and *Ncam1* was determined via normalization to *Actb* ($2^{-[\Delta Ct]}$).

Statistical Analysis—All data are expressed as means ± S.E. Data were analyzed with an unpaired Student's *t* test (two classes) or ANOVA followed by Tuckey's post hoc test (more than two classes). The number of experiments (*n*) and the level of significance (*p*) are indicated throughout the text.

RESULTS

Cell Surface Biotinylation Assay Allows the Enrichment of Membrane Proteins—Our cell surface biotinylation assay exploits the incubation of living neuronal cultures with nonpermeable biotin moieties to tag protein domains at the extracellular level. To minimize protein internalization, we performed the biotinylation step at 4 °C (24). After extensive washing, we collected via sequential centrifugation a series of biochemical fractions, namely, S1 (mainly containing cell body), S2 (cytosol), and P2 (enriched in synaptosome and mitochondria) (9). Transmission electron microscopy investigation of P2 fractions obtained from DIV6 and DIV16 cultures confirmed that both samples contained a subcellular structure recognizable as the synaptosome (supplemental Fig. S1). After solubilization in dedicated lysis buffer, we immobilized biotinylated proteins from P2 and S2 fractions on a streptavidin-agarose resin. After washing, we eluted the proteins in Laemmli buffer and analyzed the fractions via Western blotting. As *bona fide* examples of proteins located at various cellular compartments, we monitored the biochemical profiles of the synaptic proteins NMDA-R subunit 2A, syntaxin 1A, PSD-95, and NSF (Fig. 1*A*); cytoskeletal components such as MAP2, actin, and tubulin (Fig. 1*B*); and cytosolic proteins such as RpS6 and HSP-90 (Fig. 1*C*) in fractions obtained from DIV16 cultures. Western blot analysis showed that the P2 fraction was enriched in synaptic proteins such as PSD-95 and NSF and was mostly lacking in cytosolic components such as RpS6 and HSP-90; furthermore, we found that NMDA-R subunit 2A was present in the eluate of streptavidin pull-down obtained from the P2 fraction (NMDA in STREP-PD was around 26% of the input; Fig. 1*B*). A similar analysis performed on DIV6 culture produced comparable results (supplemental Fig. S2). To further explore the performance of our assay, we analyzed four biological sources obtained from DIV16 cultures by means of MS/MS spectrometry: total cell lysate, P2 fraction, or STREP-PD fraction resulting from total cell lysate or P2 fraction. We detected 1405 unique proteins, including 155 membrane proteins, in total cell lysate; 710 (147 membrane proteins) in STREP-PD from total cell lysate; 1457 (153 membrane proteins) in the P2 fraction; and 692 (166 membrane proteins) in STREP-PD from P2. In particular, STREP-PD from the P2 fraction was characterized by a peculiar subset of proteins not shared with the P2 fraction (74, 24 membrane proteins) or with STREP-PD from lysate (148, 36 membrane proteins) (Fig. 2*A* and supplemental Tables S1 and S2). When we ranked protein hits in function of the number of unique peptides assigned by MS/MS analysis, we found three membrane proteins in STREP-PD fractions, only one in the P2 fraction, and none in total cell lysate among the top four identifications (Fig. 2*B*). Gene ontology (GO) analysis performed on DAVID Bioinformatics Resources 6.7 (25, 26) indicated that the total cell lysate and P2 fraction included about

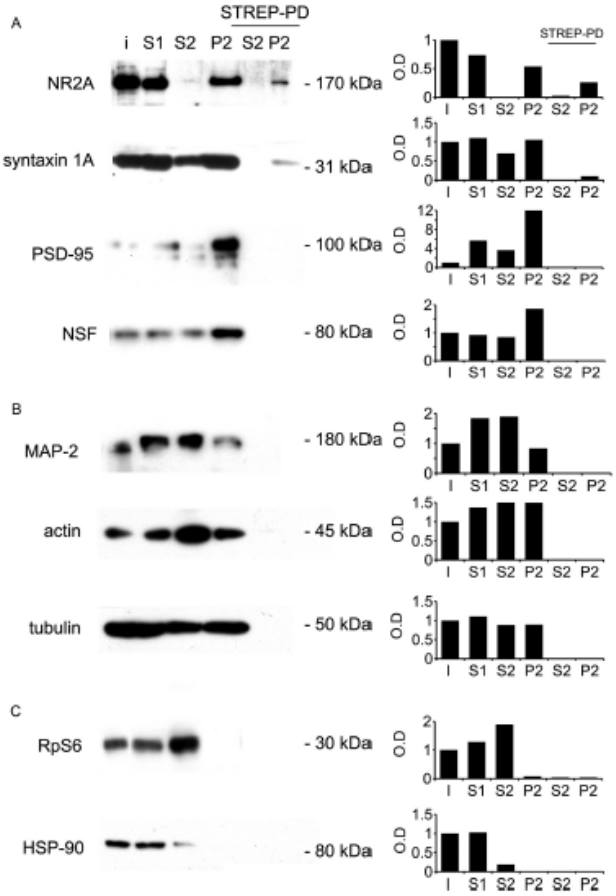

FIG. 1. **Cell surface biotinylation assay isolates membrane proteins.** We developed an assay to enrich our sample in membrane-associated proteins expressed in the synaptosomal fraction. Briefly, cell surface proteins from cortical neurons were biotinylated for 30 min at 4 °C and then processed biochemically to produce input (i, 10% of lysate) and fractions containing nucleus-free supernatant (S1), cytosol (S2), and crude synaptosomes (P2). Biotinylated membrane-associated proteins were eluted in Laemmli buffer after affinity enrichment on Streptavidin resins (STREP-PD). We monitored our protocol via Western blotting with antibodies raised against synaptic (*A*), cytoskeletal (*B*), and cytosolic markers (*C*). Postsynaptic (NMDAR2 subunit NR2A) and presynaptic (syntaxin1A) markers were enriched in the P2 fraction, whereas cytoskeletal (actin and tubulin) or cytosolic proteins (HSP-90) were not present. The left-hand panels show representative blots. For each protein blotted on the left, the histograms on the right report on the *y*-axis the optical density (O.D.) found in each fraction normalized *versus* the input amount. Quantification of the relative abundance of the different proteins in each fraction showed that NR2A was enriched in STREP-PD P2 fraction relative to the other subcellular markers.

A

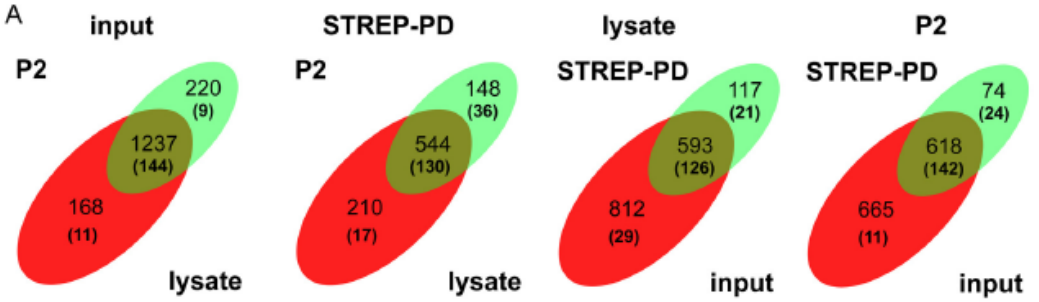

B

Top 4 STREP-PD lysate	Entry	Location	Pep
spectrin beta, non-erythrocytic 1	Q62261	cytoplasm	39
ATPase, Na+/K+ transporting, alpha 3	Q8VCE0	membrane	32
ATPase, Na+/K+ transporting, alpha 3	Q6PIC6	membrane	31
ATPase, Na+/K+ transporting, alpha 1	Q8VDN2	membrane	28

Top 4 STREP-PD P2	Entry	Location	Pep
ATPase, Na+/K+ transporting, alpha 3	Q6PIC6	membrane	29
spectrin beta, non-erythrocytic 1	Q62261	cytoplasm	27
neural cell adhesion molecule 1	P13595	membrane	25
Na+/K+ transporting, alpha 1	Q8VDN2	membrane	23

Top 4 lysate input	Entry	Location	Pep
dynein cytoplasmic 1 heavy chain 1	Q9JHU4	cytoplasm	108
spectrin beta, non-erythrocytic 1	Q62261	cytoplasm	89
clathrin, heavy polypeptide (Hc)	Q68FD5	cytoplasm	62
myosin, heavy polypeptide 10	Q61879	cytoplasm	57

Top 4 P2 input	Entry	Location	Pep
dynein cytoplasmic 1 heavy chain 1	Q9JHU4	cytoplasm	128
spectrin beta, non-erythrocytic 1	Q62261	cytoplasm	87
ankyrin 2, brain	S4R249	membrane	82
clathrin, heavy polypeptide (Hc)	Q68FD5	cytoplasm	62

C

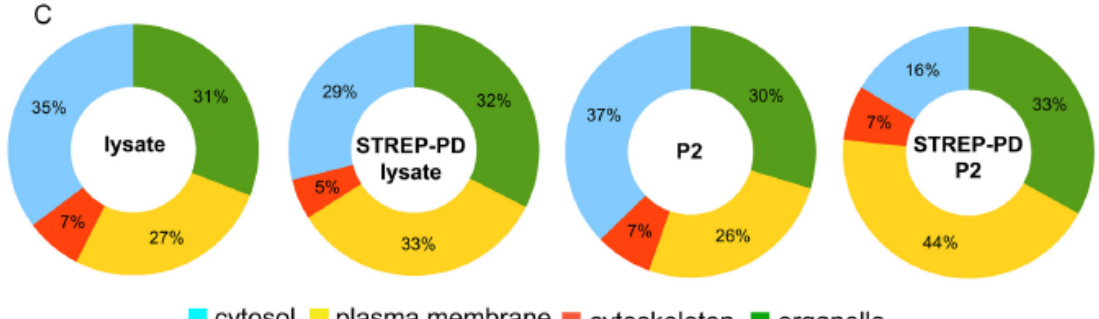

D

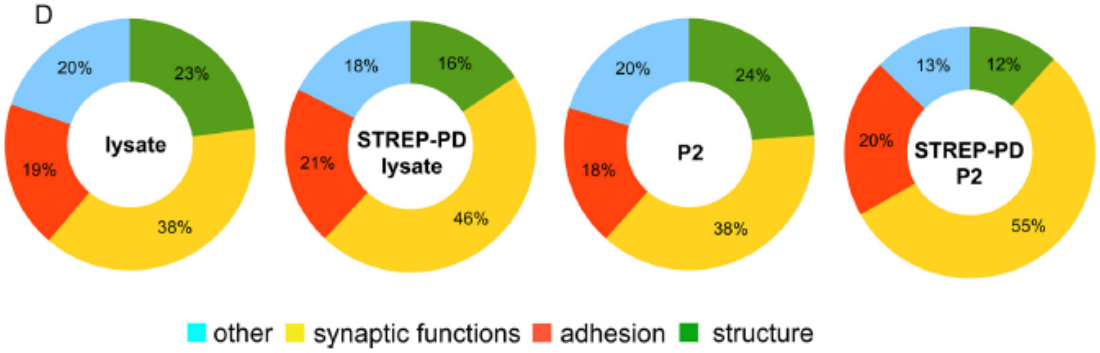

FIG. 2. **Cell surface biotinylation assay isolates membrane proteins involved in synaptic functions.** *A*, Venn diagrams compare the protein datasets identified in total cell lysate and P2 fraction (input), in the STREP-PD fraction obtained from total cell lysate and from P2 (STREP-PD), in STREP-PD from lysate and the lysate itself (lysate), and in STREP-PD from P2 and the P2 fraction itself (P2). "Input" refers to the protein source used in the streptavidin-enrichment procedure. The numbers in parentheses refer to the number of membrane proteins within each fraction. Values reported arose from a combination of four independent experiments. *B*, the tables report the four top entries for total cell lysate, STREP-PD lysate fraction, P2, and STREP-PD P2 fractions based on the number of unique peptides assigned. Protein name, UniProtKB entry, cellular location, molecular weight (MW), number of unique peptides identified (Pep), and sequence coverage (Cov) are indicated. *C*, the graphs report the GO analysis run considering cellular components relative to the proteins identified in total cell lysate, STREP-PD lysate, P2, and STREP-PD P2 fractions. *D*, the graphs report the GO analysis run considering biological processes executed by plasma membrane proteins identified in total cell lysate, STREP-PD lysate, P2, and STREP-PD P2 fractions. Additional information on protein identification, GO annotation, TMHMM prediction, and peptide identification can be found in supplemental Tables S1 and S2.

26% to 27% membrane proteins and that the incubation on streptavidin beads enriched the membrane protein yield by up to 33% and 44% in STREP-PD from total cell lysate and from P2, respectively (Fig. 2*C*). Once we considered the biological functions executed by plasma membrane proteins only, we found that 38% were involved in synaptic functions and about 18% in cell-adhesion-related processes in total cell lysate or the P2 fraction. These fractions rose to 55% and 20% in STREP-PD from P2 (46% and 21%, respectively, in STREP-PD from cell lysate; Fig. 2*D*). In STREP-PD from P2 we listed a number of proteins that had not been previously described at the synaptic site. Thus we considered for further analysis a panel of these hits, namely, Na/K ATPase subunit α, OPCML, and LSAMP. Through immunolocalization assays we were able to confirm their synaptic localization (supplemental Fig. S3). In conclusion, our cell surface biotinylation assay allowed a robust enrichment of membrane proteins. Interestingly, a high percentage of the identified hits were functionally and/or topologically related to the synapse.

Identification of Membrane Proteins Differentially Expressed during Neuronal Development—Membrane proteins play a pivotal role in the functional and structural remodeling experienced by neurons along *in vitro* culturing (27–29). Thus, we assessed the potential of our assay for identifying the membrane-associated proteins involved in neuronal development. In order to profile the main steps characterizing *in vitro* maturation, we analyzed cortical cultures at four different time points (*i.e.* DIV4, DIV8, DIV12, and DIV16) recognized as representative of neuronal maturation (30). Cortical cultures were infected with GFP-expressing viruses (miRNA control; see "Experimental Procedures") at DIV1, fixed, and imaged at DIV4, -8, -12, and -16 (Fig. 3*A* and supplemental Fig. S4*A*).

We measured the neurite number, total length, and complexity (as monitored by Sholl analysis and by the counting of processes for each order of neurite branching; Figs. 3*B*–3*D* and supplemental Fig. S4*B*). The analysis revealed that neurite arborization matured in terms of process number, length, and branching during *in vitro* culturing. To verify whether the structural maturation correlated with functional features, we measured synaptic functions at the four different time points. To this end, we monitored the SV exo-endocytotic rate by exposing cortical living neurons to an anti-synaptotagmin antibody, as previously described (15). Recycling SVs take up the antibody and thus appear as synaptotagmin-positive clusters after fixation and staining (Fig. 3*E*). The quantification of synaptotagmin-positive clusters revealed that the percentage of recycling SVs within the total SV pool increased linearly from DIV4 to DIV16 (Fig. 3*F*). The total vesicle pool estimated via staining with antibodies against an SV integral protein (synaptophysin) after fixation and permeabilization of the cells showed a bimodal profile, with an increase from DIV4 to DIV8 followed by a decrease at DIV12 and a recovery at DIV16 (Fig. 3*G*). This pattern might reveal a process of rapid synaptogenesis followed first by the elimination of unnecessary contacts and later by the establishment of new functional synapses occurring in neuronal networks during physiological development (31). Accordingly, when we examined the neuronal ultrastructure by means of electron microscopy, we noticed that both post- and presynaptic structures changed with *in vitro* culturing, as previously reported (32). In particular, a number of structural parameters such as postsynaptic density, length and width, active zone length, number of SVs in total and docked pools, and SV average diameter increased as culture proceeded *in vitro* (supplemental Fig. S5). In conclusion, we observed major changes when comparing neurons kept in culture until DIV4 with neurons kept until DIV16. Next, we used our biochemical approach to investigate cultures at two time points, DIV6 and DIV16, considered here as archetypes of the immature and mature stages, respectively. We chose DIV6 instead of DIV4 to cope with two opposing issues: the investigation of an early stage and the necessity of collecting a sufficient yield of proteins. Indeed, we noticed from preliminary experiments that we were not able to obtain an amount of proteins sufficient for our analytical purposes from DIV4 culture (data not shown). In order to identify and obtain a semi-quantitative evaluation of the transmembrane protein pattern expressed at synaptic sites in the immature and mature stages, we combined our assay with MS/MS spectrometry and label-free quantification. The analysis revealed 439 proteins differentially expressed between DIV6 and DIV16 (supplemental Tables S3 and S4). With respect to the subcellular localization, 40% of proteins were associated with the plasma membrane (Fig. 4*A* and supplemental Table S3). Functional analysis indicated that 58% of differentially regulated proteins were involved in synaptic functions and 17% in cell–cell adhesion (Figs. 4*B* and 4*C*; supplemental Table S3). Interestingly, among those differentially expressed proteins, we identified 109 transmembrane proteins including 20 cell adhesion molecules (CAMs) belonging to the IgSF (Fig. 4*D*). To support our proteomic evidence, we chose two proteins for further analysis, Negr1 (33, 34) and NCAM-1 (35, 36). Western blotting experiments indicated that Negr1 and NCAM-1 were enriched in the P2 and STREP-PD fractions (Figs. 5*A* and 5*B*) and that they were both present at the synaptic site (Fig. 5*C*). Next we confirmed that Negr1 and NCAM protein expression in both P2 and STREP-PD P2 fractions as well as Negr1 and NCAM mRNAs increased significantly from DIV6 to DIV16 (Figs. 5*D* and 5*E*; quantification in Figs. 5*G*–5*I*). Furthermore, we noticed that Negr1 and NCAM expression in cortex increased during *in vivo* development (Fig. 5*F*; quantification in Fig. 5*J*), whereas the expression of a nonrelated protein, RAB3A, remained constant (supplemental Figs. S6*A* and S6*B*). Thus, our cell biotinylation assay proved to be a valuable tool for investigation of the molecular mechanisms in play during neuronal development.

Negr1 Modulates Neuronal Structural Maturation—Of the differentially expressed CAMs identified in our assay, we fo-

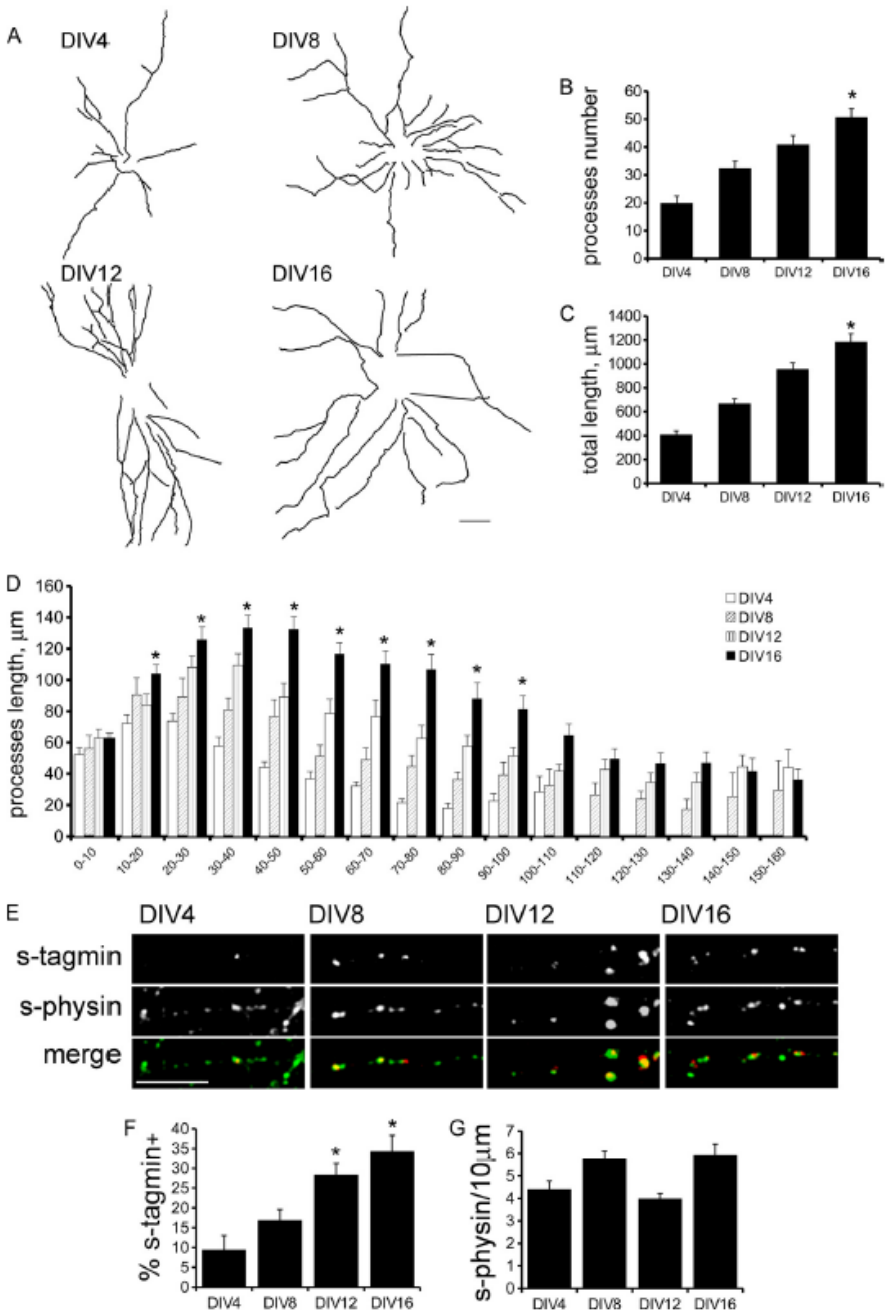

FIG. 3. **Neurons mature anatomically and functionally during *in vitro* culture.** Dissociated cortical cultures were infected at DIV1 with GFP-expressing viruses. At the indicated DIV, cells were fixed and imaged by means of confocal laser microscopy. *A*, *camera lucida* tracing of neurons kept in culture until the indicated DIV. Scale bar = 20 μm. *B*, *C*, quantification of neurite total number and length. *D*, Sholl analysis shows cumulative process length (*y*-axis) in the given spacial bin (in micrometers). Data are expressed as mean ± S.E.; $^*p < 0.01$ *versus* DIV4, ANOVA test; $n = 12$ neurons for each experimental case. *E*, the ratios of recycling synapses were estimated in incubating living cortical neurons with anti-synaptotagmin (s-tagmin) antibodies for 5 min before fixation at the indicated DIV. Post-staining with synaptophysin (s-physin) revealed the total number of synapses. Representative images were acquired with a laser-assisted confocal microscope at 63× magnification. During *in vitro* development, neurons mature functionally as indicated by the growing number of actively recycling synapses. Scale bar = 20 μm. *F*, quantification of the ratio of clusters positive for both s-tagmin and s-physin (recycling synapses) expressed as a percentage of s-physin-positive clusters (total number of synapses) in the same section. *G*, total number of s-physin-positive clusters/10 μm. Data are expressed as mean ± S.E.; $^*p < 0.05$ *versus* DIV4, ANOVA test; $n = 4$, 10 neurons for each experimental case.

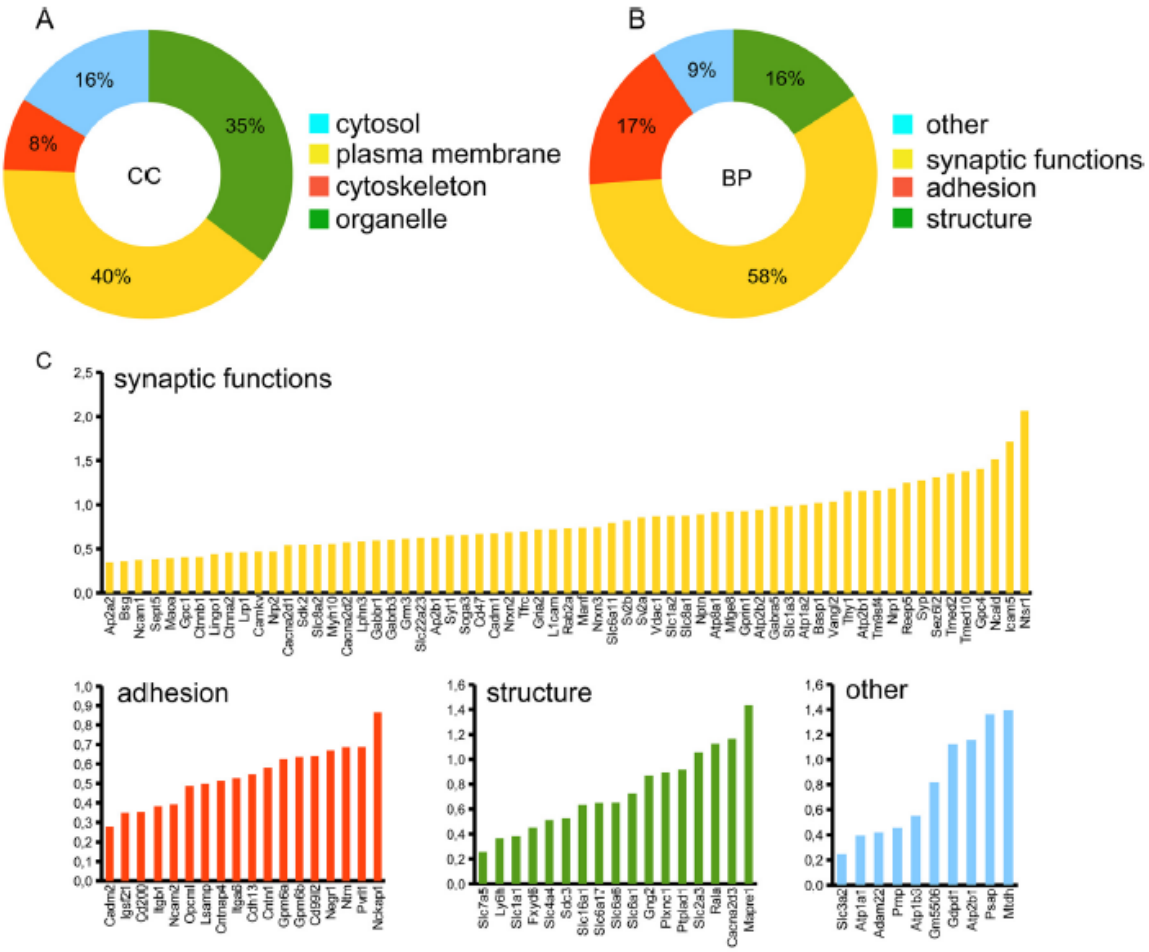

D

Description	gene	div16/div6	T-Test	#	score
basigin	Bsg	2,3	0,008	9	657
CD200 antigen	Cd200	2,3	0,048	3	114
CD47 antigen	Cd47	4,7	0,007	4	342
cell adhesion molecule 1	Cadm1	4,7	0,008	4	306
cell adhesion molecule 2	Cadm2	1,9	0,031	4	233
contactin 1	Cntn1	3,8	0,005	29	2222
immunoglobulin superfamily, member 21	Igsf21	2,2	0,004	2	161
intercellular adhesion molecule 5	Icam5	51,6	0,000	2	79
L1 cell adhesion molecule	L1cam	5,3	0,003	15	923
leucine rich repeat and Ig domain containing 1	Lingo1	2,7	0,032	6	374
limbic system-associated membrane protein	Lsamp	3,1	0,005	7	383
neural cell adhesion molecule 1	Ncam1	2,3	0,037	30	2725
neural cell adhesion molecule 2	Ncam2	2,5	0,008	10	973
neuronal growth regulator 1	Negr1	4,7	0,001	6	351
neuroplastin	Nptn	7,7	0,000	2	284
neurotrimin	Ntm	4,8	0,002	4	445
opioid binding protein/cell adhesion molecule-like	Opcml	3,1	0,004	6	551
poliovirus receptor-related 1	Pvrl1	4,9	0,010	3	322
sidekick homolog 2	Sdk2	3,5	0,001	3	140
thymus cell antigen 1, theta	Thy1	14,2	0,004	3	300

cused on Negr1. Negr1 belongs to a subgroup of the IgSF named IgLON. IgLON CAMs are implicated in synapse formation, functions, and plasticity (37). Given the expression profile we reported for *in vitro* culturing, we investigated the impact of Negr1 on neuronal morphological maturation. To this aim, we generated artificial viruses carrying GFP reporter and an miRNA-like construct able to silence Negr1 expression down to 20% of its endogenous level (supplemental Figs. S6*C*–S6*G*), reducing the short-hairpin RNA-related adverse effect (5). To evaluate the effect of Negr1 silencing on neuronal structure, we infected cortical cultures at DIV1 with viruses carrying miRNA Negr1 or miRNA control and fixed the cells at an immature (DIV6) or mature (DIV16) stage. On these cultures, we measured the neurite number, total length, and complexity (as monitored by Sholl analysis and the count of process number for each order of branching). The analysis revealed that Negr1 down-regulation did not have a significant effect on neurite arborization at DIV6 (Fig. 6). Instead, when we analyzed neurons cultured until DIV16, we found that miRNA Negr1-infected cells were characterized by significantly less complex neuritic trees than culture-matched miRNA control-infected cells (Figs. 7*A* and 7*B*). In particular we noticed that Negr1 silencing induced a decrease in neurites' total length and number (process total length, miRNA control = 1287.6 ± 91.1, miRNA Negr1 = 799.0 ± 77.1; process number, miRNA control = 54 ± 3.7, miRNA Negr1 26.7 ± 3.1; $p < 0.01$; Figs. 7*C* and 7*D*). The staining with antibodies raised against the dendritic protein MAP2 (38) suggested that Negr1 silencing affected mainly dendritic development (supplemental Fig. S7). We obtained comparable results when we down-regulated Negr1 expression via infection with a virus bearing a second Negr1 silencing construct (supplemental Fig. S8). Dendritic spines constitute the main postsynaptic elements of excitatory synapses and are morphologically distinguished as mushroom, stubby, or filopodia-like. Mushroom spines are considered mature and fully functional and are decorated by postsynaptic density markers such as PSD-95 and actin, whereas immature protrusions lack these components (39, 40). Interestingly, a previous report indicated that Negr1 overexpression positively modulates the dendritic spine number, but no evidence on the role of endogenous Negr1 has been provided so far (33). Thus we imaged dendritic protrusions in control and Negr1 silenced neurons at DIV16 and found mature protrusions stained by PSD-95 and actin or filopodial-like structures missing these markers (Fig. 8*A*). Interestingly, when we quantified the number and morphology of dendritic spines, we found that Negr1 silencing decreased the total spine number but did not have a significant impact on the morphology of these structures (spine number/10 μm: miRNA control = 1.9 ± 0.2, miRNA Negr1 = 1.33 ± 0.1, $p < 0.05$; Fig. 8*B*).

Given the implication of Negr1 involvement during neuronal morphological maturation *in vitro*, we verified its role *in vivo*. To this end, we injected miRNA control or miRNA Negr1 into the lateral ventricle of E15.5 mouse *in utero* and electroporated them into a subpopulation of neural progenitors and their progeny. After allowing *in vivo* development, we analyzed the somatosensory cortex in coronal slices obtained from pups at P7. To appreciate neuron morphology, we acquired confocal images of the GFP fluorescence in layer II/III cortical neurons that were derived from miRNA-transfected progenitors (Fig. 9*A* and supplemental Fig. S9*A*). We found that Negr1 miRNA cells displayed reduced basal dendrite arborization relative to controls, as demonstrated by the quantification of total neurite length and number (process total length: miRNA control = 538.8 ± 38.1, miRNA Negr1 = 359.8.0 ± 25.9, $p < 0.01$; process number: miRNA control = 30.4 ± 2.9, miRNA Negr1 15.7 ± 1.5, $p < 0.001$; Figs. 9*B* and 9*C*) and by Sholl analysis (supplemental Fig. S9*B*). Together, these data indicate that Negr1 down-regulation prevents normal morphological development of pyramidal neurons *in vivo*. Overall, our data suggest a critical role for Negr1 in modulating the structural maturation of neurons.

DISCUSSION

The investigation of membrane proteins is a hard task in proteomic investigations because of their low absolute amounts and their mostly hydrophobic nature. Notwithstanding the huge list of synaptosomal proteins generated by high-throughput proteomic studies, the repository of membrane protein remains poorly represented. Recently, Pielot and colleagues generated a meta-database from 12 proteomic publications describing approaches relying on enrichment of membrane fractions from different brain areas (4). The dataset included more than 2000 proteins, of which only 200 (less than 10%) were allocated to the plasma membrane. However, two articles specifically focusing on the investigation of the neuronal membrane subproteome achieved better results. Li and co-workers combined synaptic plasma membrane puri-

Fig. 4. **Identification of synaptic membrane proteins differentially expressed during neuronal development.** The comparison of STREP-PD fractions obtained from neurons at DIV6 and DIV16 via LC-MS/MS followed by label-free quantification revealed 439 differentially expressed proteins. *A*, *B*, the graphs report the GO analysis for the differentially expressed proteins considering cellular components (*A*) and biological processes (*B*). *C*, the graphs list differentially expressed membrane proteins clustered with respect to the indicated biological processes. DIV16/DIV6 ratio is expressed as Log10. *D*, we found a panel of 20 neuronal IgSF CAMs that were differentially expressed. The list reports the protein description, gene name, fold change between DIV16 and DIV6 (DIV16/DIV6), *p* value as computed after *t* test, number of peptides quantified (#), and cumulative Mascot confidence score (score). Additional protein information, including the protein accession number, description, raw abundance, GO, and peptide quantification, can be found in supplemental Tables S3 and S4.

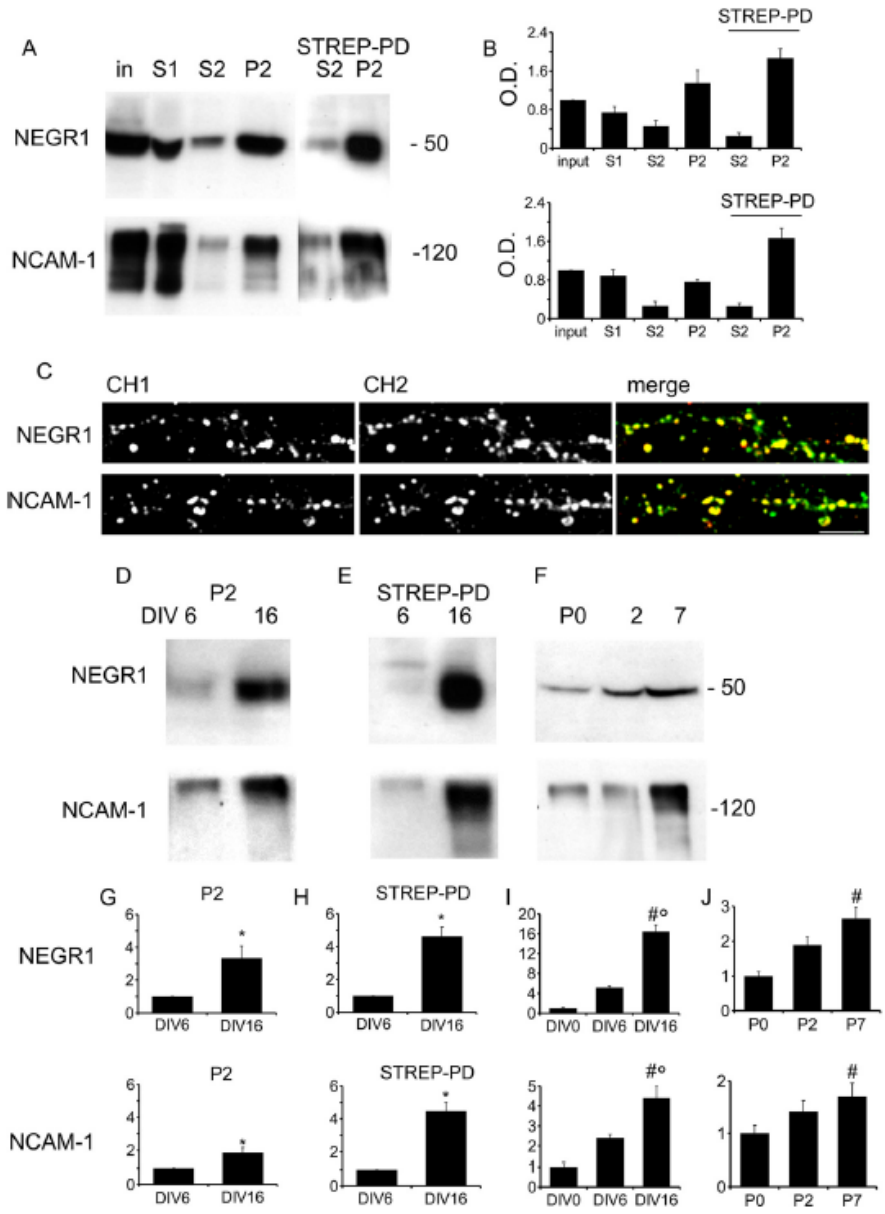

FIG. 5. **Negr1 and NCAM expression increase during *in vitro* and *in vivo* maturation.** *A*, Western blotting analysis of Negr1 and NCAM1 distribution in the biochemical fraction extracted from DIV16 cortical neurons. *B*, the quantification of the relative abundance of Negr1 and NCAM in each fraction normalized *versus* the input amount indicated that Negr1 and NCAM were enriched in STREP-PD obtained from the P2 fraction. *C*, the subcellular localization of Negr1 or NCAM was assayed via staining of DIV16 neuronal cultures with Negr1- or NCAM-specific antibodies (CH1, red) together with antibody against the synaptic marker SV2A (CH2, green). Both Negr1 and NCAM appear as clusters with overlapping with SV2A signals ("merge"). Scale bar = 50 μm. Western blotting analysis of Negr1 expression in P2 (*D*) and STREP-PD from P2 (*E*) obtained from neurons kept in culture until DIV6 and DIV16. *F*, Western blotting analysis of Negr1 expression in lysates obtained from cortexes of mice sacrificed at postnatal day 0 (P0), 2 (P2), or 7 (P7). The panels report the quantification of the relative abundance of Negr1 (upper panels) and NCAM-1 (lower panels) in P2 (*G*) and STREP-PD from P2 fractions (*H*); data were normalized *versus* the DIV6 amount. The analysis confirmed that the expression of Negr1 and NCAM-1 in P2 total and STREP-PD fractions increased during *in vitro* maturation. *I*, primary cortical neurons (DIV0 to DIV16) were analyzed by means of quantitative real-time RT-PCR for Negr-1 (upper) and Ncam-1 (lower) mRNA levels. Relative gene expression was normalized to beta-actin (ACTB) as a housekeeping gene. Expression for DIV0 was set at 1. Data are expressed as mean ± S.E.; # $p < 0.05$ *versus* DIV0, ° $p < 0.05$ *versus* DIV6 $n = 3$. Each sample was measured in triplicate. *J*, quantification of protein amount in postnatal cortices showed that the expression of Negr1 (above) and NCAM-1 (below) increased during *in vivo* maturation. Data were normalized *versus* the P0 amount. Samples containing equal amounts of proteins were resolved by means of SDS-PAGE. Data are based on protein optical density normalized as declared and expressed as mean ± S.E.; Student's *t* test, * $p < 0.05$ *versus* DIV6 or ANOVA # $p < 0.05$ *versus* P0, $n = 4$.

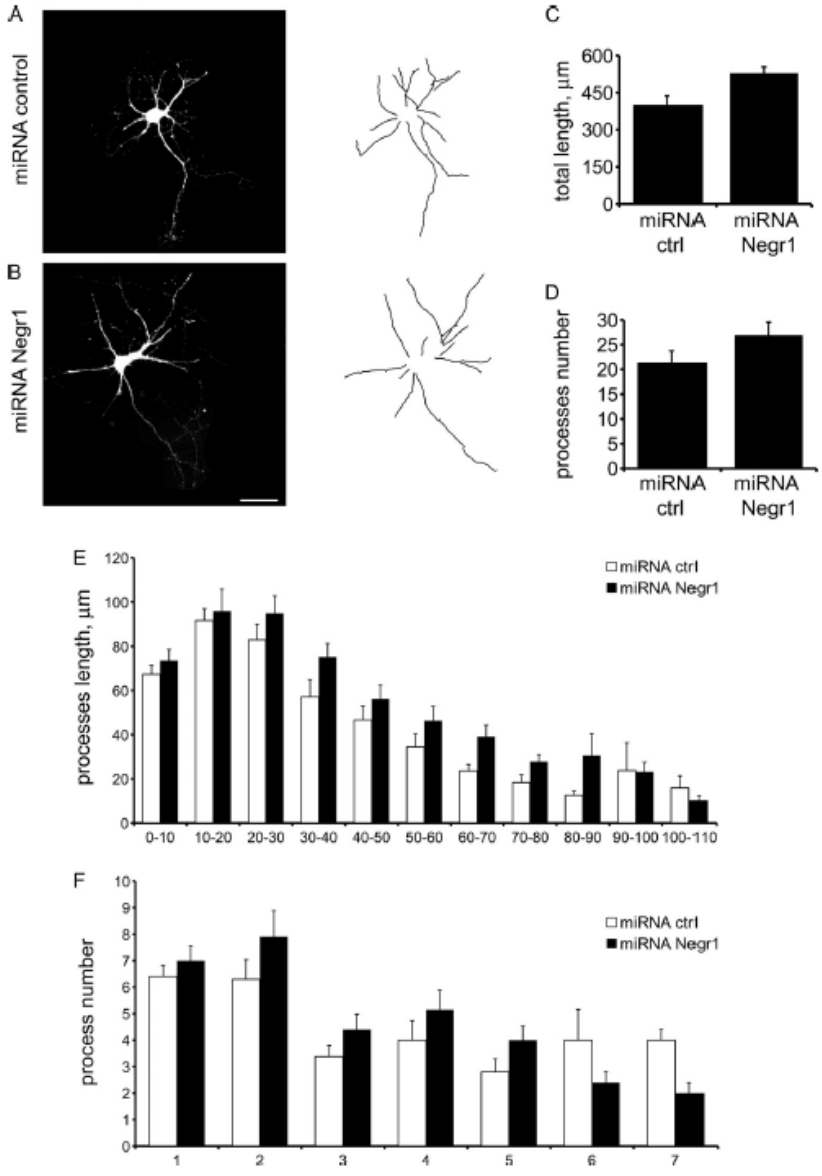

FIG. 6. **Negr1 silencing does not affect neuronal morphology at immature stages.** Cortical neurons were infected at DIV1 with miRNA control and miRNA Negr1. At DIV6, cells were fixed and imaged by means of confocal laser microscopy. *A*, *B*, confocal images highlighting the morphology of neurons infected with miRNA control and miRNA Negr1. Their relative tracings are reported on the right. *C*, *D*, quantification of the neurite total length and number for each neuron. *E*, Sholl analysis shows that Negr1 silencing did not induce significant modification of neurite immature neuronal arborization. *F*, the graph reports the number of neurites in each branching order. Scale bar = 20 μm. Data are expressed as mean ± S.E.; n = 4; 10 neurons were measured for each experimental case.

fication from rat hippocampi with blue native/SDS-PAGE and MS/MS analysis to describe 185 membrane proteins (about 36%) within a database of 514 (41). Additionally, Olsen and colleagues identified 197 membrane proteins (about 35% of 555 total hits) in plasma membrane preparations obtained from different mouse brain areas investigated by means of cation-exchange chromatography coupled with LC-MS/MS (42). In contrast to the approaches described so far in which brain tissue was used as a protein source, we applied cell surface biotinylation on primary neuronal cultures. Primary cultures constitute a robust model to recapitulate neuron physiology and ensure easy access for pharmacological and genetic manipulations that might be difficult, if not impossible, to perform in the intact brain. Furthermore, neurons can be cultured for up to 3 weeks, thus allowing the investigation of dynamic molecular modifications in a time-dependent manner. Our assay fostered the identification of up to 166 membrane proteins. Nevertheless, we found a certain amount of cytosolic/nonmembrane proteins in our dataset. The presence of cytosolic contaminants might have been due to unspecific binding to the agarose matrix of such molecules, characterized by a higher absolute cellular abundance and better solubility in aqueous buffer than membrane-passing molecules. In spite of this technical issue, the performance of our protocol far exceeds the results of similar investigations on primary cultures, to the best of our knowledge. In particular, Stella and colleagues identified about 30 membrane proteins from a preparation of membrane obtained from pri-

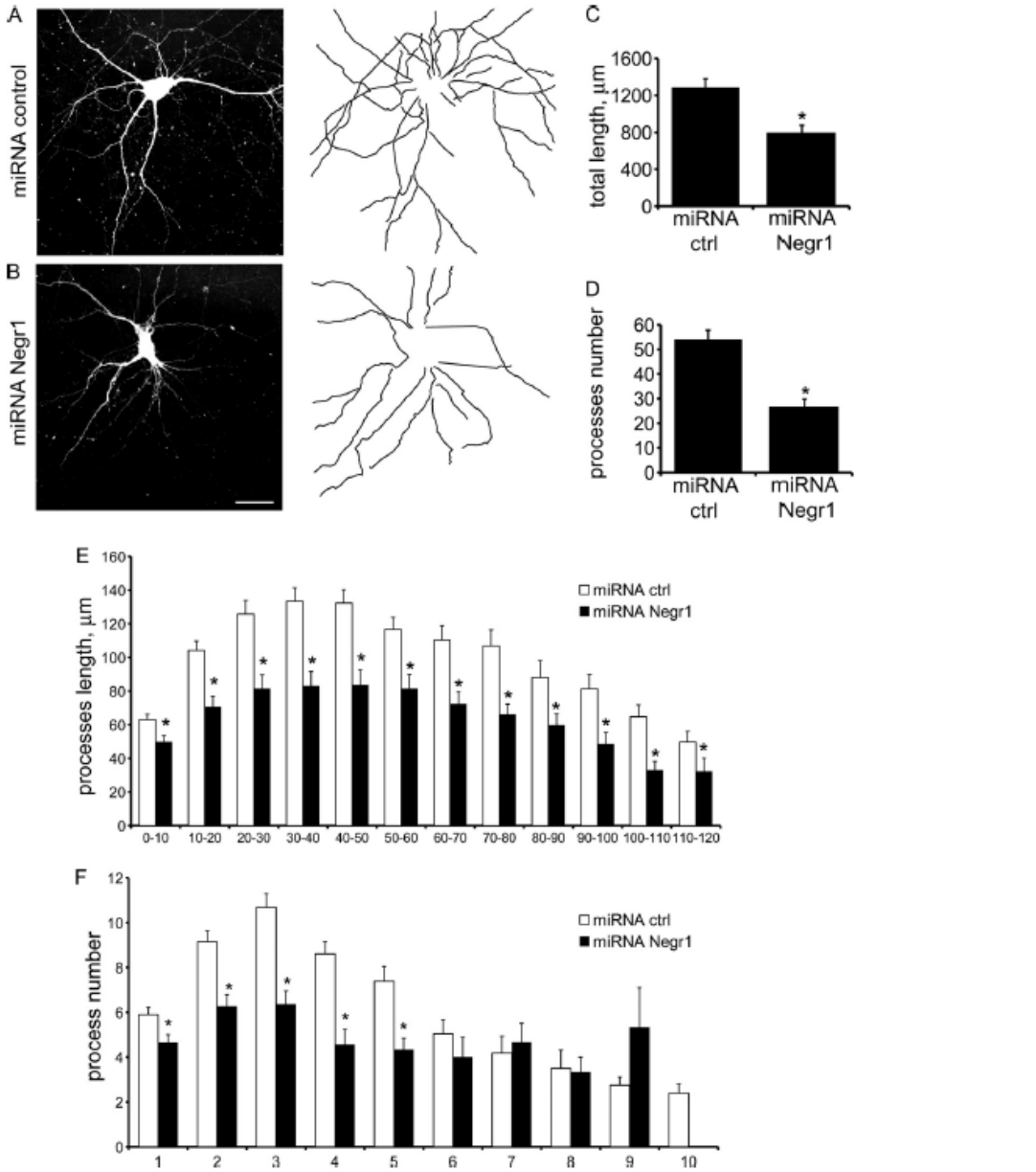

FIG. 7. **Negr1 silencing affects neuronal morphology at mature stages.** Cortical neurons were infected at DIV1 with miRNA control and miRNA Negr1. At DIV16, cells were fixed and imaged by means of confocal laser microscopy. *A*, *B*, morphology of neurons infected with miRNA control and miRNA Negr1 and relative tracing. *C*, *D*, quantification of neurite total length and number for each neuron. *E*, Sholl analysis showed that the neurite arborization was severely affected by miRNA Negr1 infection. *F*, miRNA Negr1 infection altered the distribution of neurites in each branching order. Scale bar = 20 μm. Data are expressed as mean ± S.E.; Student's *t* test, * $p < 0.01$, $n = 4$; 10 neurons were measured for each experimental case.

mary cultures of cerebellar granule neurons (43). The protocol we proposed here implies incubation with nonpermeable biotin with the aim of tagging the proteins truly exposed to the extracellular side at a given functional/developmental stage. Chen and colleagues developed a similar approach and revealed 27 proteins predicted to have at least one transmembrane domain in primary hippocampal cultures (44). Their method lacked the biochemical fractionation utilized here. This difference may account for the much higher recovery of membrane proteins we reported here in comparison to the results of Chen and colleagues. Furthermore, the P2 fraction used in our assay enriches plasma membranes and synaptosome (see supplemental Fig. S1 and Ref. 9), an artificial organelle comprising pre- and postsynaptic elements (45).

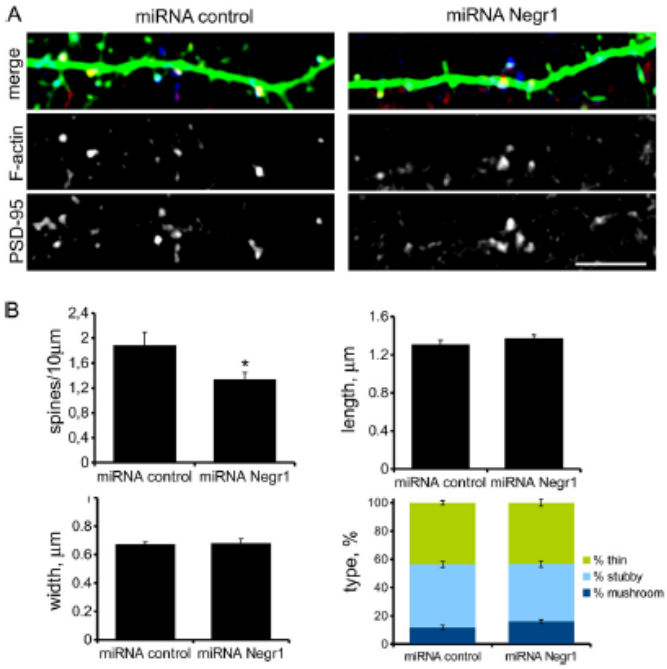

FIG. 8. **Negr1 silencing affects dendritic spine density.** Cortical neurons were infected at DIV1 with miRNA control and miRNA Negr1. At DIV16, cells were fixed, stained, and imaged by means of confocal laser microscopy. *A*, we imaged neuron processes (green) to highlight dendritic spines. Mature spines were decorated by F-actin (red) and PSD-95 (blue). *B*, quantification of morphological parameters describing spines. The panel reports spine density (spine number/10 μm), length, width, and percentage of protrusions characterized by a mushroom, stubby, or thin morphology (type). Scale bar = 10 μm. Data are expressed as mean ± S.E.; Student's *t* test, * $p < 0.05$, $n = 3$; seven neurons were measured for each experimental case.

Accordingly, about 55% of the membrane protein identified by our assay is synaptic or associated with synaptic function according to the GO annotation.

When we compared immature *versus* mature neuronal cultures, we identified a panel of 439 differentially expressed proteins. Among them, we found 109 proteins localized at the plasma membrane, and in particular we found 20 IgSF CAMs. Neuronal IgSF CAMs associate at the cell surface to form homo- and heterophilic complexes and regulate neurite outgrowth and synaptic-contact formation (3). The expression levels of Thy-1 (46), cell adhesion molecule 3 (47), cell adhesion molecule L1 (48), NrCAM (49, 50), neuroplastins (51), and basigin (52) are necessary for the proper establishment of functional neuronal circuitry. Thus, our data are perfectly in line with the fact that the above-mentioned CAMs have a precise expression profile tightly correlated to neuronal maturation. Given their pivotal role during neuronal development, several CAMs have been not surprisingly implicated in neurological disorders (53–55). Recent genetic linkages have associated NrCAM and Negr1 with autism spectrum disorder (56–58).

Negr1 is a synaptic adhesion protein member of the IgLON CAM family (59). In dissociated neurons in culture, Negr1 is mainly observed at axons and presynaptic terminals at early culture stages, but it becomes also postsynaptic at late culture stages (33). Finally, Negr1 overexpression affects the number of synapses with different outcomes depending on the culture stage. If it occurs in early stages, the overexpression of Negr1 decreases the number of synapses, whereas at later stages it is positively associated with synapse number (37). The silencing approach described here sheds light on the physiological function of endogenous Negr1. In particular, we demonstrated that Negr1 hypoexpression induced a significant decrease in the number and length of neuronal processes in mature neurons, thus causing a severe reduction of the overall complexity of neurite arborization *in vitro* and *in vivo*. Given that we reported a similar phenotype in cells overexpressing Negr1, overall our data demonstrate that the Negr1 expression level is tightly associated with neuronal maturation and that it controls the proper development of neurite arborization and dendritic spines.

The pattern of dendrite arborization exhibited by a neuron is tightly correlated to its function. Any alteration in dendrite morphology has dramatic consequences for the proper formation and functionality of the connectivity network within surrounding cells (60, 61). Recent findings point to altered brain connectivity as a key feature in autism spectrum disorder (62). Interestingly, evidence links the pathogenesis of autism spectrum disorder specifically to neuronal-network anomalies and dendritic spine dysmorphology (63–65). We hypothesize that Negr1 regulates the development, formation, and stabilization of a functional neurite network, and consequently Negr1 mutation might contribute to the anatomical aberrations reported in autism spectrum disorder. Independent approaches are needed to confirm the precise localization of the hits identified. Nevertheless, we are confident that our assay can increase the recovery of membrane proteins and facilitate the isolation of molecules functionally and/or topologically related to the synapse.

Finally, our study allowed the preliminary identification of a panel of membrane proteins whose expression was correlated with neuronal development. Although further studies

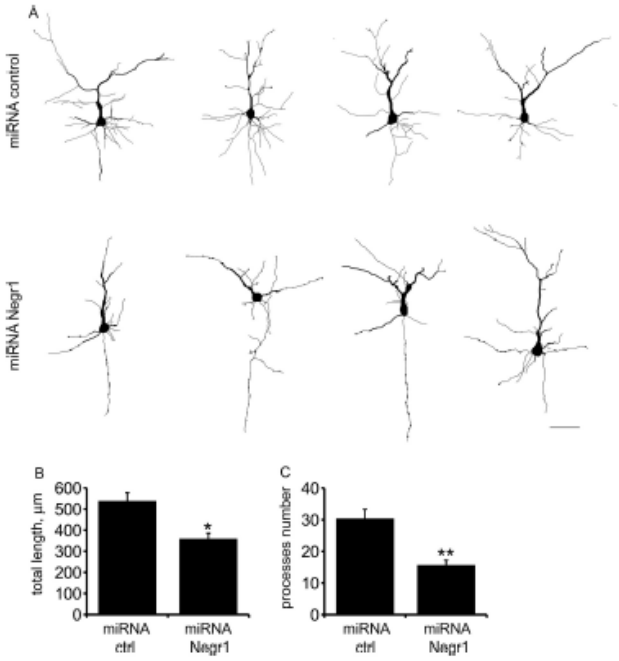

FIG. 9. **Negr1 affects neuronal morphology *in vivo*.** Mouse embryos were electroporated *in utero* at E15.5 with miRNA control or miRNA Negr1 and sacrificed at P7. *A*, *camera lucida* drawing elaborated from confocal images of GFP fluorescence in coronal sections of mouse somatosensory cortices. Negr1 down-regulation resulted in a decrease in the total length (*B*) and number (*C*) of neurite processes. Scale bar = 20 μm; Student's *t* test, * $p < 0.01$, ** $p < 0.001$, $n = 3$; 10 electroporated cells were measured for each experimental case.

will be required to clarify in detail the mechanisms orchestrated by these molecules, our assay proved to be a reliable starting point to study the extracellular proteome and monitor its implication in physiological and pathological neuronal mechanisms.

Acknowledgments—We are grateful to Dr. Ugo Cavallaro (IFOM, Milano, Italy) for reagents and critical discussion.

* This work was supported by the LRRK2 Biology LEAPS program of the Michael J. Fox Foundation (G.P. and M.U.). G.P. is supported by Fondazione Cariplo (Grant No. 2011–0540), the FIRB program (Grant No. RBFR08F82X_002), and Fondazione Telethon (Grant No. GGP12237). L.C. is grateful to the FIRB program (FIRB Grant No. RBFR08F82X). This work was supported by the EU grant 'Systems Biology of Stem Cells and Reprogramming' (SyBoSS [FP7-Health-F4-2010-242129]) and by the Helmholtz Alliance HelMA–Helmholtz Alliance for Mental Health in an Ageing Society, through the Initiative and Network Fund of the Helmholtz Association and (in part) by the Helmholtz Portfolio Theme 'Supercomputing and Modelling for the Human Brain' (SMHB) to F.G.

[S] This article contains supplemental material.

§§ To whom correspondence should be addressed: Giovanni Piccoli, Institute of Neuroscience, National Research council, IN-CNR Milano, via Vanvitelli 32, 20129 Milano, Italy. Tel.: 390250317093; Fax: 39-0250317132; E-mail: giovanni.piccoli@in.cnr.it.

REFERENCES

1. Wallin, E., and von Heijnbh, E. G. (1998) Genome-wide analysis of integral membrane proteins from eubacterial, archaean, and eukaryotic organisms. *Protein Sci.* **7,** 1029–1038
2. Gerrow, K., and El-Husseini, A. (2006) Cell adhesion molecules at the synapse. *Front. Biosci.* **11,** 2400–2419
3. Maness, P. F., and Schachner, M. (2007) Neural recognition molecules of the immunoglobulin superfamily: signaling transducers of axon guidance and neuronal migration. *Nat. Neurosci.* **10,** 19–26
4. Pielot, R., Smalla, K.-H., Müller, A., Landgraf, P., Lehmann, A.-C., Eisenschmidt, E., Haus, U.-U., Weismantel, R., Gundelfinger, E. D., and Dieterich, D. C. (2012) SynProt: a database for proteins of detergent-resistant synaptic protein preparations. *Front. Synaptic Neurosci.* **4,** 1
5. Bauer, M., Kinkl, N., Meixner, A., Kremmer, E., Riemenschneider, M., Förstl, H., Gasser, T., and Ueffing, M. (2009) Prevention of interferon-stimulated gene expression using microRNA-designed hairpins. *Gene Ther.* **16,** 142–147
6. Wiznerowicz, M., and Trono, D. (2003) Conditional suppression of cellular genes: lentivirus vector-mediated drug-inducible RNA interference. *J. Virol.* **77,** 8957–8961
7. Piccoli, G., Verpelli, C., Tonna, N., Romorini, S., Alessio, M., Nairn, A. C., Bachi, A., and Sala, C. (2007) Proteomic analysis of activity-dependent synaptic plasticity in hippocampal neurons. *J. Proteome Res.* **6,** 3203–3215
8. Brewer, G. J., Torricelli, J. R., Evege, E. K., and Price, P. J. (1993) Optimized survival of hippocampal neurons in B27-supplemented Neurobasal, a new serum-free medium combination. *J. Neurosci. Res.* **35,** 567–576
9. Corti, V., Sanchez-Ruiz, Y., Piccoli, G., Bergamaschi, A., Cannistraci, C. V., Pattini, L., Cerutti, S., Bachi, A., Alessio, M., and Malgaroli, A. (2008) Protein fingerprints of cultured CA3-CA1 hippocampal neurons: comparative analysis of the distribution of synaptosomal and cytosolic proteins. *BMC Neurosci.* **9,** 36
10. Pietrini, G., Matteoli, M., Banker, G., and Caplan, M. J. (1992) Isoforms of the Na,K-ATPase are present in both axons and dendrites of hippocampal neurons in culture. *Proc. Natl. Acad. Sci. U.S.A.* **89,** 8414–8418
11. Rudelius, M., Osanger, A., Kohlmann, S., Augustin, M., Piontek, G., Heinzmann, U., Jennen, G., Russ, A., Matiasek, K., Stumm, G., and Schlegel, J. (2006) A missense mutation in the WD40 domain of murine Lyst is linked to severe progressive Purkinje cell degeneration. *Acta Neuropathol.* **112,** 267–276
12. Wearne, S. L., Rodriguez, A., Ehlenberger, D. B., Rocher, A. B., Henderson, S. C., and Hof, P. R. (2005) New techniques for imaging, digitization and analysis of three-dimensional neural morphology on multiple scales. *Neuroscience* **136,** 661–680
13. Rodriguez, A., Ehlenberger, D. B., Dickstein, D. L., Hof, P. R., and Wearne, S. L. (2008) Automated three-dimensional detection and shape classification of dendritic spines from fluorescence microscopy images. *PLoS One* **3,** e1997
14. Matteoli, M., Takei, K., Perin, M. S., Sudhof, T. C., and De Camilli, P. (1992) Exo-endocytotic recycling of synaptic vesicles in developing processes of cultured hippocampal neurons. *J. Cell Biol.* **117,** 849–861
15. Piccoli, G., Condliffe, S. B., Bauer, M., Giesert, F., Boldt, K., De Astis, S., Meixner, A., Sarioglu, H., Vogt-Weisenhorn, D. M., Wurst, W., *et al.* (2011) LRRK2 controls synaptic vesicle storage and mobilization within the recycling pool. *J. Neurosci.* **31,** 2225–2237
16. Verderio, C., Coco, S., Rossetto, O., Montecucco, C., and Matteoli, M. (1999) Internalization and proteolytic action of botulinum toxins in CNS neurons and astrocytes. *J. Neurochem.* **73,** 372–379
17. Wiśniewski, J. R., Zougman, A., Nagaraj, N., and Mann, M. (2009) Universal sample preparation method for proteome analysis. *Nat. Methods* **6,** 359–362
18. Hauck, S. M., Dietter, J., Kramer, R. L., Hofmaier, F., Zipplies, J. K., Amann, B., Feuchtinger, A., Deeg, C. A., and Ueffing, M. (2010) Deciphering membrane-associated molecular processes in target tissue of autoimmune uveitis by label-free quantitative mass spectrometry. *Mol. Cell. Proteomics* **9,** 2292–2305
19. Olsen, J. V. (2005) Parts per million mass accuracy on an Orbitrap mass spectrometer via lock mass injection into a C-trap. *Mol. Cell. Proteomics* **4,** 2010–2021
20. Keller, A., Nesvizhskii, A. I., Kolker, E., and Aebersold, R. (2002) Empirical statistical model to estimate the accuracy of peptide identifications made by MS/MS and database search. *Anal.* **74,** 5383–5392

21. Nesvizhskii, A. I., Keller, A., Kolker, E., and Aebersold, R. (2003) A statistical model for identifying proteins by tandem mass spectrometry. *Anal.* **75,** 4646–4658
22. dal Maschio, M., Ghezzi, D., Bony, G., Alabastri, A., Deidda, G., Brondi, M., Sato, S. S., Zaccaria, R. P., Di Fabrizio, E., Ratto, G. M., and Cancedda, L. (2012) High-performance and site-directed in utero electroporation by a triple-electrode probe. *Nat. Commun.* **3,** 960
23. Giesert, F., Hofmann, A., Bürger, A., Zerle, J., Kloos, K., Hafen, U., Ernst, L., Zhang, J., Vogt-Weisenhorn, D. M., and Wurst, W. (2013) Expression analysis of Lrrk1, Lrrk2 and Lrrk2 splice variants in mice. *PLoS One* **8,** e63778
24. Sims, K. D., Straff, D. J., and Robinson, M. B. (2000) Platelet-derived growth factor rapidly increases activity and cell surface expression of the EAAC1 subtype of glutamate transporter through activation of phosphatidylinositol 3-kinase. *J. Biol. Chem.* **275,** 5228–5237
25. Huang, D. W., Sherman, B. T., and Lempicki, R. A. (2009) Bioinformatics enrichment tools: paths toward the comprehensive functional analysis of large gene lists. *Nucleic Acids Res.* **37,** 1–13
26. Huang, D. W., Sherman, B. T., and Lempicki, R. A. (2009) Systematic and integrative analysis of large gene lists using DAVID bioinformatics resources. *Nat. Protoc.* **4,** 44–57
27. Higgins, D., Burack, M., Lein, P., and Banker, G. (1997) Mechanisms of neuronal polarity. *Curr. Opin. Neurobiol.* **7,** 599–604
28. Craig, A. M., Jareb, M., and Banker, G. (1992) Neuronal polarity. *Curr. Opin. Neurobiol.* **2,** 602–606
29. Craig, A. M., and Banker, G. (1994) Neuronal polarity. *Annu. Rev. Neurosci.* **17,** 267–310
30. Dotti, C. G., Sullivan, C. A., and Banker, G. A. (1988) The establishment of polarity by hippocampal neurons in culture. *J. Neurosci.* **8,** 1454–1468
31. Trachtenberg, J. T., Chen, B. E., Knott, G. W., Feng, G., Sanes, J. R., Welker, E., and Svoboda, K. (2002) Long-term in vivo imaging of experience-dependent synaptic plasticity in adult cortex. *Nature* **420,** 788–794
32. Mozhayeva, M. G., Sara, Y., Liu, X., and Kavalali, E. T. (2002) Development of vesicle pools during maturation of hippocampal synapses. *J. Neurosci.* **22,** 654–665
33. Hashimoto, T., Yamada, M., Maekawa, S., Nakashima, T., and Miyata, S. (2008) IgLON cell adhesion molecule Kilon is a crucial modulator for synapse number in hippocampal neurons. *Brain Res.* **1224,** 1–11
34. Schäfer, M., Bräuer, A. U., Savaskan, N. E., Rathjen, F. G., and Brümmendorf, T. (2005) Neurotractin/kilon promotes neurite outgrowth and is expressed on reactive astrocytes after entorhinal cortex lesion. *Mol. Cell. Neurosci.* **29,** 580–590
35. Gascon, E., Vutskits, L., and Kiss, J. Z. (2007) Polysialic acid-neural cell adhesion molecule in brain plasticity: from synapses to integration of new neurons. *Brain Res. Rev.* **56,** 101–118
36. Durbec, P., and Cremer, H. (2001) Revisiting the function of PSA-NCAM in the nervous system. *Mol. Neurobiol.* **24,** 53–64
37. Hashimoto, T., Maekawa, S., and Miyata, S. (2009) IgLON cell adhesion molecules regulate synaptogenesis in hippocampal neurons. *Cell Biochem. Funct.* **27,** 496–498
38. Caceres, A., Binder, L. I., Payne, M. R., Bender, P., Rebhun, L., and Steward, O. (1984) Differential subcellular localization of tubulin and the microtubule-associated protein MAP2 in brain tissue as revealed by immunocytochemistry with monoclonal hybridoma antibodies. *J. Neurosci.* **4,** 394–410
39. Bosch, M., and Hayashi, Y. (2012) Structural plasticity of dendritic spines. *Curr. Opin. Neurobiol.* **22,** 383–388
40. Hayashi, Y., and Majewska, A. K. (2005) Dendritic spine geometry: functional implication and regulation. *Neuron.* **46,** 529–532
41. Li, X., Xie, C., Jin, Q., Liu, M., He, Q., Cao, R., Lin, Y., Li, J., Li, Y., Chen, P., and Liang, S. (2009) Proteomic screen for multiprotein complexes in synaptic plasma membrane from rat hippocampus by blue native gel electrophoresis and tandem mass spectrometry. *J. Proteome Res.* **8,** 3475–3486
42. Olsen, J. V., Nielsen, P. A., Andersen, J. R., Mann, M., and Wiśniewski, J. R. (2007) Quantitative proteomic profiling of membrane proteins from the mouse brain cortex, hippocampus, and cerebellum using the HysTag reagent: mapping of neurotransmitter receptors and ion channels. *Brain Res.* **1134,** 95–106
43. Stella, R., Cifani, P., Peggion, C., Hansson, K., Lazzari, C., Bendz, M., Levander, F., Sorgato, M. C., Bertoli, A., and James, P. (2012) Relative quantification of membrane proteins in wild-type and prion protein (PrP)-knockout cerebellar granule neurons. *J. Proteome Res.* **11,** 523–536
44. Chen, P., Li, X., Sun, Y., Liu, Z., Cao, R., He, Q., Wang, M., Xiong, J., Xie, J., Wang, X., and Liang, S. (2006) Proteomic analysis of rat hippocampal plasma membrane: characterization of potential neuronal-specific plasma membrane proteins. *J. Neurochem.* **98,** 1126–1140
45. Dodd, P. R., Hardy, J. A., Oakley, A. E., Edwardson, J. A., Perry, E. K., and Delaunoy, J. P. (1981) A rapid method for preparing synaptosomes: comparison, with alternative procedures. *Brain Res.* **226,** 107–118
46. Chen, C.-H., Wang, S.-M., Yang, S.-H., and Jeng, C.-J. (2005) Role of Thy-1 in in vivo and in vitro neural development and regeneration of dorsal root ganglionic neurons. *J. Cell. Biochem.* **94,** 684–694
47. Maurel, P., Einheber, S., Galinska, J., Thaker, P., Lam, I., Rubin, M. B., Scherer, S. S., Murakami, Y., Gutmann, D. H., and Salzer, J. L. (2007) Nectin-like proteins mediate axon Schwann cell interactions along the internode and are essential for myelination. *J. Cell Biol.* **178,** 861–874
48. Cui, X., Weng, Y.-Q., Frappé, I., Burgess, A., Girão da Cruz, M. T., Schachner, M., and Aubert, I. (2011) The cell adhesion molecule L1 regulates the expression of choline acetyltransferase and the development of septal cholinergic neurons. *Brain Behav.* **1,** 73–86
49. Sakurai, T. (2012) The role of NrCAM in neural development and disorders—beyond a simple glue in the brain. *Mol. Cell. Neurosci.* **49,** 351–363
50. Demyanenko, G. P., Riday, T. T., Tran, T. S., Dalal, J., Darnell, E. P., Brennaman, L. H., Sakurai, T., Grumet, M., Philpot, B. D., and Maness, P. F. (2011) NrCAM deletion causes topographic mistargeting of thalamocortical axons to the visual cortex and disrupts visual acuity. *J. Neurosci.* **31,** 1545–1558
51. Marzban, H., Khanzada, U., Shabir, S., Hawkes, R., Langnaese, K., Smalla, K.-H., Bockers, T. M., Gundelfinger, E. D., Gordon-Weeks, P. R., and Beesley, P. W. (2003) Expression of the immunoglobulin superfamily neuroplastin adhesion molecules in adult and developing mouse cerebellum and their localisation to parasagittal stripes. *J. Comp. Neurol.* **462,** 286–301
52. Munro, M., Akkam, Y., and Curtin, K. D. (2010) Mutational analysis of Drosophila basigin function in the visual system. *Gene* **449,** 50–58
53. Zoghbi, H. Y., and Bear, M. F. (2012) Synaptic dysfunction in neurodevelopmental disorders associated with autism and intellectual disabilities. Cold Spring Harb Perspect Biol 2012;4:a009886
54. Ye, H., Liu, J., and Wu, J. Y. (2010) Cell adhesion molecules and their involvement in autism spectrum disorder. *Neurosignals* **18,** 62–71
55. Melom, J. E., and Littleton, J. T. (2011) Synapse development in health and disease. *Curr. Opin. Genet. Dev.* **21,** 256–261
56. Hussman, J. P., Chung, R. H., Griswold, A. J., Jaworski, J. M., Salyakina, D., Ma, D., Konidari, I., Whitehead, P. L., Vance, J. M., Martin, E. R., Cuccaro, M. L., Gilbert, J. R., Haines, J. L., and Pericak-Vance, M. A. (2011) A noise-reduction GWAS analysis implicates altered regulation of neurite outgrowth and guidance in autism. *Mol. Autism* **2,** 1
57. Pinto, D., Pagnamenta, A. T., Klei, L., Anney, R., Merico, D., Regan, R., Conroy, J., Magalhaes, T. R., Correia, C., Abrahams, B. S., Almeida, J., Bacchelli, E., Bader, G. D., Bailey, A. J., Baird, G., Battaglia, A., Berney, T., Bolshakova, N., Bölte, S., Bolton, P. F., Bourgeron, T., Brennan, S., Brian, J., Bryson, S. E., Carson, A. R., Casallo, G., Casey, J., Chung, B. H., Cochrane, L., Corsello, C., Crawford, E. L., Crossett, A., Cytrynbaum, C., Dawson, G., de Jonge, M., Delorme, R., Drmic, I., Duketis, E., Duque, F., Estes, A., Farrar, P., Fernandez, B. A., Folstein, S. E., Fombonne, E., Freitag, C. M., Gilbert, J., Gillberg, C., Glessner, J. T., Goldberg, J., Green, A., Green, J., Guter, S. J., Hakonarson, H., Heron, E. A., Hill, M., Holt, R., Howe, J. L., Hughes, G., Hus, V., Igliozzi, R., Kim, C., Klauck, S. M., Kolevzon, A., Korvatska, O., Kustanovich, V., Lajonchere C. M., Lamb, J. A., Laskawiec, M., Leboyer, M., Le Couteur, A., Leventhal, B. L., Lionel, A. C., Liu, X. Q., Lord, C., Lotspeich, L., Lund, S. C., Maestrini, E., Mahoney, W., Mantoulan, C., Marshall, C. R., McConachie, H., McDougle, C. J., McGrath, J., McMahon, W. M., Merikangas, A., Migita, O., Minshew, N. J., Mirza, G. K., Munson, J., Nelson, S. F., Noakes, C., Noor, A., Nygren, G., Oliveira, G., Papanikolaou, K., Parr, J. R., Parrini, B., Paton, T., Pickles, A., Pilorge, M., Piven, J., Ponting, C. P., Posey, D. J., Poustka, A., Poustka, F., Prasad, A., Ragoussis, J., Renshaw, K., Rickaby, J., Roberts, W., Roeder, K., Roge, B., Rutter, M. L., Bierut, L. J., Rice, J. P., Salt, J., Sansom, K., Sato, D., Segurado,

R., Sequeira, A. F., Senman, L., Shah, N., Sheffield, V. C., Soorya, L., Sousa, I., Stein, O., Sykes, N., Stoppioni, V., Strawbridge, C., Tancredi, R., Tansey, K., Thiruvahindrapduram, B., Thompson, A. P., Thomson, S., Tryfon, A., Tsiantis, J., Van Engeland, H., Vincent, J. B., Volkmar, F., Wallace, S., Wang, K., Wang, Z., Wassink, T. H., Webber, C., Weksberg, R., Wing, K., Wittemeyer, K., Wood, S., Wu, J., Yaspan, B. L., Zurawiecki, D., Zwaigenbaum, L., Buxbaum, J. D., Cantor, R. M., Cook, E. H., Coon, H., Cuccaro, M. L., Devlin, B., Ennis, S., Gallagher, L., Geschwind, D. H., Gill, M., Haines, J. L., Hallmayer, J., Miller, J., Monaco, A. P., Nurnberger, J. I., Jr., Paterson, A. D., Pericak-Vance, M. A., Schellenberg, G. D., Szatmari, P., Vicente, A. M., Vieland, V. J., Wijsman, E. M., Scherer, S. W., Sutcliffe, J. S., and Betancur, C. (2010) Functional impact of global rare copy number variation in autism spectrum disorders. *Nature* **466,** 368–372

58. Michaelson, J. J., Shi, Y., Gujral, M., Zheng, H., Malhotra, D., Jin, X., Jian, M., Liu, G., Greer, D., Bhandari, A., Wu, W., Corominas, R., Peoples, A., Koren, A., Gore, A., Kang, S., Lin, G. N., Estabillo, J., Gadomski, T., Singh, B., Zhang, K., Akshoomoff, N., Corsello, C., McCarroll, S., Iakoucheva, L. M., Li, Y., Wang, J., and Sebat, J. (2012) Whole-genome sequencing in autism identifies hot spots for de novo germline mutation. *Cell* **151,** 1431–1442
59. Miyata, S., Matsumoto, N., Taguchi, K., Akagi, A., Iino, T., Funatsu, N., and Maekawa, S. (2003) Biochemical and ultrastructural analyses of IgLON cell adhesion molecules, Kilon and OBCAM in the rat brain. *Neuroscience* **117,** 645–658
60. Yuste, R., and Tank, D. W. (1996) Dendritic integration in mammalian neurons, a century after Cajal. *Neuron* **16,** 701–716
61. Connors, B. W., and Regehr, W. G. (1996) Neuronal firing: does function follow form? *Curr. Biol.* **6,** 1560–1562
62. Vissers, M. E., Cohen, M. X., and Geurts, H. M. (2012) Brain connectivity and high functioning autism: a promising path of research that needs refined models, methodological convergence, and stronger behavioral links. *Neurosci. Biobehav. Rev.* **36,** 604–625
63. Penzes, P., Cahill, M. E., Jones, K. A., VanLeeuwen, J.-E., and Woolfrey, K. M. (2011) Dendritic spine pathology in neuropsychiatric disorders. *Nat. Neurosci.* **14,** 285–293
64. Baudouin, S. J., Gaudias, J., Gerharz, S., Hatstatt, L., Zhou, K., Punnakkal, P., Tanaka, K. F., Spooren, W., Hen, R., De Zeeuw, C. I., Vogt, K., and Scheiffele, P. (2012) Shared synaptic pathophysiology in syndromic and nonsyndromic rodent models of autism. *Science* **338,** 128–132
65. Bailey, A., Luthert, P., Dean, A., Harding, B., Janota, I., Montgomery, M., Rutter, M., and Lantos, P. (1998) A clinicopathological study of autism. *Brain* **121 (Pt 5),** 889–905

12. APPENDIX II

MCB
Journals.ASM.org

Leucine-Rich Repeat Kinase 2 Binds to Neuronal Vesicles through Protein Interactions Mediated by Its C-Terminal WD40 Domain

Giovanni Piccoli,[a,b] Franco Onofri,[c] Maria Daniela Cirnaru,[b] Christoph J. O. Kaiser,[d] Pravinkumar Jagtap,[d,e] Andreas Kastenmüller,[d] Francesca Pischedda,[b] Antonella Marte,[c] Felix von Zweydorf,[f] Andreas Vogt,[a,f] Florian Giesert,[g] Lifeng Pan,[h] Flavia Antonucci,[i] Christina Kiel,[j] Mingjie Zhang,[h] Sevil Weinkauf,[d] Michael Sattler,[d,e] Carlo Sala,[b] Michela Matteoli,[i] Marius Ueffing,[a,f] Christian Johannes Gloeckner[a,f]

Helmholtz Zentrum München, German Research Center for Environmental Health, Research Unit Protein Science, Neuherberg, Germany[a]; Institute of Neuroscience, National Research Council, Milan, Italy[b]; Department of Experimental Medicine, University of Genoa, Genoa, Italy[c]; Center for Integrated Protein Science Munich and Technische Universität München, Department of Chemistry, Garching, Germany[d]; Helmholtz Zentrum München, German Research Center for Environmental Health, Institute of Structural Biology, Neuherberg, Germany[e]; Eberhard Karls University Tübingen, Institute for Ophthalmic Research, Medical Proteome Center, Tübingen, Germany[f]; Helmholtz Zentrum München, German Research Center for Environmental Health, Institute of Developmental Genetics, Neuherberg, Germany[g]; Division of Life Science, Centre of Systems Biology and Human Health, Institute for Advanced Study and School of Science, Hong Kong University of Science and Technology, Clear Water Bay, Kowloon, Hong Kong[h]; Department of Biotechnology and Translational Medicine, University of Milan and Humanitas Clinical and Research Center, Rozzano, Italy[i]; CRG-EMBL System Biology Program, Centre de Regulació Genòmica UPF, Barcelona, Spain[j]

Mutations in the leucine-rich repeat kinase 2 gene (*LRRK2*) are associated with familial and sporadic Parkinson's disease (PD). LRRK2 is a complex protein that consists of multiple domains, including predicted C-terminal WD40 repeats. In this study, we analyzed functional and molecular features conferred by the WD40 domain. Electron microscopic analysis of the purified LRRK2 C-terminal domain revealed doughnut-shaped particles, providing experimental evidence for its WD40 fold. We demonstrate that LRRK2 WD40 binds and sequesters synaptic vesicles via interaction with vesicle-associated proteins. In fact, a domain-based pulldown approach combined with mass spectrometric analysis identified LRRK2 as being part of a highly specific protein network involved in synaptic vesicle trafficking. In addition, we found that a C-terminal sequence variant associated with an increased risk of developing PD, G2385R, correlates with a reduced binding affinity of LRRK2 WD40 to synaptic vesicles. Our data demonstrate a critical role of the WD40 domain within LRRK2 function.

Parkinson's disease (PD) is the second most common age-related neurodegenerative disease and is clinically characterized by movement impairments, bradykinesia, rigidity, and resting tremor and pathologically by the progressive loss of dopaminergic neurons in the substantia nigra and the formation of Lewy bodies (1, 2). Although the majority of cases are sporadic, mutations in the leucine-rich repeat kinase 2 (*LRRK2*) gene (PARK8; Online Mendelian Inheritance in Man [OMIM] accession number 609007) had been unequivocally linked to late-onset autosomal dominant PD. LRRK2 mutations account for up to 13% of familial PD cases compatible with dominant inheritance and are also found in 1 to 2% of sporadic PD patients (62–64). LRRK2 is a complex 286-kDa protein that consists of multiple domains, including (in order, from the amino to carboxyl terminus) armadillo, ankyrin, and the namesake leucine-rich repeats (LRRs), followed by an ROC (Ras of complex proteins) GTPase domain, a COR (C-terminal of ROC) dimerization domain, a kinase domain, and a predicted C-terminal WD40 repeat domain (4–6). Several single-nucleotide alterations have been identified in LRRK2, but only five missense mutations within the ROC, COR, and kinase domains clearly segregate with PD in large family studies (7, 8). It has recently been shown that the WD40 domain is required to stabilize the LRRK2 dimer and to execute LRRK2-associated kinase activity as well as neurotoxicity (9, 10), but the role of this domain within LRRK2 physiological and pathological function has not yet been completely defined. The beta-propeller-forming WD40 domains are among the 10 most abundant domain types across eukaryotic proteomes (11) and constitute platforms where multiprotein complexes assemble reversibly (12). Here, we systematically analyzed the protein-protein interactions conferred by the LRRK2 WD40 domain. The nature of the LRRK2 WD40 interactors and the finding that the LRRK2 WD40 domain is able to bind to synaptic vesicles (SV) contribute to accumulating evidence suggesting that LRRK2 serves as a scaffold protein connecting vesicle trafficking and cytoskeleton (13). Strong genetic association indicates that the substitution of arginine for glycine 2385 (G2385R) within the LRRK2 WD40 domain is a pathologically relevant variant (14). This variant is considered a common risk factor for sporadic PD in Chinese Han and Korean ethnicity, but its functional impact is largely unknown (15, 16). We demonstrate that the G2385R variant alters LRRK2 WD40 binding to synaptic vesicles. Altogether, these data suggest that the LRRK2 WD40 domain is a determinant for LRRK2 physiological and pathological activities.

MATERIALS AND METHODS

Cell cultures. Cortical neuron cultures were prepared from embryonic day 15.5 to 16.5 mouse cortexes (C57BL/6). Medium-density (150 to 200

Received 23 July 2013 **Returned for modification** 14 August 2013
Accepted 18 March 2014
Published ahead of print 31 March 2014
Address correspondence to Christian Johannes Gloeckner, j.gloeckner@helmholtz-muenchen.de.
M.U. and C.J.G. contributed equally to this work.
Supplemental material for this article may be found at http://dx.doi.org/10.1128/MCB.00914-13.

doi:10.1128/MCB.00914-13

cells/mm^2) neuron cultures were plated and grown in Neurobasal culture medium supplemented with 2% B27 and 0.1% gentamicin on 24-well plastic tissue culture plates (Iwaki; Bibby Sterilin, Staffordshire, United Kingdom). In such cultures glial growth is reduced to less than 0.5% of the nearly pure neuronal population (17). HEK293T (ATCC CRL-11268) cells were cultured in Dulbecco's modified Eagle's medium (DMEM) supplemented with 10% fetal bovine serum (FBS) and 1% penicillin-streptomycin mix according to standard protocols. All media were purchased from Life Technologies.

Plasmids and transfection. Human LRRK2 LRR (amino acids [aa] 921 to 1356), LRRK2 WD40 (aa 2124 to 2527), full-length RACK1, and full-length human LRRK2 were subcloned into pDEST-15 (N-terminal glutathione *S*-transferase [GST] tag) and/or pDEST-733 (N-terminal red fluorescent protein [RFP] tag) using the Gateway system (Life Technologies) as described previously (18). The LRRK2 WD40 G2385R variant as well as FLAG- and RFP-tagged LRRK2 consisting of residues 1 to 2141 (hereinafter termed LRRK2 1–2141) were generated by site-directed mutagenesis using a QuikChange mutagenesis kit (Stratagene). Cloning of pGEX-RACK1 and full-length FLAG-LRRK2 was described previously (18–20). LRRK2 WD40 consisting of aa 2148 to 2527 with six copies of a His tag (6×His) was cloned into pETM11. pGFP (where GFP is green fluorescent protein) and pDsRed2-1 were purchased from Clontech laboratories. Neurons were transfected at 10 days of *in vitro* culture (DIV10) with GFP and RFP-tagged constructs or DsRed in a 1:3 ratio by calcium phosphate precipitation as previously described (21) and processed when indicated in the text.

Purification of GST- and His-tagged proteins. GST fusion proteins containing single LRRK2 domains and GST-RACK1 were expressed in the *Escherichia coli* BL21 strain (Life Technologies), purified as described earlier (22). The purification procedure for the N-terminal 6×His-tagged LRRK2 WD40 construct (LRRK2 2148-end), used for electron microscopy (EM) analysis, has been adapted to that used for the GST fusion proteins. Briefly, for expression, *E. coli* cells were grown in terrific broth (TB) medium with 0.1 mM isopropyl-β-D-thiogalactopyranoside (IPTG) induction overnight at 18°C. Cells were lysed in 20 mM Tris, pH 7.5, 150 mM NaCl, 2 mM beta-mercaptoethanol (BME), 0.7% Sarkosyl, and 2% Triton X-100 by sonication. The lysate was loaded onto a nickel column, and the column was then washed with 20 column volumes each of lysis buffer and high-salt buffer (20 mM Tris, pH 7.5, 150 mM NaCl, 350 mM KCl, 5 mM $MgCl_2$, 1 mM ATP). The His-tagged protein was finally eluted with lysis buffer containing 150 mM imidazole. The protein was then dialyzed overnight against 20 mM Tris, pH 7.5, 150 mM NaCl, and 5 mM dithiothreitol (DTT).

Subcellular fractionation and synaptic vesicle binding assay. Subcellular fractionation of rat forebrain tissue was carried out as previously described in the presence of protease inhibitors (23). Briefly, the freshly dissected cerebral cortex was homogenized with a glass-Teflon homogenizer in ice-cold buffered sucrose (0.32 M sucrose, 5 mM HEPES, pH 7.4) (homogenate) and centrifuged at 800 × *g* for 10 min. The nuclear pellet was discarded, and the postnuclear supernatant (containing cell membrane, cytosol, and organelles; S1 fraction) was centrifuged at 9,200 × *g* for 15 min to give a supernatant fraction (containing cytosol and microsomes; S2 fraction) and a crude mitochondrial pellet (containing mitochondria and synaptosomes; P2 fraction). The P2 fraction was subjected to osmotic lysis by homogenization in 10 volumes of ice-cold water and centrifuged at 25,000 × *g* for 20 min to yield a lysate pellet (LP1) enriched in presynaptic plasma membranes and a lysate supernatant (LS1). The LS1 fraction was further centrifuged at 16,500 × *g* for 2 h to yield a synaptosolic fraction (LS2) and a crude SV pellet (LP2) containing synaptic vesicles and small presynaptic plasma membranes. The LP2 fraction was further fractionated by centrifugation through a continuous sucrose gradient and chromatography through a controlled-pore glass column to yield highly purified SV (untreated SV [US]) and a column flowthrough (FT). When required, purified SV were partially depleted of endogenous proteins by dilution in 0.2 M NaCl (salt-treated SV, SSV). SV were centrifuged at 200,000 × *g* for 2 h after 2 h of incubation at 0°C. After centrifugation, SV were resuspended in 0.3 M glycine, 5 mM HEPES-NaOH, pH 7.4, at a protein concentration of 1.5 to 2 mg/ml. The binding of GST fusion proteins to SV was carried out using a high-speed sedimentation assay (24). Briefly, SV (5 to 10 μg of total protein) were incubated for 1 h at 0°C with increasing amounts of a GST fusion protein in a buffer containing 220 mM glycine, 30 mM NaCl, 5 mM Tris-HCl, 4 mM HEPES (pH 7.4), 0.22 mM NaN_3, and 100 μg/ml of bovine serum albumin (BSA). After the incubation, GST fusion protein which bound to SV was separated by high-speed centrifugation (400,000 × *g* for 30 min). Aliquots of the resuspended pellets were subjected to SDS-PAGE and subsequent Western blotting with GST-specific antibodies. The amount of GST protein was determined as a function of optical density in comparison to known amounts of fusion proteins. The recovery of SV, used to correct the amounts of fusion protein bound to SV, was determined by Western blotting with antisynaptophysin antibodies. FLAG-LRRK2 was purified via affinity chromatography using FLAG-M2 agarose beads (Sigma-Aldrich) from HEK293T cells transfected by lipofection using Lipofectamine 2000 (Life Technologies) according to the manufacturer's instructions. The binding of FLAG-LRRK2 to SV was performed as described above with minor modifications: only one concentration of fusion protein (50 nM) was assayed, and FLAG-LRRK2 yield was evaluated via Western blotting with FLAG-specific antibodies.

Pulldown, immunoprecipitation, and antibodies. For pulldowns, 5 μg of each GST fusion protein was loaded onto glutathione-Sepharose resin (GE Healthcare) and coincubated with adult mouse brain lysate or the LS1 fraction (1 mg of total protein). In immunoprecipitation assays, 10 μg of 1E11 anti-LRRK2 antibody was incubated with 1 mg of protein lysate and loaded onto protein G-Sepharose resin (GE Healthcare). In both procedures, resins were extensively washed in Tris-EDTA buffer (10 mM Tris-HCl, pH 8.0, 1 mM EDTA, 150 mM NaCl, 0.2% Triton X-100), followed by final elution of the samples with Laemmli buffer. For protein identification by Western blotting, samples were loaded onto 4 to 12% NuPAGE gels (Invitrogen); the proteins were transferred onto a nitrocellulose membrane (Sigma-Aldrich) at 80 V for 120 min at 4°C. The primary antibodies were applied overnight in blocking buffer (20 mM Tris, pH 7.4, 150 mM NaCl, 0.1% Tween 20, and 5% nonfat dry milk); primary antibodies (source in parentheses) included rat monoclonal anti-LRRK2 1E11 at 1:1,000 (that recognizes an epitope within the LRRK2 kinase domain [25]), mouse anti-synapsin I at 1:1,000 (Synaptic System), mouse anti-SNAP-25 at 1:1,000 (Chemicon), rabbit anti-MAP2 at 1:1,000, mouse anti-MAP6 at 1:1,000, rabbit anti-*N*-ethylmaleimide-sensitive factor (anti-NSF; 1:1,000 [Cell Signaling]), mouse anti-FLAG at 1:2,000, mouse anti-Rac1 at 1:1,000, mouse anti-β-actin at 1:1,000 mouse anti-syntaxin 1A at 1:1,000, mouse anti-Rab3A at 1:1,000, and mouse anti-α-tubulin at 1:1,000 (Sigma-Aldrich). Secondary antibodies (horseradish peroxidase [HRP]-conjugated anti-mouse, anti-rabbit, or anti-rat antibodies; Jackson ImmunoResearch) were used in a ratio of 1:8,000. The signal was detected using an enhanced chemiluminescence (ECL) detection system (GE Healthcare). Films (Hyperfilm ECL; GE Healthcare) were digitalized using a GS-800 densitometer (Bio-Rad) calibrated according to the manufacturer's instructions, and protein abundance was estimated as a function of the optical density of a specific band quantified by ImageJ software (NIH).

MS/MS identification. Liquid chromatography-tandem mass spectrometry (LC-MS/MS) analysis was performed on an Ultimate 3000 Nano high-performance liquid chromatography (HPLC) system (Dionex) coupled to a linear trap quadrupole (LTQ) OrbitrapXL mass spectrometer (Thermo Fisher Scientific) by a nanospray ion source. Tryptic peptide mixtures were automatically injected and loaded at a flow rate of 30 μl/min in 95% buffer C (0.5% trifluoroacetic acid in HPLC-grade water) and 5% buffer B (98% acetonitrile and 0.1% formic acid in HPLC-grade water) onto a nanotrap column (100-μm interior diameter [i.d.] by 2 cm; Acclaim PepMap100 C_{18} column, 5-μm particle diameter, 100-Å pore size [Dionex]). After 5 min, peptides were eluted and separated on the

analytical column (75-μm i.d. by 15 cm; Acclaim PepMap100 C_{18} column, 3-μm particle diameter, 100-Å pore size [Dionex]) by a linear gradient from 5% to 40% of buffer B in buffer A (2% acetonitrile and 0.1% formic acid in HPLC grade water) at a flow rate of 300 nl/min over 90 min. Remaining peptides were eluted by a short gradient from 40% to 100% buffer B in 5 min. The eluted peptides were analyzed by the LTQ Orbitrap XL mass spectrometer. From the high-resolution mass spectrometry prescan with a mass range of 300 to 1,500, the 10 most intense peptide ions were selected for fragment analysis in the linear ion trap if they exceeded an intensity of at least 200 counts and if they were at least doubly charged. The normalized collision energy for collision-induced dissociation was set to a value of 35, and the resulting fragments were detected with normal resolution in the linear ion trap. The lock mass option was activated; the background signal with a mass of 445.12002 was used as lock mass (26). Every ion selected for fragmentation was excluded for 30 s by dynamic exclusion. The acquired spectra were processed and analyzed by using Mascot Daemon (version 2.4.0) in combination with ExtractMSN (Thermo-Fisher) with the following settings: cysteine carbamidomethylation as a fixed modification and methionine oxidation and asparagine/glutamine deamidation as variables with a maximum of three modifications per peptide allowed. Mass tolerances for parent and fragment peptides were set to 10 ppm and 1.00 Da, respectively. The database used consisted of a combined set of mouse and *E. coli* subsets of the Swiss-Prot database (UniProt release 2012_7, published on 11 July 2012; 20,847 entries plus decoy) with spiked-in bait proteins (human LRRK2 and GST of *Schistosoma japonicum*). Reversed sequences generated by Scaffold were used as a decoy. Mascot result files were analyzed by the Scaffold software (version 4.1.1) (Proteome Software, Inc., Portland, OR) to validate MS/MS-based peptide and protein identifications. Peptide identifications were accepted if they could be established at greater than 90% probability as specified by the Peptide Prophet algorithm (27). Protein identifications were accepted if they could be established at greater than 95% probability and contained at least two identified unique peptides. Protein probabilities were assigned by the Protein Prophet algorithm (28). Proteins that contained similar peptides and could not be differentiated based on MS/MS analysis alone were grouped to satisfy the principles of parsimony. The final data sets describing the LRRK2 interactome were generated based on at least four independent experiments for each bait (LRRK2 WD40, LRRK2 LRR, and GST control). Proteins were considered specific LRRK2 WD40 interactors if they were found in at least two independent pulldown experiments and if they were, based on spectral counting, at least 2-fold enriched in the LRRK2 WD40 pulldown set compared to the GST control set. Typical contaminants, including *E. coli* proteins, ribosomal proteins, and keratins, were excluded.

Exoendocytotic assay, immunocytochemistry, and quantification. The endocytosis assay to monitor SV recycling was performed as described previously with minor modifications (13, 29) in neurons transfected at DIV12 with RFP-WD40 or RFP-RACK1 or DsRed plus GFP to visualize cellular processes. Briefly, rabbit polyclonal antibodies directed against the intravesicular domain of synaptotagmin 1 (Synaptic System) were diluted 1:400 in Tyrode solution (124 mM NaCl, 5 mM KCl, 5 mM $CaCl_2$, 1 mM $MgCl_2$, 30 mM glucose, 25 mM HEPES, pH 7.4) and applied for 5 min at room temperature (RT) on living cultures. After extensive washing with Tyrode solution, neurons were fixed in 4% paraformaldehyde and 4% sucrose at room temperature. Where indicated in the figure legends, rat anti-FLAG (1:100; kindly provided by E. Kremmer, Institute of Molecular Immunology, Helmholtz Zentrum München), rabbit anti-SV2A (1:400; Synaptic System), or mouse anti-SNAP-25 (1:1,000; Sigma-Aldrich) antibody was applied in GDB buffer (30 mM phosphate buffer, pH 7.4, containing 0.2% gelatin, 0.5% Triton X-100, and 0.8 M NaCl) overnight at 4°C. Cy5-coupled secondary antibodies and 4′,6′-diamidino-2-phenylindole (DAPI; Life Technologies) were diluted 1:1,000 in GDB buffer and applied for 1 h. Transfected neurons were randomly chosen in at least four independent experiments for each condition. The fluorescence images were acquired using an LSM Zeiss 510 confocal microscope with a Zeiss 63× objective (Karl Zeiss, Jena, Germany) at a resolution of 1 pixel equal to 0.098 μm. Image analysis was performed using ImageJ (NIH). To quantify synaptotagmin- or SV2A-positive clusters, GFP-positive processes were manually tracked, and the number of positive clusters in the region of interest was automatically counted. To evaluate neuron morphology, neurites were randomly selected and manually traced, and length and number of processes were automatically determined and logged into Microsoft Excel as described previously (30).

Electron microscopy. Purified GST- or 6×His-tagged fusion proteins were adsorbed onto carbon-coated grids that were glow discharged in air before the application of 5 μl of protein solution. Excess protein solution was blotted off after 2 min. The adsorbed molecules were negatively stained for 30 s using 5 μl of stain solution as indicated in the figure legends. Micrographs were recorded on Kodak SO-163 image film (Sigma-Aldrich) using JEOL JEM 2010 and JEOL JEM 100CX electron microscopes operated at 120 and 100 kV, respectively, at defocus values of 600 to 900 nm. Suitable micrographs were selected by optical diffraction and digitized using a Flextight Precision II (Hasselblad) scanner, resulting in pixel sizes of 1.59 or 1.28 Å at the specimen level. Particles were selected and extracted using EMAN1 (31) and classified using IMAGIC, version 5.0 (Image Science Software).

Homology modeling. Modeling templates were identified in the Protein Data Bank (PDB) (32, 33) using the profile-profile alignment program Phyre2 (3). The initial homology model was built based on the WD40 domain structure of RACK1 from *Arabidopsis thaliana* (PDB code 3DM0) (34). The model structure was further refined using the YASARA energy minimization server to increase the model accuracy (35). The quality of the final structure model was validated using PROCHECK (36). PyMOL was used for visualization of the final model.

Statistical analysis. All data are expressed as means ± standard error of the means (SE). Data were analyzed with an unpaired Student's *t* test (two classes) or by analysis of variance (ANOVA) followed by Tukey's *post hoc* test (more than two classes). The indication of the number of experiments (*n*) and level of significance (*P*) are given throughout the text.

Database accession number. The interactome data set has been submitted to the IntAct database under accession number IM-20537 (http://www.ebi.ac.uk/intact/search/do/search?searchString=imex:IM-20537).

RESULTS

WD40 links LRRK2 to presynaptic proteins. Previous findings, including our own work, suggest that LRRK2 regulates trafficking of synaptic vesicles (SV) (13, 37, 38). Here, we investigated the interaction between LRRK2 and SV at the molecular level. For this purpose, we first tested the subcellular distribution of LRRK2. Subcellular fractionation of mouse brain lysate revealed cosedimentation of LRRK2 with synapsin I and synaptophysin in a biochemically defined fraction enriched in SV (Fig. 1A, lane LS). Interestingly, mild salt treatment, reported to partially remove associated proteins such as synapsin I from SV (23), did not reduce the amount of LRRK2 or synaptophysin found in the SV fraction (Fig. 1A, lane SSV). Next, we incubated full-length FLAG-LRRK2 at a nanomolar concentration with purified SV and tested the extent of binding in a high-speed sedimentation assay (24). Western blot analysis using a FLAG-specific antibody revealed that recombinant LRRK2 associates to native SV. Interestingly, LRRK2 showed a binding affinity similar to that of SSV (Fig. 1B and C). In the same SV population we described a strong reduction in the amount of synapsin I upon salt treatment (Fig. 1B and D). These data suggest that LRRK2 forms a complex with SV. Next, we investigated if LRRK2 associates to SV through specific protein-protein interactions. The immunoprecipitation of LRRK2 showed that well-described SV proteins such as NSF, syntaxin 1A, synapsin I, dynamin-1, MUNC18-1, and VAMP2 as well

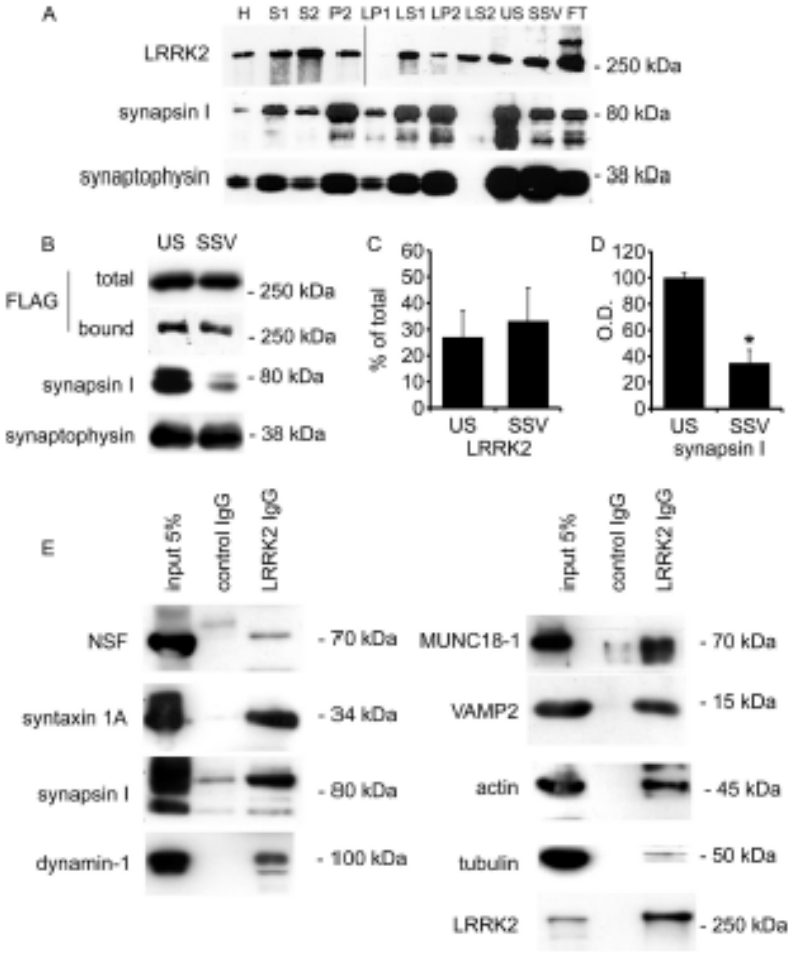

FIG 1 LRRK2 binds presynaptic proteins. (A) Distribution of LRRK2, synapsin I, and synaptophysin immunoreactivities in subcellular fractions of rat forebrain. LRRK2 is present in highly purified vesicle fractions (US), and its association with the vesicle membrane is not affected by salt treatment (SSV). H, homogenate. (B) LRRK2 binds to SV. Full-length FLAG-LRRK2, purified from transfected HEK293T cells, was incubated with unstripped SV (US) or salt-stripped SV (SSV) before high-speed sedimentation. Representative Western blots stained with anti-FLAG antibody show the initial amount of FLAG-LRRK2 protein (total), the yield of protein precipitated by US or SSV (bound), and the amount of endogenous synapsin I associated to SV. Fusion proteins were incubated with equal amounts of SV (monitored by antisynaptophysin staining). (C) The graph reports the yield of FLAG-LRRK2 precipitated by US and SSV, expressed as a fraction of FLAG-LRRK2 total protein and normalized against the SV total protein amount. (D) The graph reports the amount of endogenous synapsin I associated to US or SSV. Data are expressed as optical density (OD) in arbitrary units. *, $P < 0.05$, $n = 4$ (Student's t test). (E) Immunoprecipitation of endogenous LRRK2 from adult brain lysate confirms the interaction between LRRK2 and selected presynaptic and cytoskeletal proteins.

as actin and tubulin are LRRK2-interacting proteins (Fig. 1E) (13, 39). LRRK2 contains two domains that typically mediate protein-protein interactions, an N-terminal LRR and a C-terminal WD40 domain (5, 10, 37). Thus, we proceeded with a systematic analysis of protein-protein interactions conferred by LRRK2 LRR and WD40 domains. To this aim, we expressed the LRRK2 LRR and WD40 domains as GST fusion proteins (herein termed LRRK2 LRR and LRRK2 WD40) (see Fig. S1A in the supplemental material). GST-only served as a control in order to detect false positives caused by unspecific binding to the affinity tag or matrix. Equal amounts of each protein (baits and control) were loaded onto glutathione-Sepharose resin and incubated with adult mouse brain lysates. Interacting proteins were identified by silver staining (see Fig. S1B), Western blot assays (see Fig. S1C), and MS/MS spectrometry (see Table S1 in the supplemental material). This combined approach revealed a panel of 17 and 42 putative interactors for LRRK2 LRR and LRRK2 WD40, respectively, and suggested the C-terminal WD40 domain as an important hub for protein-protein interaction within LRRK2. Thus, we performed a more detailed investigation of the interactions conferred by LRRK2 WD40 combining Western blot assays and MS/MS spectrometry. As a protein source, we used mouse brain lysate or the LS1 fraction, partially enriched in SV. Our analysis identified 84 putative LRRK2 WD40 interactors (Table 1); in particular, we demonstrated that LRRK2 WD40 has affinity for NSF, syntaxin 1A, synapsin I, VAMP2, Rab3A, MAP2, Rac1, actin, tubulin, and Hsp90 but not for synaptophysin (Fig. 2). Surprisingly, we found that LRRK2 WD40 binds endogenous LRRK2, implying a role for this domain in LRRK2 dimerization (10). WD40 repeats commonly constitute a molecular platform for protein-protein inter-

TABLE 1 Identification of LRRK2 WD40 interactors

Accession no.[a]	Protein name	Gene	Experiment(s)[b]	Mass (kDa)	Coverage (%)[c]	No. of WD40 repeats[d]	Source[e]
P60711 (P60710)	Actin, beta	*Actb*	MS, WB, IP	42	46.0	17	LS1, total brain
P85515	Alpha-centractin	*Actr1a*	MS, WB	43	16.0	4	LS1 fraction
P39069	Adenylate kinase 1	*Ak1*	MS	22	14.0	2	LS1 fraction
Q9DBG3	Adaptor-related protein complex 2, beta 1 subunit	*Ap2b1*	MS	105	4.0	4	Total brain
Q08163	Adenylyl cyclase-associated protein 1	*Cap1*	MS	52	6.0	2	LS1 fraction
P84079	ADP-ribosylation factor 1	*Arf1*	MS	21	15.0	2	LS1 fraction
Q5XI73	Rho GDP dissociation inhibitor (GDI) alpha	*Arhgdia*	MS	23	33.0	4	LS1 fraction
Q8VDN2	ATPase, Na^+/K^+ transporting, alpha 1 polypeptide	*Atp1a1*	MS	113	17.0	4	Total brain
Q6PIE5	ATPase, Na^+/K^+ transporting, alpha 2 polypeptide	*Atp1a2*	MS	112	17.0	5	Total brain
P06687	ATPase, Na^+/K^+ transporting, alpha 3 polypeptide	*Atp1a3*	MS	112	12.0	10	LS1 fraction
Q9R0K7	ATPase, Ca^{2+} transporting, plasma membrane 2	*Atp2b2*	MS	133	4.0	3	Total brain
Q03265	ATP synthase alpha subunit, isoform 1	*Atp5a1*	MS	60	21.0	12	LS1 fraction
P56480 (P10719)	ATP synthase beta subunit	*Atp5b*	MS	56	13.0	5	LS1 fraction, total brain
P62815	V-type proton ATPase subunit B, brain isoform	*Atp6v1b2*	MS	57	36.0	14	LS1 fraction
Q6PCU2	ATPase, H^+ transporting, lysosomal V1 subunit E1	*Atp6v1e1*	MS	26	15.0	4	LS1 fraction
P47728	Calbindin 2	*Calb2*	MS	31	14.0	3	LS1 fraction
P28480	T-complex protein 1 subunit alpha	*Tcp1*	MS	60	11.0	5	LS1 fraction
Q5XIM9	T-complex protein 1 subunit beta	*Cct2*	MS	57	18.0	6	LS1 fraction
Q68FD5	Clathrin, heavy polypeptide (Hc)	*Cltc*	MS	192	24.0	28	Total brain
P63041	Complexin 1	*Cplx1*	MS	15	17.0	2	LS1 fraction
P39053	Dynamin 1	*Dnm1*	MS, IP	98	8.0	7	Total brain
Q62952	Dihydropyrimidinase-like 3	*Dpysl3*	MS	62	31.0	7	LS1 fraction
P38650	Dynein cytoplasmic 1 heavy chain 1	*Dync1h1*	MS	532	18.0	4	LS1 fraction
P85845	Fascin homolog	*Fscn1*	MS	54	9.0	3	LS1 fraction
P50398	Rab GDP dissociation inhibitor alpha	*Gdi1*	MS	51	49.0	16	LS1 fraction
P50399	Rab GDP dissociation inhibitor beta	*Gdi2*	MS	51	25.0	5	LS1 fraction
P59215 (P18872)	Guanine nucleotide-binding protein G(o) subunit alpha	*Gnao1*	MS	40	12.0	3	LS1 fraction, total brain
P07901	Heat shock protein 90, alpha	*Hsp90aa1*	MS, WB	85	5.0	2	Total brain
P11499	Heat shock protein 90, beta	*Hsp90ab1*	MS, WB	83	7.0	2	Total brain
O35814	Stress-induced phosphoprotein 1	*Stip1*	MS	63	10.0	4	LS1 fraction
Q2PQA9	Kinesin-1 heavy chain	*Kif5b*	MS	110	4.0	3	LS1 fraction
Q9WV63	Kinesin-like protein KIF2A	*Kif2a*	MS	80	5.0	3	LS1 fraction
P63086	Mitogen-activated protein kinase 1	*Mapk1*	MS	41	20.0	6	LS1 fraction
Q3B8Q0	Microtubule-associated protein RP/EB family member 2	*Mapre2*	MS	37	11.0	2	LS1 fraction
P19332	Microtubule-associated protein tau	*Mapt*	MS	76	7.0	5	LS1 fraction
P34926	Microtubule-associated protein 1A	*Map1a*	MS	300	2.0	3	LS1 fraction
P15205	Microtubule-associated protein 1B	*Map1b*	MS	270	2.0	5	LS1 fraction
P15146 (P20357)	Microtubule-associated protein 2	*Map2*	MS	199	6.0	6	LS1 fraction, total brain
Q9QYF3	Myosin VA	*Myo5a*	MS	212	5.0	8	LS1 fraction
Q63610	Tropomyosin alpha-3	*Tpm3*	MS	29	19.0	4	LS1 fraction
P85969	Beta-soluble NSF attachment protein	*Napb*	MS	34	11.0	3	LS1 fraction
Q9Z0E0	Neurochondrin	*Ncdn*	MS	79	4.0	2	LS1 fraction
P46460	*N*-Ethylmaleimide sensitive fusion protein	*Nsf*	MS, WB, IP	83	10.0	6	Total brain
Q9QXU9	ProSAAS	*Pcsk1n*	MS	27	18.0	5	LS1 fraction
Q9EPC6	Profilin 2	*Pfn2*	MS	15	18.0	3	LS1 fraction
P60203	Proteolipid protein (myelin) 1	*Plp1*	MS	30	9.0	2	LS1 fraction
P63329	PP2B catalytic subunit alpha isoform	*Ppp3ca*	MS	59	28.0	11	LS1 fraction
Q63716	Peroxiredoxin 1	*Prdx1*	MS	22	20.0	3	LS1 fraction
P35704	Peroxiredoxin 2	*Prdx2*	MS	22	31.0	8	LS1 fraction
O35244	Similar to peroxiredoxin 6	*Prdx6*	MS	25	32.0	5	LS1 fraction
P63011	Ras-related protein Rab-3A	*Rab3a*	WB	25	31.0	7	Total brain
Q9WU34	Neuron-specific septin-3	*Sept3*	MS	41	11.0	4	LS1 fraction
Q9JIM9	Septin 5	*Sept5*	MS	43	10.0	3	LS1 fraction
Q9WVC0	Septin 7	*Sept7*	MS	51	15.0	5	LS1 fraction
O35179	Endophilin-A1	*Sh3gl2*	MS	40	29.0	9	LS1 fraction
Q5PPJ9	Endophilin-B2	*Sh3glb2*	MS	45	8.0	3	LS1 fraction

(Continued on following page)

TABLE 1 (Continued)

Accession no.[a]	Protein name	Gene	Experiment(s)[b]	Mass (kDa)	Coverage (%)[c]	No. of WD40 repeats[d]	Source[e]
P60881	Synaptosome-associated protein 25	*Snap25*	MS, WB	23	14.0	2	LS1 fraction
Q61548	Synaptosome-associated protein 91	*Snap91*	MS	92	4.0	3	Total brain
P37377	Synuclein, alpha	*Snca*	MS	14	39.0	3	LS1 fraction
Q91ZZ3	Synuclein, beta	*Sncb*	MS	14	50.0	5	LS1 fraction
P16546	Spectrin alpha 2	*Spna2*	MS	285	4.0	9	Total brain
Q62261	Spectrin beta 2	*Spnb2*	MS	274	1.0	2	Total brain
P63039	60-kDa heat shock protein	*Hspd1*	MS	61	46.0	25	LS1 fraction
O35814	Stress-induced phosphoprotein 1	*Stip1*	MS	63	10.0	4	LS1 fraction
P13668	Stathmin	*Stmn1*	MS	17	36.0	5	LS1 fraction
P61264	Syntaxin 1B	*Stx1b*	MS	33	13.0	3	Total brain
P61765 (O08599)	Syntaxin-binding protein 1	*Stxbp1*	MS, IP	68	19.0	10	LS1 fraction, total brain
Q9JIS5	Synaptic vesicle glycoprotein 2A	*Sv2a*	MS	83	5.0	2	Total brain
O88935	Synapsin-1	*Syn1*	WB, IP	75	16.0	5	Total brain
Q63537 (Q64332)	Synapsin-2	*Syn2*	WB, IP	63	17.0	7	LS1 fraction, total brain
Q62910	Synaptojanin 1	*Synj1*	MS	173	4.0	5	LS1 fraction
Q6P9V9 (Q99KA2)	Tubulin alpha-1B chain	*Tuba1b*	MS, WB, IP	50	45.0	21	LS1 fraction, total brain
Q5XIF6	Tubulin alpha-4A chain	*Tuba4a*	MS	50	36.0	5	LS1 fraction
P85108	Tubulin beta-2A chain	*Tubb2a*	MS	50	64.0	2	LS1 fraction
Q3KRE8	Tubulin beta-2B chain	*Tubb2b*	MS	50	64.0	10	LS1 fraction
Q4QRB4	Tubulin beta-3 chain	*Tubb3b*	MS	50	66.0	12	LS1 fraction
Q6P9T8	Tubulin beta-4B chain	*Tubb4b*	MS	50	63.0	28	LS1 fraction
P69897	Tubulin beta-5 chain	*Tubb5b*	MS	50	63.0	6	LS1 fraction
Q00981	Ubiquitin carboxyl-terminal hydrolase isozyme L1	*Uchl1*	MS	25	37.0	6	LS1 fraction
P63045	Vesicle-associated membrane protein 2	*Vamp2*	MS, WB, IP	13	46.0	6	LS1 fraction
P35213	14-3-3 protein beta polypeptide	*Ywhab*	MS	28	30.0	2	LS1 fraction
P62259	14-3-3 protein epsilon polypeptide	*Ywhae*	MS	29	16.0	2	Total brain
P68511	14-3-3 protein eta polypeptide	*Ywhah*	MS	28	52.0	7	LS1 fraction
P68255	14-3-3 protein theta	*Ywhaq*	MS	28	30.0	4	LS1 fraction

[a] UniProtKB/Swiss-Prot accession numbers.
[b] Interactors were found by immunoprecipitation of endogenous LRRK2 (IP) or LRRK2 WD40 pulldown assays analyzed by Western blotting (WB) and mass spectrometry (MS).
[c] Sequence coverage for proteins identified by LC-MS/MS.
[d] Number of identified unique peptides.
[e] Lysate from adult mouse brain (total brain) or the LS1 fraction.

actions (12). In order to determine the specificity/exclusiveness of the protein interactions determined by LRRK2 WD40, we investigated the interactome of RACK1, an unrelated protein encompassing a well-defined WD40 repeat domain (40). We performed pulldown experiments using full-length RACK1 fused to GST as a bait protein and analyzed the coprecipitated proteins by Western blotting (see Fig. S2A and B in the supplemental material) and mass spectrometry (see Table S2). As a result of this analysis, we found that only seven putative LRRK2 WD40 binding partners demonstrated affinity also for RACK1. Notably, among them, we did not identify LRRK2 itself, MAP2, actin, syntaxin 1A, and NSF, indicating that these proteins are bona fide specific binders of LRRK2 WD40.

For further analysis, we elaborated the interactome conferred to LRRK2 by its WD40 domain, *in silico*, using the STRING protein database tools (accessible online at http://string-db.org) (41). The resulting scale-free network was visualized by Cytoscape software (42). The network included 85 nodes (84 interactors plus LRRK2) connected by 160 edges (see Fig. S3 and Table S3 in the supplemental material). In order to identify major hubs within the network, the complete data set was filtered for those nodes qualified by a degree of connectivity higher than four. The filtered data set formed a subnetwork of 21 nodes associated through 62 edges (Fig. 3A). Interestingly, proteins represented in this subnetwork are key determinants of SV trafficking (Fig. 3B). Taken together, our data suggest that the C-terminal WD40 domain of LRRK2 serves as a major hub for its interaction with other proteins and that LRRK2 is part of a highly interconnected protein network involved in synaptic vesicle trafficking.

The LRRK2 WD40 domain induces neurotoxicity. It has been reported that the C-terminal LRRK2 WD40 domain is required for LRRK2-associated neurotoxicity (10). To gain a better understanding of this phenomenon, we cotransfected cortical neurons at DIV3 with GFP and vectors expressing either DsRed, the isolated LRRK2 WD40 domain (RFP-LRRK2 WD40), truncated LRRK2 lacking the C-terminal domain (RFP LRRK2 1–2141), full-length LRRK2 (RFP-LRRK2), or full-length RACK1 (RFP-RACK1) and analyzed neuron morphology at DIV16 (Fig. 4). The overexpression of the full-length RFP LRRK2 severely reduced the number of processes compared to control neurons expressing DsRed. This outcome might be related to the high expression of recombinant full-length LRRK2 achieved in our model (43). Interestingly, while ectopic LRRK2 1–2141 expression did not significantly alter neuron morphology, overexpression of the single

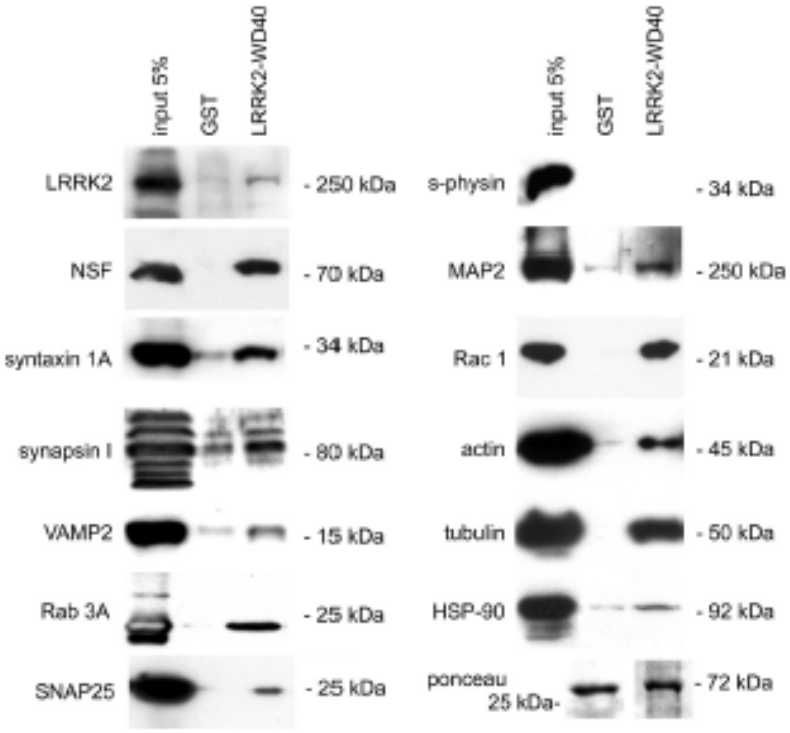

FIG 2 The C-terminal WD40 domain of LRRK2 represents a hub for protein-protein interactions. Western blots are shown, confirming the specific interaction of proteins following a domain-based pulldown assay for the LRRK2 WD40 domain. s-physin, synaptophysin.

LRRK2 WD40 domain significantly impaired process number. Given the severe neurotoxicity observed upon expression of RFP WD40 and RFP LRRK2 from DIV3 to DIV16, we modified our experimental setup and investigated the effect of ectopic LRRK2 construct expression in neurons transfected at DIV10 and imaged at DIV16 (Fig. 5A). Given that we experienced an extremely low efficiency when transfecting full-length LRRK2 in primary cultures at DIV10 (data not shown), we excluded this condition in subsequent experiments. While ectopic DsRed, RACK1, and LRRK2 1–2141 were diffusely distributed in neuronal soma and along neuronal processes, partially colocalizing with the synaptic marker SNAP-25, we found that the ectopically expressed LRRK2 WD40 domain was mainly localized in a perinuclear somatic region, with low colocalization with SNAP-25 (see Fig. S4 in the supplemental material). Next, we considered neuron morphology. The overexpression of RFP-LRRK2 WD40 significantly reduced the number of processes and increased the amount of swollen or fragmented neurites compared to control neurons. In contrast, ectopic LRRK2 1–2141 expression did not influence total neurite number and was associated to a milder increase of swollen processes than LRRK2 WD40. Finally, we found an increased number of processes in RACK1-overexpressing neurons (Fig. 5B and C). Given that neuronal fragmentation represents the first sign of neuronal sufferance (44), our data indicate that the prolonged expression of the isolated LRRK2 WD40 domain induces toxicity in neurons.

LRRK2 WD40 domain and RACK1 alter SV trafficking. Given the interactions described between the LRRK2 WD40 domain and presynaptic proteins, we wondered whether the LRRK2 WD40 domain affects proper SV trafficking and distribution. To test this hypothesis, we cotransfected cortical neurons at DIV10 with GFP and either DsRed, RFP-LRRK2 WD40, RFP-RACK1, or LRRK2 1–2141 expression vectors. At DIV12 we determined the SV exoendocytic rate by exposing living cortical neurons to an antisynaptotagmin antibody as previously described (13). Transfected neurons were then tracked via laser confocal microscopy. Recycling vesicles appeared as synaptotagmin-positive clusters along GFP-positive neuronal processes (Fig. 6A). The total vesicle pool was estimated by staining with antibodies directed against an integral SV protein (SV2A) after fixation and permeabilization of the cells (Fig. 6B). While ectopic LRRK2 1–2141 did not influence synaptotagmin uptake, the overexpression of RFP-LRRK2 WD40 as well as RFP-RACK1 induced a significant decrease in the number of synaptotagmin-positive clusters (Fig. 6C). At the same time, neither LRRK2 WD40 nor RACK1 nor LRRK2 1–2141 overexpression affected the amount of SV2A-positive clusters compared to DsRed transfected neurons (Fig. 6D). Next, we examined if the expression of LRRK2 WD40, RACK1, or LRRK2 1–2141 had an impact on the distribution of cycling or total SV pools. To this end, we tracked the distribution of synaptotagmin (cycling SV) and SV2A-positive (total SV) clusters along GFP-positive processes. Interestingly, in LRRK2 WD40 transfected neurons, synaptotagmin-positive clusters were mainly distributed proximally to the cellular soma while SV2A-positive clusters were homogeneously diffused along the entire length of the neurites (Fig. 6E and F). Taken together, these data strongly indicate that ectopic expression of the LRRK2 WD40 domain influences trafficking, distribution, and topology of the SV cycling pool.

A

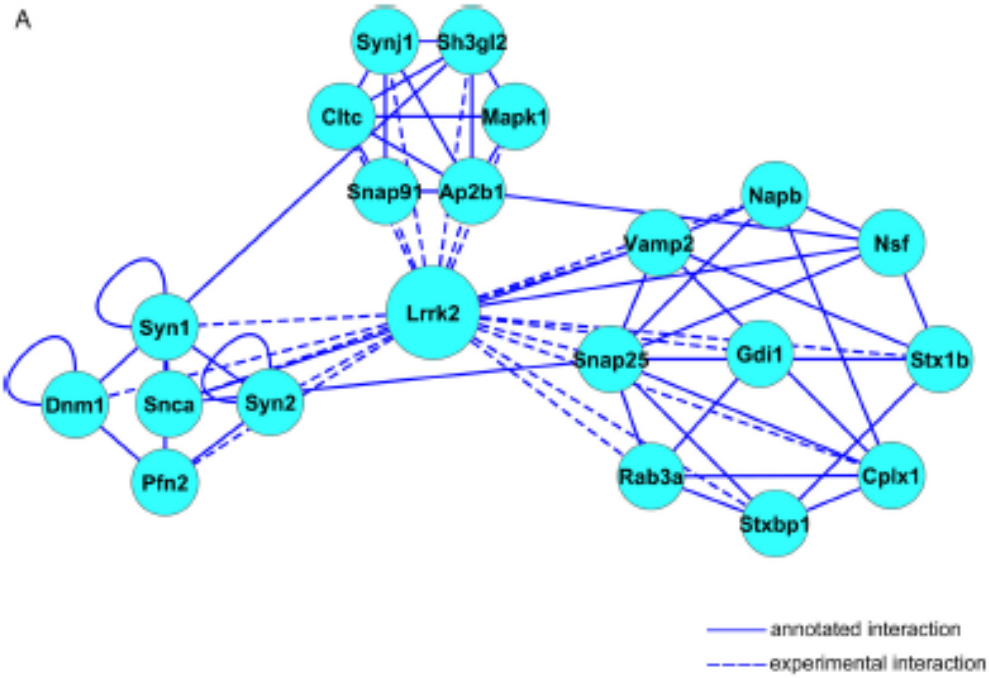

B

gene	protein name	GO biological function
Ap2b1	adaptor-related protein complex 2, beta 1 subunit	vesicle-mediated transport
Cltc	clathrin, heavy polypeptide (Hc)	vesicle-mediated transport
Cplx1	complexin 1	vesicle-mediated transport
Dnm1	dynamin 1	vesicle-mediated transport
Gdi1	guanosine diphosphate (GDP) dissociation inhibitor 1	regulation biological process
Lrrk2	leucine-rich repeat kinase 2	regulation biological process
Mapk1	mitogen-activated protein kinase 1	regulation biological process
Napb	N-ethylmaleimide sensitive fusion protein attachment protein beta	vesicle-mediated transport
Nsf	N-ethylmaleimide sensitive fusion protein	vesicle-mediated transport
Pfn2	profilin 2	regulation biological process
Rab3a	RAB3A, member RAS oncogene family	vesicle-mediated transport
Sh3gl2	SH3-domain GRB2-like 2	vesicle-mediated transport
Snap25	synaptosome-associated protein 25	vesicle-mediated transport
Snap91	synaptosome-associated protein 91	vesicle-mediated transport
Snca	synuclein, alpha	vesicle-mediated transport
Stx1b	syntaxin 1B	vesicle-mediated transport
Stxbp1	syntaxin binding protein 1	vesicle-mediated transport
Syn1	synapsin I	synaptic transmission
Syn2	synapsin II	synaptic transmission
Synj1	synaptojanin 1	vesicle-mediated transport
Vamp2	vesicle-associated membrane protein 2	vesicle-mediated transport

FIG 3 LRRK2 interacts with presynaptic proteins. (A) The network of LRRK2 interactors was modeled from STRING annotation on the Cytoscape representation. annotated, interactions annotated on STRING; experimental, interactions described in the manuscript. (B) Gene symbols, names, and gene ontology (GO) terms for the proteins included in the network.

The G2385R PD risk variant alters LRRK2 WD40 binding properties to synaptic vesicles. The critical role conferred by the LRRK2 WD40 domain is suggested by the existence of the G2385R polymorphism, described as a risk factor for the development of PD (14–16).

Sequence alignments and secondary structure predictions suggest that the LRRK2 C terminus contains a WD40 propeller domain composed of seven β-blades. We assessed the structure of the region comprising LRRK2 residues 2124 to 2499 using homology modeling in order to gain information about the structural features of the LRRK2 C terminus (Fig. 7A; see also Fig. S5A in the supplemental material). Our model, based on the structure of the WD40 protein RACK1 from *Arabidopsis thaliana* (34), shows that the LRRK2 C-terminal domain is compatible with the characteristic structure of WD40 domains, i.e., seven β-propeller repeats combined to a cleft of basic residues (5, 15). A more detailed analysis of the region surrounding the residue G2385 revealed that G2385 lies in close vicinity of two hydrophobic residues, V2375

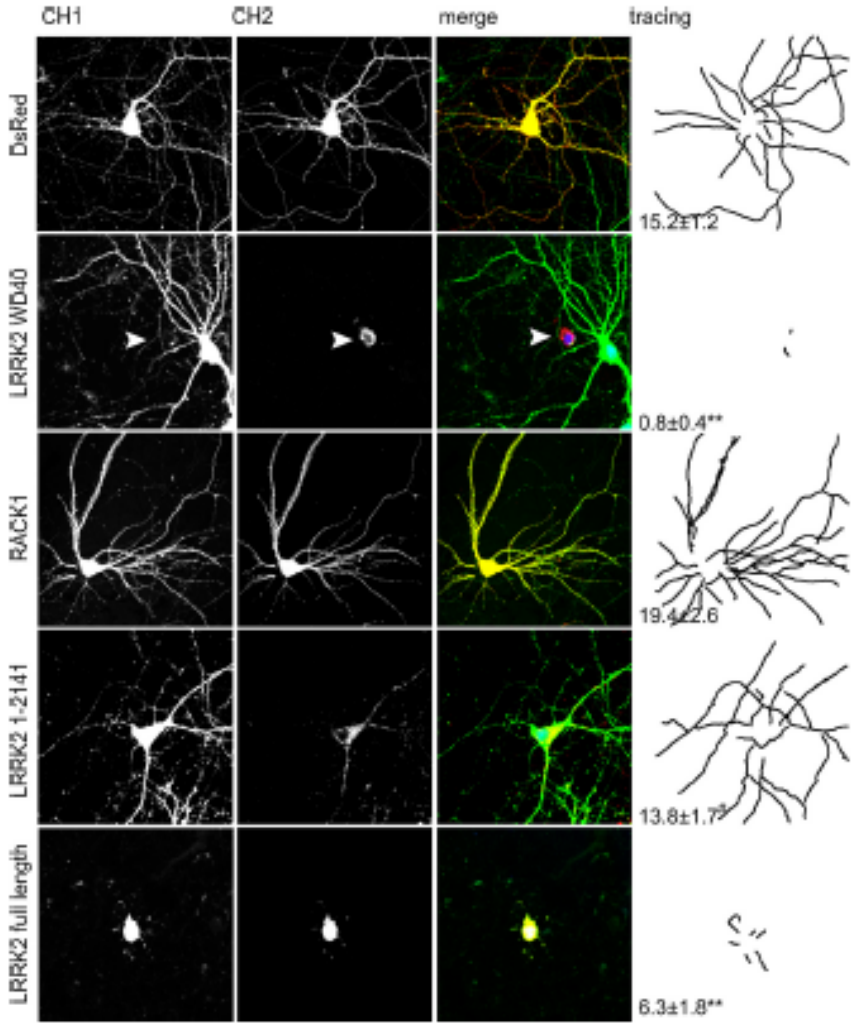

FIG 4 Expression of an LRRK2 WD40 domain construct is sufficient to induce neurotoxicity in primary neurons. Neurons were transfected at DIV3 and imaged at DIV16. Long-lasting overexpression of RFP-LRRK2 WD40 and full-length RFP-LRRK2 significantly reduced the number of processes and increased the amount of swollen or fragmented neurites compared to levels in DsRed-, RFP LRRK2 1–2141-, or RFP-RACK1-transfected neurons. Images show signals acquired for GFP (channel 1, CH1), DsRed or RFP (channel 2, CH2), superimposed channel signals (merge), and tracings. Arrow heads indicate an RFP-LRRK2 WD40-positive cell. Numbers in the tracing panel indicate total process numbers and are expressed as means ± SE. **, $P < 0.01$ versus DsRed; #, $P < 0.01$ versus full-length RFP-LRRK2 (ANOVA; Tukey's *post hoc* test, $n = 3$; 8 neurons were analyzed for each experimental case). Panel size shown is 200 by 200 μm.

and L2439, on one side and with R2442 and R2443 on the other side. Even with its limitations, the structural model suggests that the substitution of G2385 with a bulky and positively charged arginine residue would lead to unfavorable charge repulsions and potentially conformational changes of the protein near the interface between β-blades 5 and 6. This might not only alter the local conformation but also affect the binding surface of WD40 for interaction with interacting proteins and thus impair LRRK2 activity. In order to experimentally assess the structural properties of the LRRK2 C terminus and the alterations caused by the G2385R variant, purified GST fusion proteins LRRK2 WD40 and LRRK2 WD40 G2385R were analyzed by transmission electron microscopy (EM). To meet the demand of EM for highly pure material, purity and concentration of the GST fusion proteins were confirmed by SDS-PAGE (see Fig. S2A in the supplemental material). While particles with distinct shapes were discernible on electron micrographs of negatively stained LRRK2 WD40 fusion proteins, similar structures were not visible for the GST tag alone (see Fig. S5B). Single-particle classification and averaging indicated the existence of particle populations with an annular, doughnut-like appearance and diameters ranging from 5 to 8 nm for LRRK2 WD40 (Fig. 7B). Structures similar in size and shape were also detected for the GST-RACK1 fusion protein (Fig. 7B), indicating that the fold of the LRRK2 WD40 domain is comparable despite limited sequence homology. To ensure that the fusion of the WD40 domains to the GST tag does not induce ring-like structures, N-terminal 6×His-tagged LRRK2 WD40 was subjected to EM (see Fig. S5C in the supplemental material). Although the

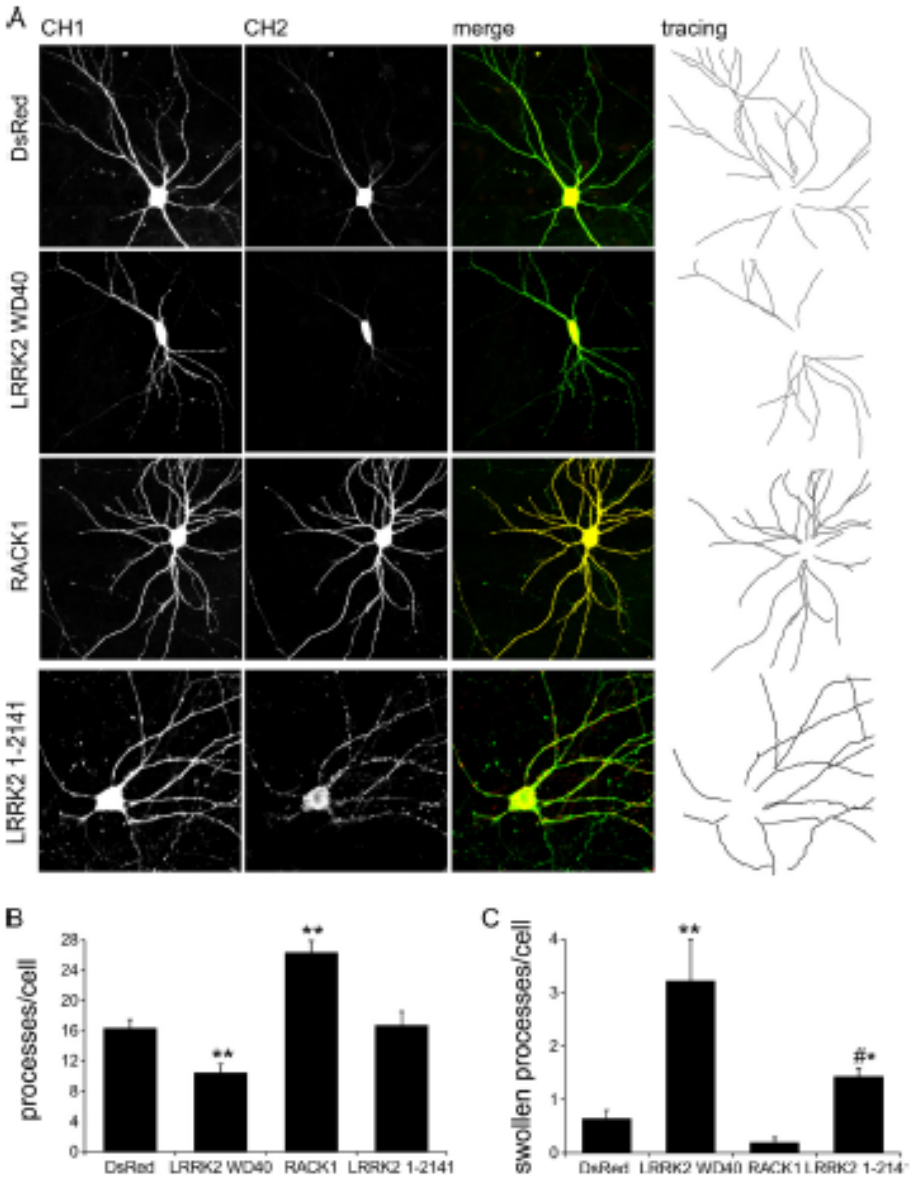

FIG 5 Expression of an LRRK2 WD40 domain construct induces neurotoxicity in primary neurons. (A) Neurons were transfected at DIV10 and imaged at DIV16. Long-lasting overexpression of RFP-LRRK2 WD40 significantly reduced the number of processes and increased the amount of swollen or fragmented neurites compared to levels in DsRed-, LRRK2 1–2141-, or RFP-RACK1-transfected neurons. Images show signals acquired for GFP (channel 1, CH1), DsRed or RFP (channel 2, CH2), superimposed channel signals (merge), and tracings. Graphs report the number of total processes (B) and number of fragmented processes (C) (means ± SE). *, $P < 0.05$ versus DsRed; **, $P < 0.01$ versus DsRed; #, $P < 0.05$ versus LRRK2 WD40 (ANOVA; Tukey's *post hoc* test, $n = 4$; 7 neurons were analyzed for each experimental case). Panel size shown is 200 by 200 μm.

protein lacking the GST tag turned out to be more aggregation prone, doughnut-like structures similar in size and appearance to those observed in GST fusion proteins were still present. The analysis of the LRRK2 WD40 G2385R variant by EM revealed strong similarity to the other WD40 domain constructs, however, with a wider size distribution ranging from 5 to 13 nm. This larger size heterogeneity may be due to structural alterations in WD40 induced by electrostatic repulsion in the β-propeller fold, as suggested by the structural model.

In order to further characterize the G2385R variant, we investigated the impact of LRRK2 WD40 G2385R overexpression on neurons. Ectopic LRRK2 WD40 G2385R induced neuronal toxicity and sequestered cycling SV to a similar extent as LRRK2 WD40 (see Fig. S6 in the supplemental material).

The data presented above suggest that the WD40 domain plays a major role in tethering LRRK2 to SV via protein interactions; thus, we asked if the G2385R variant can influence LRRK2 binding to SV. To explore this hypothesis, we incubated

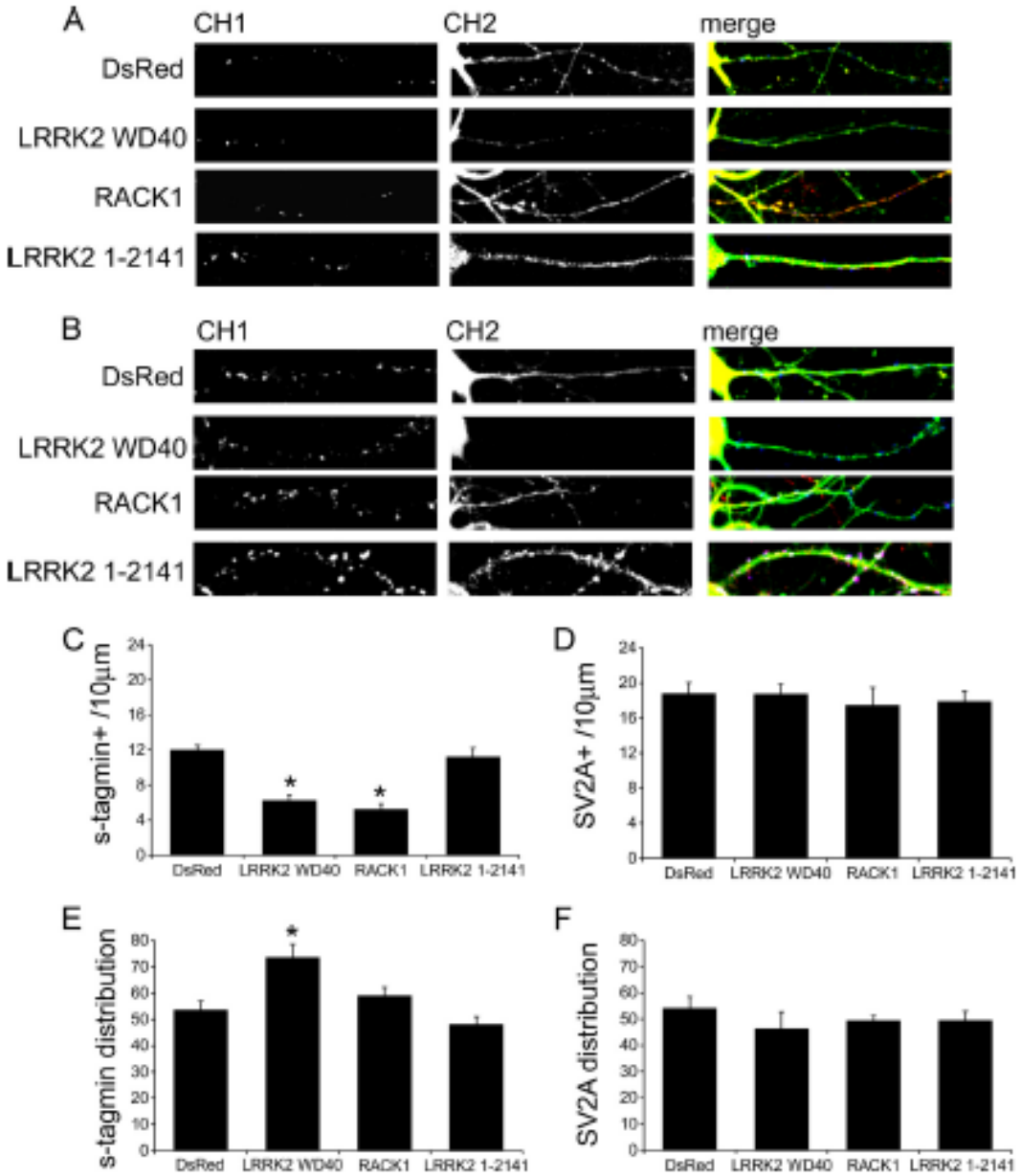

FIG 6 The LRRK2 WD40 domain sequesters cycling synaptic vesicles. The exoendocytotic assay was performed at DIV12 on cortical neurons transfected at DIV10. (A) Cycling SV appear as synaptotagmin (s-tagmin)-positive clusters along neuron processes. Images show signals acquired for synaptotagmin (channel 1, CH1) and DsRed or RFP or FLAG (channel 2, CH2) and their superimposition plus GFP (merge). (B) The total SV pool was revealed by staining with anti-SV2A antibodies upon permeabilization. Images show signals acquired for SV2A (channel 1, CH1) and DsRed or RFP (channel 2, CH2) and their superimposition plus GFP (merge). (C) SV cycling is strongly reduced upon either LRRK2 WD40 or RACK1 overexpression. The graph reports the number of synaptotagmin-positive clusters per 10 µm of GFP-positive process. (D) The total number of SV pools was not altered by LRRK2 WD40, RACK1, or LRRK2 1–2141 overexpression. (E and F) Ectopically expressed LRRK2 WD40 confines cycling SV within a perisomatic region, while total SV pool distribution is not affected. The graph reports the percentage of synaptotagmin- or SV2A-positive clusters distributed within the proximal half of the process. Data are expressed as means ± SE. *, $P < 0.01$ versus DsRed (ANOVA; Tukey's *post hoc* test, $n = 4$; 7 neurons were analyzed for each experimental case). Panel length is 10 µm.

LRRK2 WD40 and LRRK2 WD40 G2385R as well as RACK1 GST fusion proteins at nanomolar concentrations with purified SV and tested the extent of binding by the means of a high-speed sedimentation assay (24). Western blot analysis using a GST-specific antibody revealed that LRRK2 WD40 as well as LRRK2 WD40 G2385R and RACK1 binds to purified SV (Fig. 7C to E) while GST alone failed to bind SV at significant rates (see Fig. S5D in the supplemental material). As mild salt treatment partially washes away peripheral SV proteins, we exploited this feature to further investigate the binding properties

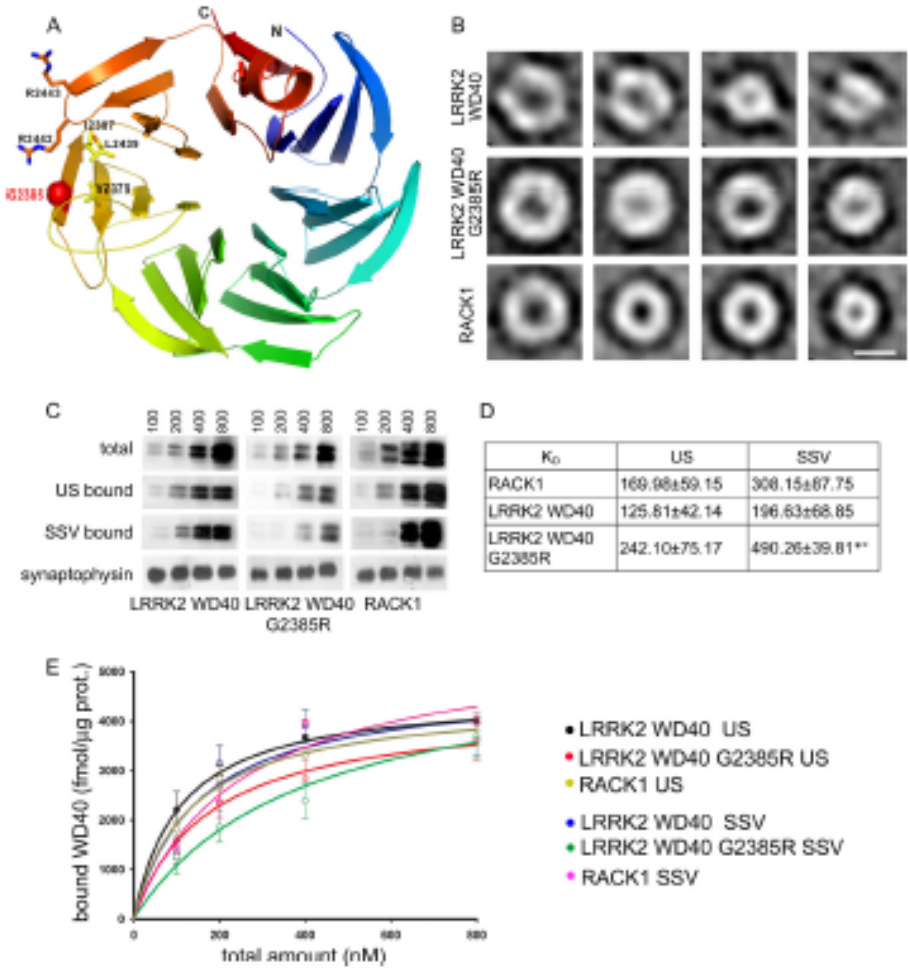

K_D	US	SSV
RACK1	169.98±59.15	308.15±67.75
LRRK2 WD40	125.81±42.14	196.63±68.85
LRRK2 WD40 G2385R	242.10±75.17	490.26±39.81**

FIG 7 The G2385R substitution impacts the local structure of LRRK2 WD40. (A) Combined stick-and-ribbon representation showing a structural homology model (based on RACK1 from *Arabidopsis thaliana*, PDB 3DM0) for the LRRK2 WD40 domain. The N terminus, C terminus, and the position of G2385 (red sphere) are indicated. (B) Transmission EM images of negatively stained (1% uranyl acetate) LRRK2 WD40, LRRK2 WD40 G2385R, and RACK1 proteins show doughnut-shaped particles consistent with the characteristic structure of WD40 folds. Four representative averaged single-particle two-dimensional projections are shown for each protein (scale bar, 5 nm). (C) LRRK2 WD40 binds SV. Increasing nanomolar amounts of LRRK2 WD40, LRRK2 WD40 G2385R domains, and RACK1 protein were incubated with unstripped SV (US) or salt-stripped SV (SSV) before high-speed sedimentation. Representative Western blots show initial amount of fusion protein (total) and the yield of GST fusion proteins precipitated by US or SSV (bound). Fusion proteins were incubated with equal amounts of SV (monitored by antisynaptophysin staining). (D) The table reports the dissociation constant (K_D) describing the binding between the indicated fusion protein and US or SSV. Data are expressed as means ± SE. *, $P < 0.05$ versus LRRK2 WD40 G2385R binding to US; **, $P < 0.01$ versus LRRK2 WD40 binding to SSV (ANOVA; Tukey's *post hoc* test, $n = 4$). (E) The graph reports the yield of precipitated GST fusion protein normalized versus the SV total protein amount (average data plus fitting) on the *y* axis and the initial amount of GST fusion protein on the *x* axis.

of the three fusion proteins. Interestingly, the salt treatment did not alter the SV association of LRRK2 WD40 and RACK1, whereas the affinity/binding strength of the LRRK2 WD40 G2385R domain to salt-treated SV was significantly reduced (Fig. 7C to E).

Taken together, these results suggest that the structural alteration induced by the G2385R substitution functionally disturbs LRRK2 WD40 binding properties to SV.

DISCUSSION

Since the first description of LRRK2 as a PD-causative gene, major attention has been devoted to its GTPase and kinase activity, linking disease-associated mutations to altered functional and (patho)physiological enzymatic properties of the protein (45–50). However, LRRK2 C-terminal deletion mutants fail to induce apoptosis and toxicity and demonstrate a reduced kinase activity (Fig. 4 and 5) (10, 51). These reports, however, do not address the question of whether the kinase domain or WD40 domain or both are causative for PD pathology. We, on the other hand, observed that the severe toxicity induced by overexpression of full-length LRRK2 in primary cultures is mimicked by ectopic expression of a construct containing only the C-terminal WD40 domain of LRRK2. Noticeably, in contrast to LRRK2 WD40, RACK1, another WD40 protein, has a positive effect on neurite complexity. These data suggest that the C-terminal WD40 domain has a major role in LRRK2-associated toxicity (43).

From structural prediction it appears likely that the LRRK2 WD40 domain folds as a seven-bladed propeller (15, 52). However, sequence homology is considerably low, and no experimental evidence for this assumption has existed so far. According to our EM analysis, the purified LRRK2 WD40 fusion protein forms doughnut-like structures with an average diameter of 5 to 8 nm, resembling EM structures reported for known WD40-containing proteins such as the splicing factor Prp19p (53) or RACK1 (this paper). These findings suggest that the LRRK2 C terminus may indeed form a propeller-like structure, in agreement with a WD40 fold. WD repeat-containing proteins execute a broad spectrum of critical functions. They participate in organizing cytoskeleton assembly, mitotic spindle formation, and vesicular trafficking (11, 12, 54, 55). Furthermore, increasing evidence describes WD40 repeat domains as molecular hubs orchestrating complex protein-protein interactions. Structurally, this feature is based on the evolutionary principle to generate binding epitopes with different specificities by concatenation of stable folded repeats and loops with variable sequences (11). Following the "guilt by association" principle (56), we systematically analyzed the domain-specific interactome of the LRRK2 C terminus in order to assign specific physiological functions to this domain. Through its WD40 domain, LRRK2 interacts with critical players of the SV cycle such as NSF, syntaxin 1A, synapsin I, dynamin-1, MUNC18-1, VAMP2, synaptojanin, and synuclein. Thus, the ability of LRRK2 to influence vesicle trafficking (13, 37, 38) is likely to involve its WD40 domain. Accordingly, we observed a severe reduction in the transport of synaptotagmin-labeled (cycling) SV to distal parts of neuronal processes upon overexpression of LRRK2 WD40 domain constructs; such output might be read as a dominant negative effect of ectopic LRRK2 WD40 executed on endogenous LRRK2 function. RACK1 is a seven-bladed WD40 propeller protein (19, 40), reported to bind and anchor recycling endosomal vesicles to centrosomes (57). Accordingly, we reported that RACK1 significantly reduces SV recycling (but not spatial segregation) once it is overexpressed in neurons and that it cosediments with pure SV. Thus, the ability to bind and sequester SV might be a biochemical property common to several WD40-containing proteins or, alternatively, might arise as an *in vitro* effect due to high local concentrations of WD40 domains. Even if we cannot completely rule out the latter explanation, our data suggest a peculiar physiological role for LRRK2 at the synaptic site. In fact, we demonstrated here that endogenous LRRK2 can be detected in a pure SV fraction, that full-length LRRK2 binds SV, and that LRRK2 WD40, but not LRRK2 LRR or full-length RACK1, interacts with several proteins involved in SV trafficking. Thus, we propose that LRRK2 association with SV is mediated by the interaction of its WD40 domain with SV-integral and -associated proteins.

The description of the G2385R point mutation within the WD40 domain as the main PD risk variant in the Chinese Han and Korean population further underlines the functional and pathological role of this domain (14). G2385R carrier patients demonstrate clinical features similar to noncarrier patients; however, the G2385R variant does correlate to a small but significant effect in lowering the age of PD onset (16). It has recently been reported that G2385R has a mild impact on LRRK2 biochemical properties, such as reduced LRRK2 kinase activity and interactions with other proteins (9), while it neither influences LRRK2 toxicity in neuron cultures nor affects overall autophosphorylation (46). Accordingly, we reported here that LRRK2 WD40 G2385R behaved similarly to LRRK2 WD40 once it was overexpressed in primary neurons. Comparative protein models predict that the glycine 2385 residue stays at the surface of the WD40 domain (Fig. 7A) (15). The G2385R variant replaces the glycine with a long, positively charged arginine residue, thus increasing the net positive charge of the domain and likely inducing an electrostatic repulsion between WD40 repeats 5 and 6. This may explain the increased mean diameter observed for LRRK2 WD40 G2385R in our EM analysis. The changes in surface charge and local structural features in the WD40 fold are expected to result in altered biochemical properties which affect protein-protein interaction strength and quality. Indeed, we reported that the association with SV is partially impaired by the glycine-to-arginine change. In particular, while LRRK2 WD40 showed a high affinity toward both native and salt-treated SV, LRRK2 WD40 G2385R binding to SV was significantly sensitive to salt treatment. In line with our proposal of LRRK2 as a synaptic scaffold protein involved in vesicular trafficking and vesicle storage, our data strongly support the idea that in addition to increased kinase activity, other molecular mechanisms, such as altered protein binding, may underlie LRRK2-associated forms of PD. In particular, given the recent independent evidence linking LRRK2 dysfunction to neurotransmission defects in PD models (58–60) and in patients carrying LRRK2 mutations (61), an altered presynaptic vesicle transport, storage, and release kinetics may arise as a common pathway disturbed by the different LRRK2 pathological mutations described so far and become a future target for pharmacological treatment.

ACKNOWLEDGMENTS

We are grateful to Nathalie Théret (INSERM, Rennes, France) for reagents, to Sandra Helm for technical assistance, and to Peijian Zou and Arie Geerlof for initial bacterial expression clones of the WD40 domain. In addition we thank Pablo Porras and Henning Hermjakob (EMBL-EBI) for data integration into the IntAct database.

This work was supported by the National Genome Research Framework program NGFN-Plus (grant 01GS08140, subproject 12), the Helmholtz Alliance for Mental Health in an Aging Society (grant HA-215, topic 3 WP11), the European Community's Seventh Framework Program FP7/2009 under grant agreement number 241955, number 278568, PRIMES, and number 241481, AFFINOMICS (to M.U.), and the LRRK2 Biology LEAPS 2012 award of the Michael J. Fox Foundation to G.P., C.J.G., M.S., and M.U. G.P. and F.O. are supported by Fondazione Cariplo (grant 2011-0540), MJFF, and Fondazione Telethon (grant GGP12237). G.P. is supported also by the FIRB program (grant RBFR08F82X_002) and Fondazione Grigioni per il morbo di Parkinson. F.O. is grateful to PRIN 2010-11. M.M. is supported by Fondazione Cariplo (grant 2008-3184).

Author contributions are as follows. G.P., C.J.G., F.O. and M.U. designed the study. G.P., C.J.G., and M.U. wrote the paper. G.P., M.D.C., A.M., F.P., F.A., F.G., P.J., C.J.K., F.V.Z., and A.K. performed experiments. G.P., C.J.G., C.S., C.J.O.K., M.M., A.V., C.J.O.K., L.P., M.Z, S.W., M.S., and M.U. analyzed the data and/or provided data analysis expertise.

REFERENCES

1. Clarke C, Moore AP. 2005. Parkinson's disease. Clin. Evid. 13:1658–1677.
2. Fahn S. 2003. Description of Parkinson's disease as a clinical syndrome. Ann. N. Y. Acad. Sci. 991:1–14. http://dx.doi.org/10.1111/j.1749-6632.2003.tb07458.x.
3. Kelley LA, Sternberg MJE. 2009. Protein structure prediction on the Web: a case study using the Phyre server. Nat. Protoc. 4:363–371. http://dx.doi.org/10.1038/nprot.2009.2.
4. Bosgraaf L, Van Haastert PJ. 2003. Roc, a Ras/GTPase domain in complex proteins. Biochim. Biophys. Acta 1643:5–10. http://dx.doi.org/10.1016/j.bbamcr.2003.08.008.

5. Mills RD, Mulhern TD, Cheng H-C, Culvenor JG. 2012. Analysis of LRRK2 accessory repeat domains: prediction of repeat length, number and sites of Parkinson's disease mutations. Biochem. Soc. Trans. 40:1086–1089. http://dx.doi.org/10.1042/BST20120088.
6. Guo L, Wang W, Chen SG. 2006. Leucine-rich repeat kinase 2: relevance to Parkinson's disease. Int. J. Biochem. Cell Biol. 38:1469–1475. http://dx.doi.org/10.1016/j.biocel.2006.02.009.
7. Goldwurm S, Zini M, Di Fonzo A, De Gaspari D, Siri C, Simons EJ, van Doeselaar M, Tesei S, Antonini A, Canesi M, Zecchinelli A, Mariani C, Meucci N, Sacilotto G, Cilia R, Isaias IU, Bonetti A, Stroni F, Ricca S, Oostra BA, Bonifati V, Pezzoli G. 2006. LRRK2 G2019S mutation and Parkinson's disease: a clinical, neuropsychological and neuropsychiatric study in a large Italian sample. Parkinsonism Relat. Disord. 12:410–419. http://dx.doi.org/10.1016/j.parkreldis.2006.04.001.
8. Bonifati V. 2006. Parkinson's disease: the LRRK2–G2019S mutation: opening a novel era in Parkinson's disease genetics. Eur. J. Hum. Genet. 14:1061–1062. http://dx.doi.org/10.1038/sj.ejhg.5201695.
9. Rudenko IN, Kaganovich A, Hauser DN, Beylina A, Chia R, Ding J, Maric D, Jaffe H, Cookson MR. 2012. The G2385R variant of leucine-rich repeat kinase 2 associated with Parkinson's disease is a partial loss-of-function mutation. Biochem. J. 446:99–111. http://dx.doi.org/10.1042/BJ20120637.
10. Jorgensen ND, Peng Y, Ho CC-Y, Rideout HJ, Petrey D, Liu P, Dauer WT. 2009. The WD40 domain is required for LRRK2 neurotoxicity. PLoS One 4:e8463. http://dx.doi.org/10.1371/journal.pone.0008463.
11. Stirnimann CU, Petsalaki E, Russell RB, Müller CW. 2010. WD40 proteins propel cellular networks. Trends Biochem. Sci. 35:565–574. http://dx.doi.org/10.1016/j.tibs.2010.04.003.
12. Smith TF. 2008. Diversity of WD-repeat proteins. Subcell. Biochem. 48:20–30. http://dx.doi.org/10.1007/978-0-387-09595-0_3.
13. Piccoli G, Condliffe SB, Bauer M, Giesert F, Boldt K, De Astis S, Meixner A, Sarioglu H, Vogt-Weisenhorn DM, Wurst W, Gloeckner CJ, Matteoli M, Sala C, Ueffing M. 2011. LRRK2 controls synaptic vesicle storage and mobilization within the recycling pool. J. Neurosci. 31:2225–2237. http://dx.doi.org/10.1523/JNEUROSCI.3730-10.2011.
14. Tan E-K. 2006. Identification of a common genetic risk variant (LRRK2 Gly2385Arg) in Parkinson's disease. Ann. Acad. Med. Singapore 35:840–842.
15. Tan EK, Zhao Y, Skipper L, Tan MG, Di Fonzo A, Sun L, Fook-Chong S, Tang S, Chua E, Yuen Y, Tan L, Pavanni R, Wong MC, Kolatkar P, Lu CS, Bonifati V, Liu JJ. 2007. The LRRK2 Gly2385Arg variant is associated with Parkinson's disease: genetic and functional evidence. Hum. Genet. 120:857–863. http://dx.doi.org/10.1007/s00439-006-0268-0.
16. Tan EK, Peng R, Wu YR, Wu RM, Wu-Chou YH, Tan LC, An XK, Chen CM, Fook-Chong S, Lu CS. 2009. LRRK2 G2385R modulates age at onset in Parkinson's disease: A multi-center pooled analysis. Am. J. Med. Genet. B Neuropsychiatr. Genet. 150B:1022–1023. http://dx.doi.org/10.1002/ajmg.b.30923.
17. Brewer GJ, Torricelli JR, Evege EK, Price PJ. 1993. Optimized survival of hippocampal neurons in B27-supplemented Neurobasal, a new serum-free medium combination. J. Neurosci. Res. 35:567–576. http://dx.doi.org/10.1002/jnr.490350513.
18. Gloeckner CJ, Boldt K, Schumacher A, Ueffing M. 2009. Tandem affinity purification of protein complexes from mammalian cells by the Strep/FLAG (SF)-TAP tag. Proteomics 564:359–372. http://dx.doi.org/10.1007/978-1-60761-157-8_21.
19. Bourd-Boittin K, Le Pabic H, Bonnier D, L'Helgoualc'h A, Théret N. 2008. RACK1, a new ADAM12 interacting protein. Contribution to liver fibrogenesis. J. Biol. Chem. 283:26000–26009. http://dx.doi.org/10.1074/jbc.M709829200.
20. Gloeckner CJ, Kinkl N, Schumacher A, Braun RJ, O'Neill E, Meitinger T, Kolch W, Prokisch H, Ueffing M. 2006. The Parkinson disease causing LRRK2 mutation I2020T is associated with increased kinase activity. Hum. Mol. Genet. 15:223–232. http://dx.doi.org/10.1093/hmg/ddl439.
21. Xia Z, Dudek H, Miranti CK, Greenberg ME. 1996. Calcium influx via the NMDA receptor induces immediate early gene transcription by a MAP kinase/ERK-dependent mechanism. J. Neurosci. 16:5425–5436.
22. Frangioni JV, Neel BG. 1993. Solubilization and purification of enzymatically active glutathione S-transferase (pGEX) fusion proteins. Anal. Biochem. 210:179–187. http://dx.doi.org/10.1006/abio.1993.1170.
23. Huttner WB, Schiebler W, Greengard P, De Camilli P. 1983. Synapsin I (protein I), a nerve terminal-specific phosphoprotein. III. Its association with synaptic vesicles studied in a highly purified synaptic vesicle preparation. J. Cell Biol. 96:1374–1388.
24. Messa M, Congia S, Defranchi E, Valtorta F, Fassio A, Onofri F, Benfenati F. 2010. Tyrosine phosphorylation of synapsin I by Src regulates synaptic-vesicle trafficking. J. Cell Sci. 123:2256–2265. http://dx.doi.org/10.1242/jcs.068445.
25. Gillardon F, Kremmer E, Froehlich T, Ueffing M, Hengerer B, Gloeckner CJ. 2013. ATP-competitive LRRK2 inhibitors interfere with monoclonal antibody binding to the kinase domain of LRRK2 under native conditions. A method to directly monitor the active conformation of LRRK2? J. Neurosci. Methods 214:62–68. http://dx.doi.org/10.1016/j.jneumeth.2012.12.015.
26. Olsen JV. 2005. Parts per million mass accuracy on an Orbitrap mass spectrometer via lock mass injection into a C-trap. Mol. Cell. Proteomics 4:2010–2021. http://dx.doi.org/10.1074/mcp.T500030-MCP200.
27. Keller A, Nesvizhskii AI, Kolker E, Aebersold R. 2002. Empirical statistical model to estimate the accuracy of peptide identifications made by MS/MS and database search. Anal. Chem. 74:5383–5392. http://dx.doi.org/10.1021/ac025747h.
28. Nesvizhskii AI, Keller A, Kolker E, Aebersold R. 2003. A statistical model for identifying proteins by tandem mass spectrometry. Anal. Chem. 75:4646–4658. http://dx.doi.org/10.1021/ac0341261.
29. Matteoli M, Takei K, Perin MS, Sudhof TC, De Camilli P. 1992. Exo-endocytotic recycling of synaptic vesicles in developing processes of cultured hippocampal neurons. J. Cell Biol. 117:849–861. http://dx.doi.org/10.1083/jcb.117.4.849.
30. Piccoli G, Verpelli C, Tonna N, Romorini S, Alessio M, Nairn AC, Bachi A, Sala C. 2007. Proteomic analysis of activity-dependent synaptic plasticity in hippocampal neurons. J. Prot. Res. 6:3203–3215. http://dx.doi.org/10.1021/pr0701308.
31. Ludtke SJ, Baldwin PR, Chiu W. 1999. EMAN: semiautomated software for high-resolution single-particle reconstructions. J. Struct. Biol. 128:82–97. http://dx.doi.org/10.1006/jsbi.1999.4174.
32. Berman HM, Bhat TN, Bourne PE, Feng Z, Gilliland G, Weissig H, Westbrook J. 2000. The Protein Data Bank and the challenge of structural genomics. Nat. Struct. Biol. 7(Suppl):957–959. http://dx.doi.org/10.1038/80734.
33. Berman HM, Battistuz T, Bhat TN, Bluhm WF, Bourne PE, Burkhardt K, Feng Z, Gilliland GL, Iype L, Jain S, Fagan P, Marvin J, Padilla D, Ravichandran V, Schneider B, Thanki N, Weissig H, Westbrook JD, Zardecki C. 2002. The Protein Data Bank. Acta Crystallogr. D. Biol. Crystallogr. 58:899–907. http://dx.doi.org/10.1107/S0907444902003451.
34. Ullah H, Scappini EL, Moon AF, Williams LV, Armstrong DL, Pedersen LC. 2008. Structure of a signal transduction regulator, RACK1, from *Arabidopsis thaliana*. Protein Sci. 17:1771–1780. http://dx.doi.org/10.1110/ps.035121.108.
35. Krieger E, Koraimann G, Vriend G. 2002. Increasing the precision of comparative models with YASARA NOVA-a self-parameterizing force field. Proteins 47:393–402. http://dx.doi.org/10.1002/prot.10104.
36. Laskowski R, Rullmann JA, MacArthur M, Kaptein R, Thornton J. 1996. AQUA and PROCHECK-NMR: programs for checking the quality of protein structures solved by NMR. J. Biomol. NMR 8:477–486.
37. Shin N, Jeong H, Kwon J, Heo HY, Kwon JJ, Yun HJ, Kim C-H, Han BS, Tong Y, Shen J, Hatano T, Hattori N, Kim KS, Chang S, Seol W. 2008. LRRK2 regulates synaptic vesicle endocytosis. Exp. Cell Res. 314:2055–2065. http://dx.doi.org/10.1016/j.yexcr.2008.02.015.
38. Xiong Y, Coombes CE, Kilaru A, Li X, Gitler AD, Bowers WJ, Dawson VL, Dawson TM, Moore DJ. 2010. GTPase activity plays a key role in the pathobiology of LRRK2. PLoS Genet. 6:e1000902. http://dx.doi.org/10.1371/journal.pgen.1000902.
39. Meixner A, Boldt K, Van Troys M, Askenazi M, Gloeckner CJ, Bauer M, Marto JA, Ampe C, Kinkl N, Ueffing M. 2011. A QUICK screen for Lrrk2 interaction partners-leucine-rich repeat kinase 2 is involved in actin cytoskeleton dynamics. Mol. Cell Proteomics 10:M110.001172. http://dx.doi.org/10.1074/mcp.M110.001172.
40. Sengupta J, Nilsson J, Gursky R, Spahn CMT, Nissen P, Frank J. 2004. Identification of the versatile scaffold protein RACK1 on the eukaryotic ribosome by cryo-EM. Nat. Struct. Mol. Biol. 10:957–962. http://dx.doi.org/10.1038/nsmb822.
41. Szklarczyk D, Franceschini A, Kuhn M, Simonovic M, Roth A, Minguez P, Doerks T, Stark M, Muller J, Bork P, Jensen LJ, von Mering C. 2011. The STRING database in 2011: functional interaction networks of pro-

teins, globally integrated and scored. Nucleic Acids Res. 39:D561–D568. http://dx.doi.org/10.1093/nar/gkq973.
42. Shannon P, Markiel A, Ozier O, Baliga NS, Wang JT, Ramage D, Amin N, Schwikowski B, Ideker T. 2003. Cytoscape: a software environment for integrated models of biomolecular interaction networks. Genome Res. 13:2498–2504. http://dx.doi.org/10.1101/gr.1239303.
43. Skibinski G, Nakamura K, Cookson MR, Finkbeiner S. 2014. Mutant LRRK2 toxicity in neurons depends on LRRK2 levels and synuclein but not kinase activity or inclusion bodies. J. Neurosci. 34:418–433. http://dx.doi.org/10.1523/JNEUROSCI.2712-13.2014.
44. Chernova T, Steinert JR, Guerin CJ, Nicotera P, Forsythe ID, Smith AG. 2007. Neurite degeneration induced by heme deficiency mediated via inhibition of NMDA receptor-dependent extracellular signal-regulated kinase 1/2 activation. J. Neurosci. 27:8475–8485. http://dx.doi.org/10.1523/JNEUROSCI.0792-07.2007.
45. Gloeckner CJ, Schumacher A, Boldt K, Ueffing M. 2009. The Parkinson disease-associated protein kinase LRRK2 exhibits MAPKKK activity and phosphorylates MKK3/6 and MKK4/7, in vitro. J. Neurochem. 109:959–968. http://dx.doi.org/10.1111/j.1471-4159.2009.06024.x.
46. West AB, Moore DJ, Choi C, Andrabi SA, Li X, Dikeman D, Biskup S, Zhang Z, Lim KL, Dawson VL, Dawson TM. 2007. Parkinson's disease-associated mutations in LRRK2 link enhanced GTP-binding and kinase activities to neuronal toxicity. Hum. Mol. Genet. 16:223–232. http://dx.doi.org/10.1093/hmg/ddl471.
47. Lee BD, Shin J-H, VanKampen J, Petrucelli L, West AB, Ko HS, Lee Y-I, Maguire-Zeiss KA, Bowers WJ, Federoff HJ, Dawson VL, Dawson TM. 2010. Inhibitors of leucine-rich repeat kinase-2 protect against models of Parkinson's disease. Nat. Med. 16:998–1000. http://dx.doi.org/10.1038/nm.2199.
48. Kett LR, Boassa D, Ho CC-Y, Rideout HJ, Hu J, Terada M, Ellisman M, Dauer WT. 2012. LRRK2 Parkinson disease mutations enhance its microtubule association. Hum. Mol. Genet. 21:890–899. http://dx.doi.org/10.1093/hmg/ddr526.
49. Greggio E, Jain S, Kingsbury A, Bandopadhyay R, Lewis P, Kaganovich A, van der Brug MP, Beilina A, Blackinton J, Thomas KJ, Ahmad R, Miller DW, Kesavapany S, Singleton A, Lees A, Harvey RJ, Harvey K, Cookson MR. 2006. Kinase activity is required for the toxic effects of mutant LRRK2/dardarin. Neurobiol. Dis. 23:329–341. http://dx.doi.org/10.1016/j.nbd.2006.04.001.
50. Imai Y, Gehrke S, Wang HQ, Takahashi R, Hasegawa K, Oota E, Lu B. 2008. Phosphorylation of 4E-BP by LRRK2 affects the maintenance of dopaminergic neurons in *Drosophila*. EMBO J. 27:2432–2443. http://dx.doi.org/10.1038/emboj.2008.163.
51. Iaccarino C, Crosio C, Vitale C, Sanna G, Carri MT, Barone P. 2007. Apoptotic mechanisms in mutant LRRK2-mediated cell death. Hum. Mol. Genet. 16:1319–1326. http://dx.doi.org/10.1093/hmg/ddm080.
52. Wang Y, Jiang F, Zhuo Z, Wu X-H, Wu Y-D. 2013. A method for WD40 repeat detection and secondary structure prediction. PLoS One 8:e65705. http://dx.doi.org/10.1371/journal.pone.0065705.
53. Ohi MD, Koot CWV, Rosenberg JA, Ren L, Hirsch JP, Chazin WJ, Walz T, Gould KL. 2005. Structural and functional analysis of essential pre-mRNA splicing factor Prp19p. Mol. Cell. Biol. 25:451–460. http://dx.doi.org/10.1128/MCB.25.1.451-460.2005.
54. Pryer NK, Salama NR, Schekman R, Kaiser CA. 1993. Cytosolic Sec13p complex is required for vesicle formation from the endoplasmic reticulum in vitro. J. Cell Biol. 120:865–875. http://dx.doi.org/10.1083/jcb.120.4.865.
55. Vaisman N, Tsouladze A, Robzyk K, Ben-Yehuda S, Kupiec M, Kassir Y. 1995. The role of *Saccharomyces cerevisiae* Cdc40p in DNA replication and mitotic spindle formation and/or maintenance. Mol. Gen. Genet. 247:123–136. http://dx.doi.org/10.1007/BF00705642.
56. Wang PI, Marcotte EM. 2010. It's the machine that matters: predicting gene function and phenotype from protein networks. J. Proteomics 73:2277–2289. http://dx.doi.org/10.1016/j.jprot.2010.07.005.
57. Ai E, Skop AR. 2009. Endosomal recycling regulation during cytokinesis. Commun. Integr. Biol. 2:444–447. http://dx.doi.org/10.4161/cib.2.5.8931.
58. Li X, Patel JC, Wang J, Avshalumov MV, Nicholson C, Buxbaum JD, Elder GA, Rice ME, Yue Z. 2010. Enhanced striatal dopamine transmission and motor performance with LRRK2 overexpression in mice is eliminated by familial Parkinson's disease mutation G2019S. J. Neurosci. 30:1788–1797. http://dx.doi.org/10.1523/JNEUROSCI.5604-09.2010.
59. Tong Y, Pisani A, Martella G, Karouani M, Yamaguchi H, Pothos EN, Shen J. 2009. R1441C mutation in LRRK2 impairs dopaminergic neurotransmission in mice. Proc. Natl. Acad. Sci. 106:14622–14627. http://dx.doi.org/10.1073/pnas.0906334106.
60. Li Y, Liu W, Oo TF, Wang L, Tang Y, Jackson-Lewis V, Zhou C, Geghman K, Bogdanov M, Przedborski S, Beal MF, Burke RE, Li C. 2009. Mutant LRRK2R1441G BAC transgenic mice recapitulate cardinal features of Parkinson's disease. Nat. Neurosci. 12:826–828. http://dx.doi.org/10.1038/nn.2349.
61. Sossi V, de la Fuente-Fernández R, Nandhagopal R, Schulzer M, McKenzie J, Ruth TJ, Aasly JO, Farrer MJ, Wszolek ZK, Stoessl JA. 2010. Dopamine turnover increases in asymptomatic LRRK2 mutations carriers. Mov. Disord. 25:2717–2723. http://dx.doi.org/10.1002/mds.23356.
62. Berg D, Schweitzer KJ, Leitner P, Zimprich A, Lichtner P, Belcredi P, Brüssel T, Schulte C, Maass S, Nägele T, Wszolek ZK, Gasser T. 2005. Type and frequency of mutations in the LRRK2 gene in familial and sporadic Parkinson's disease*. Brain 128:3000–3011. http://dx.doi.org/10.1093/brain/awh666.
63. Brice A. 2005. Genetics of Parkinson's disease: LRRK2 on the rise. Brain 128:2760–2762. http://dx.doi.org/10.1093/brain/awh676.
64. Hardy J, Lewis P, Revesz T, Lees A, Paisan-Ruiz C. 2009. The genetics of Parkinson's syndromes: a critical review. Curr. Opin. Genet. Dev. 19:254–265. http://dx.doi.org/10.1016/j.gde.2009.03.008.